The Cahn-Larché system: A model for spinodal decomposition in eutectic solder

–Modelling, analysis and simulation–

Von der Fakultät Mathematik und Physik der Universität Stuttgart
zur Erlangung der Würde eines Doktors der
Naturwissenschaften (Dr. rer. nat.) genehmigte Abhandlung

Vorgelegt von

Dipl.-Math. Thomas Merkle

aus Göppingen

Hauptberichter:	Apl. Prof. Dr. A.-M. Sändig
Mitberichter:	Prof. Dr. A. Mielke
	Prof. Dr. H. Garcke
Tag der Einreichung:	8. März 2005
Tag der mündlichen Prüfung:	25. April 2005

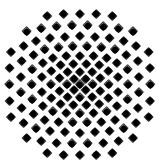

Institut für Angewandte Analysis und Numerische Simulation
Universität Stuttgart
2005

Dipl.-Math. Thomas Merkle
Robert Bosch GmbH
Automotive Electronics
Engineering Design Powertrain 5
Tübinger Straße 123
72 762 Reutlingen
Germany

This document can be downloaded from http://elib.uni-stuttgart.de/opus/index.php.

This document is typeset with PDFLaTeX.

This thesis is dedicated to my wife

Monika

in honour of her lovely support during the time I spent on this work.

Preface

This thesis has been arisen from the dissertation project *„Mathematische Modellbildung und Analyse von Weichloten unter mechanischen und thermischen Belastungen mit Anwendung auf die Steuergerätekonstruktion“* in cooperation with the *Robert Bosch GmbH, Automotive Electronics, Engineering Design Powertrain 5* in Reutlingen.

It is a great pleasure to thank my supervisor apl. Prof. Dr. A.-M. Sändig for her valuable advice, her support during the time I spent on this thesis and for many interesting discussions.

I would also thank my co-advisors Prof. Dr. A. Mielke and Prof. Dr. H. Garcke for their encouragement and review of this thesis.

I gratefully acknowledge the financial support of the *Robert Bosch GmbH*. Many thanks are also due to Dr. A. Rössle and Dr. I. Durdevic for valuable discussions and for having given me the opportunity to attend several workshops and summer schools. I have benefited a great deal from the interaction with so many kind and encouraging people from science and industry.

There are many colleagues from the *“Institut für Angewandte Analysis und Numerische Simulation“* whom I owe a lot of gratitude for their support and discussions. Among them are Dr. D. Knees and Dipl.-Math. W. Geis, who gave me helpful suggestions for this work.

Stuttgart, 10th June 2005

Contents

Introduction

Electronic control of mechanical procedures in particular within an automobile becomes recently more and more important. Control devices undertake responsible and security relevant tasks, hence they effect essentially the performance of a car. Due to this fact control devices have to satisfy high standards even under extreme thermal and mechanical loadings. Among the number of challenging problems, which appear by the development of control devices, we focus our attention to the reliability of solder joints. In Surface Mount Technology (SMT) silicon wafers and Printed Circuit Boards (PCB) are connected electrically and mechanically with solder.

The reliability and life time of a solder joint in SMT becomes more and more significant to electronic and automotive industry. The thermal mismatch between various materials involved in microelectronic composites in combination with advanced temperatures and mechanical loadings is the key issue in solder joint reliability.

Usually, solder is an alloy consisting of two or more components. Materials like tin (Sn), lead (Pb), silver (Ag) and copper (Cu) are normally used as components of a solder alloy. We have to remark, that Pb free solder plays an import role due to the fact, that heavy metals are forbidden by law in automotive technology.

Fig. 1 shows a cross section cut through a Sn-Pb solder bump, which has been subjected to several thousand power cycles. The experimental investigations show different damages of the solder joint.

Obviously, the large amount of power cycles essentially changes the microstructure of the alloy. In fig. 1 regions of gray and white shades demonstrate, that the original fine mixture of Sn and Pb separates into islands of high Sn and high Pb concentration. Furthermore, the coarsening process of the microstructure is not uniform all over the alloy. There are regions, which have a much more coarser microstructure than others. However, these regions are not randomly distributed over the solder joint. They start e.g. from a notch or a reentrant corner or lie nearby a hard clamped boundary part of the solder joint. These observations give rise to the conjecture, that the boundary of the solder bump as well as the type of loading additionally effect the separation and coarsening process.

In the worst case cracks appear within the alloy after a sufficient amount of power cycles. Fig. 1 shows that cracks propagate between regions of coarse and fine

microstructures. All these phenomena together are denoted as disruption of solder.

The first step in order to understand disruption and aging of solder is to simulate the evolution of microstructure on a mesoscopic level. In general, the simulation of microstructure formation is restricted only on small parts of a solder joint due to computational complexity. A small part of the solder bump could be a Representative Volume Element (RVE) lying inside the alloy or more interesting a RVE, which has a connection with the boundary and undergoes the influence of changing boundary loadings and geometrical effects.

The results of mesoscopic simulations can be used to develop strength and local damage criteria. In particular, the design optimisation of a solder joint and of a microelectronic composite avoiding disruption and aging of the alloy is the essential purpose of these simulations.

Furthermore, the mesoscopic simulation results can be used for deriving a macroscopic material model in order to simulate a whole solder joint inside a microelectronic device. For this reasons we concentrate our attention on the simulation of microstructure formation within a solder alloy on a mesoscopic level.

The evolution of microstructure within an alloy is described by a diffusive process. We have to decide between an early and a late stage of this evolution.

In the beginning of the process we observe the following phenomena: At temperatures larger than a critical temperature θ_c the mixture of the alloy consists of one homogeneous phase only, which is arranged in an energetic stable state. By decreasing the temperature below a critical temperature θ_c two or more phases develop. This can be seen in the phase diagram e.g. of a Sn-Pb solder, see fig. 2. Each phase is characterised by a distinct composition of individual components such that it is again energetic stable and the energy becomes small. The formation of microstructure happens on a very fast time scale and is called *spinodal decomposition* or *phase separation*. We denote a connected region of a distinct phase as a particle.

In a later stage of the evolution another phenomena is observed: The particles developed after spinodal decomposition are separated by interfaces. With these interfaces an interfacial energy is associated. After spinodal decomposition there are

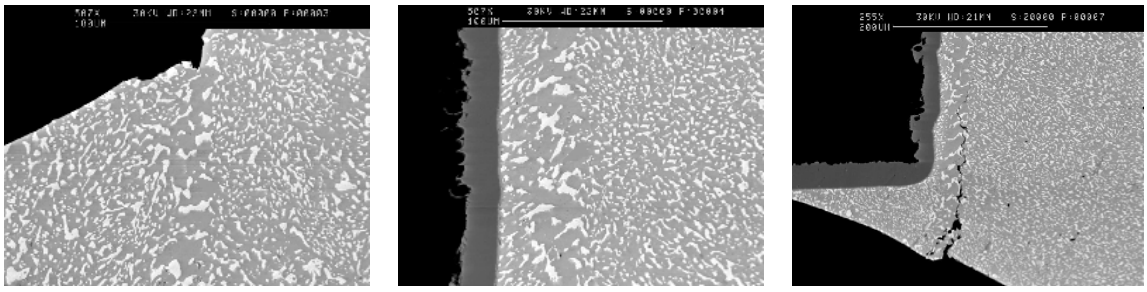

Fig. 1: Microstructure and damage within a solder joint

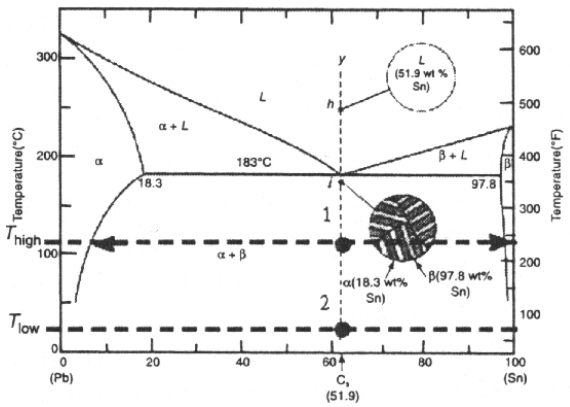

Fig. 2: Phase diagram of a Sn-Pb alloy

a lot of small particles, hence the interfacial energy is very large. In the second stage of the evolution, the microstructure starts to coarsen in order to reduce energy. This means that large particles become even larger on costs of the small particles, which shrink and finally vanish. This part of the evolution is called *coarsening* or *Ostwald ripening* and is mainly driven by the reduction of interfacial energy. We remark, that in the case of negligible elastic effects, the particles become round, see fig. 3. In this case, there exists a theory, which provides a relation for the growth of the averaged particle size. This theory goes back to Lifshitz and Slyozov [70] as well as Wagner [100] and is called LSW-theory.

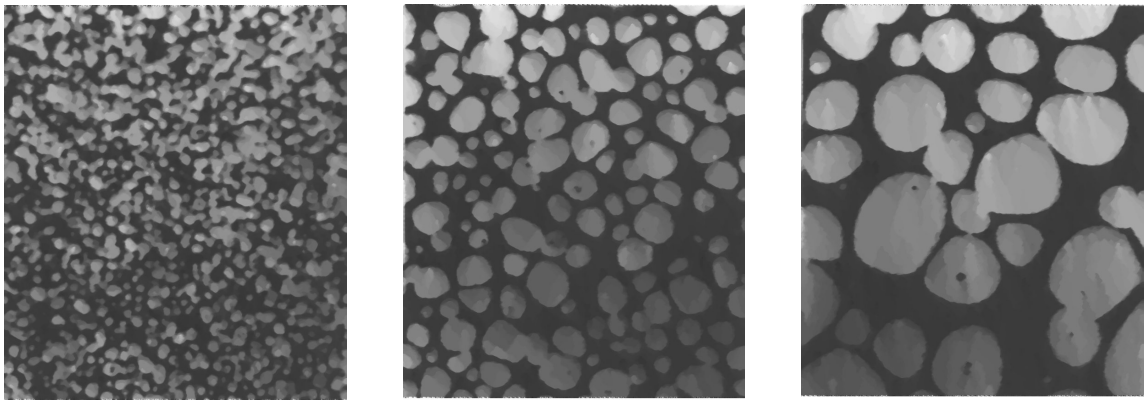

Fig. 3: Formation of round particles

In a solder alloy there are various materials involved, which have very different elastic moduli or different lattice structures. This fact has a great influence on the phase separation as well as on the coarsening process. Furthermore, stress effects form essentially the morphology of the particles. Material scientists discuss the situation in which stress effects slow down the rate of coarsening, see [44, 45]. Some experiments suggested that even inverse coarsening is possible. Additionally, stress

singularities resulting from notches, reentrant corners or different boundary loadings might influence the coarsening process.

In order to simulate these phenomena there exist at least three different types of material models, for a detailed overview we refer to [44]:

- atomistic models
- concentration dependent models with sharp interfaces
- concentration dependent models with diffusive interfaces

On a micromechanical level atomistic models are used to simulate the behaviour of atoms inside the lattice structure. This models base on probability assumptions describing the exchange of atoms in the lattice (Kawasaki dynamic), see [61]. With this type of model it is possible to simulate a bounded amount of atoms only, which is in general not enough for realistic simulations.

In order to make realistic simulations, continuum mechanical models are used, which are based on the mass concentration of one or more components. The main difference of these models is the description of an interface as a sharp or diffusive interface.

In general an interface between two phases is very small, so it is acceptable to describe an interface as a manifold with infinite small thickness. One type of sharp interface models for coarsening phenomena is derived by Mullins and Sekerka [77]. The main goal of this model is to simulate the motion of an interface. This model uses one concentration value inside the particle and one concentration value outside the particle only. The diffusion is driven by a potential inside each phase and the velocity of an interface is given by the jump of the gradient of the potential across the interface into normal direction.

The Mullin-Sekerka model is generalised to consider elastic effects in [69]. Boundary Element Methods (BEM) are used in [3, 4, 59] to simulate the coarsening process with sharp interfaces. BEM are frequently applied in this context, because only the manifold of an interface must be discretised. The advantage of this model is to simulate the coarsening process at a late stage, where only large particles appear.

A diffusive phase interface model describes an interface as a thin, but not infinitesimal thin region with a large gradient of the concentration. A mathematical model of this type is derived by Cahn and Hilliard [20, 21] and know as Cahn-Hilliard equation. The evolution of the concentration field is driven by the gradient of the chemical potential of the mixture, which enters the model as the variational derivative of the energy with respect to the concentration. Due to this fact the Cahn-Hilliard model has a flow gradient structure, an important property for the mathematical analysis as well as for the numerical simulation. Numerical simulations of the Cahn-Hilliard equation are done e.g. in [36, 37].

The extension of the model taking into account elastic interactions goes back to Cahn [19], Khachaturyan [62], Larché and Cahn [68] as well as Onuki [84]. Numerical investigations of phase separation under elastic loadings are made e.g. in [50, 51, 102]. We have to remark, that Garcke [49] shows the convergence of the diffusive interface model to the sharp interface model, when the interface thickness goes to zero.

Motivated by these observations the important aspects in the modelling of the phase separation under elastic loadings are the following in this thesis:

- We present a mathematical rigorous derivation of the Cahn-Larché system, which contributes the influence of the external mechanical loadings and viscosity to the classical model derived in [62, 68, 84].

- The examination of the general entropy principle is done by applying Lagrangian multipliers to the thermodynamics of the spinodal decomposition.

The method of Lagrangian multipliers in thermodynamic was developed by Liu in [71]. This technique was applied to phase transition problems with a order parameter and temperature by Alt and Pawlow in [6, 7]. The Lagrangian multipliers provide an alternative concept to the theory of configurational forces derived by Fried and Gurtin in [46, 47], which is also applied to the Cahn-Larché model in [56]. A new result concerning the analysis for the Cahn-Larché system is the following:

- The existence of weak solutions of the viscous Cahn-Larché system is proved taking into account a concentration dependent mobility tensor and external mechanical forces.

In order to attain this result, we extend the method, which is developed by Garcke in [48, 49] consisting of a time discretisation, minimising the Helmholtz free energy and maximising the dissipation. An interesting result of our investigations is the fact that the a-priori estimates do not depend on the friction coefficient. Due to this observation we get simultaneously the existence of weak solutions of the viscous and non-viscous problem. Thereby we observe that a weak solution of the viscous system is smoother with respect to time than a solution of the non-viscous system.

In the numerical simulation of the phase separation without viscosity we observe Gibbs phenomena. This means that high overshoots and undershoots appear within a diffusive phase interface. Consequently, a discrete solution starts to oscillate and the computational results are unusable.

This observation motivates the development of stable numerical approximation methods for the Cahn-Larché system. Stable means that high overshoots and undershoots do not appear in a discrete solution. We attain this goal by the following methods:

- A Faedo-Galerkin method of the viscous Cahn-Larché equations is derived. The friction term is used for stabilising the method applied to the non-viscous system.

- A second viscous approximation method is observed, where friction is formulated in terms of driving forces. We show that both methods are equivalent taking into account the flow gradient structure of the system.

Both methods state a new stable simulation method for the spinodal decomposition. Nevertheless, it is of great advantage to derive a stable numerical approximation method for the non-viscous Cahn-Larché system. This is done by the following:

- We derive an operator-splitting method for the non-viscous Cahn-Larché system, which decomposes the Gibbs free energy density into a convex and a concave part.

Operator-splitting methods for semilinear parabolic equations were considered by Elliott and Stuart in [41] and applied to the Cahn-Hilliard equation by Barrett and Blowey in [9, 10]. A similar technique was developed by Rumpf and Grün in [54] for the thin film equation. Our investigations show that the operator-splitting method is stable, but the viscous method are more efficient, since for the operator-splitting method the time discretisation must be chosen very small.

The different numerical simulations performed essentially by using the viscous method stabilised by driving forces yield the following results:

- The Cahn-Larché model with a concentration dependent elasticity tensor fits qualitatively better to the experiment than the simpler model with a constant elasticity tensor.

- Mechanical stress singularities, which result from changing boundary conditions, affect the development of the microstructure essentially.

- Similar results are observed at reentrant corners. In both cases a phase consisting of the softer material develops in a vicinity of a point with a stress singularity.

This thesis is organised as follows:

In **chapter 1** the Cahn-Larché equations are derived. The mathematical model coincides basically with the material model in [68, 84], however, it is expanded by a viscosity term. We realise a mathematical rigorous derivation of the Cahn-Larché system by using the concept of overlapping continua. In order to make the material model thermodynamical consistent Lagrangian multipliers are used. Finally, the

general phase separation model taking stress effects into account is applied on solder materials. We use the quantitative approach by Dreyer and Müller [33], in order to formulate the dependence of the material parameters from the concentration.

In **chapter 2** the existence of weak solutions of the Cahn-Larché system with concentration dependent mobility, elasticity and viscosity is proved. First, assumptions are formulated, which guarantee the existence of a solution. Moreover, we show that these assumptions are valid for practical applications described in chapter 1. The used function spaces as well as different types of weak formulations are introduced. The existence proof uses the flow gradient structure of the problem in order to minimise the energy and maximise the dissipation. We generalise the approach from [49] in a way, that for concentration dependent mobility and viscosity existence of a solution can be proved. The viscous term provides more regularity of the solution with respect to time, which is a useful result for the numerical simulations.

In the following parts, we deal with the numerical simulation of phase separation under elastic loadings. In general a finite element discretisation with respect to space and an implicit time discretisation is applied.

In **chapter 3** we introduce numerical basics. Here we formulate the different trial spaces, which are used to approximate a solution of the Cahn-Larché system. Moreover, we present basic properties of the Clement operator from [26], which are necessary in the following chapters. Since the Cahn-Larché equations state a time dependent problem, we have to analyse some preprocessing tasks. The initial data are projected onto the trial space by a $L_2(\Omega)$-projection and the corresponding initial displacement must be computed.

In **chapter 4** new types of Faedo-Galerkin methods for the Cahn-Larché system are studied, which are stabilised by introducing artificial friction. In the first method artificial friction is involved by the dynamical variable $\dot{c}$, where in the second method artificial friction is introduced by driving forces. Due to the flow gradient structure of the problem, it is possible to show that both methods are equivalent. For both methods existence and uniqueness of a discrete solution is proved. Furthermore we show the convergence of discrete solutions to a solution of the non-viscous problem.

In **chapter 5** we investigate an operator-splitting method in order to stabilise the Faedo-Galerkin scheme. This method splits the Gibbs free energy density additively into a convex and a concave function. The concave part of the Gibbs free energy density is discretised explicitly, because it creates the instability. In contrast to this, the convex part is handled implicitly, because it belongs to the stable state of the system. For this method existence and uniqueness of a discrete solution is proved as well. The chapter ends with a convergence proof of discrete solutions to a solution of the continuous problem.

In **chapter 6** various numerical simulations are presented. First of all we test the above explained method for the Cahn-Hilliard equation neglecting elastic effects.

Furthermore, we perform simulations for the Cahn-Larché system with constant and concentration dependent elasticity tensor. These simulations are compared and it is shown that the model with concentration dependent elasticity tensor fits to the experiment qualitatively very well. Finally, numerical simulations are presented, which show the influence of changing boundary conditions and reentrant corners on the development of the microstructure.

Chapter 7 contains the conclusion and a summary of the results following from this thesis. We also formulate open problems, which are related to the problems discussed in this thesis.

Chapter 1

Modelling of phase separation including stress effects

We consider a binary alloy, e.g. a Sn-Pb or a Sn-Ag system, which is modelled as a mixture of two different components. In order to describe the spinodal decomposition of the mixture we use the concept of overlapping continua [76, 97] and derive a diffusive phase interface model taking into account stress effects similar to [19, 62, 68]. This leads to the well known Cahn-Larché system. The general Cahn-Larché system is adapted to eutectic solder by formulating appropriate constitutive equations, which are a modification of those from [31, 32, 33, 34].

The main goal of this chapter is the mathematical rigorous derivation of the Cahn-Larché system under consideration of external mechanical boundary loadings. Furthermore, we present a thermodynamical framework for this model of spinodal decomposition, which consists of the evaluation of the general entropy principle by a Lagrangian multiplier technique. Finally, sufficiently exact material parameters for quantitative significant numerical simulations of the coarsening process are proposed.

This chapter is arranged in the following way: A mathematical rigorous derivation of the Cahn-Larché model requires the introduction of all kinematic quantities of the mixture. Due to this fact, in section 1.1, first the motion of each component is introduced and then the motion of the mixture is described by using a mass averaging technique.

In the diffusive phase interface model the mass concentration described within the reference configuration is used as a phase field variable. In section 1.2 the corresponding diffusion equation is derived from the balance of mass for each component and from the balance of mass for the whole mixture. Furthermore, in section 1.2 the balance of linear momentum for the mixture is derived, additionally the balance of energy and entropy of the mixture are observed. The derivation of the field equations bases on the Reynolds transport theorem see [55, 76], which in general is formulated within the actual configuration. The transformation of fields from the

actual configuration into the reference configuration is rigorously done by applying the Piola transformation formulated in [24]. Due to this transformation a unique relation between the Eulerian (spatial) and Lagrangian (material) description of a field is observed.

In [56] a thermodynamical framework for the Cahn-Larché system is developed by using the method of microforces introduced by Fried, Gurtin [46, 47] and Gurtin [57]. In section 1.3 we show an alternative method for evaluating the general entropy principle, presented in [74, 75, 76] by applying a Lagrange multiplier technique developed by Liu [71]. The exploration of the entropy principle leads to restrictions on the constitutive equations. Finally, in section 1.3 we give the formulation of constitutive equations for an alloy satisfying the second law of thermodynamic.

The methods for deriving constitutive equations in [31, 32, 33, 34] are expanded by formulating a new shape function in order to get bounded constitutive equations for the material parameters. Similar as in [31, 32, 33, 34] we take the material data for the Gibbs free energy density from MTData report [73]. In [73] there are two Gibbs free energy densities for each phase respectively, but the Cahn-Larché system needs one Gibbs free energy density for both phases. We present an interpolation of the material data in order to fit the Gibbs free energy density, such that it is appropriate for efficient numerical simulations.

1.1 Kinematic basics

The binary alloy occupies at initial time $t = 0$ a spatial domain $\Omega \subset \mathbb{R}^d$ with an outer normal vector $\boldsymbol{n}$, where the space dimensions $d = 2, 3$ are observed. The domain $\Omega \subset \mathbb{R}^d$ is used as reference configuration of the solder joint and $\boldsymbol{x} \in \Omega$ denotes the material coordinate in the reference configuration. We describe the phase separation process in a finite time interval $(0, T)$ and introduce the time space cylinder $\Omega_T := (0, T) \times \Omega$, furthermore we denote its cylindric shell by $\Gamma_T := (0, T) \times \partial\Omega$.

With each component of the mixture we identify an index k and in case of a binary mixture obviously holds $1 \leq k \leq 2$. In the beginning of the separation process only one homogeneous phase exists. This observation gives rise to the assumption that not only the mixture, but also all different components occupy the whole reference domain $\Omega \subset \mathbb{R}^d$. Thus the motion of a component k is given by a sufficiently smooth vector field

$$\boldsymbol{\varphi}_k : \Omega_T \longrightarrow \mathbb{R}^d,$$

which for fixed time is injective, orientation preserving and satisfies the condition $\boldsymbol{\varphi}_k(0, \boldsymbol{x}) = \boldsymbol{x}$. Naturally, the velocity of component k in material description is

calculated by the smooth vector field

$$\boldsymbol{v}_k : \Omega_T \longrightarrow \mathbb{R}^d, \qquad \boldsymbol{v}_k(t,\boldsymbol{x}) := \frac{\partial}{\partial t}\boldsymbol{\varphi}_k(t,\boldsymbol{x}). \tag{1.1}$$

The derivation of all field equations, like mass, linear momentum, energy and entropy, occurs in the actual configuration. Due to this fact the actual configuration of component k at time $t \in (0,T)$ is defined by $\Omega_{t,k}^{\varphi} := \boldsymbol{\varphi}_k(t,\Omega)$. During spinodal decomposition of the binary alloy two phases develop. For example, in a Sn-Pb system a Sn-rich and a Pb-rich phase are observed, but both components appear in both phases. This observation gives rise to the assumption that the ranges of both motions are equal. Consequently this assumption leads to $\Omega_{t,1}^{\varphi} = \Omega_{t,2}^{\varphi} =: \Omega_t^{\varphi}$. We denote Ω_t^{φ} as the actual configuration of the mixture and $\boldsymbol{y} \in \Omega_t^{\varphi}$ as the spatial coordinate in the actual configuration. Appropriate to the time space cylinder we get a non cylindric time space domain defined by $\Omega_T^{\varphi} := \{(t,\boldsymbol{y}) : t \in (0,T), \boldsymbol{y} \in \Omega_t^{\varphi}\}$. In the spatial description the velocity of the component k is a smooth vector field defined by

$$\boldsymbol{v}_k^{\varphi} : \Omega_T^{\varphi} \longrightarrow \mathbb{R}^d, \qquad \boldsymbol{v}_k^{\varphi}(t,\boldsymbol{y}) := \boldsymbol{v}_k(t,\boldsymbol{x}) \ : \ \boldsymbol{y} = \boldsymbol{\varphi}_k(t,\boldsymbol{x}). \tag{1.2}$$

In order to apply a mass averaging technique, we have to introduce the mass density of component k, which is assumed to be a strict positive and sufficiently smooth spatial field

$$\rho_k^{\varphi} : \Omega_T^{\varphi} \longrightarrow \mathbb{R}^+.$$

Due to the fact that mass is an additive quantity the mass density of the mixture is a strict positive and smooth spatial field given by

$$\rho^{\varphi} : \Omega_T^{\varphi} \longrightarrow \mathbb{R}^+, \qquad \rho^{\varphi}(t,\boldsymbol{y}) := \sum_{k=1}^{2} \rho_k^{\varphi}(t,\boldsymbol{y}). \tag{1.3}$$

As phase field variable we use the concentration of a component k, which represents the percentage amount of component k within the mixture. Moreover, the concentration is needed for averaging quantities of the mixture. In the actual configuration the concentration is a smooth scalar field introduced by

$$c_k^{\varphi} : \Omega_T^{\varphi} \longrightarrow [0,1], \qquad c_k^{\varphi}(t,\boldsymbol{y}) := \frac{\rho_k^{\varphi}(t,\boldsymbol{y})}{\rho^{\varphi}(t,\boldsymbol{y})}. \tag{1.4}$$

We remark that c_k^{φ} is well defined due to the fact that ρ^{φ} is strict positive. Obviously, the concentrations satisfy the condition $c_1^{\varphi} + c_2^{\varphi} = 1$. In particular, the mean velocity of the mixture is defined by averaging the velocities of all continua with respect to the distribution of mass

$$\boldsymbol{v}^{\varphi} : \Omega_T^{\varphi} \longrightarrow \mathbb{R}^d, \qquad \boldsymbol{v}^{\varphi}(t,\boldsymbol{y}) := \sum_{k=1}^{2} c_k^{\varphi}(t,\boldsymbol{y}) \boldsymbol{v}_k^{\varphi}(t,\boldsymbol{y}). \tag{1.5}$$

We use this definition to introduce the mass averaged motion of the mixture by solving the following ordinary differential equation:

$$\begin{aligned} &\boldsymbol{\varphi} : \Omega_T \longrightarrow \mathbb{R}^d, \\ &\frac{\partial}{\partial t}\boldsymbol{\varphi} = \boldsymbol{v}^\varphi(t, \boldsymbol{\varphi}) \quad \text{with} \quad \boldsymbol{\varphi}(0, \boldsymbol{x}) = \boldsymbol{x}, \quad \text{for all } \boldsymbol{x} \in \Omega. \end{aligned} \tag{1.6}$$

The smoothness of ρ_k^φ and $\boldsymbol{v}_k^\varphi$ implies the smoothness of $\boldsymbol{v}^\varphi$, in fact we have Lipschitz continuity for $\boldsymbol{v}^\varphi$ on the bounded time space cylinder Ω_T. By applying the Picard-Lindelöf theorem, see [101], we deduce for all $\boldsymbol{x} \in \Omega$ a unique solution of (1.6). The smoothness of $\boldsymbol{v}^\varphi$ leads to the smoothness of $\boldsymbol{\varphi}$ with respect to $t \in (0, T)$ and $\boldsymbol{x} \in \Omega$. Clearly, the mass averaged velocity in the reference configuration follows from (1.6) by

$$\boldsymbol{v} : \Omega_T \longrightarrow \mathbb{R}^d, \qquad \boldsymbol{v}(t, \boldsymbol{x}) := \frac{\partial}{\partial t}\boldsymbol{\varphi}(t, \boldsymbol{x}). \tag{1.7}$$

1.1.1 Reynolds transport theorem

The evolution of a spatial field is basically described by the Reynolds transport theorem. In case of a scalar field, like mass density, the Reynolds transport theorem is the following:

Theorem 1.1. *Let $\phi^\varphi : \Omega_T^\varphi \to \mathbb{R}$ be a smooth scalar field in the actual configuration. Furthermore, let $\boldsymbol{v}^\varphi : \Omega_T^\varphi \to \mathbb{R}^d$ be the corresponding smooth spatial velocity and let $\hat{\phi}^\varphi : \Omega_T^\varphi \to \mathbb{R}$ be a volume source of this field also in the actual configuration. Then for any time $t \in (0, T)$ and any part $\mathscr{P}_t^\varphi \subset \Omega_t^\varphi$ holds*

$$\frac{d}{dt}\int_{\mathscr{P}_t^\varphi} \phi^\varphi \, d\boldsymbol{y} = \int_{\mathscr{P}_t^\varphi} \phi^{\varphi\prime} + \operatorname{div}_{\boldsymbol{y}}(\phi^\varphi \boldsymbol{v}^\varphi) \, d\boldsymbol{y} = \int_{\mathscr{P}_t^\varphi} \hat{\phi}^\varphi \, d\boldsymbol{y}.$$

In fact, this relation holds for all parts $\mathscr{P}_t^\varphi \subset \Omega_t^\varphi$, then we have almost everywhere

$$\phi^{\varphi\prime} + \operatorname{div}_{\boldsymbol{y}}(\phi^\varphi \boldsymbol{v}^\varphi) = \hat{\phi}^\varphi.$$

Proof. The proof basically uses transformation of integrals. For details see Gurtin [55, page 78]. □

In case of a vector field, like linear momentum, the Reynolds transport theorem is the following:

Theorem 1.2. *Let $\boldsymbol{\phi}^\varphi : \Omega_T^\varphi \to \mathbb{R}^d$ be a smooth vector field in the actual configuration. Furthermore, let $\boldsymbol{v}^\varphi : \Omega_T^\varphi \to \mathbb{R}^d$ be the corresponding smooth spatial velocity*

and let $\hat{\boldsymbol{\phi}}^{\varphi} : \Omega_T^{\varphi} \to \mathbb{R}^d$ *be a volume source of this vector field also in the actual configuration. Then for any time* $t \in (0,T)$ *and for any part* $\mathscr{P}_t^{\varphi} \subset \Omega_t^{\varphi}$ *holds*

$$\frac{d}{dt}\int_{\mathscr{P}_t^{\varphi}} \boldsymbol{\phi}^{\varphi}\, d\boldsymbol{y} = \int_{\mathscr{P}_t^{\varphi}} \boldsymbol{\phi}^{\varphi\prime} + \operatorname{div}_{\boldsymbol{y}}(\boldsymbol{\phi}^{\varphi}\boldsymbol{v}^{\varphi T})\, d\boldsymbol{y} = \int_{\mathscr{P}_t^{\varphi}} \hat{\boldsymbol{\phi}}^{\varphi}\, d\boldsymbol{y}.$$

In fact, this relation holds for all parts $\mathscr{P}_t^{\varphi} \subset \Omega_t^{\varphi}$*, then we have almost everywhere*

$$\boldsymbol{\phi}^{\varphi\prime} + \operatorname{div}_{\boldsymbol{y}}(\boldsymbol{\phi}^{\varphi}\boldsymbol{v}^{\varphi T}) = \hat{\boldsymbol{\phi}}^{\varphi}.$$

Proof. The proof is similar to Gurtin [55, page 78]. □

1.1.2 Piola transformation

In order to agree with the notation in classical continuum mechanics we introduce the deformation gradient of the mass averaged motion by

$$\boldsymbol{F} : \Omega_T \longrightarrow \mathbb{R}^{d\times d}, \qquad \boldsymbol{F}(t,\boldsymbol{x}) := \mathrm{D}_{\boldsymbol{x}}\boldsymbol{\varphi}(t,\boldsymbol{x}).$$

Furthermore, we have to show that at least for small strains the mass averaged motion is orientation preserving. From [55] we take the derivative of the determinant and exploit a Taylor expansion in order to follow

$$\begin{aligned}\det(\boldsymbol{F}(t,\boldsymbol{x})) &= \det(\boldsymbol{F}(0,\boldsymbol{x})) + \mathrm{D}_{\boldsymbol{A}}\det(\boldsymbol{F}(0,\boldsymbol{x}))[\boldsymbol{F}(t,\boldsymbol{x}) - \boldsymbol{F}(0,\boldsymbol{x})] \\ &\quad + \mathcal{O}(\|\boldsymbol{F}(t,\boldsymbol{x}) - \boldsymbol{F}(0,\boldsymbol{x})\|) \\ &= 1 + \operatorname{tr}(\boldsymbol{F}(t,\boldsymbol{x}) - \boldsymbol{F}(0,\boldsymbol{x})) + \mathcal{O}(\|\boldsymbol{F}(t,\boldsymbol{x}) - \boldsymbol{F}(0,\boldsymbol{x})\|).\end{aligned}$$

For small strain holds $\det(\boldsymbol{F}(t,\boldsymbol{x})) > 0$ and $\boldsymbol{\varphi}$ is a motion in the sense of [24, 55].

The Piola transformation is established in order to define the corresponding field in the reference configuration of a surface dependent field, like the diffusive flux or stress tensor. The Piola transformation basically uses transformation of surface integrals. Due to this fact we introduce the cofactor matrix, which is defined in Ciarlet [24, page 4].

Definition 1.3. Let $\boldsymbol{A} \in \mathrm{GL}(\mathbb{R})$ be an invertible matrix, then the cofactor matrix is defined by

$$\operatorname{Cof}(\boldsymbol{A}) := \det(\boldsymbol{A})\boldsymbol{A}^{-T}$$

The first version of the Piola transformation is taken from Ciarlet [24, page 53] and defined for vector fields.

Definition 1.4 (Piola transformation for vector fields). Let $\boldsymbol{\phi}^{\varphi} : \Omega_T^{\varphi} \to \mathbb{R}^d$ be a smooth spatial field in the actual configuration and let $\boldsymbol{\varphi} : \Omega_T \to \mathbb{R}^d$ be the mass averaged deformation with the corresponding deformation gradient $\boldsymbol{F} : \Omega_T \longrightarrow \mathbb{R}^{d\times d}$. Then the Piola transformation is defined by

$$\begin{aligned}&\boldsymbol{P} : \mathbb{R}^d \longrightarrow \mathbb{R}^d\\ &\boldsymbol{\phi}(t,\boldsymbol{x}) := (\boldsymbol{P}\boldsymbol{\phi}^{\varphi})(t,\boldsymbol{x}) := \operatorname{Cof}(\boldsymbol{F}^T(t,\boldsymbol{x}))\boldsymbol{\phi}^{\varphi}(t,\boldsymbol{\varphi}(t,\boldsymbol{x})).\end{aligned}$$

The main interest of the Piola transformation is that it yields a simple relation between the divergence of spatial and material fields and the desired relation between corresponding surface integrals.

Lemma 1.5. *The material vector field $\boldsymbol{\phi} = \boldsymbol{P}\boldsymbol{\phi}^{\varphi}$ of a sufficiently smooth spatial vector field $\boldsymbol{\phi}^{\varphi}$ satisfies under consideration of $\mathscr{P}_t^{\varphi} := \boldsymbol{\varphi}(t,\mathscr{P})$ with $\mathscr{P} \subset \Omega$:*

(1) $\operatorname{div}_{\boldsymbol{x}}(\boldsymbol{\phi}) = \det(\boldsymbol{F}) \operatorname{div}_{\boldsymbol{y}}(\boldsymbol{\phi}^{\varphi})$,

(2) $\displaystyle\int_{\partial\mathscr{P}_t^{\varphi}} \boldsymbol{\phi}^{\varphi}\cdot\boldsymbol{n}^{\varphi}\, d\boldsymbol{a}_{\boldsymbol{y}} = \int_{\partial\mathscr{P}} \boldsymbol{\phi}\cdot\boldsymbol{n}\, d\boldsymbol{a}_{\boldsymbol{x}}.$

Proof. For the proof the Piola identity and transformation of surface integrals are used, see [24, page 39, 53]. □

The second version of the Piola transformation is used to establish material tensor fields.

Definition 1.6 (Piola transformation for tensor fields). Let $\boldsymbol{T}^{\varphi} : \Omega_T^{\varphi} \to \mathbb{R}^{d\times d}$ be a smooth spatial tensor field and let $\boldsymbol{\varphi} : \Omega_T \to \mathbb{R}^d$ be the mass averaged deformation, with the corresponding deformation gradient. The Piola transformation for tensor valued fields is given by

$$\begin{aligned}&\boldsymbol{P} : \mathbb{R}^{d\times d} \longrightarrow \mathbb{R}^{d\times d},\\ &\boldsymbol{T}(t,\boldsymbol{x}) := (\boldsymbol{P}\boldsymbol{T}^{\varphi})(t,\boldsymbol{x}) := \boldsymbol{T}^{\varphi}(t,\boldsymbol{\varphi}(t,\boldsymbol{x}))\operatorname{Cof}(\boldsymbol{F}(t,\boldsymbol{x})).\end{aligned}$$

The similar relation between the divergence of spatial and material fields and the desired relation between corresponding surface integrals is satisfied.

Lemma 1.7. *The material tensor field $\boldsymbol{T} = (\boldsymbol{P}\boldsymbol{T}^{\varphi})$ of a sufficiently smooth spatial tensor field $\boldsymbol{T}^{\varphi}$ satisfies under consideration of $\mathscr{P}_t^{\varphi} := \boldsymbol{\varphi}(t,\mathscr{P})$ with $\mathscr{P} \subset \Omega$:*

(1) $\operatorname{div}_{\boldsymbol{x}}(\boldsymbol{T}) = \det(\boldsymbol{F}) \operatorname{div}_{\boldsymbol{y}}(\boldsymbol{T}^{\varphi})$,

(2) $\displaystyle\int_{\partial\mathscr{P}_t^{\varphi}} \boldsymbol{T}^{\varphi}\boldsymbol{n}^{\varphi}\, d\boldsymbol{a}_{\boldsymbol{y}} = \int_{\partial\mathscr{P}} \boldsymbol{T}\boldsymbol{n}\, d\boldsymbol{a}_{\boldsymbol{x}}.$

Proof. This proof also uses the Piola identity and transformation of surface integrals, see [24, page 39]. □

Finally the mass averaged deformation of the mixture is calculated by a smooth vector field

$$\boldsymbol{u} : \Omega_T \longrightarrow \mathbb{R}^d, \qquad \boldsymbol{u}(t, \boldsymbol{x}) := \boldsymbol{\varphi}(t, \boldsymbol{x}) - \boldsymbol{x}. \tag{1.8}$$

It is acceptable to assume that the solder joint undergoes only small deformations, thus we work with the linearised strain tensor defined by

$$\boldsymbol{\varepsilon} : \Omega_T \longrightarrow \mathbb{R}^{d\times d}_{\mathrm{sym}}, \qquad \boldsymbol{\varepsilon}(t, \boldsymbol{x}) := \frac{1}{2}(\mathrm{D}_{\boldsymbol{x}}\boldsymbol{u}(t, \boldsymbol{x}) + (\mathrm{D}_{\boldsymbol{x}}\boldsymbol{u})^T(t, \boldsymbol{x})). \tag{1.9}$$

1.2 Conservation laws

In this section we apply the fundamental physical principle that mass, linear momentum, energy and entropy are conservation quantities. We derive the corresponding balance laws in the actual configuration by applying the Reynolds transport theorem 1.1 respectively 1.2 and refer for detailed calculations to [55, 76]. Our model will later be analysed in the fixed reference configuration, therefore we transform the resulting field equations into the material description by using the Piola transformation definition 1.4 respectively 1.6 and for details we refer to [24, 55].

1.2.1 Balance of mass

We begin our considerations with the mass balance of each component. Experimental observations of spinodal decomposition of a solder alloy lead to the constitutive assumption that no chemical reactions happen within the mixture. Due to this fact no volume source of mass in component k is observed. The application of the Reynolds transport theorem 1.1 on the mass density ρ_k^φ and the velocity $\boldsymbol{v}_k^\varphi$ yields the continuity equation of the component k

$$\rho_k^{\varphi\prime} + \mathrm{div}_{\boldsymbol{y}}(\rho_k^\varphi \boldsymbol{v}_k^\varphi) = 0. \tag{1.10}$$

Similar, the total mass of the mixture is also conserved and the Reynolds transport theorem 1.1 yields for the mass density ρ^φ and the velocity $\boldsymbol{v}^\varphi$ the continuity equation of the alloy

$$\rho^{\varphi\prime} + \mathrm{div}_{\boldsymbol{y}}(\rho^\varphi \boldsymbol{v}^\varphi) = 0. \tag{1.11}$$

Diffusion describes the relative motion of one component with respect to the motion of the mixture. Thus we observe the diffusive flux of component k as a spatial smooth vector field calculated by

$$\boldsymbol{J}_k^\varphi : \Omega_T^\varphi \longrightarrow \mathbb{R}^d, \qquad \boldsymbol{J}_k^\varphi(t, \boldsymbol{y}) := \rho_k^\varphi(t, \boldsymbol{y})(\boldsymbol{v}_k^\varphi(t, \boldsymbol{y}) - \boldsymbol{v}^\varphi(t, \boldsymbol{y})). \tag{1.12}$$

Taking into account (1.3) and (1.5) the diffusive fluxes satisfy the property $\boldsymbol{J}_1^\varphi + \boldsymbol{J}_2^\varphi = \boldsymbol{0}$. Furthermore, we assume that no mass is transfered over the boundary $\Gamma_T^\varphi := \{(t, \boldsymbol{y}) : t \in [0,T], \boldsymbol{y} \in \partial\Omega_t^\varphi\}$, which leads to the boundary condition $\boldsymbol{J}^\varphi \cdot \boldsymbol{n}^\varphi = 0$ on Γ_T^φ. From (1.4) we get $\rho_k^\varphi = \rho^\varphi c_k^\varphi$ and calculate by using (1.10), (1.11) and (1.12) the diffusion equation in the actual configuration

$$\begin{aligned}(\rho^\varphi c_k^\varphi)' + \operatorname{div}_{\boldsymbol{y}}(\rho_k^\varphi \boldsymbol{v}_k^\varphi) &= \rho^\varphi c_k^{\varphi\prime} + \rho^{\varphi\prime} c_k^\varphi + \operatorname{div}_{\boldsymbol{y}}(\rho_k^\varphi \boldsymbol{v}_k^\varphi) \\ &= \rho^\varphi c_k^{\varphi\prime} - \operatorname{div}_{\boldsymbol{y}}(\rho^\varphi \boldsymbol{v}^\varphi) c_k^\varphi + \operatorname{div}_{\boldsymbol{y}}(\rho_k^\varphi \boldsymbol{v}_k^\varphi) \\ &= \rho^\varphi (c_k^{\varphi\prime} + \nabla_{\boldsymbol{y}} c_k^\varphi \cdot \boldsymbol{v}^\varphi) + \operatorname{div}_{\boldsymbol{y}}(\boldsymbol{J}_k^\varphi) = 0. \end{aligned} \tag{1.13}$$

In order to observe this equation in material description we transform the mass density of a component and of the mixture by

$$\begin{aligned} \rho_k : \Omega_T \longrightarrow \mathbb{R}^+, \qquad & \rho_k(t, \boldsymbol{x}) := \rho_k^\varphi(t, \boldsymbol{\varphi}(t, \boldsymbol{x})) \det(\boldsymbol{F}(t, \boldsymbol{x})), \\ \rho : \Omega_T \longrightarrow \mathbb{R}^+, \qquad & \rho(t, \boldsymbol{x}) := \rho^\varphi(t, \boldsymbol{\varphi}(t, \boldsymbol{x})) \det(\boldsymbol{F}(t, \boldsymbol{x})). \end{aligned}$$

This definition is clear due to transformation of volume integrals. The concentration is a specific quantity, which means that it is independent of volume changes. Thus its representation in the reference configuration is given by a reparametrisation

$$c_k : \Omega_T \longrightarrow [0,1], \qquad c_k(t, \boldsymbol{x}) := c_k^\varphi(t, \boldsymbol{\varphi}(t, \boldsymbol{x})).$$

Obviously for the concentrations holds $c_1 + c_2 = 1$. We remark that for the material time derivative of the concentration holds due to the chain rule $\dot{c} = c_k^{\varphi\prime} + \nabla_{\boldsymbol{y}} c_k^\varphi \cdot \boldsymbol{v}^\varphi$. The diffusive flux in material description, which is treated as a constitutive quantity in the following, is defined by the Piola transformation given in definition 1.4

$$\boldsymbol{J}_k : \Omega_T \longrightarrow \mathbb{R}^d, \qquad \boldsymbol{J}_k(t, \boldsymbol{x}) := (\boldsymbol{P}\boldsymbol{J}_k^\varphi)(t, \boldsymbol{x}).$$

The linearity of the Piola transformation yields $\boldsymbol{J}_1 + \boldsymbol{J}_2 = 0$. The no flux boundary condition takes the form $\boldsymbol{J} \cdot \boldsymbol{n} = 0$ on Γ_T due to lemma 1.5. From these considerations and from (1.13) we deduce the diffusion equation in material description

$$\rho \dot{c}_k + \operatorname{div}_{\boldsymbol{x}}(\boldsymbol{J}_k) = 0.$$

Finally, we assume that ρ is constant. This assumption is motivated by the fact that in the beginning of the phase separation process only a homogeneous phase exists. We choose $\rho = \overline{\rho}_1 c_{eut} + \overline{\rho}_2(1 - c_{eut})$, where $\overline{\rho}_k$ are the mass densities of the pure constituents and c_{eut} denotes the eutectic concentration of the alloy taken from the phase diagram, which is outlined in fig. 2. In a binary alloy we can simplify the notation by denoting $c := c_1$ and $\boldsymbol{J} := \boldsymbol{J}_1$, because $c_2 = 1 - c$ and $\boldsymbol{J}_2 = -\boldsymbol{J}$. The

initial mass distribution is described by a sufficiently smooth mapping $c_0 : \Omega \longrightarrow [0,1]$ and we get the first field equation

$$\rho\dot{c} + \operatorname{div}_{\boldsymbol{x}}(\boldsymbol{J}) = 0 \qquad \text{in } \Omega_T, \tag{1.14}$$

$$\boldsymbol{J} \cdot \boldsymbol{n} = 0 \qquad \text{on } \Gamma_T, \tag{1.15}$$

$$c(0, \boldsymbol{x}) = c_0(\boldsymbol{x}) \qquad \text{in } \Omega. \tag{1.16}$$

In this field equation c is the unknown phase field variable and $\boldsymbol{J}$ is a constitutive quantity, which must be derived from thermodynamical considerations.

A further conclusion from the principle of mass conservation leads to a constraint on the mass concentration c. By using the diffusion equation (1.14) and the Gauß theorem we calculate

$$\frac{d}{dt}\rho \int_\Omega c \, d\boldsymbol{x} = -\int_\Omega \operatorname{div}_{\boldsymbol{x}}(\boldsymbol{J}) \, d\boldsymbol{x} = -\int_{\partial\Omega} \boldsymbol{J} \cdot \boldsymbol{n} \, d\boldsymbol{a}_{\boldsymbol{x}} = 0.$$

Due to this calculation the mass concentration c has to satisfy at each time $t \in (0,T)$ the constraint

$$\int_\Omega c \, d\boldsymbol{x} = m = \text{const.} \tag{1.17}$$

1.2.2 Conservation of linear momentum

In the second part of this section we consider the conservation of linear momentum in order to derive the equation of motion of the mixture. The linear momentum density of the mixture in the actual configuration is defined by $\rho^\varphi \boldsymbol{v}^\varphi$. Experimental observations show that only the linear momentum balance of the mixture must be considered, the influence of several continua on the motion is formulated by constitutive equations. For completeness we remark that relations between the linear momentum of several components and of the mixture are calculated in [72, 76].

The change of linear momentum in a body is equal to the force acting on it. In general this force is divided into a surface and a volume force. In our model we neglect the action of a volume force like an electrostatic force and assume that only a surface force appears. The surface force is given by a sufficiently smooth density on the Neumann boundary part $\Gamma_T^{\varphi,N} \subset \Gamma_T^\varphi$,

$$\boldsymbol{g}^\varphi : \Gamma_T^{\varphi,N} \longrightarrow \mathbb{R}^d.$$

Moreover, we assume that the alloy is hard clamped on the remaining Dirichlet boundary $\Gamma_T^{\varphi,D} := \Gamma_T^\varphi \setminus \Gamma_T^{\varphi,N}$. From the Cauchy theorem [24, page 62] we get the existence and uniqueness of a sufficiently smooth and symmetric stress tensor

$$\boldsymbol{S}^\varphi : \Omega_T^\varphi \longrightarrow \mathbb{R}^{d\times d}_{sym},$$

such that on the Neumann boundary holds $\boldsymbol{S}^{\varphi}\boldsymbol{n}^{\varphi} = \boldsymbol{g}^{\varphi}$. Applying the Reynolds transport theorem 1.2 onto the linear momentum density $\rho^{\varphi}\boldsymbol{v}^{\varphi}$ and taking into account the Cauchy stress tensor, we get the well known balance of linear momentum

$$(\rho^{\varphi}\boldsymbol{v}^{\varphi})' + \operatorname{div}_{\boldsymbol{y}}(\rho^{\varphi}\boldsymbol{v}^{\varphi}\boldsymbol{v}^{\varphi T} - \boldsymbol{S}^{\varphi}) = \boldsymbol{0}. \tag{1.18}$$

In view of the continuity equation (1.11) we calculate from (1.18) the equation of motion in the actual configuration

$$\begin{aligned}\rho^{\varphi\prime}\boldsymbol{v}^{\varphi} + \rho^{\varphi}\boldsymbol{v}^{\varphi\prime} + \operatorname{div}_{\boldsymbol{y}}(\rho^{\varphi}\boldsymbol{v}^{\varphi}\boldsymbol{v}^{\varphi T} - \boldsymbol{S}^{\varphi}) \\ = \rho^{\varphi}\boldsymbol{v}^{\varphi\prime} - \operatorname{div}_{\boldsymbol{y}}(\rho^{\varphi}\boldsymbol{v}^{\varphi})\boldsymbol{v}^{\varphi} + \operatorname{div}_{\boldsymbol{y}}(\rho^{\varphi}\boldsymbol{v}^{\varphi}\boldsymbol{v}^{\varphi T} - \boldsymbol{S}^{\varphi}) \\ = \rho^{\varphi}(\boldsymbol{v}^{\varphi\prime} + \mathrm{D}_{\boldsymbol{y}}(\boldsymbol{v}^{\varphi})\boldsymbol{v}^{\varphi}) - \operatorname{div}_{\boldsymbol{y}}(\boldsymbol{S}^{\varphi}) = \boldsymbol{0}.\end{aligned} \tag{1.19}$$

In order to get the equation of motion in material description the Cauchy stress tensor must be transformed into the reference configuration. This is done by the Piola transformation given in definition 1.6 and we get analogously to [24] the 1. Piola-Kirchoff stress tensor

$$\boldsymbol{S} : \Omega_T \longrightarrow \mathbb{R}^{d\times d}, \qquad \boldsymbol{S}(t,\boldsymbol{x}) := (\boldsymbol{P}\boldsymbol{S}^{\varphi})(t,\boldsymbol{x}).$$

The transformation of surface integrals leads corresponding to [24] to a formulation of the surface forces in material description

$$\boldsymbol{g} : \Gamma_T^N \longrightarrow \mathbb{R}^d, \quad \boldsymbol{g}(t,\boldsymbol{x}) := \det(\boldsymbol{F}(t,\boldsymbol{x}))|\boldsymbol{F}(t,\boldsymbol{x})^{-T}\boldsymbol{n}(t,\boldsymbol{x})|\boldsymbol{g}^{\varphi}(t,\boldsymbol{\varphi}(t,\boldsymbol{x}))$$

and it holds $\boldsymbol{S}\boldsymbol{n} = \boldsymbol{g}$ on the corresponding Neumann boundary Γ_T^N due to lemma 1.7. Again taking into account the material time derivative $\dot{\boldsymbol{v}} = \boldsymbol{v}^{\varphi\prime} + \mathrm{D}_{\boldsymbol{y}}(\boldsymbol{v}^{\varphi})\boldsymbol{v}^{\varphi}$, we calculate from (1.19) and in view of lemma 1.7 the equation of motion

$$\rho\dot{\boldsymbol{v}} - \operatorname{div}_{\boldsymbol{x}}(\boldsymbol{S}) = \boldsymbol{0}.$$

Note, that in general the 1. Piola-Kirchoff stress tensor is not symmetric, but in continuum mechanics it is desirable to work with a symmetric stress tensor. Thus we introduce from [24] the 2. Piola-Kirchoff stress tensor by

$$\boldsymbol{\sigma} : \Omega_T \longrightarrow \mathbb{R}^{d\times d}_{sym}, \qquad \boldsymbol{\sigma}(t,\boldsymbol{x}) := \boldsymbol{F}^{-1}(t,\boldsymbol{x})\boldsymbol{S}(t,\boldsymbol{x}),$$

which in the following is treated as a constitutive quantity and must be calculated from thermodynamical observations. The initial deformation as well as the initial velocity is described by a sufficiently smooth mapping $\boldsymbol{u}_0 : \Omega \longrightarrow \mathbb{R}^d$ and $\boldsymbol{v}_0 : \Omega \longrightarrow \mathbb{R}^d$. Moreover, we derive in view of (1.7) for the acceleration $\ddot{\boldsymbol{u}} := \frac{\partial^2}{\partial t^2}\boldsymbol{u} = \dot{\boldsymbol{v}}$. Due

to the fact that the solder joint undergoes only small deformations, we assume that the strain is very small and follow the second field equation of our model

$$\rho\ddot{\boldsymbol{u}} - \operatorname{div}_{\boldsymbol{x}}(\boldsymbol{\sigma}) = \boldsymbol{0} \qquad \text{in } \Omega_T, \tag{1.20}$$

$$\boldsymbol{u} = \boldsymbol{0} \qquad \text{on } \Gamma_T^D, \tag{1.21}$$

$$\boldsymbol{\sigma}\boldsymbol{n} = \boldsymbol{g} \qquad \text{on } \Gamma_T^N, \tag{1.22}$$

$$\boldsymbol{u}(0,\boldsymbol{x}) = \boldsymbol{u}_0(\boldsymbol{x}) \qquad \text{in } \Omega, \tag{1.23}$$

$$\dot{\boldsymbol{u}}(0,\boldsymbol{x}) = \boldsymbol{v}_0(\boldsymbol{x}) \qquad \text{in } \Omega. \tag{1.24}$$

1.2.3 Energy balance

We continue our considerations with the energy conservation law of the solder alloy. Relations between the energy balance of several continua and of the mixture are formulated in [14, 72, 76]. The internal energy of the solder joint is represented by a sufficiently smooth spatial specific energy density

$$\epsilon^\varphi : \Omega_T^\varphi \longrightarrow \mathbb{R}.$$

The total energy density consisting of the internal and kinematic energy density is given by $\rho^\varphi(\epsilon^\varphi + \frac{1}{2}(\boldsymbol{v}^\varphi)^2)$. The change of energy is equal to the supply of energy, which consists of a surface flux and a volume energy source.

We assume within our model that no volume source appears, because as mentioned above we observe no chemical reactions and do not model the action of a volume force like an electrostatic force.

Moreover, the spinodal decomposition is assumed to be an isothermal process. We have to point out that this is a very strong restriction on the model, but it reduces the computational complexity essentially. Consequently no heat flux occurs and we work with a constant temperature θ. From [76] we deduce the energy balance equation by applying the Reynolds transport theorem 1.1 onto the energy density

$$\left(\rho^\varphi\left(\epsilon^\varphi + \frac{1}{2}(\boldsymbol{v}^\varphi)^2\right)\right)' + \operatorname{div}_{\boldsymbol{y}}\left(\rho^\varphi\left(\epsilon^\varphi + \frac{1}{2}(\boldsymbol{v}^\varphi)^2\right)\boldsymbol{v}^\varphi - \boldsymbol{S}^\varphi\boldsymbol{v}^\varphi\right) = 0.$$

In order to transform the energy balance equation into the reference configuration we take into account the continuity equation (1.11), the equation of motion (1.19) and calculate

$$\begin{aligned}&\left(\rho^\varphi\left(\epsilon^\varphi + \frac{1}{2}(\boldsymbol{v}^\varphi)^2\right)\right)' + \operatorname{div}_{\boldsymbol{y}}\left(\rho^\varphi\left(\epsilon^\varphi + \frac{1}{2}(\boldsymbol{v}^\varphi)^2\right)\boldsymbol{v}^\varphi - \boldsymbol{S}^\varphi\boldsymbol{v}^\varphi\right)\\ &\quad = \rho^\varphi(\epsilon^{\varphi\prime} + \nabla_{\boldsymbol{y}}\epsilon^\varphi \cdot \boldsymbol{v}^\varphi) - \boldsymbol{S}^\varphi : \mathrm{D}_{\boldsymbol{y}}\boldsymbol{v}^\varphi = 0.\end{aligned} \tag{1.25}$$

The specific internal energy density is independent of volume changes, thus its representation in material description is calculated by a simple reparametrisation

$$\epsilon : \Omega_T \longrightarrow \mathbb{R}, \qquad \epsilon(t, \boldsymbol{x}) := \epsilon^{\varphi}(t, \boldsymbol{\varphi}(t, \boldsymbol{x})).$$

In view of the material time derivative of the specific internal energy density $\dot{\epsilon} = \epsilon^{\varphi\prime} + \nabla_{\boldsymbol{y}} \epsilon^{\varphi} \cdot \boldsymbol{v}^{\varphi}$ we derive the energy balance from (1.25) by taking into account lemma 1.7 and the assumption that only small strains occur

$$\rho \dot{\epsilon} - \boldsymbol{\sigma} : \dot{\boldsymbol{\varepsilon}} = 0. \tag{1.26}$$

1.2.4 Consideration of entropy

This section ends with the observation of the entropy in order to develop relations for the constitutive moduli $\boldsymbol{J}$ and $\boldsymbol{\sigma}$. From [76] we know that the entropy is an auxiliary quantity in material theory. Similar to [76] we consider a specific entropy density introduced by a sufficiently smooth scalar field in the actual configuration

$$\eta^{\varphi} : \Omega_T^{\varphi} \longrightarrow \mathbb{R}.$$

The change of entropy is equal to the supply of entropy given by an entropy flux and an entropy volume source. The entropy flux is denoted by a sufficiently smooth spatial vector field

$$\boldsymbol{\phi}^{\varphi} : \Omega_T^{\varphi} \longrightarrow \mathbb{R}^d.$$

Similar to Müller [76] we introduce a specific non-negative entropy volume source, which has to satisfy the second law of thermodynamic. This source is again given by a sufficiently smooth scalar field

$$\hat{\eta}^{\varphi} : \Omega_T^{\varphi} \longrightarrow \mathbb{R}_0^+.$$

The conservation of entropy is derived from the Reynolds transport theorem 1.1 and we get

$$(\rho^{\varphi} \eta^{\varphi})' + \operatorname{div}_{\boldsymbol{y}}(\rho^{\varphi} \eta^{\varphi} \boldsymbol{v}^{\varphi} + \boldsymbol{\phi}^{\varphi}) = \rho^{\varphi} \hat{\eta}^{\varphi} \geq 0. \tag{1.27}$$

The formulation of the entropy conservation equation in the reference configuration works similar as for all other conservation equations. The specific entropy density is independent of volume changes and thus the material description is defined by a reparametrisation

$$\eta : \Omega_T \longrightarrow \mathbb{R}, \qquad \eta(t, \boldsymbol{x}) := \eta^{\varphi}(t, \boldsymbol{\varphi}(t, \boldsymbol{x})).$$

The entropy flux is transformed by using the Piola transformation given in definition 1.4 and it is also treated as a constitutive quantity in the following

$$\boldsymbol{\phi} : \Omega_T \longrightarrow \mathbb{R}^d, \qquad \boldsymbol{\phi}(t, \boldsymbol{x}) := (\boldsymbol{P}\boldsymbol{\phi})(t, \boldsymbol{x}).$$

The entropy volume source is again a specific quantity and thus it is independent of volume changes. In material description it is given by a reparametrisation

$$\hat{\eta} : \Omega_T \longrightarrow \mathbb{R}_0^+, \qquad \hat{\eta}(t, \boldsymbol{x}) := \hat{\eta}^{\varphi}(t, \boldsymbol{\varphi}(t, \boldsymbol{x})).$$

Taking into account the above considerations using the continuity equation (1.11), applying the material derivative of the specific entropy density $\dot{\eta} = \eta^{\varphi\prime} + \nabla_{\boldsymbol{y}}\eta^{\varphi} \cdot \boldsymbol{v}^{\varphi}$ and lemma 1.5, we get the entropy balance equation in the reference configuration

$$\rho\dot{\eta} + \operatorname{div}_{\boldsymbol{x}}(\boldsymbol{\phi}) = \hat{\eta} \geq 0. \tag{1.28}$$

1.3 Material model

Whenever the properties of a material are investigated the entropy principle is used to impose restrictions on the constitutive relations of the material. In this section we derive the constitutive equations for the diffusive flux $\boldsymbol{J}$ and for the 2. Piola-Kirchoff stress tensor $\boldsymbol{\sigma}$. We have to ensure that the resulting field equations satisfy the second law of thermodynamics, therefore the general entropy principle proposed by Müller [74, 75, 76] is evaluated by using Lagrangian multipliers developed by Liu in [71]. For phase transition problems with conserved order parameters and temperature this is done in [6, 7]. We apply the Lagrangian multiplier technique in order to derive the Cahn-Larché equations with viscous effects in a thermodynamical rigorous way.

A dimensional analysis is done to simplify the mathematical model in order to reduce the computational complexity for numerical simulations. Finally, constitutive equations are formulated for a binary system and outlined for a Sn-Pb alloy as an example.

1.3.1 Evaluation of the entropy inequality

The basic fields in thermodynamics of spinodal decomposition are the concentration $c(t, \boldsymbol{x})$ describing the percentage amount of one component within the mixture, $\nabla_{\boldsymbol{x}} c(t, \boldsymbol{x})$ identifying diffusive phase interfaces and $\dot{c}(t, \boldsymbol{x})$ taking into account viscous effects. Furthermore, the influence of mechanical effects on the spinodal decomposition is described by the velocity $\boldsymbol{v}(t, \boldsymbol{x})$ and the linearised strain $\boldsymbol{\varepsilon}(t, \boldsymbol{x})$. The field

equations are based on the diffusion equation (1.14), the balance of linear momentum (1.20) and the balance of energy (1.26). In order to have enough independent variables second and third derivatives of the concentration field are observed.

From these observations follows that the thermodynamical process of phase separation is described by $\boldsymbol{Y}^T := (c, \boldsymbol{v}^T, (c_{,\boldsymbol{\alpha}})_{1\leq|\boldsymbol{\alpha}|\leq 3}, \dot{c}, \boldsymbol{\varepsilon}^T) \in \mathbb{R}^n$, where $\boldsymbol{\alpha}$ is a multi-index and we use Voigt's notation of the symmetric linearised strain tensor $\boldsymbol{\varepsilon}$. The physical understanding of viscous effects is the key issue for the derivation of stable numerical methods even for the non-viscous case.

The evaluation of the entropy principle for calculating restrictions onto the constitutive equations of a material under consideration is done with the method of Lagrangian multipliers developed by Liu [71].

Lemma 1.8. *Let $\boldsymbol{A} \in \mathbb{R}^{p\times n}$, $\boldsymbol{B} \in \mathbb{R}^p$, $\boldsymbol{\alpha} \in \mathbb{R}^n \setminus \{\boldsymbol{0}\}$ and $\beta \in \mathbb{R}$ be given. Let $\mathscr{S} := \{\boldsymbol{X} \in \mathbb{R}^n : \boldsymbol{A}\boldsymbol{X} + \boldsymbol{B} = \boldsymbol{0}\}$ and assume that $\mathscr{S}$ be not-empty. Then the following statements are equivalent:*

(1) $\boldsymbol{\alpha} \cdot \boldsymbol{X} + \beta \geq 0, \qquad \forall \boldsymbol{X} \in \mathscr{S}.$

(2) There exists $\boldsymbol{\Lambda} \in \mathbb{R}^p \setminus \{\boldsymbol{0}\}$, such that

$$\boldsymbol{\alpha} \cdot \boldsymbol{X} + \beta - \boldsymbol{\Lambda} \cdot (\boldsymbol{A}\boldsymbol{X} + \boldsymbol{B}) \geq 0, \qquad \forall \boldsymbol{X} \in \mathbb{R}^n.$$

(3) There exists $\boldsymbol{\Lambda} \in \mathbb{R}^p \setminus \{\boldsymbol{0}\}$, such that

$$\boldsymbol{\alpha} - \boldsymbol{A}^T\boldsymbol{\Lambda} = 0, \qquad \beta - \boldsymbol{\Lambda} \cdot \boldsymbol{B} \geq 0.$$

Proof. This lemma is proved by Liu [71, section 3]. □

The first step in order to evaluate the entropy principle by using the concept of Lagrangian multipliers is to show that a thermodynamical process $\boldsymbol{Y}$ exists. The field equations for $\boldsymbol{Y}$ result from (1.14), (1.20) and (1.26), when constitutive equations for the diffusive flux $\boldsymbol{J}$, the 2. Piola-Kirchoff stress tensor $\boldsymbol{\sigma}$ and the internal energy density ϵ are formulated. These equations depend on the material under consideration.

We assume that $\boldsymbol{J}$, $\boldsymbol{\sigma}$ and ϵ are real analytic functions depending on the thermodynamical process $\boldsymbol{Y}$, which also is assumed to be real and analytic

$$\boldsymbol{J} = \boldsymbol{J}(\boldsymbol{Y}), \qquad \boldsymbol{\sigma} = \boldsymbol{\sigma}(\boldsymbol{Y}), \qquad \epsilon = \epsilon(\boldsymbol{Y}). \tag{1.29}$$

Inserting (1.29) into the diffusion equation (1.14), into the balance of linear momentum (1.20) and into the balance of energy (1.26), this leads to a first order partial

differential equation system of $m = (d+2)$ equations and $n = |\boldsymbol{Y}|$ unknown functions. This system can be written in the following form, where $\boldsymbol{Y}_0 : \Omega \longrightarrow \mathbb{R}^n$ denotes the real analytic initial condition

$$\begin{aligned}
&\boldsymbol{A}(\boldsymbol{Y})\dot{\boldsymbol{Y}} = \boldsymbol{B}(\boldsymbol{Y}), \qquad \boldsymbol{Y}(0,\boldsymbol{x}) = \boldsymbol{Y}_0(\boldsymbol{x}), \qquad (1.30)\\
&\boldsymbol{A}(\boldsymbol{Y}) := \begin{pmatrix} \rho & \mathbf{0} & 0\cdots\cdots\cdots 0 & 0 & \mathbf{0} \\ \mathbf{0} & \rho\boldsymbol{I} & 0\cdots\cdots\cdots 0 & 0 & \mathbf{0} \\ \rho\frac{\partial\epsilon}{\partial c} & \rho\frac{\partial\epsilon}{\partial\boldsymbol{v}} & \rho\left(\frac{\partial\epsilon}{\partial c,\boldsymbol{\alpha}}\right)_{1\leq|\boldsymbol{\alpha}|\leq 3} & \rho\frac{\partial\epsilon}{\partial\dot{c}} & \rho\frac{\partial\epsilon}{\partial\boldsymbol{\varepsilon}} - \boldsymbol{\sigma} \end{pmatrix} \in \mathbb{R}^{m\times n},\\
&\boldsymbol{B}^T(\boldsymbol{Y}) := \left(-\frac{\partial J_i}{\partial Y_k}\frac{\partial Y_k}{\partial x_i}, \quad -\frac{\partial\sigma_{1,i}}{\partial Y_k}\frac{\partial Y_k}{\partial x_i}, \quad \cdots, \quad -\frac{\partial\sigma_{d,i}}{\partial Y_k}\frac{\partial Y_k}{\partial x_i}, \quad 0\right)^T \in \mathbb{R}^m.
\end{aligned}$$

Similar as in [71] we divide the thermodynamic process $\boldsymbol{Y}$ into $\tilde{\boldsymbol{Y}}^T := (Y_1,\ldots,Y_m) \in \mathbb{R}^m$, which are treated as unknown functions and $\hat{\boldsymbol{Y}}^T := (Y_{m+1},\ldots,Y_n) \in \mathbb{R}^{n-m}$, which are chosen arbitrary, but assumed to be real analytic functions. Moreover, we define $\tilde{\boldsymbol{A}}(\tilde{\boldsymbol{Y}}) := (A_{i,j}(\boldsymbol{Y}))$ with $1 \leq i,j \leq m$. Finally, the $m \times n$ system (1.30) is reduced to a $m \times m$ system in the following way

$$\begin{aligned}
&\tilde{\boldsymbol{A}}(\tilde{\boldsymbol{Y}})\dot{\tilde{\boldsymbol{Y}}} := \tilde{\boldsymbol{B}}(\tilde{\boldsymbol{Y}}), \qquad \tilde{\boldsymbol{Y}}(0,\boldsymbol{x}) = \tilde{\boldsymbol{Y}}_0(\boldsymbol{x}), \qquad (1.31)\\
&\tilde{\boldsymbol{B}}^T(\boldsymbol{Y}) := \left(-\frac{\partial J_i}{\partial Y_k}\frac{\partial Y_k}{\partial x_i}, \quad -\frac{\partial\sigma_{1,i}}{\partial Y_k}\frac{\partial Y_k}{\partial x_i}, \quad \ldots, \quad -\frac{\partial\sigma_{d,i}}{\partial Y_k}\frac{\partial Y_k}{\partial x_i}, \quad -A_{m,k}(\boldsymbol{Y})\hat{Y}_k\right)^T \in \mathbb{R}^m.
\end{aligned}$$

We know from [20] that the internal energy density ϵ contains the surface energy identified with the diffusive phase interfaces. This fact gives rise to the assumption that $\frac{\partial\epsilon}{\partial\nabla_{\boldsymbol{x}}c} \neq \mathbf{0}$. Due to this reason $\tilde{\boldsymbol{A}}^{-1}$ exists and the system (1.31) is formulated in Kowalevskaya normal form

$$\dot{\tilde{\boldsymbol{Y}}} = \tilde{\boldsymbol{A}}^{-1}(\tilde{\boldsymbol{Y}})\tilde{\boldsymbol{B}}(\tilde{\boldsymbol{Y}}), \qquad \tilde{\boldsymbol{Y}}(0,\boldsymbol{x}) = \tilde{\boldsymbol{Y}}_0(\boldsymbol{x}). \qquad (1.32)$$

In order to proof that a thermodynamical process $\boldsymbol{Y}$ of spinodal decomposition exists, we need a existence theorem for first order partial differential equations.

Theorem 1.9 (Cauchy-Kowalevskaya). *Assume that $\boldsymbol{B}_j : \mathbb{R}^d \times \mathbb{R}^m \longrightarrow \mathbb{R}^{m\times d}$ with $1 \leq j \leq d$ and $\boldsymbol{c} : \mathbb{R}^d \times \mathbb{R}^m \longrightarrow \mathbb{R}^m$ are real analytic functions. Then there exists a unique real analytic function $\tilde{\boldsymbol{Y}} : \mathbb{R}\times\mathbb{R}^d \longrightarrow \mathbb{R}^m$ in a neighbourhood of the real analytic initial condition $\tilde{\boldsymbol{Y}}_0 : \mathbb{R}^d \longrightarrow \mathbb{R}^m$ solving the initial value problem*

$$\dot{\tilde{\boldsymbol{Y}}} = \sum_{j=1}^{d} \boldsymbol{B}_j(\boldsymbol{x},\tilde{\boldsymbol{Y}})\nabla_{\boldsymbol{x}}\tilde{\boldsymbol{Y}}_j + \boldsymbol{c}(\boldsymbol{x},\tilde{\boldsymbol{Y}}), \qquad \tilde{\boldsymbol{Y}}(0,\boldsymbol{x}) = \tilde{\boldsymbol{Y}}(\boldsymbol{x})_0.$$

Proof. See [43], page 229. □

From Cauchy-Kowalevskaya theorem 1.9 follows that there exists a unique real analytic solution $\tilde{\boldsymbol{Y}}$ in a neighbourhood of real analytic initial condition $\tilde{\boldsymbol{Y}}_0$ of the partial differential equation (1.32). Due to this fact a thermodynamical process $\boldsymbol{Y}$ exists satisfying (1.30) and the admissible set $\mathscr{S}$ in lemma 1.8 is not empty.

The second step for the evaluation of the entropy principle using Lagrangian multipliers is the formulation of the entropy inequality in terms of the thermodynamical process $\boldsymbol{Y}$. In a supply free body the entropy inequality (1.28) has the special form

$$\rho\dot{\eta} + \operatorname{div}_{\boldsymbol{x}}(\boldsymbol{\phi}) \geq 0. \tag{1.33}$$

In particular, for spinodal decomposition the constitutive equations for the entropy η and for the entropy flux $\boldsymbol{\phi}$ are assumed to depend on the thermodynamical process

$$\eta = \eta(\boldsymbol{Y}), \qquad \boldsymbol{\phi} = \boldsymbol{\phi}(\boldsymbol{Y}). \tag{1.34}$$

We directly calculate from the entropy inequality (1.33) and from the approach (1.34) a version of the entropy inequality corresponding to lemma 1.8

$$\begin{aligned} &\boldsymbol{\alpha}(\boldsymbol{Y}) \cdot \dot{\boldsymbol{Y}} + \beta(\boldsymbol{Y}) \geq 0, \\ &\qquad \boldsymbol{\alpha}^T(\boldsymbol{Y}) = \left(\rho\frac{\partial\eta}{\partial Y_1}, \ldots, \rho\frac{\partial\eta}{\partial Y_n}\right) \in \mathbb{R}^n, \qquad \beta(\boldsymbol{Y}) = \frac{\partial\phi_i}{\partial Y_k}\frac{\partial Y_k}{\partial x_i}. \end{aligned}$$

Obviously $\boldsymbol{\alpha}$ and β satisfy the assumptions of lemma 1.8 and we deduce from Liu's lemma 1.8 the existence of Lagrangian multipliers $\Lambda^c, \Lambda^e \in \mathbb{R}$ and $\boldsymbol{\Lambda}^v \in \mathbb{R}^d$ such that for all thermodynamical processes holds

$$\begin{aligned} \rho\dot{\eta} + \operatorname{div}_{\boldsymbol{x}}(\boldsymbol{\phi}) - \Lambda^c(\rho\dot{c} + \operatorname{div}_{\boldsymbol{x}}(\boldsymbol{J})) - \boldsymbol{\Lambda}^v \cdot (\rho\dot{\boldsymbol{v}} - \operatorname{div}_{\boldsymbol{x}}(\boldsymbol{\sigma})) \\ - \Lambda^e(\rho\dot{\epsilon} - \boldsymbol{\sigma} : \dot{\boldsymbol{\varepsilon}}) \geq 0. \end{aligned} \tag{1.35}$$

We continue our observations by introducing the Helmholtz free energy density in order to calculate the dissipation inequality. The Helmholtz free energy density is defined by a smooth scalar field

$$e : \Omega_T \longrightarrow \mathbb{R}, \qquad e(t, \boldsymbol{x}) = \epsilon(t, \boldsymbol{x}) - \theta\eta(t, \boldsymbol{x}).$$

Note, that in our model the temperature θ is constant, thus for the time derivative of the Helmholtz free energy density holds $\dot{e} = \dot{\epsilon} - \theta\dot{\eta}$ and we calculate form (1.35)

$$\begin{aligned} (\rho - \rho\Lambda^e\theta)\dot{\eta} + \operatorname{div}_{\boldsymbol{x}}(\boldsymbol{\phi}) - \Lambda^c(\rho\dot{c} + \operatorname{div}_{\boldsymbol{x}}(\boldsymbol{J})) - \boldsymbol{\Lambda^v} \cdot (\rho\dot{\boldsymbol{v}} - \operatorname{div}_{\boldsymbol{x}}(\boldsymbol{\sigma})) \\ - \Lambda^e(\rho\dot{e} - \boldsymbol{\sigma} : \dot{\boldsymbol{\varepsilon}}) \geq 0. \end{aligned} \tag{1.36}$$

The entropy principle developed by Müller [75, 74, 76] says that equation (1.36) must hold for all thermodynamical processes, in particular for all velocities $\boldsymbol{v}$. Consequently the inequality is linear with respect to $\dot{\boldsymbol{v}}$ and we observe an isothermal process such that it turns out

$$\Lambda^e = \frac{1}{\theta}, \qquad \boldsymbol{\Lambda}^v = \mathbf{0}.$$

Taking this relations into account and introducing the chemical potential $\mu := -\theta\Lambda^c$ as well as the generalised entropy flux $\tilde{\boldsymbol{\phi}} := (\theta\boldsymbol{\phi} + \mu\boldsymbol{J})$ we derive from (1.36) the dissipation inequality

$$\begin{aligned} \operatorname{div}_{\boldsymbol{x}}(\boldsymbol{\phi}) - \Lambda^c(\rho\dot{c} + \operatorname{div}_{\boldsymbol{x}}(\boldsymbol{J})) - \frac{1}{\theta}(\rho\dot{e} - \boldsymbol{\sigma} : \dot{\boldsymbol{\varepsilon}}) &\geq 0, \\ \rho\dot{e} - \operatorname{div}_{\boldsymbol{x}}(\theta(\boldsymbol{\phi} - \Lambda^c\boldsymbol{J})) + \theta\Lambda^c\rho\dot{c} - \boldsymbol{\sigma} : \dot{\boldsymbol{\varepsilon}} &\leq 0, \\ \rho\dot{e} - \operatorname{div}_{\boldsymbol{x}}(\tilde{\boldsymbol{\phi}}) - \rho\mu\dot{c} + \nabla_{\boldsymbol{x}}\mu \cdot \boldsymbol{J} - \boldsymbol{\sigma} : \dot{\boldsymbol{\varepsilon}} &\leq 0. \end{aligned} \tag{1.37}$$

Finally, the Helmholtz free energy density depends on all fields of the thermodynamical process and we make the approach $e = e(\boldsymbol{Y})$. Due to the chain rule we follow for the time derivative

$$\dot{e} = \frac{\partial e}{\partial c}\dot{c} + \frac{\partial e}{\partial \boldsymbol{v}} \cdot \dot{\boldsymbol{v}} + \frac{\partial e}{\partial \nabla_{\boldsymbol{x}} c} \cdot \nabla_{\boldsymbol{x}}\dot{c} + \frac{\partial e}{\partial (c_{,\boldsymbol{\alpha}})_{2\leq|\boldsymbol{\alpha}|\leq 3}}\dot{c}_{,\boldsymbol{\alpha}} + \frac{\partial e}{\partial \dot{c}}\ddot{c} + \frac{\partial e}{\partial \boldsymbol{\varepsilon}} : \dot{\boldsymbol{\varepsilon}}.$$

The simplest way to achieve consistence with the second law of thermodynamics is to assume a linear dependence of the general entropy flux $\tilde{\boldsymbol{\phi}} = \rho\boldsymbol{\phi}_1\dot{c}$. Inserting this approach into the dissipation inequality (1.37), we calculate the relation

$$\begin{aligned} \rho\left(\frac{\partial e}{\partial c} - \operatorname{div}_{\boldsymbol{x}}(\boldsymbol{\phi}_1) - \mu\right)\dot{c} + \rho\frac{\partial e}{\partial \boldsymbol{v}} \cdot \dot{\boldsymbol{v}} + \rho\left(\frac{\partial e}{\partial \nabla_{\boldsymbol{x}} c} - \boldsymbol{\phi}_1\right) \cdot \nabla_{\boldsymbol{x}}\dot{c} \\ + \rho\frac{\partial e}{\partial (c_{,\boldsymbol{\alpha}})_{2\leq|\boldsymbol{\alpha}|\leq 3}}\dot{c}_{,\boldsymbol{\alpha}} + \rho\frac{\partial e}{\partial \dot{c}}\ddot{c} + \left(\rho\frac{\partial e}{\partial \boldsymbol{\varepsilon}} - \boldsymbol{\sigma}\right) : \dot{\boldsymbol{\varepsilon}} + \nabla_{\boldsymbol{x}}\mu \cdot \boldsymbol{J} \leq 0. \end{aligned} \tag{1.38}$$

Arguing as before, this inequality has to hold for all thermodynamical processes. Moreover, it is linear with respect to $\dot{\boldsymbol{v}}$, $(\dot{c}_{,\boldsymbol{\alpha}})_{1\leq|\boldsymbol{\alpha}|\leq 3}$, $\ddot{c}$ and $\dot{\boldsymbol{\varepsilon}}$, thus we deduce

$$\rho\frac{\partial e}{\partial \boldsymbol{v}} = \mathbf{0}, \qquad \boldsymbol{\phi}_1 = \frac{\partial e}{\partial \nabla_{\boldsymbol{x}} c}, \qquad \rho\frac{\partial e}{\partial (c_{,\boldsymbol{\alpha}})_{2\leq|\boldsymbol{\alpha}|\leq 3}} = 0, \tag{1.39}$$

$$\rho\frac{\partial e}{\partial \dot{c}} = 0, \qquad \boldsymbol{\sigma} = \rho\frac{\partial e}{\partial \boldsymbol{\varepsilon}}, \tag{1.40}$$

$$\rho\left(\frac{\partial e}{\partial c} - \operatorname{div}_{\boldsymbol{x}}(\boldsymbol{\phi}_1) - \mu\right)\dot{c} + \nabla_{\boldsymbol{x}}\mu \cdot \boldsymbol{J} \leq 0. \tag{1.41}$$

Consequently follows that the Helmholtz free energy density depends only on the concentration c, corresponding to the configurational part of the energy, on $\nabla_{\boldsymbol{x}} c$

identifying the surface energy of the diffusive interfaces and on the strain $\boldsymbol{\varepsilon}$ describing the elastic energy. We get the relation $e = e(c, \nabla_{\boldsymbol{x}} c, \boldsymbol{\varepsilon})$.

We continue our considerations with the observation of the dissipation (1.41) and define for further calculations

$$\boldsymbol{A} := \begin{pmatrix} \rho\left(\frac{\partial e}{\partial c} - \operatorname{div}_{\boldsymbol{x}}(\boldsymbol{\phi}_1) - \mu\right) \\ \boldsymbol{J} \end{pmatrix}, \qquad \boldsymbol{X} := \begin{pmatrix} \dot{c} \\ \nabla_{\boldsymbol{x}} \mu \end{pmatrix}. \tag{1.42}$$

The dissipation inequality (1.41) takes the simple form $\boldsymbol{A} \cdot \boldsymbol{X} \leq 0$ under consideration of (1.42). Furthermore, we assume that $\boldsymbol{A} = \boldsymbol{A}(\boldsymbol{X})$ is sufficiently smooth.

For an arbitrary $\lambda \geq 0$ holds $\boldsymbol{A}(\lambda \boldsymbol{X}) \cdot \boldsymbol{X} \leq 0$. Letting $\lambda \to 0$, the smoothness of $\boldsymbol{A}$ yields $\boldsymbol{A}(\boldsymbol{0}) \cdot \boldsymbol{X} \leq 0$ for all $\boldsymbol{X} \in \mathbb{R}^{d+1}$ and this leads to the result $\boldsymbol{A}(\boldsymbol{0}) = \boldsymbol{0}$. Moreover, we calculate a Taylor expansion and set $\boldsymbol{B} := -\,\mathrm{D}_{\boldsymbol{X}}\, \boldsymbol{A}(\boldsymbol{X})$, which is treated as a constitutive quantity in the following. We get

$$\boldsymbol{A}(\boldsymbol{X}) = -\boldsymbol{B}\boldsymbol{X} + \mathcal{O}(\|\boldsymbol{X}\|).$$

The constitutive parameter $\boldsymbol{B}$ contains friction in view of (1.42), given by a friction coefficient γ, diffusion, formulated by the mobility tensor $\boldsymbol{M}$ and some coupling terms between friction and diffusion denoted by $\boldsymbol{a}$ and $\boldsymbol{b}$. After neglecting higher order terms the dissipation inequality takes the form

$$-\boldsymbol{X} \cdot \boldsymbol{B}\boldsymbol{X} \leq 0, \qquad \boldsymbol{B} = \rho \begin{pmatrix} \gamma & \boldsymbol{a}^T \\ \boldsymbol{b} & \boldsymbol{M} \end{pmatrix}. \tag{1.43}$$

The second law of thermodynamics yields that $\boldsymbol{B}$ must be a positive definite tensor. In view of (1.42) we calculate from (1.43) the dissipation inequality

$$-\rho(\gamma \dot{c}^2 + \dot{c}\boldsymbol{a} \cdot \nabla_{\boldsymbol{x}} \mu + \nabla_{\boldsymbol{x}} \mu \cdot \boldsymbol{b}\dot{c} + \nabla_{\boldsymbol{x}} \mu \cdot \boldsymbol{M} \nabla_{\boldsymbol{x}} \mu) \leq 0.$$

Assuming that friction and diffusion are decoupled, then it follows $\boldsymbol{a} = \boldsymbol{0}$ and $\boldsymbol{b} = \boldsymbol{0}$. Finally the dissipation inequality is given by a friction coefficient $\gamma \geq 0$ and a positive definite mobility tensor $\boldsymbol{M}$, which is additionally symmetric due to Onsager's reciprocal law [82, 83]. The dissipation inequality is given under these assumptions by

$$-\rho(\gamma \dot{c}^2 + \nabla_{\boldsymbol{x}} \mu \cdot \boldsymbol{M} \nabla_{\boldsymbol{x}} \mu) \leq 0. \tag{1.44}$$

The second law of thermodynamics yields constitutive equations for the diffusive flux $\boldsymbol{J}$, for the chemical potential μ and for the 2. Piola-Kirchoff stress tensor given by

$$\boldsymbol{J} = -\rho \boldsymbol{M} \nabla_{\boldsymbol{x}} \mu \qquad \mu = -\operatorname{div}_{\boldsymbol{x}} \left(\frac{\partial e}{\partial \nabla_{\boldsymbol{x}} c} \right) + \frac{\partial e}{\partial c} + \gamma \dot{c} \qquad \boldsymbol{\sigma} = \rho \frac{\partial e}{\partial \boldsymbol{\varepsilon}} \tag{1.45}$$

We have to remark that the driving force of the diffusion is given by the gradient of the chemical potential. Moreover, from (1.45) follows that the chemical potential enters the material model as the variational derivative of the Helmholtz free energy plus a friction term. This agrees with classical thermodynamics, formulated e.g. in [99].

1.3.2 Dimensional analysis

The restriction of the equation of motion on the characteristic length scale will be done by a dimensional analysis. For this purpose we consider the following characteristic parameters resulting from experimental investigations:

- **characteristic length**: For our application we consider a RVE of the solder joint, which has the shape of a cube with side length

  $$L_0 = 10^{-6}[m].$$

- **characteristic velocity**: From measurements we know, that the wave speed of the deformation is bounded by a value

  $$v_0 = 10[\frac{m}{s}]$$

- **characteristic time**: The spinodal decomposition occurs on a small time scale, we observe as characteristic time

  $$t_0 = 100[s].$$

Using the characteristic parameters, we have to transform the equation of motion (1.20) into dimensionless parameters

$$\boldsymbol{x}^* = \frac{\boldsymbol{x}}{L_0}, \quad t^* = \frac{t}{t_0}, \quad \boldsymbol{v}^* = \frac{\boldsymbol{v}}{v_0}, \quad \boldsymbol{\sigma}^* = \frac{\boldsymbol{\sigma}}{\rho v_0^2}.$$

Furthermore, we have to transform the derivative operators into dimensionless parameters

$$\frac{\partial}{\partial x_i^*} = L_0 \frac{\partial}{\partial x_i}, \quad \frac{\partial}{\partial t^*} = t_0 \frac{\partial}{\partial t}.$$

The application of these transformations yields for the linearised equation of motion (1.20),

$$\rho \dot{\boldsymbol{v}} - \mathrm{div}_{\boldsymbol{x}}(\boldsymbol{\sigma}) = \frac{\rho v_o}{t_0} \frac{\partial}{\partial t^*} \boldsymbol{v}^* - \frac{\rho v_0^2}{L_0} \mathrm{div}_{\boldsymbol{x}^*}(\boldsymbol{\sigma}^*) = 0.$$

This calculation directly leads to the relation

$$\frac{L_0}{t_0 v_0}\frac{\partial}{\partial t^*}\boldsymbol{v}^* = \mathrm{div}_{\boldsymbol{x}^*}(\boldsymbol{\sigma}^*). \tag{1.46}$$

The factor on the left hand side of equation (1.46) is called Strouhol's number,

$$S_r = \frac{L_0}{t_0 v_0}$$

and by using the characteristic parameters, an estimate of this quantity yields

$$S_r \leq 10^{-9}.$$

This estimate shows, that the mechanical wave propagation can be neglected, because the right hand side of (1.46) is of order one. The dimensional analysis yields a quasi static mechanical equilibrium

$$-\mathrm{div}_{\boldsymbol{x}}(\boldsymbol{\sigma}) = \mathbf{0}. \tag{1.47}$$

1.3.3 Constitutive equations with application to solder

Energy and dissipation

For the Cahn-Larché system we have to formulate a constitutive relation for the Helmholtz free energy density $e = e(c, \nabla_{\boldsymbol{x}} c, \boldsymbol{\varepsilon})$. In the famous work of Cahn and Hilliard [20, 21] and Larché and Cahn [68] statistical arguments lead to the relation

$$e(c, \nabla_{\boldsymbol{x}} c, \boldsymbol{\varepsilon}) = \frac{1}{2}\boldsymbol{\Gamma}\nabla_{\boldsymbol{x}} c \cdot \nabla_{\boldsymbol{x}} c + \psi(c) + W(c, \boldsymbol{\varepsilon}). \tag{1.48}$$

The first term is called gradient or surface energy density, where the surface stress tensor $\boldsymbol{\Gamma}$ is directly related to the thickness of a diffusive interface. The Gibbs free energy density is denoted by $\psi(c)$ corresponding to Fickian diffusion. The last term describes the elastic energy density W, which additionally depends on the concentration c, because the elastic properties of the material vary within the alloy. The energy of the system then is given by the functional

$$E(t, c, \boldsymbol{u}) = \int_\Omega \left(\frac{1}{2}\boldsymbol{\Gamma}\nabla_{\boldsymbol{x}} c \cdot \nabla_{\boldsymbol{x}} c + \psi(c) + W(c, \boldsymbol{\varepsilon}(\boldsymbol{u}))\right)\, d\boldsymbol{x} - \int_{\Gamma_N} \boldsymbol{g}(t)\cdot\boldsymbol{u}\, d\boldsymbol{a}_{\boldsymbol{x}}. \tag{1.49}$$

Moreover, the dissipation functional of the viscous Cahn-Larché model follows from (1.44) by

$$D_\gamma(c, \dot{c}, \mu) = -\frac{1}{2}\int_\Omega \boldsymbol{M}(c)\nabla_{\boldsymbol{x}}\mu \cdot \nabla_{\boldsymbol{x}}\mu + \gamma\dot{c}^2\, d\boldsymbol{x}. \tag{1.50}$$

Consequently we formulate the field equations of the viscous Cahn-Larché model, which follows from the diffusion equation (1.14) and from the quasi static equilibrium (1.47) by taking into account the constitutive equations (1.45) and (1.48),

$$\begin{aligned}
\dot{c} - \operatorname{div}_{\boldsymbol{x}}(\boldsymbol{M}(c)\nabla_{\boldsymbol{x}}\mu) &= 0 && \text{in } \Omega_T, && (1.51)\\
\mu &= -\operatorname{div}_{\boldsymbol{x}}(\boldsymbol{\Gamma}\nabla_{\boldsymbol{x}}c) + \psi_{,c}(c) + W_{,c}(c,\boldsymbol{\varepsilon}) + \gamma\dot{c} && \text{in } \Omega_T, && (1.52)\\
-\operatorname{div}_{\boldsymbol{x}}(W_{,\boldsymbol{\varepsilon}}(c,\boldsymbol{\varepsilon})) &= \boldsymbol{0} && \text{in } \Omega_T, && (1.53)\\
\boldsymbol{M}(c)\nabla_{\boldsymbol{x}}\mu \cdot \boldsymbol{n} &= 0 && \text{on } \Gamma_T, && (1.54)\\
\boldsymbol{\Gamma}\nabla_{\boldsymbol{x}}c \cdot \boldsymbol{n} &= 0 && \text{on } \Gamma_T, && (1.55)\\
\boldsymbol{u} &= \boldsymbol{0} && \text{on } \Gamma_T^D, && (1.56)\\
W_{,\boldsymbol{\varepsilon}}(c,\boldsymbol{\varepsilon})\boldsymbol{n} &= \boldsymbol{g} && \text{on } \Gamma_T^N, && (1.57)\\
c(0,\boldsymbol{x}) &= c_0(\boldsymbol{x}) && \text{in } \Omega. && (1.58)
\end{aligned}$$

As mentioned above the greatest interest in understanding the viscosity is the fact to develop efficient numerical methods for the non-viscous case. In this case the thermodynamical process $\boldsymbol{Y}$ does not depend on $\dot{c}$ and due to this fact (1.38) is linear with respect to $\dot{c}$. Furthermore, in the non-viscous model dissipation only contains diffusion and we have the dissipation functional

$$D(c,\mu) = -\frac{1}{2}\int_\Omega \boldsymbol{M}(c)\nabla_{\boldsymbol{x}}\mu \cdot \nabla_{\boldsymbol{x}}\mu \, d\boldsymbol{x}. \tag{1.59}$$

The field equations for this model are given by neglecting the friction coefficient γ and consequently we have

$$\begin{aligned}
\dot{c} - \operatorname{div}_{\boldsymbol{x}}(\boldsymbol{M}(c)\nabla_{\boldsymbol{x}}\mu) &= 0 && \text{in } \Omega_T, && (1.60)\\
\mu &= -\operatorname{div}_{\boldsymbol{x}}(\boldsymbol{\Gamma}\nabla_{\boldsymbol{x}}c) + \psi_{,c}(c) + W_{,c}(c,\boldsymbol{\varepsilon}) && \text{in } \Omega_T, && (1.61)\\
-\operatorname{div}_{\boldsymbol{x}}(W_{,\boldsymbol{\varepsilon}}(c,\boldsymbol{\varepsilon})) &= \boldsymbol{0} && \text{in } \Omega_T, && (1.62)\\
\boldsymbol{M}(c)\nabla_{\boldsymbol{x}}\mu \cdot \boldsymbol{n} &= 0 && \text{on } \Gamma_T, && (1.63)\\
\boldsymbol{\Gamma}\nabla_{\boldsymbol{x}}c \cdot \boldsymbol{n} &= 0 && \text{on } \Gamma_T, && (1.64)\\
\boldsymbol{u} &= \boldsymbol{0} && \text{on } \Gamma_T^D, && (1.65)\\
W_{,\boldsymbol{\varepsilon}}(c,\boldsymbol{\varepsilon})\boldsymbol{n} &= \boldsymbol{g} && \text{on } \Gamma_T^N, && (1.66)\\
c(0,\boldsymbol{x}) &= c_0(\boldsymbol{x}) && \text{in } \Omega. && (1.67)
\end{aligned}$$

Finally we have to formulate relations for the surface stress tensor $\boldsymbol{\Gamma}$, for the Gibbs free energy density $\psi(c)$, for the strain energy density $W(c,\boldsymbol{\varepsilon})$ and for the mobility tensor $\boldsymbol{M}(c)$. This is done for the example of a Sn-Pb system in [31, 32, 33, 34] and we modify these constitutive equations in order to use them directly in the numerical simulations.

Shape function

First of all we have to observe how the material properties between both phases are interpolated. In [31, 32, 33, 34] this is done by a linear shape function, which causes in general none bounded material equations. Therefore, in our model we use the following different shape function

$$\vartheta(c) := \begin{cases} 1 & : \ c \leq c^\alpha, \\ \frac{(c-c^\beta)^3}{(c^\alpha-c^\beta)^3}\left(6\frac{(c-c^\alpha)^2}{(c^\alpha-c^\beta)^2} - 3\frac{(c-c^\alpha)}{(c^\alpha-c^\beta)} + 1\right) & : \ c^\alpha < c < c^\beta, \\ 0 & : \ c^\beta \leq c, \end{cases}$$

where c^α and c^β are the equilibrium concentrations of the α- and β-phase. For a given temperature θ these values can be read from the phase diagram, which is shown in fig. 2. In our model the shape function is twice continuously differentiable and we have the derivatives

$$\vartheta_{,c}(c) = \begin{cases} 1 & : \ c \leq c^\alpha, \\ 30\frac{(c-c^\alpha)^2(c-c^\beta)^2}{(c^\alpha-c^\beta)^5} & : \ c^\alpha < c < c^\beta, \\ 0 & : \ c^\beta \leq c, \end{cases}$$

$$\vartheta_{,cc}(c) = \begin{cases} 1 & : \ c \leq c^\alpha, \\ 60\frac{(c-c^\alpha)(c-c^\beta)(2c-c^\alpha-c^\beta)}{(c^\alpha-c^\beta)^5} & : \ c^\alpha < c < c^\beta, \\ 0 & : \ c^\beta \leq c. \end{cases}$$

In order to illustrate the behaviour of the shape function we plot the shape function in fig. 1.1 for a Sn-Pb alloy at the different temperatures with the corresponding equilibrium concentrations taken from [73].

θ in $[^\circ C]$	c^α	c^β
$20^\circ C$	0.020	0.9967
$125^\circ C$	0.0918	0.9786

Tab. 1.1: Equilibrium concentration of Sn-Pb

Surface stress tensor

The surface stress tensor of the mixture is related to the surface stress tensor of the individual phase $\mathbf{\Gamma}^{\alpha/\beta}$ by a convex combination with respect to the shape function. In our numerical simulations we work with a constant surface stress tensor calculated by

$$\mathbf{\Gamma} = \vartheta(c_{eut})\mathbf{\Gamma}^\alpha + (1 - \vartheta(c_{eut}))\mathbf{\Gamma}^\beta$$

(a) $\vartheta(c)$ at temperature $\theta = 20°C$ (b) $\vartheta(c)$ at temperature $\theta = 125°C$

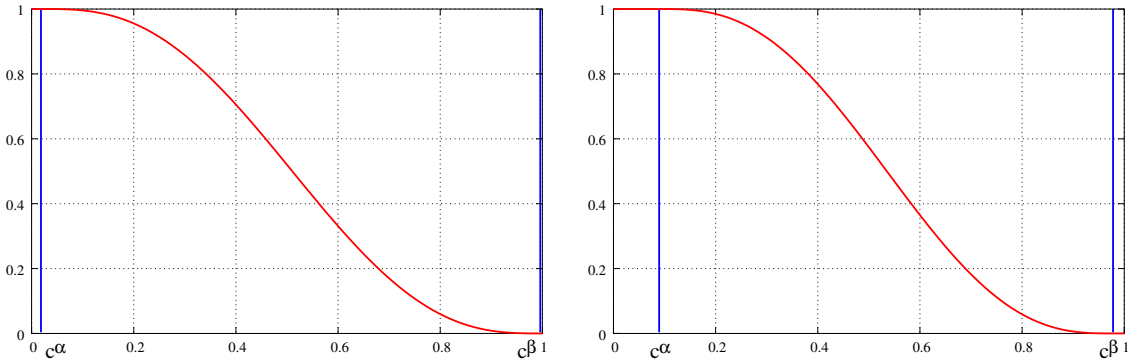

Fig. 1.1: Shape function at different temperatures

in the unit $\left[\frac{J}{m}\right]$. It is very difficult to obtain reliable data for the surface stress tensor $\mathbf{\Gamma}^{\alpha/\beta}$. Dreyer and Müller have calculated these quantities in [32] for a Sn-Pb alloy from the lattice structure of the pure constitutes

$$\tilde{\gamma} = \frac{2\bar{\gamma}\Delta x}{(c^\alpha - c^\beta)^2}, \qquad \bar{\gamma} = 1.5\frac{J}{m^2}, \qquad \Delta x = 25nm,$$

$$\mathbf{\Gamma}^\alpha = \begin{pmatrix} 1.5\tilde{\gamma} & 0 & 0 \\ 0 & 1.5\tilde{\gamma} & 0 \\ 0 & 0 & 1.5\tilde{\gamma} \end{pmatrix}, \qquad \mathbf{\Gamma}^\beta = \begin{pmatrix} \tilde{\gamma} & 0 & 0 \\ 0 & \tilde{\gamma} & 0 \\ 0 & 0 & 14\tilde{\gamma} \end{pmatrix}.$$

In these formulas $\bar{\gamma}$ denotes the surface energy and Δx describes the thickness of the diffusive phase interface between the Sn-rich and Pb-rich phase. The structure of the surface stress tensors $\mathbf{\Gamma}^{\alpha/\beta}$ clearly demonstrates that the α-phase (Pb rich phase) has a cubic lattice structure, in contrast to the β-phase (Sn rich phase), which has a tetragonal lattice structure.

θ in $[°C]$	$\tilde{\gamma}$ in $\left[\frac{J}{m}\right]$
$20°C$	$7.862105 \times 10^{-8}\frac{J}{m}$
$125°C$	$9.536959 \times 10^{-8}\frac{J}{m}$

Tab. 1.2: Values for the surface stress tensors

Gibbs free energy

From the MTData report [73] we take the formula for the Gibbs free energy density for a binary system A/B. The Gibbs free energy density is obtained for both phases α/β individually in the unit $\left[\frac{J}{mol}\right]$ as a function of the particle density y

$$g^{\alpha/\beta}(y) = yg_A^{\alpha/\beta} + (1-y)g_B^{\alpha/\beta} + R\theta(y\ln(y) + (1-y)\ln(1-y)) + y(1-y)l^\alpha.$$

In this relation $R = 8.31434 \frac{J}{Kmol}$ denotes the gas constant, where the functions g_j^i and l^i for $i \in \{\alpha, \beta\}$ and $j \in \{A, B\}$ depend on the absolute temperature. They are obtained from fits to experimental data by the following curves

$$g_j^i = A_j^i + B_j^i\theta + C_j^i\theta\ln(\theta) + D_j^i\theta^2 + E_j^i\theta^3 + \frac{F_j^i}{\theta}, \quad i \in \{\alpha, \beta\}, \quad j \in \{A, B\},$$
$$l^i = A^i + B^i\theta \qquad\qquad i \in \{\alpha, \beta\}.$$

For a Sn-Pb alloy MTData report [73] provides numerical values for the fit parameters valid within a temperature range $250K < \theta < 505K$. They are outlined in tab.1.3.

	A_j^i $\left[\frac{kJ}{mol}\right]$	B_j^i $\left[\frac{J}{mol}\right]$	C_j^i $\left[\frac{J}{molK}\right]$	D_j^i $\left[\frac{mJ}{molK}\right]$	E_j^i $\left[\frac{\mu J}{molK}\right]$	F_j^i $\left[\frac{MJK}{mol}\right]$
$i = \alpha$						
j =Pb	-7.650085	101.700244	-24.524223	-3.65895	-0.24395	0
j =Sn	-1.705135	60.2433150	-15.9610	-18.8702	3.121167	-0.06196
$i = \beta$						
j =Pb	-7.161085	105.220244	C^α_{Pb}	D^α_{Pb}	E^α_{Pb}	F^α_{Pb}
j =Sn	-5.855135	65.4433150	C^α_{Sn}	D^α_{Sn}	E^α_{Sn}	F^α_{Sn}

	A^i $\left[\frac{kJ}{mol}\right]$	B^i $\left[\frac{J}{mol}\right]$
$i = \alpha$	5.13241	1.56312
$j = \beta$	17.11778	-11.80656

Tab. 1.3: Fit parameter of the Gibbs free energy density

The Cahn-Larché model is originally developed in terms of the mass concentration c and not in terms of the particle density y. In order to avoid this difficulty we have to reformulate the Gibbs free energy in terms of the concentration c. This is done by arguing similarly as in [31] and using the non-linear relation between the mass concentration c and the particle density y,

$$y(c) = \frac{M_B c}{M_A - c(M_A - M_B)}. \tag{1.68}$$

In this relation $M_{A/B}$ denotes the atomic weights for the individual constituents, e.g. in a Sn-Pb alloy we have

$$M_{\mathrm{Sn}} = 118.69, \qquad M_{\mathrm{Pb}} = 207.19.$$

Moreover, in order to convert the free energy density from $Jmol^{-1}$ into Jm^{-3} it is useful to introduce an averaged molecular weight $M = M(c)$, which changes as a function of concentration c. We take from [31] the relation

$$M(c) = \frac{M_A M_B}{M_A - c(M_A - M_B)}. \tag{1.69}$$

By means of Avogardo's number $N_{Avo} = 6.0225 \times 10^{23} \frac{1}{mol}$ and the atomic weight of a hydrogen atom $\mu_H = 1.675 \times 10^{-27} kg$ the Gibbs free energy density for an individual phase i is given by

$$\psi^i(c) = \rho \frac{g^i(y(c))}{M(c) N_{Avo} \mu_H}, \qquad i \in \{\alpha, \beta\}. \tag{1.70}$$

In fig. 1.2 we plot the Gibbs free energy densities $\psi^i(c)$ with $i \in \{\alpha, \beta\}$ for a Sn-Pb system after Maxwell tangent construction. Maxwell tangent construction means that we transform the Gibbs free energy density in such a way that both phase equilibria are on the same energy level.

(a) $\psi^{\alpha/\beta}$ at temperature $\theta = 20°C$ (b) $\psi^{\alpha/\beta}$ at temperature $\theta = 125°C$

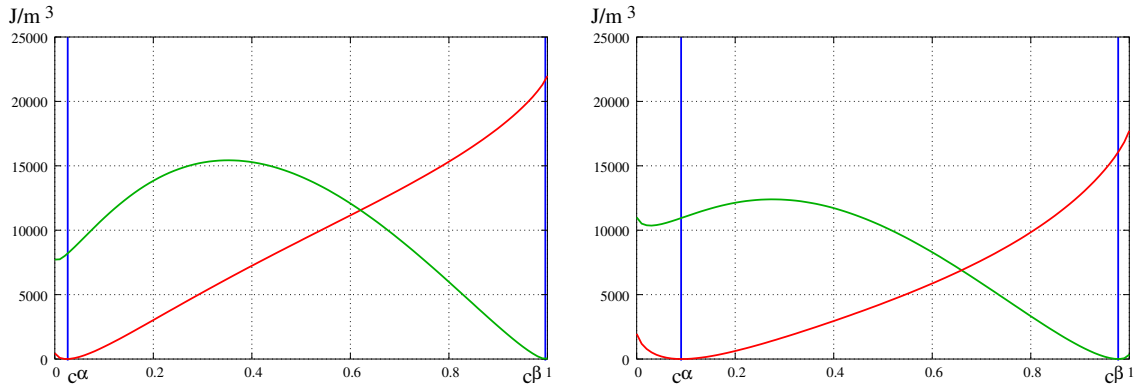

Fig. 1.2: Specific Gibbs free energy for a Sn-Pb alloy

The Helmholtz free energy formulated by Cahn and Hilliard in [20, 21] as well as Larché and Cahn in [68] contains only one Gibbs free energy density for both phases. Dreyer and Müller [31] proposed to choose for the Gibbs free energy the minimum of $\psi^i(c)$. For the analysis as well as for the numerical simulation this choice causes large difficulties due to the resulting kink at c^γ, where it holds $\psi^\alpha(c^\gamma) = \psi^\beta(c^\gamma)$. Therefore we propose an interpolation of $\min_{i \in \{\alpha,\beta\}} \psi^i(c)$ satisfying the following properties

$$\begin{aligned}
\psi(0) &= \min_{i \in \{\alpha,\beta\}} \psi^i(0), \\
\psi(c^\alpha) &= \min_{i \in \{\alpha,\beta\}} \psi^i(c^\alpha), \qquad \psi_{,c}(c^\alpha) = 0, \qquad \psi_{,cc}(c^\alpha) \quad \text{continuous}, \\
\psi(c^\beta) &= \min_{i \in \{\alpha,\beta\}} \psi^i(c^\beta), \qquad \psi_{,c}(c^\beta) = 0, \qquad \psi_{,cc}(c^\beta) \quad \text{continuous}, \\
\psi(c^\gamma) &= \min_{i \in \{\alpha,\beta\}} \psi^i(c^\gamma), \qquad \psi_{,c}(c^\gamma) = 0, \qquad \psi_{,cc}(c^\gamma) \quad \text{continuous}, \\
\psi(1) &= \min_{i \in \{\alpha,\beta\}} \psi^i(1).
\end{aligned}$$

In order to keep the polynomial degree as small as possible, we use a spline interpolation with Bernstein polynomials as formulated e.g. in [88]. The i-th Bernstein polynomial of degree n is defined by

$$B_i^n(x) = \binom{n}{i} x^i (1-x)^{n-i}, \qquad 0 \le i \le n, \qquad 0 \le x \le 1.$$

The interval $[0,1]$ is divided into four parts $[0,c^\alpha]$, $[c^\alpha,c^\gamma]$, $[c^\gamma,c^\beta]$ and $[c^\beta,1]$. In order to satisfy the eleven interpolation conditions, which are formulated above, we use Bernstein polynomials of degree three except in the interval $[c^\gamma,c^\beta]$, where Bernstein polynomials of degree four are used. This approach leads to a spline function for the Gibbs free energy density having the form

$$\psi(c) := \begin{cases} \sum_{k=0}^{3} b_k^0 B_k^3\left(\frac{c}{c^\alpha}\right), & 0 \le c < c^\alpha \\ \sum_{k=0}^{3} b_k^1 B_k^3\left(\frac{c-c^\alpha}{c^\gamma-c^\alpha}\right), & c^\alpha \le c < c^\beta \\ \sum_{k=0}^{4} b_k^2 B_k^4\left(\frac{c-c^\gamma}{c^\beta-c^\gamma}\right), & c^\gamma \le c < c^\beta \\ \sum_{k=0}^{3} b_k^3 B_k^3\left(\frac{c-c^\beta}{1-c^\beta}\right), & c^\beta \le c \le 1 \end{cases}. \tag{1.71}$$

The interpolation weights satisfying the interpolation conditions are calculated in the following way

$$\begin{aligned} &b_0^0 = \min_{i\in\{\alpha,\beta\}} \psi^i(0), && b_0^1 = b_3^0, && b_0^2 = b_3^1, && b_0^3 = b_4^2, \\ &b_1^0 = \frac{\psi^\alpha(c^\gamma)c^{\alpha\,2}}{(c^\gamma-c^\alpha)^2}, && b_1^1 = b_3^0, && b_1^2 = b_0^2, && b_1^3 = b_0^3, \\ &b_2^0 = b_3^0, && b_2^1 = b_3^1, && b_2^2 = \frac{(1-(c^\beta-c^\gamma)^2)b_0^1}{2(c^\gamma-c^\alpha)^2}, && b_2^3 = \frac{2(1-c^\beta)^2 b_2^2}{(c^\gamma-c^\alpha)^2}, \\ &b_3^0 = 0, && b_3^1 = \min_{i\in\{\alpha,\beta\}} \psi^i(c^\gamma), && b_3^2 = b_4^2, && b_3^3 = \min_{i\in\{\alpha,\beta\}} \psi^i(1), \\ & && && b_4^2 = 0. && \end{aligned}$$

Fig. 1.3 shows the Gibbs free energy density ψ at temperature $\theta = 20°C$ and $\theta = 125°C$.

Strain energy

As mentioned before, the solder joint undergoes only small deformations and small strains. Due to this fact a Hook's law is taken into account, which is derived e.g. in [24]. The strain energy density for a Hook's law with concentration dependent material parameters is given by

$$W(c,\boldsymbol{\varepsilon}) := \frac{1}{2}\boldsymbol{C}(c)(\boldsymbol{\varepsilon}-\overline{\boldsymbol{\varepsilon}}(c)) : (\boldsymbol{\varepsilon}-\overline{\boldsymbol{\varepsilon}}(c)). \tag{1.72}$$

(a) $\psi(c)$ at temperature $\theta = 20°C$

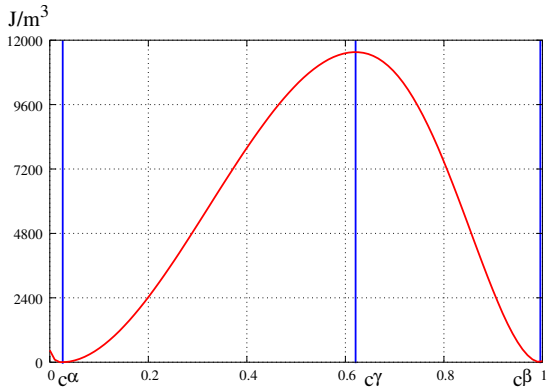

(b) $\psi(c)$ at temperature $\theta = 125°C$

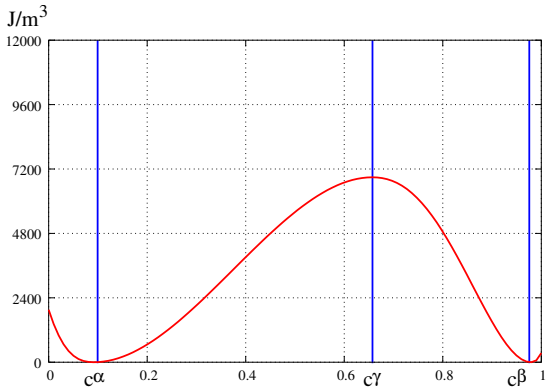

(c) $\psi_{,c}(c)$ at temperature $\theta = 20°C$

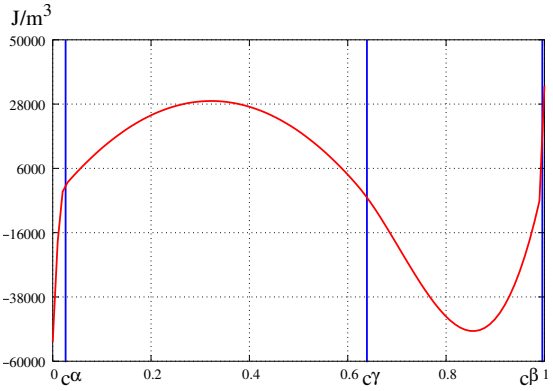

(d) $\psi_{,c}(c)$ at temperature $\theta = 125°C$

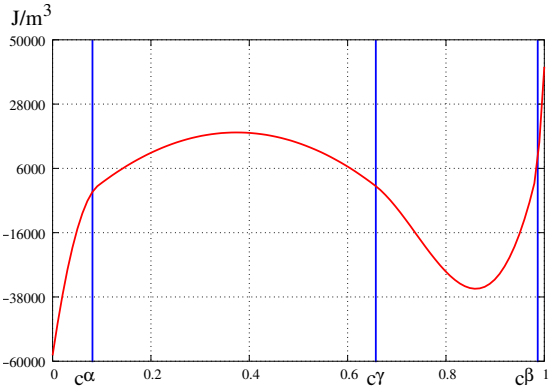

(e) $\psi_{,cc}(c)$ at temperature $\theta = 20°C$

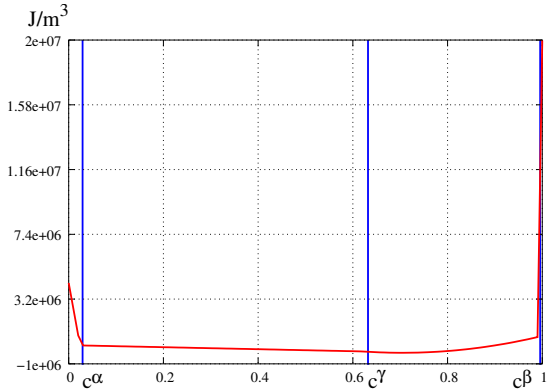

(f) $\psi_{,cc}(c)$ at temperature $\theta = 125°C$

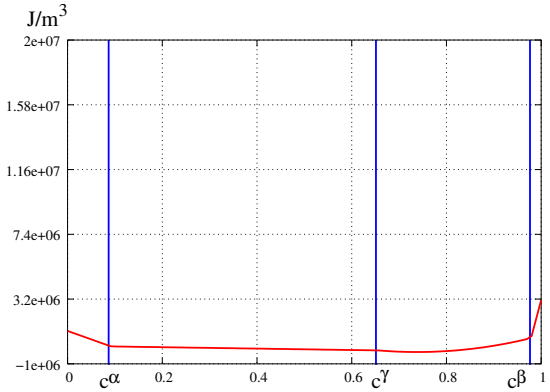

Fig. 1.3: Interpolated Gibbs free energy

In (1.72) $\boldsymbol{C}(c)$ denotes the elasticity tensor of the mixture, $\boldsymbol{\varepsilon}$ the linearised strain tensor defined in (1.9) and $\overline{\boldsymbol{\varepsilon}}(c)$ the eigenstrain of the alloy. For modelling solder, the elasticity tensor $\boldsymbol{C}$ as well as the eigenstrain tensor $\overline{\boldsymbol{\varepsilon}}$ are assumed to depend on the concentration c, because the lattice structure of the α- and β-phase may be different. For example in a Sn-Pb solder the α- phase has a cubic lattice structure, while the β-phase has a tetragonal lattice structure.

The elasticity tensor $\boldsymbol{C}$ is related to the elasticity tensors of the individual phases $\boldsymbol{C}^{\alpha/\beta}$ by a convex combination with respect to the shape function

$$\boldsymbol{C}(c) := \vartheta(c)\boldsymbol{C}^{\alpha} + (1-\vartheta(c))\boldsymbol{C}^{\beta}. \tag{1.73}$$

In view of the uncertain determined material parameters involved in this model, we use for $\boldsymbol{C}^{\alpha/\beta}$ the elasticity tensor of the pure constituents. For a Sn-Pb alloy we have the following elasticity tensor in the unit $[GPa]$

$$\boldsymbol{C}^{\alpha} = \begin{pmatrix} 49.6 & 42.3 & 42.3 & 0 & 0 & 0 \\ 42.3 & 49.6 & 42.3 & 0 & 0 & 0 \\ 42.3 & 42.3 & 49.6 & 0 & 0 & 0 \\ 0 & 0 & 0 & 14.9 & 0 & 0 \\ 0 & 0 & 0 & 0 & 14.9 & 0 \\ 0 & 0 & 0 & 0 & 0 & 14.9 \end{pmatrix}, \qquad \boldsymbol{C}^{\beta} = \begin{pmatrix} 75.2 & 61.5 & 44.0 & 0 & 0 & 0 \\ 61.5 & 75.2 & 44.0 & 0 & 0 & 0 \\ 44.0 & 44.0 & 95.5 & 0 & 0 & 0 \\ 0 & 0 & 0 & 21.9 & 0 & 0 \\ 0 & 0 & 0 & 0 & 21.9 & 0 \\ 0 & 0 & 0 & 0 & 0 & 23.3 \end{pmatrix}.$$

In a similar way the eigenstrain tensor $\overline{\boldsymbol{\varepsilon}}$ of the alloy is related to the thermal expansion coefficients of the individual phases $\overline{\boldsymbol{\varepsilon}}^{\alpha/\beta}$ and the temperature increase $\Delta\theta$ by the following formula

$$\overline{\boldsymbol{\varepsilon}}(c) := \Delta\theta(\vartheta(c)\overline{\boldsymbol{\varepsilon}}^{\alpha} + (1-\vartheta(c))\overline{\boldsymbol{\varepsilon}}^{\beta}). \tag{1.74}$$

In this formula $\Delta\theta$ denotes the temperature increase and $\overline{\boldsymbol{\varepsilon}}^{\alpha/\beta}$ are the thermal expansion coefficients of the pure components formulated in the unit $\left[\frac{1}{K}\right]$,

$$\overline{\boldsymbol{\varepsilon}}^{\alpha} = \begin{pmatrix} 28.9 & 0 & 0 \\ 0 & 28.9 & 0 \\ 0 & 0 & 28.9 \end{pmatrix}, \qquad \overline{\boldsymbol{\varepsilon}}^{\beta} = \begin{pmatrix} 16.7 & 0 & 0 \\ 0 & 16.7 & 0 \\ 0 & 0 & 36.4 \end{pmatrix}.$$

Mobility tensor

Similar, for the mobility tensor we have to consider the different lattice structures in both phases. This is the reason why the mobility tensor also has to depend on the concentration c. We relate this constitutive quantity to the mobility tensors $\boldsymbol{M}^{\alpha/\beta}$ of the individual phase by a convex combination with respect to the shape function,

$$\boldsymbol{M}(c) = \vartheta(c)\boldsymbol{M}^{\alpha} + (1-\vartheta(c))\boldsymbol{M}^{\beta}.$$

The material parameters $\boldsymbol{M}^{\alpha/\beta}$ are not directly available from literature, moreover they are not directly measurable from experiments. Therefore, we follow Dreyer and Müller [31], who take arguments from [66] in order to relate the mobility tensor to

the diffusion tensor. In [66] Cahn-Hilliard diffusion is neglected and only diffusion of Fickian type is observed and we get approximately

$$\boldsymbol{J} \approx -\rho \boldsymbol{M} \nabla_{\boldsymbol{x}} \left(\frac{\partial \psi(c)}{\partial c} \right) = -\rho \boldsymbol{M} \frac{\partial^2 \psi(c)}{\partial c^2} \nabla_{\boldsymbol{x}} c =: -\rho \boldsymbol{D} \nabla_{\boldsymbol{x}} c.$$

This approach yields the definition of the diffusion matrix $\boldsymbol{D}$, which naturally depends on the concentration c. Furthermore, we conclude that mobility and diffusion tensor is related as follows

$$\boldsymbol{M}(c) = \left(\frac{\partial^2 \psi(c)}{\partial c^2} \right)^{-1} \boldsymbol{D}(c), \qquad \boldsymbol{D}(c) = \vartheta(c) \boldsymbol{D}^{\alpha} + (1 - \vartheta(c)) \boldsymbol{D}^{\beta} \tag{1.75}$$

In this relation $\boldsymbol{D}^{\alpha/\beta}$ denote the diffusion tensor of the α- respectively β-phase. Again the diffusion tensors of pure Sn and pure Pb are used.

In order to compute the mobilities $\boldsymbol{M}^{\alpha/\beta}$ we have to evaluate the second derivative of the Gibbs free energy density ψ. In [66] this is done for the eutectic concentration. In contrast to this method, Dreyer and Müller [31] evaluate the relation (1.75) at the equilibrium concentrations $c^{\alpha/\beta}$ and we get

$$\boldsymbol{M}^{\alpha} = \left(\frac{\partial^2 \psi(c^{\alpha})}{\partial c^2} \right)^{-1} \boldsymbol{D}(c^{\alpha}), \qquad \boldsymbol{M}^{\beta} = \left(\frac{\partial^2 \psi(c^{\beta})}{\partial c^2} \right)^{-1} \boldsymbol{D}(c^{\beta}).$$

We take the following mobility coefficients of a Sn-Pb alloy from [31], where they are calculated for the temperature $\theta = 20°C$ and $\theta = 125°C$ given in the unit $\left[\frac{m^5}{Js}\right]$.

θ in $[°C]$	$\boldsymbol{M}^{\alpha}$ in $\left[\frac{m^5}{Js}\right]$	$\boldsymbol{M}^{\beta}$ in $\left[\frac{m^5}{Js}\right]$
$20[°C]$	$\begin{pmatrix} 1.27\times10^{-32} & 0 & 0 \\ 0 & 1.27\times10^{-32} & 0 \\ 0 & 0 & 1.27\times10^{-32} \end{pmatrix}$	$\begin{pmatrix} 1.11\times10^{-27} & 0 & 0 \\ 0 & 1.11\times10^{-27} & 0 \\ 0 & 0 & 1.11\times10^{-27} \end{pmatrix}$
$125[°C]$	$\begin{pmatrix} 2.42\times10^{-27} & 0 & 0 \\ 0 & 2.42\times10^{-27} & 0 \\ 0 & 0 & 2.42\times10^{-27} \end{pmatrix}$	$\begin{pmatrix} 4.52\times10^{-24} & 0 & 0 \\ 0 & 4.52\times10^{-24} & 0 \\ 0 & 0 & 4.52\times10^{-24} \end{pmatrix}$

Tab. 1.4: Mobility tensors

Chapter 2

Analysis for weak solutions of the viscous Cahn-Larché system

The second chapter deals with the analysis of weak solutions of the viscous Cahn-Larché system (1.51) - (1.58) and weak solutions of the non-viscous Cahn-Larché system (1.60) - (1.67). The main goal of this chapter is to show the existence of a weak solution of the Cahn-Larché system with concentration dependent mobility, viscosity and mixed boundary conditions, which extends the results from [48, 49]. We additionally focus on the fact that uniform a-priori estimates of the solution do not depend on the friction coefficient γ, which is an important property for the following chapters where numerical methods are discussed.

The existence proof is organised in such a way that it works for both cases, the viscous and non-viscous system. During this proof we point out the different properties between weak solutions of the viscous and non-viscous Cahn-Larché system.

The existence proof in this work bases essentially on the methods developed by Garcke in [48, 49]. Garcke applies a time discretisation of the Cahn-Larché system and uses the flow gradient structure in order to reformulate the model as a variational problem minimising the Helmholtz free energy and maximising the dissipation. Here, Garcke's techniques are expanded in order to show the existence of solutions for concentration dependent mobilities, mixed boundary conditions for the mechanical equilibrium and additional viscosity.

There are a lot of papers on Cahn-Hilliard and Cahn-Larché equations, which are related to our subject. In [40] an existence result for weak solutions of Cahn-Hilliard's equation without elasticity, constant material parameters and smooth Gibbs free energy densities is proved. The more interesting case of a logarithmic Gibbs free energy density is considered in [39], which holds also for systems of Cahn-Hilliard equations. There is an existence result for the Cahn-Hilliard equation with concentration dependent and degenerating mobilities in [38]. The Cahn-Hilliard equation with viscous effects is considered in [52].

Furthermore, we refer to existence results of Cahn-Larché's equations, which take into account elastic effects. An existence result for this system with constant material parameters is formulated in [22]. In [48] this result is generalised to the case of concentration dependent elasticity, but considers a constant mobility tensor. The result from [48] holds also for systems as well as for logarithmic Gibbs free energy densities. A viscous Cahn-Larché system with concentration dependent material parameters is observed in [13]. But this model differs from the one discussed here, because the field equations in [13] do not satisfy a gradient flow structure and therefore the model is not thermodynamical consistent. Recently an existence result for weak solutions of the viscous Cahn-Larché system with constant mobility and constant elasticity tensor is achieved in [12]. They use a Galerkin method for proving the existence result whereas here an energy minimisation is applied.

2.1 Weak formulation

In this work, we restrict our considerations as mentioned in the beginning on space dimensions $d = 2; 3$. In order to develop an existence theory for weak solutions of the viscous Cahn-Larché system (1.51) - (1.58) we assume further restrictions on the domain:

(H-1) **Domain**: Let $\Omega \subset \mathbb{R}^d$ be an open, bounded and polyhedral domain with a Lipschitz boundary. The decomposition of the boundary $\partial\Omega$ into a Dirichlet part Γ_D and a Neumann part Γ_N has to satisfy the following properties:

$$\partial\Omega = \overline{\Gamma}_D \cup \overline{\Gamma}_N; \quad \Gamma_D \cap \Gamma_N = \emptyset; \quad \text{meas}(\Gamma_D) > 0.$$

2.1.1 Function spaces

In general, let X be a Banach space equipped with the norm $\|\cdot\|_X$, its dual space is denoted with X'. The conjugate pairing of an element $f \in X'$ with an element $v \in X$ is described by $\langle f, v\rangle$. X' is also a Banach space endowed with the operator norm

$$\|f\|_{X'} := \sup_{v \in X} \frac{|\langle f, v\rangle|}{\|v\|_X}.$$

Additionally, we use the notation $\boldsymbol{X}$ for a Banach space of vector valued functions.

Let $(v_n)_{n\in\mathbb{N}} \subset X$ be a sequence, which converges weakly to $v \in X$, in a reflexive Banach space, then we use the notation

$$v_n \rightharpoonup v.$$

Furthermore, if the sequence $(v_n)_{n\in\mathbb{N}} \subset X'$ is a weak-$\star$ convergent sequence in a non-reflexive Banach space, then we use the notation

$$v_n \overset{*}{\rightharpoonup} v.$$

Throughout this work we denote by $C^{k,l}(\Omega)$ with $k, l \in \mathbb{N}_0$ the space of k times Hölder continuous functions with Hölder exponent l. Furthermore we write $L_p(\Omega)$ with $1 \leq p \leq \infty$ for the usual Lebesgue spaces as defined in [42]. These spaces are Banach spaces equipped with the classical norm denoted by $\|\cdot\|_{L_p(\Omega)}$. Moreover, the space $L_2(\Omega)$ is a separable Hilbert space with the usual inner product $\langle\cdot,\cdot\rangle_{L_2(\Omega)}$. For functions in $L_p(\Omega)$ Hölder's inequality holds as proved in [42] and especially yields a Cauchy-Schwartz inequality on the Hilbert space $L_2(\Omega)$.

Let $l \in \mathbb{N}_0$, then we use the Sobolev spaces denoted by $H^l(\Omega)$, which are defined in [2, 104]. These spaces are separable Hilbert spaces endowed with the usual norm $\|\cdot\|_{H^l(\Omega)}$ or semi-norm $|\cdot|_{H^l(\Omega)}$. Furthermore, let $s = l + \sigma$ where $l \in \mathbb{N}_0$, $0 < \sigma < 1$, then $H^s(\Omega)$ denotes the Sobolev-Slobodeckij spaces as defined in [104], which are also separable Hilbert spaces equipped with the usual norm $\|\cdot\|_{H^s(\Omega)}$ or semi-norm $|\cdot|_{H^s(\Omega)}$.

In order to show the existence of weak solutions of the viscous Cahn-Larché system, we have to take into account the mass conservation (1.17). Therefore a function space is defined, which contains functions satisfying the mass conservation,

$$X_m(\Omega) := \left\{ v \in H^1(\Omega) \ : \ \int_\Omega v \, d\boldsymbol{x} = m, \quad m \geq 0 \text{ const} \right\}.$$

The space $X_m(\Omega)$ is equipped with the usual Sobolev norm $\|\cdot\|_{H^1(\Omega)}$ or semi-norm $|\cdot|_{H^1(\Omega)}$. We remark, that if $m = 0$, $X_0(\Omega)$ is a linear subspace of $H^1(\Omega)$, and if $m > 0$, $X_m(\Omega)$ is an affine subspace of $H^1(\Omega)$.

We have Poincaré's inequality in $X_m(\Omega)$ as a special case of [104] theorem 7.7.

Lemma 2.1 (Poincaré's inequality). *Let $\Omega \subset \mathbb{R}^d$ be an open and bounded Lipschitz domain, then there exists a constant $c_p > 0$, such that for all $v \in X_m(\Omega)$ with $m \geq 0$ holds*

$$\|v\|^2_{H^1(\Omega)} \leq c_p(|v|^2_{H^1(\Omega)} + m^2). \tag{2.1}$$

Moreover, we introduce the space of linear functionals on $H^1(\Omega)$, which provide the solvability condition of a homogeneous Neumann problem,

$$Y_0(\Omega) := \left\{ f \in (H^1(\Omega))' \ : \ \langle f, 1\rangle = 0 \right\}.$$

This space is endowed with the operator norm $\|\cdot\|_{(H^1(\Omega))'}$.

We further need trace spaces corresponding to $H^l(\Omega)$ on a boundary part $\Gamma \subset \partial\Omega$, Γ is an open subset of $\partial\Omega$. Trace spaces are defined in the sense of Sobolev-Slobodeckij spaces on compact manifolds. A detailed introduction of these spaces is presented in [53] chapter 1.5.2. Here we need $C^{k,1}$-smoothness of $\partial\Omega$ for the definition of $H^s(\Gamma)$, where s and k are related by $k \in \mathbb{N}_0,\ |s| \leq k+1$.

As a special case of [53] theorem 1.5.2.1 we have the following trace theorem with $s = 1$ and $k = 0$:

Theorem 2.2 (Trace theorem). *Let $\Omega \subset \mathbb{R}^d$ be an open and bounded domain with a Lipschitz boundary, $\Gamma \subset \partial\Omega$ be an open subset. Then the mapping*

$$\gamma|_\Gamma : H^1(\Omega) \longrightarrow H^{\frac{1}{2}}(\Gamma),$$
$$\gamma|_\Gamma(v) = v|_\Gamma$$

exists and is understood in the sense of traces. Furthermore, this operator is continuous and there exists a constant $c_\gamma > 0$, such that the following estimate holds

$$\|\gamma|_\Gamma(v)\|_{H^{\frac{1}{2}}(\Gamma)} = \|v\|_{H^{\frac{1}{2}}(\Gamma)} \leq c_\gamma \|v\|_{H^1(\Omega)}. \tag{2.2}$$

In order to consider the viscous Cahn-Larché equations with mixed boundary conditions, we need the trace space $H^{\frac{1}{2}}(\Gamma_D)$ to describe Dirichlet data. The Neumann boundary condition acting on the boundary part Γ_N is understood in a weak sense. Therefore we define the spaces of linear functionals on boundary parts Γ_N and Γ_D by

$$H^{-\frac{1}{2}}(\Gamma_N) := \left(\widetilde{H}^{\frac{1}{2}}(\Gamma_N)\right)', \qquad \widetilde{H}^{-\frac{1}{2}}(\Gamma_D) := \left(H^{\frac{1}{2}}(\Gamma_D)\right)',$$

which are equipped with the usual operator norms. In this definition the space $\widetilde{H}^{\frac{1}{2}}(\Gamma_N)$ is given by

$$\widetilde{H}^{\frac{1}{2}}(\Gamma_N) := \left\{v :\ v = \tilde{v}|_{\Gamma_N},\ \text{where } \tilde{v} \in H^{\frac{1}{2}}(\partial\Omega) \text{ with } \operatorname{supp}(\tilde{v}) \subset \overline{\Gamma}_N\right\},$$

which is endowed with the norm $\|v\|_{\widetilde{H}^{\frac{1}{2}}(\Gamma_N)} := \|\tilde{v}\|_{H^{\frac{1}{2}}(\partial\Omega)}$.

We have to remark that for vector valued boundary loadings the same definitions hold. The space of vector valued Dirichlet data is denoted by $\boldsymbol{H}^{\frac{1}{2}}(\Gamma_D)$, furthermore the space of vector valued Neumann data is described by $\boldsymbol{H}^{-\frac{1}{2}}(\Gamma_N)$.

The function space used for the displacement $\boldsymbol{u}$ must take into account the Dirichlet boundary condition (1.56). In order to consider the hard clamped boundary part we define the space

$$\boldsymbol{X}(\Omega) := \left\{\boldsymbol{v} \in \boldsymbol{H}^1(\Omega) :\ \gamma|_{\Gamma_D}(\boldsymbol{v}) = \boldsymbol{0}\right\},$$

which is endowed with the usual Sobolev norm $\|\cdot\|_{\boldsymbol{H}^1(\Omega)}$ or semi-norm $|\cdot|_{\boldsymbol{H}^1(\Omega)}$.

Lemma 2.3 (Korn's inequality). *Let $\Omega \subset \mathbb{R}^d$ be a domain satisfying condition (H-1), then there exists a constant $c_k > 0$, such that for all $\boldsymbol{v} \in \boldsymbol{X}(\Omega)$ holds*

$$\|\boldsymbol{v}\|^2_{\boldsymbol{H}^1(\Omega)} \leq c_k \int_\Omega \boldsymbol{\varepsilon}(\boldsymbol{v}) : \boldsymbol{\varepsilon}(\boldsymbol{v})\, d\boldsymbol{x}. \tag{2.3}$$

Proof. See for instance [79] page 79. □

As a special case of [2] theorem 6.2 we have the following compact embedding result:

Theorem 2.4 (Rellich-Kondrachov). *Let $\Omega \subset \mathbb{R}^d$ be an open and bounded domain with Lipschitz boundary, then there exists a constant $c_r > 0$ and the following compact embedding holds*

$$H^1(\Omega) \Subset L_q(\Omega); \quad \|v\|_{L_q(\Omega)} \leq c_r \|v\|_{H^l(\Omega)}; \quad 1 \leq q \leq \frac{2d}{d-2}.$$

Furthermore, we need the definition of a Carathéodory function, which is taken from [95].

Definition 2.5 (Carathéodory function). A function $f : \Omega \times \mathbb{R} \times \mathbb{R}^d \longrightarrow \mathbb{R}$ is called Carathéodory function, if and only if

(1) f is measurable in $\boldsymbol{x} \in \Omega$ for all $y \in \mathbb{R}$, $\boldsymbol{p} \in \mathbb{R}^d$,

(2) f is continuous in $y \in \mathbb{R}$ and $\boldsymbol{p} \in \mathbb{R}^d$ for all $\boldsymbol{x} \in \Omega$.

Moreover, we consider a density $f : \Omega \times \mathbb{R} \times \mathbb{R}^d \longrightarrow \mathbb{R}$ and a variational integral

$$I(v) := \int_\Omega f(\boldsymbol{x}, v, \nabla_{\boldsymbol{x}} v)\, d\boldsymbol{x}. \tag{2.4}$$

In [95] theorem 1.6, there is proved the following result on sequentially lower semi weak continuity:

Theorem 2.6. *Let $\Omega \subset \mathbb{R}^d$ an open and bounded domain with Lipschitz boundary. The density $f : \Omega \times \mathbb{R} \times \mathbb{R}^d \longrightarrow \mathbb{R}$ satisfies the following properties:*

(1) f is a Carathéodory function,

(2) $f(\boldsymbol{x}, y, \boldsymbol{p}) \geq \phi(\boldsymbol{x})$ for almost every $\boldsymbol{x} \in \Omega$, $y \in \mathbb{R}$ and $\boldsymbol{p} \in \mathbb{R}^d$, where $\phi \in L_1(\Omega)$,

(3) $f(\boldsymbol{x}, y, \boldsymbol{p})$ is convex in $\boldsymbol{p} \in \mathbb{R}^d$ for almost every $\boldsymbol{x} \in \Omega$ and $y \in \mathbb{R}$.

For a sequence $(v_k)_{k\in\mathbb{N}} \subset H^1(\Omega)$ and $v \in H^1(\Omega)$ with $v_k \rightharpoonup v$ in $H^1(\Omega)$ and $I(\cdot)$ defined by (2.4) follows

$$I(v) \leq \liminf_{k\to\infty} I(v_k).$$

In order to minimise the Helmholtz free energy and maximise the dissipation, we need the following theorem on the existence of minimisers, which is proofed in [29] theorem 1.1 respectively [108].

Theorem 2.7. *Let X be a reflexive Banach space, $I : X \longrightarrow \mathbb{R} \cup \{\infty\}$ be a variational functional. Assuming that there exist constants $C_I, c_I > 0$ such that*

(1) I is coercive, this means $I(v) \geq c_I \|v\|_X - C_I$ for all $v \in X$,

(2) I is weakly lower semi-continuous over X,

(3) there exists a $\bar{u} \in X$ such that $I(\bar{u}) < \infty$,

then there exists at least one solution $u \in X$ of the minimising problem

$$I(u) = \min_{v \in X} I(v).$$

Considering the Gâteaux derivative of the variational functional, then the following lemma holds, which is also proved in [29] theorem 1.3 respectively [108].

Theorem 2.8. *Let X be a Banach space, $I : X \longrightarrow \mathbb{R}$ be a Gâteaux differentiable functional and let $I(u) = \min_{v \in X} I(v)$, then it holds*

$$\langle \mathrm{D}\, I(u), v \rangle = 0 \qquad \text{for all } v \in X.$$

Finally, we introduce Lebesgue spaces with Banach space valued functions, which are necessary to consider time dependent weak problems. Let X be a Banach space, then we get from [30] chapter 18 the definition

$$L_p(0,T;X) := \left\{ v : \ (0,T) \longrightarrow X : \ \|v\|_{L_p(0,T;X)} < \infty \right\},$$

which is in view of [30] also a Banach space equipped with the norm

$$\begin{aligned} \|v\|^p_{L_p(0,T;X)} &:= \int_0^T \|v\|^p_X dt, && 1 \leq p < \infty, \\ \|v\|_{L_\infty(0,T;X)} &:= \operatorname*{ess\,sup}_{t \in (0,T)} \|v\|_X, && p = \infty. \end{aligned}$$

The existence proof of weak solutions of the viscous Cahn-Larché equation system needs essentially the theorem of Arselà-Ascoli for which we refer to [91].

Theorem 2.9 (Arzelà-Ascoli). *Let X be a Banach space, then a set $F \subset C([0,T];X)$ is relatively compact if and only if:*

(1) $F(t) := \{f(t) \ : \ f \in F\}$ is relatively compact in X for all $0 < t < T$,

(2) F is uniformly equicontinuous: $\forall \varepsilon > 0$, $\exists \delta > 0$ such that

$$\|f(t_2)-f(t_1)\|_X \leq \varepsilon, \quad \forall f \in F, \quad \forall\, 0 \leq t_1 \leq t_2 \leq T \quad \text{such that} \quad |t_2-t_1| \leq \delta.$$

In the existence proof of weak solutions of the viscous Cahn-Larché system we use the well known Lebesgue convergence theorem, see e.g. [42] theorem 5.2. But sometimes it is of great advantage to apply the generalised Lebesgue convergence theorem as formulated in [5] theorem A 1.23.

Theorem 2.10 (Generalised Lebesgue convergence theorem). *Let $\Omega \subset \mathbb{R}^d$ be a measurable domain, let $(g_n)_{n\in\mathbb{N}} \subset L_q(\Omega)$ a sequence and $g \in L_q(\Omega)$ with $1 \leq q < \infty$ such that $g_n \longrightarrow g$ in $L_q(\Omega)$. Moreover, let $(f_n)_{n\in\mathbb{N}}$ a sequence of measurable functions and f a measurable function with the property*

$$f_n \longrightarrow f \quad \text{a.e. in } \Omega, \qquad\qquad |f_n|^p \leq |g_n|^q \quad \text{a.e. in } \Omega,$$

with $1 \leq p < \infty$, then it follows $f_n \longrightarrow f$ in $L_p(\Omega)$.

In order to show convergence in $L_1(\Omega)$ we use Vitali's convergence theorem, which is formulated e.g. in [5] theorem A 1.22. For a more general version of Vitali's convergence theorem we refer to [42] chapter 6 theorem 5.6.

Theorem 2.11 (Vitali convergence theorem). *Let $(f_n)_{n\in\mathbb{N}} \subset L_p(\Omega)$ with $1 \leq p < \infty$ and let $f_n \longrightarrow f$ almost everywhere for $n \longrightarrow \infty$. Then the following statements are equivalent:*

(1) $f \in L_p(\Omega)$ and $\|f_n - f\|_{L_p(\Omega)} \longrightarrow 0$ for $n \longrightarrow \infty$.

(2) It holds for all $\mathscr{E} \subset \Omega$

$$\sup_{n\in\mathbb{N}} \int_{\mathscr{E}} |f_n|^p \, d\boldsymbol{x} \longrightarrow 0, \quad \text{if } \operatorname{meas}(\mathscr{E}) \longrightarrow 0,$$

and for all $\varepsilon > 0$ exists a set $\mathscr{E}_\varepsilon$ with $\operatorname{meas}(\mathscr{E}_\varepsilon) < \infty$ and

$$\sup_{n\in\mathbb{N}} \int_{\mathscr{E}_\varepsilon^c} |f_n|^p \, d\boldsymbol{x} \leq \varepsilon.$$

Corollary 2.12. *Let $(f_n)_{n\in\mathbb{N}} \subset L_p(\Omega)$ and $f \in L_p(\Omega)$ with $1 \leq p \leq \infty$ a convergent sequence $f_n \longrightarrow f$, then there exists a convergent subsequence $(f_{n_k})_{k\in\mathbb{N}}$, which is almost everywhere convergent.*

Proof. For the proof see [42]. □

2.1.2 Assumptions

In this section we formulate all sufficient conditions in order to show the existence of weak solutions of the viscous and non-viscous Cahn-Larché system. Moreover, these assumptions also guarantee the existence of a discrete solution of the numerical approximation techniques in chapter four and five. Finally, these assumptions are sufficient to prove the convergence of the approximation methods. We point out whether these assumptions are of physical nature or formulated for technical reasons only. We assume the following constraints on the material parameters and constitutive functions:

(A-1) **Surface stress tensor**: Let $\boldsymbol{\Gamma} \in \mathbb{R}^{d\times d}_{\text{sym}}$ be a symmetric positive definite second order tensor, such that there exist constants $C_\Gamma, c_\Gamma > 0$ with the property, that for all $\boldsymbol{a}, \boldsymbol{b} \in \mathbb{R}^d \setminus \{\boldsymbol{0}\}$ holds

$$|\boldsymbol{\Gamma a} \cdot \boldsymbol{b}| \leq C_\Gamma |\boldsymbol{a}||\boldsymbol{b}|, \qquad \boldsymbol{\Gamma a} \cdot \boldsymbol{a} \geq c_\Gamma |\boldsymbol{a}|^2.$$

We remark, that this assumption is a direct consequence of the formulation of surface energy by Cahn and Hilliard [20, 21] and Cahn [19].

(A-2) **Gibbs free energy density**: Let $\psi(c) := \psi^+(c) + \psi^-(c)$ be a function with $\psi^+, \psi^- \in C^2(\mathbb{R}, \mathbb{R})$, where ψ^+ is a convex function and ψ^- is a concave function. Additionally, we assume, that for all $c \in X_m(\Omega)$ follows $\psi(c) \in L_1(\Omega)$. Furthermore, there exists a constant $c_\psi \geq 0$, such that the homogeneous free energy is bounded below by

$$\psi(c) \geq -c_\psi.$$

Additionally, we assume, that for all $\delta > 0$ exists a constant $C_\delta > 0$ and an upper estimate of the convex part

$$|\psi^+_{,c}(c)| \leq \delta \psi^+(c) + C_\delta.$$

Moreover, there exists a constant $C_\psi > 0$, such that a polynomial estimate of the concave part holds

$$|\psi^-(c)| \leq C_{\psi^-}(|c|^q + 1),$$

where in the case $d = 2$ we have $1 \leq q < \infty$ and in the case $d = 3$, we have $1 \leq q < 6$.
This assumption looks quite technical. In fact it is formulated in such a way, that the following calculations become clearer. But we point out that the spline interpolation of the Gibbs free energy density (1.71) satisfies this condition. In chapter five we calculate explicitly a decomposition of the spline interpolation into a convex and a concave part.

(A-3) **Mobility**: Let $\boldsymbol{M} \in C^0(\mathbb{R}, \mathbb{R}^{d\times d}_{\text{sym}})$ be a second order tensor valued function, such that there exist constants $C_M, c_M > 0$, with the property, that for all $\boldsymbol{a}, \boldsymbol{b} \in \mathbb{R}^d \setminus \{\boldsymbol{0}\}$ and for all $c \in \mathbb{R}$ hold

$$|\boldsymbol{M}(c)\boldsymbol{a} \cdot \boldsymbol{b}| \leq C_M|\boldsymbol{a}||\boldsymbol{b}|, \qquad \boldsymbol{M}(c)\boldsymbol{a} \cdot \boldsymbol{a} \geq c_M|\boldsymbol{a}|^2.$$

(A-4) **Friction**: The friction coefficient is assumed to be non negative,

$$\gamma \geq 0.$$

Assumption (A-3) and (A-4) are a direct consequence of the second law of thermodynamics, which in detail is discussed in (1.44).

(A-5) **Initial condition**: The initial mass concentration has to satisfy the condition

$$c_0 \in H^1(\Omega), \quad \text{with} \quad 0 \leq c_0(\boldsymbol{x}) \leq 1 \text{ almost everywhere.}$$

In view of mass conservation the gauge condition of the concentration field c is given by

$$m := \int_\Omega c_0(\boldsymbol{x})\, d\boldsymbol{x} \quad \text{and it follows} \quad c_0 \in X_m(\Omega).$$

(A-6) **Elasticity tensor**: This quantity is assumed to be a fourth order tensor valued function $\boldsymbol{C}(c) := \{C_{ijkl}(c)\}_{i,j,k,l=1}^d$, such that $C_{i,j,k,l} \in C^2(\mathbb{R}, \mathbb{R})$ and the symmetry property $C_{i,j,k,l} = C_{j,i,k,l} = C_{i,j,l,k}$ must be valid. Additionally, there exist constants $C_C, c_C, C_{C'}, C_{C''} > 0$, such that for all $\boldsymbol{A}, \boldsymbol{B} \in \mathbb{R}^{d\times d} \setminus \{\boldsymbol{0}\}$ and for all $c \in \mathbb{R}$ hold

$$\begin{aligned} &|\boldsymbol{C}(c)\boldsymbol{A} : \boldsymbol{B}| \leq C_C|\boldsymbol{A}||\boldsymbol{B}|, && |\boldsymbol{C}_{,c}(c)\boldsymbol{A} : \boldsymbol{B}| \leq C_{C'}|\boldsymbol{A}||\boldsymbol{B}|, \\ &\boldsymbol{C}(c)\boldsymbol{A} : \boldsymbol{A} \geq c_C|\boldsymbol{A}|^2, && |\boldsymbol{C}_{,cc}(c)\boldsymbol{A} : \boldsymbol{B}| \leq C_{C''}|\boldsymbol{A}||\boldsymbol{B}|. \end{aligned}$$

(A-7) **Eigenstrain**: Let $\overline{\boldsymbol{\varepsilon}} \in C^2(\mathbb{R}, \mathbb{R}^{d\times d}_{\text{sym}})$ be a second order tensor valued function, such that there exist constants $C_{\overline{\boldsymbol{\varepsilon}}}, C_{\overline{\boldsymbol{\varepsilon}}'}, C_{\overline{\boldsymbol{\varepsilon}}''} > 0$, that for all $c \in \mathbb{R}$ hold

$$|\overline{\boldsymbol{\varepsilon}}(c)| \leq C_{\overline{\boldsymbol{\varepsilon}}}, \qquad |\overline{\boldsymbol{\varepsilon}}_{,c}(c)| \leq C_{\overline{\boldsymbol{\varepsilon}}'}, \qquad |\overline{\boldsymbol{\varepsilon}}_{,cc}(c)| \leq C_{\overline{\boldsymbol{\varepsilon}}''}.$$

(A-8) **Mechanical loading**: The mechanical loading can be a distribution $\boldsymbol{g}$. We assume that there exists a constant $c_{\boldsymbol{g}} > 0$, such that

$$\boldsymbol{g} \in C^{0,1}(0, T; \boldsymbol{H}^{-\frac{1}{2}}(\Gamma_N)), \qquad \|\boldsymbol{g}(t_2) - \boldsymbol{g}(t_1)\|_{H^{-\frac{1}{2}}(\Gamma_N)} \leq c_g|t_2 - t_1|.$$

We remark, that in view of the assumptions (A-1), (A-3) the field equations (1.51) and (1.52) represent a fourth order parabolic equation with respect to the mass concentration c, while assumption (A-6) generates a second order elliptic equation for the displacement $\boldsymbol{u}$ by equation (1.53).

2.1.3 Different weak formulations

In this work we distinguish between a semi-weak and a weak formulation of the viscous Cahn-Larché system (1.51) - (1.58). The semi-weak formulation is related to a weak formulation of the field equations (1.51) - (1.53) with respect to space only.

Definition 2.13 (Semi-weak solution). At each time $t \in (0,T)$ a triple $c(t,\cdot) \in X_m(\Omega)$ with $\dot{c}(t,\cdot) \in Y_0(\Omega)$, $\mu(t,\cdot) \in H^1(\Omega)$ and $\boldsymbol{u}(t,\cdot) \in \boldsymbol{X}(\Omega)$ is called semi-weak solution of the field equations (1.51) - (1.53), if it holds

$$\int_\Omega \dot{c}\zeta \, d\boldsymbol{x} + \int_\Omega \boldsymbol{M}(c)\nabla_{\boldsymbol{x}}\mu \cdot \nabla_{\boldsymbol{x}}\zeta \, d\boldsymbol{x} = 0 \qquad \forall \zeta \in X_0(\Omega), \tag{2.5}$$

$$\int_\Omega \mu\xi \, d\boldsymbol{x} = \int_\Omega \boldsymbol{\Gamma}\nabla_{\boldsymbol{x}}c \cdot \nabla_{\boldsymbol{x}}\xi + \psi_{,c}(c)\xi + W_{,c}(c,\boldsymbol{\varepsilon}(\boldsymbol{u}))\xi + \gamma\dot{c}\xi \, d\boldsymbol{x}$$

$$\forall \xi \in H^1(\Omega) \cap L_\infty(\Omega), \tag{2.6}$$

$$\int_\Omega W_{,\boldsymbol{\varepsilon}}(c,\boldsymbol{\varepsilon}(\boldsymbol{u})) : \boldsymbol{\varepsilon}(\boldsymbol{\eta}) \, d\boldsymbol{x} = \int_{\Gamma_N} \boldsymbol{g} \cdot \boldsymbol{\eta} \, d\boldsymbol{a}_{\boldsymbol{x}} \qquad \forall \boldsymbol{\eta} \in \boldsymbol{X}(\Omega), \tag{2.7}$$

$$c(0,\boldsymbol{x}) = c_0(\boldsymbol{x}) \qquad \text{almost everywhere.}$$

Formally, we derive the semi-weak formulation by multiplying the field equations (1.51) - (1.53) with the corresponding test function, integrating over the domain Ω, using Gauß's theorem and taking into account the corresponding boundary conditions (1.54) - (1.57). We remark that in the non-viscous case the term $\gamma\dot{c}\xi$ vanishes and we get the semi-weak formulation of the field equations (1.60) - (1.62).

In this formulation the time derivative of the mass concentration $\dot{c}(t,\cdot) \in Y_0(\Omega)$ is a distribution, which guarantees mass conservation. We further remark, that all integrals in definition 2.13 exist, due to assumption (A-1) - (A-4) and (A-6) - (A-8), and the fact, that we use almost everywhere bounded test functions for the chemical potential.

In order to get some technical estimates, we consider the semi-weak formulation of the quasi steady momentum balance (2.7) with an arbitrary, but fixed mass concentration $c \in X_m(\Omega)$.

Lemma 2.14. *Let $\Omega \subset \mathbb{R}^d$ be a domain satisfying condition (H-1), let the assumption (A-6) - (A-8) be satisfied and let $c \in X_m(\Omega)$ arbitrary, but fixed. Then for the semi-weak momentum balance* (2.7) *the following estimates hold*

(1) $$\left| \int_\Omega \boldsymbol{C}(c)\boldsymbol{\varepsilon}(\boldsymbol{u}) : \boldsymbol{\varepsilon}(\boldsymbol{\eta}) \, d\boldsymbol{x} \right| \leq C_C \|\boldsymbol{u}\|_{\boldsymbol{H}^1(\Omega)} \|\boldsymbol{\eta}\|_{\boldsymbol{H}^1(\Omega)} \qquad \forall \boldsymbol{u}, \boldsymbol{\eta} \in \boldsymbol{X}(\Omega),$$

(2) $$\int_\Omega \boldsymbol{C}(c)\boldsymbol{\varepsilon}(\boldsymbol{\eta}) : \boldsymbol{\varepsilon}(\boldsymbol{\eta}) \, d\boldsymbol{x} \geq \frac{c_C}{c_k} \|\boldsymbol{\eta}\|^2_{\boldsymbol{H}^1(\Omega)} \qquad \forall \boldsymbol{\eta} \in \boldsymbol{X}(\Omega),$$

(3) $$\left| \int_\Omega \boldsymbol{C}(c)\overline{\boldsymbol{\varepsilon}}(c) : \boldsymbol{\varepsilon}(\boldsymbol{\eta}) \, d\boldsymbol{x} + \int_{\Gamma_N} \boldsymbol{g} \cdot \boldsymbol{\eta} \, d\boldsymbol{a}_{\boldsymbol{x}} \right|$$
$$\leq C \left(\|\boldsymbol{g}\|_{C^0(0,T;\boldsymbol{H}^{-\frac{1}{2}}(\Gamma_N))} + \operatorname{meas}^{\frac{1}{2}}(\Omega) \right) \|\boldsymbol{\eta}\|_{H^1(\Omega)} \qquad \forall \boldsymbol{\eta} \in \boldsymbol{X}(\Omega),$$

with a constant $C = C(C_C, C_{\overline{\boldsymbol{\varepsilon}}}, c_\gamma)$.

Proof. (1) follows directly from assumption (A-6) and from Hölder's inequality. *(2)* is a direct consequence of assumption (A-6) and of Korn's inequality (2.3). *(3)* is calculated by using assumptions (A-6) - (A-8), the trace theorem 2.2 and Hölder's inequality. We get

$$\begin{aligned}
&\left| \int_\Omega \boldsymbol{C}(c)\overline{\boldsymbol{\varepsilon}}(c) : \boldsymbol{\varepsilon}(\boldsymbol{\eta})\, d\boldsymbol{x} + \int_{\Gamma_N} \boldsymbol{g}\cdot\boldsymbol{\eta}\, d\boldsymbol{a}_{\boldsymbol{x}} \right| \\
&\quad \leq C_C C_{\overline{\boldsymbol{\varepsilon}}} \int_\Omega |\boldsymbol{\varepsilon}(\boldsymbol{\eta})|\, d\boldsymbol{x} + c_\gamma \|\boldsymbol{g}\|_{C^0(0,T;\boldsymbol{H}^{-\frac{1}{2}}(\Gamma_N))} \|\boldsymbol{\eta}\|_{\boldsymbol{H}^1(\Omega)} \\
&\quad \leq C \left(\|\boldsymbol{g}\|_{C^0(0,T;\boldsymbol{H}^{-\frac{1}{2}}(\Gamma_N))} + \mathrm{meas}^{\frac{1}{2}}(\Omega) \right) \|\boldsymbol{\eta}\|_{\boldsymbol{H}^1(\Omega)},
\end{aligned}$$

with a constant $C = C(C_C, C_{\overline{\boldsymbol{\varepsilon}}}, c_\gamma)$. □

For an arbitrary, but fixed mass concentration $c \in X_m(\Omega)$, due to lemma 2.14 and Lax-Milgram's theorem, see [104] theorem 17.9, there exists a unique displacement $\boldsymbol{u} \in \boldsymbol{X}(\Omega)$ satisfying the semi-weak formulation of the quasi steady equilibrium (2.7). This displacement $\boldsymbol{u}$ satisfies by Lax-Milgram's theorem the following a-priori estimate

$$\|\boldsymbol{u}\|_{\boldsymbol{H}^1(\Omega)} \leq \frac{c_k C}{c_{\boldsymbol{C}}} \left(\|\boldsymbol{g}\|_{C^0(0,T;\boldsymbol{H}^{-\frac{1}{2}}(\Gamma_N))} + \mathrm{meas}^{\frac{1}{2}}(\Omega) \right) =: C_{\boldsymbol{u}}, \tag{2.8}$$

with a constant $C_{\boldsymbol{u}} = C_{\boldsymbol{u}}(C_C, C_{\overline{\boldsymbol{\varepsilon}}}, c_C, c_k, c_\gamma, \boldsymbol{g}, \mathrm{meas}(\Omega))$. As a special case of this result, there exists a unique initial displacement $\boldsymbol{u}_0 \in \boldsymbol{X}(\Omega)$ corresponding to the initial mass concentration $c_0 \in X_m(\Omega)$.

Finally, we give the complete weak formulation of the field equations (1.51) - (1.53), which is a weak formulation with respect to time and space.

Definition 2.15 (Weak solution). A triple $c \in L_2(0,T;X_m(\Omega))$, $\mu \in L_2(0,T;H^1(\Omega))$ and $\boldsymbol{u} \in L_2(0,T;\boldsymbol{X}(\Omega))$ is called weak solution of the field equations (1.51) - (1.53), if it holds

$$\begin{aligned}
&-\int_{\Omega_T} \dot{\zeta}(c-c_0)\, d\boldsymbol{x}dt + \int_{\Omega_T} \boldsymbol{M}(c)\nabla_{\boldsymbol{x}}\mu \cdot \nabla_{\boldsymbol{x}}\zeta\, d\boldsymbol{x}dt = 0 \\
&\qquad \forall \zeta \in L_2(0,T;X_0(\Omega)) \text{ with } \dot{\zeta} \in L_2(\Omega_T) \text{ and } \zeta(T,\boldsymbol{x}) = 0 \text{ a.e.},
\end{aligned} \tag{2.9}$$

$$\begin{aligned}
&\int_{\Omega_T} \mu\xi\, d\boldsymbol{x}dt = \int_{\Omega_T} \boldsymbol{\Gamma}\nabla_{\boldsymbol{x}}c \cdot \nabla_{\boldsymbol{x}}\xi + \psi_{,c}(c)\xi + W_{,c}(c,\boldsymbol{\varepsilon}(\boldsymbol{u}))\xi - \gamma(c-c_0)\dot{\xi}\, d\boldsymbol{x}dt \\
&\forall \xi \in L_2(0,T;H^1(\Omega)) \cap L_\infty(\Omega_T) \text{ with } \dot{\xi} \in L_2(\Omega_T) \text{ and } \xi(T,\boldsymbol{x}) = 0 \text{ a.e.},
\end{aligned} \tag{2.10}$$

$$\int_{\Omega_T} W_{,\boldsymbol{\varepsilon}}(c,\boldsymbol{\varepsilon}(\boldsymbol{u})) : \boldsymbol{\varepsilon}(\boldsymbol{\eta})\, d\boldsymbol{x}dt = \int_{\Gamma_T^N} \boldsymbol{g}\cdot\boldsymbol{\eta}\, d\boldsymbol{a}_{\boldsymbol{x}}dt \quad \forall \boldsymbol{\eta} \in L_2(0,T;\boldsymbol{X}(\Omega)). \tag{2.11}$$

Formally, we get this weak formulation by multiplying the field equations (1.51) - (1.53) with the corresponding test functions, integrating over the domain Ω and time $(0,T)$, using Gauß's theorem and taking into account the boundary conditions (1.54) - (1.57) as well as the initial condition (1.58). Similar as above, all integrals in definition 2.15 exist due to assumption (A-1) - (A-8) and the fact, that we use bounded test functions for the chemical potential. It is obvious that in the non-viscous case the term $\gamma(c-c_0)\dot{\xi}$ does not appear and this leads to the weak formulation of the system (1.60) - (1.62).

2.2 Existence of weak solutions

In this section we prove the existence of weak solutions of the viscous Cahn-Larché system in the sense of definition 2.15.

Theorem 2.16 (Existence of weak solutions). *Let $\Omega \subset \mathbb{R}^d$ be a domain satisfying condition (H-1) and let the assumption (A-1) - (A-8) be satisfied. Then there exists at least one triple $c \in L_\infty(0,T;X_m(\Omega))$, $\mu \in L_2(0,T;H^1(\Omega))$ and $\boldsymbol{u} \in L_\infty(0,T;\boldsymbol{X}(\Omega))$ satisfying the field equations* (1.51) - (1.53) *in the sense of definition 2.15. Moreover, if $\gamma \gneqq 0$ then for the concentration field c additionally holds $\dot{c} \in L_2(\Omega_T)$.*

At this point we give a small overview about the following existence proof, which is similar to Garcke [48], but additionally takes into account the nonlinearity within the mobility tensor, viscous effects and mechanical boundary loadings.

In subsection 2.2.1 we derive a time discretisation of the semi-weak Cahn-Larché system (2.5) - (2.7) similar to [48]. Moreover, we use the time discretisation in order to linearise the mobility tensor. Finally, we are able to eliminate the diffusion equation, such that we end up with a time discrete equation system with two equations for the discrete mass concentration c^n and the discrete displacement $\boldsymbol{u}^n$ at each discrete time. At this point of the proof the flow gradient structure is needed essentially. A corresponding time discrete functional $E^n_{\Delta t}$ is also formulated containing energy and dissipation.

In subsection 2.2.2 we prove the existence of a time discrete solution c^n, μ^n and $\boldsymbol{u}^n$ of the Cahn-Larché system. This is done by minimising the time discrete functional $E^n_{\Delta t}$. From a physical point of view we minimise the Helmholtz free energy (1.49) and maximise the dissipation (1.50). Furthermore, we show for the minimiser, that the weak Euler-Lagrange differential equations corresponds to the discrete semi-weak formulation of the Cahn-Larché system. This is possible, because the time discrete semi-weak formulation of the Cahn-Larché equation system and the discrete energy have a gradient flow structure.

In subsection 2.2.3 we derive uniform a-priori estimates for the discrete solutions of the Cahn-Larché system. Here we essentially use the Lyapunov property of the time discrete energy functional, which means that the system has decreasing energy and goes into an energetic stable state.

In subsection 2.2.4 we show, that the piecewise constant expansion c_N, μ_N and $\boldsymbol{u}_N$ of the time discrete solutions of the Cahn-Larché system converge to a weak solution in the sense of definition 2.15.

2.2.1 Time discretisation

In the first step of this existence proof, we observe a uniform decomposition of the time interval $(0, T)$ into N parts and define a time step by

$$\Delta t := \frac{T}{N}.$$

For a short notation we introduce the boundary loading at time $t = n\Delta t$ for all $0 \leq n \leq N$ by

$$\boldsymbol{g}^n(\boldsymbol{x}) := \boldsymbol{g}(n\Delta t, \boldsymbol{x}).$$

The boundary loading will be approximated by a piecewise constant expansion $\boldsymbol{g}_N(t, \boldsymbol{x}) = \boldsymbol{g}^n(\boldsymbol{x})$ for $t \in ((n-1)\Delta t, n\Delta t]$ with $1 \leq n \leq N$. Further, we denote the time discrete solution of the viscous Cahn-Larché system at time $t = n\Delta t$ for all $0 \leq n \leq N$ by

$$c^n(\boldsymbol{x}) := c(n\Delta t, \boldsymbol{x}); \quad \mu^n(\boldsymbol{x}) := \mu(n\Delta t, \boldsymbol{x}); \quad \boldsymbol{u}^n(\boldsymbol{x}) := \boldsymbol{u}(n\Delta t, \boldsymbol{x}). \tag{2.12}$$

In the following, the functions c^n, μ^n and $\boldsymbol{u}^n$ are considered as unknowns. Moreover, we formulate a piecewise constant expansion of these functions with respect to time and define for all $1 \leq n \leq N$ at time $t \in ((n-1)\Delta t, n\Delta t]$

$$c_N(t, \boldsymbol{x}) := c^n(\boldsymbol{x}); \quad \mu_N(t, \boldsymbol{x}) := \mu^n(\boldsymbol{x}); \quad \boldsymbol{u}_N(t, \boldsymbol{x}) := \boldsymbol{u}^n(\boldsymbol{x}). \tag{2.13}$$

The time derivative of the mass concentration in the diffusion equation (1.51) will be approximated by an implicit Eulerian scheme. We get for all $1 \leq n \leq N$

$$\dot{c}_N(n\Delta t, \boldsymbol{x}) \approx \frac{c^n(\boldsymbol{x}) - c^{n-1}(\boldsymbol{x})}{\Delta t} =: \partial_{\Delta t} c^n(\boldsymbol{x}). \tag{2.14}$$

Additionally to the piecewise constant interpolant c_N, we introduce a piecewise linear interpolant of the mass concentration $\bar{c}_N$. For all $1 \leq n \leq N$ we define at time $t \in ((n-1)\Delta t, n\Delta t]$

$$\bar{c}_N(t, \boldsymbol{x}) := c^n(\boldsymbol{x}) \left(\frac{t - (n-1)\Delta t}{\Delta t} \right) - c^{n-1}(\boldsymbol{x}) \left(\frac{t - n\Delta t}{\Delta t} \right), \tag{2.15}$$

$$\dot{\bar{c}}_N(t, \boldsymbol{x}) = \frac{c^n(\boldsymbol{x}) - c^{n-1}(\boldsymbol{x})}{\Delta t}. \tag{2.16}$$

Finally, we apply the time discretisation (2.12) to linearise the mobility tensor in order to get a linear diffusion equation. Therefore, we define the linearised mobility tensor

$$\boldsymbol{M}^{n-1}(\boldsymbol{x}) := \boldsymbol{M}(c^{n-1}(\boldsymbol{x})). \tag{2.17}$$

Inserting the time discretisation (2.12) and (2.14) as well as the linearised mobility tensor (2.17) into the semi-weak problem given by definition 2.13, we end up with the definition of a discrete semi-weak solution. Time t is observed as a parameter in the definition of a discrete semi-weak solution.

Definition 2.17. At each discrete time $t = n\Delta t$, $1 \leq n \leq N$, a triple $c^n \in X_m(\Omega)$, $\mu^n \in H^1(\Omega)$ and $\boldsymbol{u}^n \in \boldsymbol{X}(\Omega)$ is called discrete semi-weak solution of the field equations (1.51) - (1.53), if it holds

$$\int_\Omega \partial_{\Delta t} c^n \zeta \, d\boldsymbol{x} + \int_\Omega \boldsymbol{M}^{n-1} \nabla_{\boldsymbol{x}} \mu^n \cdot \nabla_{\boldsymbol{x}} \zeta \, d\boldsymbol{x} = 0 \qquad \forall \zeta \in X_0(\Omega), \tag{2.18}$$

$$\int_\Omega \mu^n \xi \, d\boldsymbol{x} = \int_\Omega \boldsymbol{\Gamma} \nabla_{\boldsymbol{x}} c^n \cdot \nabla_{\boldsymbol{x}} \xi + \psi_{,c}(c^n)\xi + W_{,c}(c^n, \boldsymbol{\varepsilon}(\boldsymbol{u}^n))\xi + \gamma \partial_{\Delta t} c^n \xi \, d\boldsymbol{x} \qquad \forall \xi \in H^1(\Omega) \cap L_\infty(\Omega), \tag{2.19}$$

$$\int_\Omega W_{,\boldsymbol{\varepsilon}}(c^n, \boldsymbol{\varepsilon}(\boldsymbol{u}^n)) : \boldsymbol{\varepsilon}(\boldsymbol{\eta}) \, d\boldsymbol{x} = \int_{\Gamma_N} \boldsymbol{g}^n \cdot \boldsymbol{\eta} \, d\boldsymbol{a}_{\boldsymbol{x}} \qquad \forall \boldsymbol{\eta} \in \boldsymbol{X}(\Omega). \tag{2.20}$$

We calculate a discrete semi-weak solution of the Cahn-Larché system by minimising the energy. In order to apply this technique, we eliminate the diffusion equation (2.18) by using a shift operator corresponding to the linearised mobility tensor (2.17). From a physical point of view we derive a relation between the diffusion equation and the dissipation functional.

Definition 2.18. Let $\Omega \subset \mathbb{R}^d$ be an open and bounded domain with a Lipschitz boundary, then the operator $\mathcal{M}^n$ is defined by

$$\begin{aligned} &\mathcal{M}^n : \ X_0(\Omega) \longrightarrow Y_0(\Omega), \\ &\langle \mathcal{M}^n \mu, \zeta \rangle := \int_\Omega \boldsymbol{M}^{n-1} \nabla_{\boldsymbol{x}} \mu \cdot \nabla_{\boldsymbol{x}} \zeta \, d\boldsymbol{x} \qquad \forall \zeta \in X_0(\Omega). \end{aligned}$$

The operator $\mathcal{M}^n$ corresponds to a Laplace operator with a material tensor $\boldsymbol{M}^{n-1}$ and homogeneous Neumann boundary conditions.

Lemma 2.19. *Let $\Omega \subset \mathbb{R}^d$ be an open and bounded Lipschitz domain and let assumption (A-3) be satisfied, then for the operator $\mathcal{M}^n$ the following estimates hold*

(1) $|\langle \mathcal{M}^n \mu, \zeta \rangle| \leq C_M \|\mu\|_{H^1(\Omega)} \|\zeta\|_{H^1(\Omega)} \qquad \forall \mu, \zeta \in X_0(\Omega),$

(2) $\langle \mathcal{M}^n \zeta, \zeta \rangle \geq \dfrac{c_M}{c_p} \|\zeta\|^2_{H^1(\Omega)} \qquad \forall \zeta \in X_0(\Omega).$

Proof. (1) follows directly from (A-3) and Hölder's inequality. *(2)* is a consequence of (A-3) and Poincaré's inequality (2.1). □

In view of Lax-Milgram's theorem the inverse operator of $\mathcal{M}^n$ exists and it is denoted by $(\mathcal{M}^n)^{-1}$. By using the operator $(\mathcal{M}^n)^{-1}$ we introduce an inner product and a norm on the space $Y_0(\Omega)$, corresponding to the dissipation of spinodal decomposition.

Definition 2.20. Let $f, g \in Y_0(\Omega)$, then the inner product with respect to $(\mathcal{M}^n)^{-1}$ is defined by

$$\langle f, g \rangle_{\mathcal{M}^n} := \int_\Omega \boldsymbol{M}^{n-1} \nabla_{\boldsymbol{x}} (\mathcal{M}^n)^{-1} f \cdot \nabla_{\boldsymbol{x}} (\mathcal{M}^n)^{-1} g \, d\boldsymbol{x},$$

the corresponding norm is given by

$$\|f\|^2_{\mathcal{M}^n} := \langle f, f \rangle_{\mathcal{M}^n}.$$

We identify a function $v \in X_0(\Omega)$ with a functional in $Y_0(\Omega)$ via the following shift operator,

$$\begin{aligned} &\mathcal{S} : \ X_0(\Omega) \longrightarrow Y_0(\Omega), \qquad (2.21)\\ &\langle \mathcal{S} v, \zeta \rangle = \int_\Omega v\zeta \, d\boldsymbol{x}, \qquad \forall \zeta \in X_0(\Omega). \end{aligned}$$

Finally, we are able to eliminate the discrete semi-weak diffusion equation (2.18), in order to reduce the equation system (2.18) - (2.20) onto a system with only two equations for the unknowns c^n and $\boldsymbol{u}^n$. Therefore, we identify $\partial_{\Delta t} c^n$ with an element from $Y_0(\Omega)$ by the shift operator $\mathcal{S}$ and apply the operator $(\mathcal{M}^n)^{-1}$ onto the discrete semi-weak diffusion equation (2.18) in order to deduce

$$\mu^n = -(\mathcal{M}^n)^{-1} \partial_{\Delta t} c^n \in X_0(\Omega). \qquad (2.22)$$

We remark, that for any Lagrangian multiplier $\lambda^n \in \ker(\mathcal{M}^n) = \mathbb{R}$

$$\mu^n = -(\mathcal{M}^n)^{-1} \partial_{\Delta t} c^n + \lambda^n \in H^1(\Omega) \qquad (2.23)$$

holds and is also a solution of the discrete semi-weak diffusion equation (2.18).

Let $\xi \in X_0(\Omega)$ be a test function, then we use assumption (A-3), the symmetry of $\boldsymbol{M}^{n-1}$ and definition 2.18 and calculate

$$\begin{aligned}\int_\Omega \mu^n \xi \, d\boldsymbol{x} &= -\int_\Omega (\mathcal{M}^n)^{-1}\partial_{\Delta t} c^n \xi \, d\boldsymbol{x} = -\big\langle (\mathcal{M}^n)^{-1}\partial_{\Delta t} c^n, \mathcal{M}^n(\mathcal{M}^n)^{-1}\xi \big\rangle \\ &= -\int_\Omega \boldsymbol{M}^{n-1}\nabla_{\boldsymbol{x}}(\mathcal{M}^n)^{-1}\partial_{\Delta t} c^n \cdot \nabla_{\boldsymbol{x}}(\mathcal{M}^n)^{-1}\xi \, d\boldsymbol{x} = -\langle \partial_{\Delta t} c^n, \xi\rangle_{\mathcal{M}^n}\end{aligned} \tag{2.24}$$

In view of calculation (2.24) we restrict the discrete semi-weak problem given by definition 2.17 to a weak problem with only two equations for the mass concentration c^n and the displacement $\boldsymbol{u}^n$.

Problem 2.21. At each discrete time $t = n\Delta t$, $1 \le n \le N$, we have to find $c^n \in X_m(\Omega)$ and $\boldsymbol{u}^n \in \boldsymbol{X}(\Omega)$, such that holds

$$\int_\Omega \boldsymbol{\Gamma}\nabla_{\boldsymbol{x}} c^n \cdot \nabla_{\boldsymbol{x}}\xi + \psi_{,c}(c^n)\xi + W_{,c}(c^n, \boldsymbol{\varepsilon}(\boldsymbol{u}^n))\xi + \gamma\partial_{\Delta t} c^n \xi \, d\boldsymbol{x} = -\langle \partial_{\Delta t} c^n, \xi\rangle_{\mathcal{M}^n}$$

$$\forall \xi \in X_0(\Omega) \cap L_\infty(\Omega),$$

$$\int_\Omega W_{,\boldsymbol{\varepsilon}}(c^n, \boldsymbol{\varepsilon}(\boldsymbol{u}^n)) : \boldsymbol{\varepsilon}(\boldsymbol{\eta}) \, d\boldsymbol{x} = \int_{\Gamma_N} \boldsymbol{g}^n \cdot \boldsymbol{\eta} \, d\boldsymbol{a}_{\boldsymbol{x}} \qquad \boldsymbol{\eta} \in \boldsymbol{X}(\Omega).$$

The corresponding energy to problem 2.21 is called discrete energy. At time $t_n = n\Delta t$ it contains the Helmholtz free energy functional $E(t_n, \cdot, \cdot)$ defined by (1.49) and the dissipation. For all $d \in X_m(\Omega)$ and $\boldsymbol{v} \in \boldsymbol{X}(\Omega)$ the discrete energy is given by

$$E^n_{\Delta t}(d, \boldsymbol{v}) := E(t_n, d, \boldsymbol{v}) + \frac{1}{2\Delta t}\|d - c^{n-1}\|^2_{\mathcal{M}^n} + \frac{\gamma}{2\Delta t}\|d - c^{n-1}\|^2_{L_2(\Omega)}. \tag{2.25}$$

We directly see, that problem 2.21 and the discrete energy (2.25) satisfy a gradient flow structure with respect to the inner product $\langle\cdot,\cdot\rangle_{\mathcal{M}^n}$ and $\langle\cdot,\cdot\rangle_{L_2(\Omega)}$. For a physical understanding we make the following calculation

$$\begin{aligned}&\frac{1}{2\Delta t}\|c^n - c^{n-1}\|^2_{\mathcal{M}^n} + \frac{\gamma}{2\Delta t}\|c^n - c^{n-1}\|^2_{L_2(\Omega)} \\ &\quad= \frac{\Delta t}{2}\int_\Omega \boldsymbol{M}^{n-1}\nabla_{\boldsymbol{x}}(\mathcal{M}^n)^{-1}\partial_{\Delta t} c^n \cdot \nabla_{\boldsymbol{x}}(\mathcal{M}^n)^{-1}\partial_{\Delta t} c^n + \gamma(\partial_{\Delta t} c^n)^2 \, d\boldsymbol{x} \\ &\quad= \frac{\Delta t}{2}\int_\Omega \boldsymbol{M}^{n-1}\nabla_{\boldsymbol{x}}\mu^n \cdot \nabla_{\boldsymbol{x}}\mu^n + \gamma(\dot{\bar{c}}_N)^2 \, d\boldsymbol{x} = -\Delta t D_\gamma(c^{n-1}, \dot{\bar{c}}^n, \mu^n).\end{aligned} \tag{2.26}$$

This calculation shows, that minimisation of the discrete energy (2.25) means minimisation of the Helmholtz free energy and maximisation of the dissipation.

2.2.2 Energy minimisation

In the second step of this existence proof we calculate a solution of problem 2.21 by minimising the discrete energy (2.25).

Lemma 2.22. *Let $\Omega \subset \mathbb{R}^d$ be a domain satisfying condition (H-1), let the assumptions (A-1) - (A-8) be satisfied. Then there exists at least one tuple $c^n \in X_m(\Omega)$ and $\boldsymbol{u}^n \in \boldsymbol{X}(\Omega)$ such that*

$$E^n_{\Delta t}(c^n, \boldsymbol{u}^n) = \min_{\substack{d \in X_m(\Omega), \\ \boldsymbol{v} \in \boldsymbol{X}(\Omega)}} E^n_{\Delta t}(d, \boldsymbol{v}).$$

We remark, that the tuple of the mass concentration c^n and the displacement $\boldsymbol{u}^n$ is called the minimiser of the discrete energy $E^n_{\Delta t}$.

Proof. **Step 1**: In order to prove lemma 2.22 we first show, that $E^n_{\Delta t}$ is a coercive functional on the space $X_m(\Omega) \times \boldsymbol{X}(\Omega)$, see [29] chapter 3.0.

We consider the surface energy, take into account (A-1) and apply Poincaré's inequality (2.1) in order to calculate

$$\int_\Omega \frac{1}{2} \boldsymbol{\Gamma} \nabla_{\boldsymbol{x}} d \cdot \nabla_{\boldsymbol{x}} d \, d\boldsymbol{x} \geq \frac{c_\Gamma}{2c_p} \|d\|^2_{H^1(\Omega)} - \frac{c_\Gamma}{2} m^2.$$

The homogeneous free energy is bounded below as outlined in assumption (A-2) and therefore we get

$$\int_\Omega \psi(d) \, d\boldsymbol{x} \geq -c_\psi \operatorname{meas}(\Omega).$$

The strain energy is estimated below by using assumption (A-6) and (A-7), Young's inequality, Hölder's inequality and Korn's inequality (2.3). We get

$$\begin{aligned} \int_\Omega W(d, \boldsymbol{\varepsilon}(\boldsymbol{v})) \, d\boldsymbol{x} &\geq \frac{c_C}{2} \int_\Omega \boldsymbol{\varepsilon}(\boldsymbol{v}) : \boldsymbol{\varepsilon}(\boldsymbol{v}) - 2\overline{\boldsymbol{\varepsilon}}(d) : \boldsymbol{\varepsilon}(\boldsymbol{v}) + \overline{\boldsymbol{\varepsilon}}(d) : \overline{\boldsymbol{\varepsilon}}(d) \, d\boldsymbol{x} \\ &\geq \frac{c_C}{2} \int_\Omega \frac{1}{2} \boldsymbol{\varepsilon}(\boldsymbol{v}) : \boldsymbol{\varepsilon}(\boldsymbol{v}) - \overline{\boldsymbol{\varepsilon}}(d) : \overline{\boldsymbol{\varepsilon}}(d) \, d\boldsymbol{x} \\ &\geq \frac{c_C}{4c_k} \|\boldsymbol{v}\|^2_{H^1(\Omega)} - \frac{c_c C^2_{\overline{\boldsymbol{\varepsilon}}}}{2} \operatorname{meas}(\Omega). \end{aligned}$$

The energy of the boundary loading is estimated by using assumption (A-8), the trace theorem with estimate (2.2) and Young's inequality. We estimate

$$\begin{aligned} \int_{\Gamma_N} \boldsymbol{g}^n \cdot \boldsymbol{v} \, d\boldsymbol{a}_{\boldsymbol{x}} &\leq c_\gamma \|\boldsymbol{g}\|_{C^0(0,T;\boldsymbol{H}^{-\frac{1}{2}}(\Gamma_N))} \|\boldsymbol{v}\|_{\boldsymbol{H}^1(\Omega)} \\ &\leq \frac{c^2_\gamma}{\delta} \|\boldsymbol{g}\|^2_{C^0(0,T;\boldsymbol{H}^{-\frac{1}{2}}(\Gamma_N))} + \delta \|\boldsymbol{v}\|^2_{\boldsymbol{H}^1(\Omega)}. \end{aligned}$$

Finally, we choose $\delta = \frac{c_C}{8c_k}$, summarise the above calculations and estimate the dissipative terms of the time discrete functional $E^n_{\Delta t}$ below by zero. We get

$$\begin{aligned} E^n_N(d,\boldsymbol{v}) &\geq \frac{c_\Gamma}{2c_p}\|d\|^2_{H^1(\Omega)} + \frac{c_C}{8c_k}\|\boldsymbol{v}\|^2_{\boldsymbol{H}^1(\Omega)} + \frac{1}{2\Delta t}\|d-c^{n-1}\|^2_{\mathcal{M}^n} \\ &\quad + \frac{\gamma}{2\Delta t}\|d-c^{n-1}\|^2_{L_2(\Omega)} - C \\ &\geq \frac{c_\Gamma}{2c_p}\|d\|^2_{H^1(\Omega)} + \frac{c_C}{8c_k}\|\boldsymbol{v}\|^2_{\boldsymbol{H}^1(\Omega)} - C, \end{aligned}$$

with a constant $C = C(C_{\overline{\boldsymbol{\varepsilon}}}, c_\gamma, c_c, c_\psi, m, c_k, c^{n-1}, \boldsymbol{g}, \mathrm{meas}(\Omega))$.

Step 2: In the next step we show, that the discrete energy is sequentially weakly lower semi-continuous, see [29] chapter 3.1.1. Let $(d_k)_{k\in\mathbb{N}} \subset X_m(\Omega)$ and $(\boldsymbol{v}_k)_{k\in\mathbb{N}} \subset \boldsymbol{X}(\Omega)$ be weak-convergent sequences,

$$d_k \rightharpoonup d \quad \text{in } X_m(\Omega), \qquad \boldsymbol{v}_k \rightharpoonup \boldsymbol{v} \quad \text{in } \boldsymbol{X}(\Omega), \qquad k \to \infty.$$

Due to Rellich-Kondrachov's embedding theorem, we know, that $X_m(\Omega) \Subset L_q(\Omega)$, where q is chosen as in (A-2) assumed, and therefore $(d_k)_{k\in\mathbb{N}}$ converges strongly in $L_q(\Omega)$,

$$d_k \to d \quad \text{in } L_q(\Omega), \qquad k \to \infty.$$

We first consider the surface energy and remark, that the density $\frac{1}{2}\boldsymbol{\Gamma}\nabla_{\boldsymbol{x}} d \cdot \nabla_{\boldsymbol{x}} d$ is continuous in $\nabla_{\boldsymbol{x}} d$. Furthermore, the positive definiteness of $\boldsymbol{\Gamma}$, postulated in assumption (A-1), yields a boundedness from below and convexity with respect to $\nabla_{\boldsymbol{x}} d$. Applying theorem 2.6, we get

$$\int_\Omega \frac{1}{2}\boldsymbol{\Gamma}\nabla_{\boldsymbol{x}} d \cdot \nabla_{\boldsymbol{x}} d \; d\boldsymbol{x} \leq \liminf_{k\to\infty} \int_\Omega \frac{1}{2}\boldsymbol{\Gamma}\nabla_{\boldsymbol{x}} d_k \cdot \nabla_{\boldsymbol{x}} d_k \; d\boldsymbol{x}.$$

The first term of the homogeneous free energy ψ^+ is a continuous and convex function with respect to d, see assumption (A-2), and therefore the convergence follows from [29] chapter 2. The second part ψ^- is a continuous function with respect to d and polynomial bounded by assumption (A-2), hence the convergence follows from the generalised Lebesgue convergence theorem 2.10. Therefore we get

$$\int_\Omega \psi(d) \; d\boldsymbol{x} \leq \liminf_{k\to\infty} \int_\Omega \psi(d_k) \; d\boldsymbol{x}.$$

The strain energy is observed by using the convexity of W with respect to the strain

$\boldsymbol{\varepsilon}(\boldsymbol{v})$, which follows from assumption (A-6).

$$\begin{aligned}
&\int_\Omega W(d_k, \boldsymbol{\varepsilon}(\boldsymbol{v}_k)) - W(d, \boldsymbol{\varepsilon}(\boldsymbol{v}))\, d\boldsymbol{x} \\
&\quad = \int_\Omega W(d_k, \boldsymbol{\varepsilon}(\boldsymbol{v}_k)) - W(d_k, \boldsymbol{\varepsilon}(\boldsymbol{v})) + W(d_k, \boldsymbol{\varepsilon}(\boldsymbol{v})) - W(d, \boldsymbol{\varepsilon}(\boldsymbol{v}))\, d\boldsymbol{x} \\
&\quad \geq \int_\Omega W_{,\boldsymbol{\varepsilon}}(d_k, \boldsymbol{\varepsilon}(\boldsymbol{v})) : (\boldsymbol{\varepsilon}(\boldsymbol{v}_k) - \boldsymbol{\varepsilon}(\boldsymbol{v})) + W(d_k, \boldsymbol{\varepsilon}(\boldsymbol{v})) - W(d, \boldsymbol{\varepsilon}(\boldsymbol{v}))\, d\boldsymbol{x} \\
&\quad = \int_\Omega (W_{,\boldsymbol{\varepsilon}}(d_k, \boldsymbol{\varepsilon}(\boldsymbol{v})) - W_{,\boldsymbol{\varepsilon}}(d, \boldsymbol{\varepsilon}(\boldsymbol{v}))) : (\boldsymbol{\varepsilon}(\boldsymbol{v}_k) - \boldsymbol{\varepsilon}(\boldsymbol{v}))
\end{aligned}$$

This calculation together with the almost everywhere convergence of $(d_k)_{k\in\mathbb{N}}$, assumptions (A-6), (A-7) and Lebesgue's convergence theorem as well as the weak convergence of $(\boldsymbol{v}_k)_{k\in\mathbb{N}}$ yield

$$\int_\Omega W(d, \boldsymbol{\varepsilon}(\boldsymbol{v}))\, d\boldsymbol{x} \leq \liminf_{k\to\infty} \int_\Omega W(d_k, \boldsymbol{\varepsilon}(\boldsymbol{v}_k))\, d\boldsymbol{x}.$$

The convergence of the energy of the boundary loading is achieved due to the fact that it provides a linear functional with respect to $\boldsymbol{v}$ and we have the weak convergence of $(\boldsymbol{v}_k)_{k\in\mathbb{N}}$. This leads to

$$\int_{\Gamma_N} \boldsymbol{g}^n \cdot \boldsymbol{v}\, d\boldsymbol{a}_{\boldsymbol{x}} = \lim_{k\to\infty} \int_{\Gamma_N} \boldsymbol{g}^n \cdot \boldsymbol{v}_k\, d\boldsymbol{a}_{\boldsymbol{x}}.$$

For the dissipation part of the discrete energy, we use the convexity of the norms $\|\cdot\|_{\mathcal{M}^n}$ and $\|\cdot\|_{L_2(\Omega)}$ as well as the weak convergence of $(d_k)_{k\in\mathbb{N}}$ and theorem 2.6 in order to derive directly

$$\begin{aligned}
\frac{1}{2\Delta t}\|d - c^{n-1}\|^2_{\mathcal{M}^n} &\leq \liminf_{k\to\infty} \frac{1}{2\Delta t}\|d_k - c^{n-1}\|^2_{\mathcal{M}^n}, \\
\frac{\gamma}{2\Delta t}\|d - c^{n-1}\|^2_{L_2(\Omega)} &\leq \liminf_{k\to\infty} \frac{\gamma}{2\Delta t}\|d_k - c^{n-1}\|^2_{L_2(\Omega)}.
\end{aligned}$$

Summing up all calculations of this step, we get the sequentially weak lower semi continuity of the discrete energy

$$E^n_{\Delta t}(d, \boldsymbol{v}) \leq \liminf_{k\to\infty} E^n_{\Delta t}(d_k, \boldsymbol{v}_k).$$

Step 1 and step 2 present all conditions, which are necessary to apply theorem 2.7, from which the existence of a minimiser $c^n \in X_m(\Omega)$ and $\boldsymbol{u}^n \in \boldsymbol{X}(\Omega)$ follows. □

We now show, that c^n and $\boldsymbol{u}^n$ solve the discrete problem 2.21.

Lemma 2.23. *Let $\Omega \subset \mathbb{R}^d$ be a domain satisfying condition (H-1) and let the assumptions (A-1) - (A-8) be satisfied. For an arbitrary test function $\xi \in H^1(\Omega) \cap L_\infty(\Omega)$ and $\boldsymbol{\eta} \in \boldsymbol{X}(\Omega)$ the Gâteaux derivative of $E^n_{\Delta t}$ exists and it holds*

$$\begin{aligned}
&\lim_{\delta\to 0} \frac{E^n_{\Delta t}(d+\delta\xi, \boldsymbol{v}+\delta\boldsymbol{\eta}) - E^n_{\Delta t}(d,\boldsymbol{v})}{\delta} \\
&\quad = \int_\Omega \boldsymbol{\Gamma}\nabla_{\boldsymbol{x}} d\cdot\nabla_{\boldsymbol{x}}\xi + \psi_{,c}(d)\xi + W_{,c}(d,\boldsymbol{\varepsilon}(\boldsymbol{v}))\xi + W_{,\boldsymbol{\varepsilon}}(d,\boldsymbol{\varepsilon}(\boldsymbol{v})) : \boldsymbol{\varepsilon}(\boldsymbol{\eta})\, d\boldsymbol{x} \\
&\qquad - \int_{\Gamma_N} \boldsymbol{g}\cdot\boldsymbol{\eta}\, d\boldsymbol{a}_{\boldsymbol{x}} + \frac{1}{\Delta t}\big\langle d - c^{n-1}, \xi\big\rangle_{\mathcal{M}^n} + \frac{\gamma}{\Delta t}\big\langle d - c^{n-1}, \xi\big\rangle_{L_2(\Omega)}. \qquad (2.27)
\end{aligned}$$

Proof. We start this proof by considering the surface energy, using assumption (A-1) and calculate

$$\begin{aligned}
&\lim_{\delta\to 0}\frac{1}{\delta}\int_\Omega \frac{1}{2}\boldsymbol{\Gamma}\nabla_{\boldsymbol{x}}(d+\delta\xi)\cdot\nabla_{\boldsymbol{x}}(d+\delta\xi) - \frac{1}{2}\boldsymbol{\Gamma}\nabla_{\boldsymbol{x}} d\cdot\nabla_{\boldsymbol{x}} d\, d\boldsymbol{x} \\
&\quad = \lim_{\delta\to 0}\frac{1}{\delta}\int_\Omega \frac{1}{2}\boldsymbol{\Gamma}\nabla_{\boldsymbol{x}} d\cdot\nabla_{\boldsymbol{x}} d + \delta\boldsymbol{\Gamma}\nabla_{\boldsymbol{x}} d\cdot\nabla_{\boldsymbol{x}}\xi + \frac{1}{2}\delta^2\boldsymbol{\Gamma}\nabla_{\boldsymbol{x}}\xi\cdot\nabla_{\boldsymbol{x}}\xi - \frac{1}{2}\boldsymbol{\Gamma}\nabla_{\boldsymbol{x}} d\cdot\nabla_{\boldsymbol{x}} d\, d\boldsymbol{x} \\
&\quad = \int_\Omega \boldsymbol{\Gamma}\nabla_{\boldsymbol{x}} d\cdot\nabla_{\boldsymbol{x}}\xi\, d\boldsymbol{x}.
\end{aligned}$$

Furthermore, we observe ψ^+, the first term of the homogeneous free energy, which is in view of assumption (A-2) a convex function. Without loss of generality we work with a test function $\xi \in H^1(\Omega)\cap L_\infty(\Omega)$ with $\|\xi\|_{L_\infty(\Omega)} \le 1$ and get

$$\begin{aligned}
\psi^+(d+\delta\xi) &\le \psi^+(d) + \delta\psi^+_{,c}(d+\delta\xi)\xi \le \psi^+(d) + \delta|\psi^+_{,c}(d+\delta\xi)|\|\xi\|_{L_\infty(\Omega)} \\
&\le \psi^+(d) + \delta(\psi^+(d+\delta\xi) + C) \qquad (2.28)\\
(1-\delta)\psi^+(d+\delta\xi) &\le \psi^+(d) + \delta C.
\end{aligned}$$

Since we are interested in the case $\delta \to 0$, we determine for all $\delta \le \frac{1}{2}$,

$$\psi^+(d+\delta\xi) \le 2\psi^+(d) + C. \qquad (2.29)$$

We show that for all $\delta \le \frac{1}{2}$ the difference quotient of ψ^+ is uniformly bounded by using estimate (2.28) and (2.29)

$$\begin{aligned}
&\left|\frac{\psi^+(d+\delta\xi)-\psi^+(d)}{\delta}\right| \le \left|\frac{\psi^+(d)+\delta(\psi^+(d+\delta\xi)+C)-\psi^+(d)}{\delta}\right| \\
&\quad \le 2(\psi^+(d)+C).
\end{aligned}$$

From assumption (A-2) we get $\psi^+ \in C^2(\mathbb{R},\mathbb{R})$, in combination with the uniform boundedness of the difference quotient and Lebesgue's convergence theorem we calculate

$$\lim_{\delta\to 0}\int_\Omega \frac{\psi^+(d+\delta\xi)-\psi^+(d)}{\delta}\, d\boldsymbol{x} = \int_\Omega \psi^+_{,c}(d)\xi\, d\boldsymbol{x}.$$

Considering the non-convex term of the homogeneous free energy we know from assumption (A-2) that $\psi^- \in C^2(\mathbb{R},\mathbb{R})$ and we have a polynomial boundedness. Due to this fact, we get by using the generalised Lebesgue's convergence theorem

$$\lim_{\delta\to 0}\int_\Omega \frac{\psi^-(d+\delta\xi)-\psi^-(d)}{\delta}\,d\boldsymbol{x} = \int_\Omega \psi^-_{,c}(d)\xi\,d\boldsymbol{x}.$$

Moreover, the strain energy is observed by using again the mean value theorem together with assumptions (A-6) and (A-7) as well as Lebesgue's convergence theorem to calculate

$$\begin{aligned}
&\lim_{\delta\to 0}\frac{1}{\delta}\int_\Omega W(d+\delta\xi,\boldsymbol{\varepsilon}(\boldsymbol{v}+\delta\boldsymbol{\eta}))-W(d,\boldsymbol{\varepsilon}(\boldsymbol{v}))\,d\boldsymbol{x}\\
&\quad=\lim_{\delta\to 0}\frac{1}{\delta}\int_\Omega W(d+\delta\xi,\boldsymbol{\varepsilon}(\boldsymbol{v}+\delta\boldsymbol{\eta}))-W(d,\boldsymbol{\varepsilon}(\boldsymbol{v}+\delta\boldsymbol{\eta}))\\
&\qquad\qquad+W(d,\boldsymbol{\varepsilon}(\boldsymbol{v}+\delta\boldsymbol{\eta}))-W(d,\boldsymbol{\varepsilon}(\boldsymbol{v}))\,d\boldsymbol{x}\\
&\quad=\lim_{\delta\to 0}\int_\Omega W_{,c}(d+\nu(\delta)\xi,\boldsymbol{\varepsilon}(\boldsymbol{v}+\delta\boldsymbol{\eta}))\xi+W_{,\boldsymbol{\varepsilon}}(d,\boldsymbol{\varepsilon}(\boldsymbol{v}+\nu(\delta)\boldsymbol{\eta})):\boldsymbol{\varepsilon}(\boldsymbol{\eta})\,d\boldsymbol{x}\\
&\quad=\int_\Omega W_{,c}(d,\boldsymbol{\varepsilon}(\boldsymbol{v}))\xi+W_{,\boldsymbol{\varepsilon}}(d,\boldsymbol{\varepsilon}(\boldsymbol{v})):\boldsymbol{\varepsilon}(\boldsymbol{\eta})\,d\boldsymbol{x}.
\end{aligned}$$

The dissipative terms of the time discrete functional $E^n_{\Delta t}$ are observed and we calculate directly

$$\begin{aligned}
&\lim_{\delta\to 0}\frac{1}{2\delta\Delta t}\left(\|d+\delta\xi-c^{n-1}\|^2_{\mathcal{M}^n}-\|d-c^{n-1}\|^2_{\mathcal{M}^n}\right)\\
&\quad=\lim_{\delta\to 0}\frac{1}{\Delta t}\left(\langle d-c^{n-1},\xi\rangle_{\mathcal{M}^n}+\frac{1}{2}\delta\langle\xi,\xi\rangle_{\mathcal{M}^n}\right)=\frac{1}{\Delta t}\langle d-c^{n-1},\xi\rangle_{\mathcal{M}^n},\\
&\lim_{\delta\to 0}\frac{\gamma}{2\delta\Delta t}\left(\|d+\delta\xi-c^{n-1}\|^2_{L_2(\Omega)}-\|d-c^{n-1}\|^2_{L_2(\Omega)}\right)\\
&\quad=\lim_{\delta\to 0}\frac{\gamma}{\Delta t}\left(\langle d-c^{n-1},\xi\rangle_{L_2(\Omega)}+\frac{1}{2}\delta\langle\xi,\xi\rangle_{L_2(\Omega)}\right)=\frac{\gamma}{\Delta t}\langle d-c^{n-1},\xi\rangle_{L_2(\Omega)}.
\end{aligned}$$

The energy of the boundary loading is a linear functional with respect to the displacement $\boldsymbol{v}$ and therefore holds

$$\lim_{\delta\to 0}\frac{1}{\delta}\left(\int_{\Gamma_N}\boldsymbol{g}^n\cdot(\boldsymbol{v}+\delta\boldsymbol{\eta})-\boldsymbol{g}^n\cdot\boldsymbol{v}\right)\,d\boldsymbol{a}_{\boldsymbol{x}}=\int_{\Gamma_N}\boldsymbol{g}^n\cdot\boldsymbol{\eta}\,d\boldsymbol{a}_{\boldsymbol{x}}.$$

The summary of all calculations shows the statement of this lemma. □

We remark, that due to theorem 2.8 for a minimiser $c^n \in X_m(\Omega)$ and $\boldsymbol{u}^n \in \boldsymbol{X}(\Omega)$ the Gâteaux derivative is equal to zero. Consequently we get for test functions

$\xi \in X_0(\Omega) \cap L_\infty(\Omega)$ and $\boldsymbol{\eta} \in \boldsymbol{X}(\Omega)$

$$\int_\Omega \boldsymbol{\Gamma} \nabla_{\boldsymbol{x}} c^n \cdot \nabla_{\boldsymbol{x}} \xi + \psi_{,c}(c^n)\xi + W_{,c}(c^n, \boldsymbol{\varepsilon}(\boldsymbol{u}^n))\xi + W_{,\boldsymbol{\varepsilon}}(c^n, \boldsymbol{\varepsilon}(\boldsymbol{u}^n)) : \boldsymbol{\varepsilon}(\boldsymbol{\eta})\, d\boldsymbol{x} - \int_{\Gamma_N} \boldsymbol{g}^n \cdot \boldsymbol{\eta}\, d\boldsymbol{a}_{\boldsymbol{x}} + \frac{1}{\Delta t}\langle c^n - c^{n-1}, \xi \rangle_{\mathcal{M}^n} + \frac{\gamma}{\Delta t}\langle c^n - c^{n-1}, \xi \rangle_{L_2(\Omega)} = 0.$$

Due to the fact that the test functions $\xi \in X_0(\Omega) \cap L_\infty(\Omega)$ and $\boldsymbol{\eta} \in \boldsymbol{X}(\Omega)$ are independent, a minimiser $c^n \in X_m(\Omega)$, $\boldsymbol{u}^n \in \boldsymbol{X}(\Omega)$ provides a solution of the discrete weak problem 2.21.

Furthermore, the minimiser $c^n \in X_m(\Omega)$ and $\boldsymbol{u}^n \in \boldsymbol{X}(\Omega)$ with a chemical potential $\mu^n \in H^1(\Omega)$ given by (2.23) generates a discrete weak solution in the sense of definition 2.17. This holds, because the Gâteaux derivative exists for all test functions $\xi \in H^1(\Omega) \cap L_\infty(\Omega)$ and $\boldsymbol{\eta} \in \boldsymbol{X}(\Omega)$ and we can choose the constant Lagrange multiplier

$$\lambda^n = \frac{1}{\text{meas}(\Omega)} \int_\Omega \mu^n\, d\boldsymbol{x} = \frac{1}{\text{meas}(\Omega)} \int_\Omega \psi_{,c}(c^n) + W_{,c}(c^n, \boldsymbol{\varepsilon}(\boldsymbol{u}^n))\, d\boldsymbol{x}. \tag{2.30}$$

Now, we have calculated the piecewise constant interpolants of the mass concentration $(c_N)_{N\in\mathbb{N}} \subset L_2(0,T;X_m(\Omega))$, of the chemical potential $(\mu_N)_{N\in\mathbb{N}} \subset L_2(0,T;H^1(\Omega))$ and of the displacement $(\boldsymbol{u}_N)_{N\in\mathbb{N}} \subset L_2(0,T;\boldsymbol{X}(\Omega))$. Moreover, the piecewise linear interpolant of the mass concentration $(\overline{c}_N)_{n\in\mathbb{N}} \subset L_2(0,T;X_m(\Omega))$ is also calculated. Finally, we have to prove, that these sequences converge to a weak solution of the field equations (1.51) - (1.53) in the sense of definition 2.15.

2.2.3 A-priori estimates

In the third step of this existence proof, we derive uniform a-priori estimates for the discrete weak solutions $(c_N)_{N\in\mathbb{N}}$, $(\overline{c}_N)_{N\in\mathbb{N}}$, $(\mu_N)_{N\in\mathbb{N}}$ and $(\boldsymbol{u}_N)_{N\in\mathbb{N}}$. In order to calculate an a-priori estimate, we use the Lyapunov property of the system. This property says that the binary alloy is transfered into an energetic more stable state due to spinodal decomposition.

Lemma 2.24 (Lyapunov property). *Let $\Omega \subset \mathbb{R}^d$ be a domain satisfying condition (H-1). At each discrete time $t_n = n\Delta t$ holds for a discrete semi-weak solution c_N, μ_N and $\boldsymbol{u}_N$ the following energy estimate*

$$E(t_n, c^n, \boldsymbol{u}^n) + \frac{1}{2}\int_0^{t_n}\int_\Omega \boldsymbol{M}(c_N(t-\Delta t,\cdot))\nabla_{\boldsymbol{x}}\mu_N \cdot \nabla_{\boldsymbol{x}}\mu_N\, d\boldsymbol{x}dt + \frac{\gamma}{2}\int_0^{t_n}\int_\Omega (\dot{\overline{c}}_N)^2\, d\boldsymbol{x}dt \le E(0, c^0, \boldsymbol{u}^0) + CT,$$

with a constant $C = C(C_C, c_C, C_{\overline{\boldsymbol{\varepsilon}}}, \boldsymbol{g}, \text{meas}(\Omega))$.

Proof. We consider the discrete energy functional $E^n_{\Delta t}$ defined in (2.25) at time $t_n = n\Delta t$, $1 \le n \le N$, with a corresponding minimiser $c^n \in X_m(\Omega)$ and $\boldsymbol{u}^n \in \boldsymbol{X}(\Omega)$ and use $c^{n-1} \in X_m(\Omega)$ and $\boldsymbol{u}^{n-1} \in \boldsymbol{X}(\Omega)$ as comparison functions. Then we directly get by taking into account (2.26)

$$\begin{aligned} E^n_{\Delta t}(c^n, \boldsymbol{u}^n) &= E(t_n, c^n, \boldsymbol{u}^n) + \frac{1}{2\Delta t}\|c^n - c^{n-1}\|^2_{\mathcal{M}_n} + \frac{\gamma}{2\Delta t}\|c^n - c^{n-1}\|^2_{L_2(\Omega)} \\ &= E(t_n, c^n, \boldsymbol{u}^n) + \frac{1}{2}\int_{t_{n-1}}^{t_n}\int_\Omega \boldsymbol{M}^{n-1}\nabla_{\boldsymbol{x}}\mu^n \cdot \nabla_{\boldsymbol{x}}\mu^n \, d\boldsymbol{x}dt + \frac{\gamma}{2}\int_{t_{n-1}}^{t_n}\int_\Omega (\dot{\bar{c}}_N)^2 \, d\boldsymbol{x}dt \\ &\le E^n_{\Delta t}(c^{n-1}, \boldsymbol{u}^{n-1}) = E(t_n, c^{n-1}, \boldsymbol{u}^{n-1}). \end{aligned}$$

Considering the last term of this calculation, we derive from assumption (A-8), from the trace theorem 2.2 and from estimate (2.8) the relation

$$\begin{aligned} &E(t_n, c^{n-1}, \boldsymbol{u}^{n-1}) \\ &\quad= \int_\Omega \frac{1}{2}\boldsymbol{\Gamma}\nabla_{\boldsymbol{x}}c^{n-1} \cdot \nabla_{\boldsymbol{x}}c^{n-1} + \psi(c^{n-1}) + W(c^{n-1}, \boldsymbol{\varepsilon}(\boldsymbol{u}^{n-1})) \, d\boldsymbol{x} \\ &\qquad- \int_{\Gamma_N} \boldsymbol{g}^n \cdot \boldsymbol{u}^{n-1} \, d\boldsymbol{a}_{\boldsymbol{x}} \\ &\quad= E(t_{n-1}, c^{n-1}, \boldsymbol{u}^{n-1}) + \int_{\Gamma_N} (\boldsymbol{g}^{n-1} - \boldsymbol{g}^n) \cdot \boldsymbol{u}^{n-1} \, d\boldsymbol{a}_{\boldsymbol{x}} \\ &\quad\le E(t_{n-1}, c^{n-1}, \boldsymbol{u}^{n-1}) + C\Delta t. \end{aligned}$$

Summing up the above formulated estimates we get for the time step $t_n = n\Delta t$ the energy estimate

$$\begin{aligned} E(t_n, c^n, \boldsymbol{u}^n) + \frac{1}{2}\int_{t_{n-1}}^{t_n}\int_\Omega \boldsymbol{M}^{n-1}\nabla_{\boldsymbol{x}}\mu^n \cdot \nabla_{\boldsymbol{x}}\mu^n \, d\boldsymbol{x}dt \\ + \frac{\gamma}{2}\int_{t_{n-1}}^{t_n}\int_\Omega (\dot{\bar{c}}_N)^2 \, d\boldsymbol{x}dt \le E(t_{n-1}, c^{n-1}, \boldsymbol{u}^{n-1}) + C\Delta t. \end{aligned}$$

Finally, we have to apply the above energy estimate recursively in order to deduce the statement of this lemma. □

It is obvious to see in view of (2.16), that $\bar{c}_N$ is a solution of the discrete semi-weak diffusion equation (2.18). For $t \in ((n-1)\Delta t, n\Delta t]$, $1 \le n \le N$ we get

$$\int_\Omega \dot{\bar{c}}_N \zeta \, d\boldsymbol{x} + \int_\Omega \boldsymbol{M}^{n-1}\nabla_{\boldsymbol{x}}\mu_N \cdot \nabla_{\boldsymbol{x}}\zeta \, d\boldsymbol{x} = 0 \qquad \forall \zeta \in X_0(\Omega). \tag{2.31}$$

In order to show the existence of a weak solution of the viscous Cahn-Larché system, we prove uniform a-priori estimates for the interpolants c_N, $\bar{c}_N$, μ_N and $\boldsymbol{u}_N$.

Lemma 2.25. *Let $\Omega \subset \mathbb{R}^d$ be a domain satisfying condition (H-1) and let the assumptions (A-1), (A-2), (A-6) - (A-8) be satisfied. Then there exists a constant $C_E > 0$ depending on the material parameters formulated in the above mentioned assumptions, on the initial condition c_0 and on the boundary loading g such that*

$$E(0, c_0, \boldsymbol{u}_0) \leq C_E.$$

Proof. We observe the energy at initial time $t = 0$ by using the assumptions (A-1), (A-2), (A-6) - (A-8) and take into account the a-priori estimate (2.8) for $\boldsymbol{u}_0$, which is the initial displacement corresponding to c_0. We calculate by using the Hölder inequality and the trace theorem 2.2

$$\begin{aligned}
E(0, c_0, \boldsymbol{u}_0) &= \int_\Omega \frac{1}{2}\boldsymbol{\Gamma}\nabla_{\boldsymbol{x}} c_0 \cdot \nabla_{\boldsymbol{x}} c_0 + \psi(c_0) + W(c_0, \boldsymbol{\varepsilon}(\boldsymbol{u}_0))\, d\boldsymbol{x} - \int_{\Gamma_N} \boldsymbol{g}^0 \cdot \boldsymbol{u}_0 \, d\boldsymbol{a}_{\boldsymbol{x}} \\
&\leq \frac{C_\Gamma}{2}|c_0|^2_{H^1(\Omega)} + \|\psi(c_0)\|_{L_1(\Omega)} + C_C(|\boldsymbol{u}_0|^2_{\boldsymbol{H}^1(\Omega)} + C^2_{\overline{\boldsymbol{\varepsilon}}}\,\mathrm{meas}(\Omega)) \\
&\quad + c_\gamma \|\boldsymbol{g}\|_{C^0(0,T;\boldsymbol{H}^{-\frac{1}{2}}(\Gamma_N))} \|\boldsymbol{u}_0\|_{\boldsymbol{H}^1(\Omega)} \\
&\leq \bar{C}(\|c_0\|^2_{H^1(\Omega)} + \|\psi(c_0)\|_{L_1(\Omega)} + \|\boldsymbol{g}\|^2_{C^0(0,T;\boldsymbol{H}^{-\frac{1}{2}}(\Gamma_N))} + \mathrm{meas}(\Omega)) =: C_E,
\end{aligned}$$

with a constant $C_E = C_E(C_{\boldsymbol{u}}, C_\Gamma, C_C, C_{\overline{\boldsymbol{\varepsilon}}}, c_\gamma)$. □

Lemma 2.26. *Let $\Omega \subset \mathbb{R}^d$ be a domain satisfying condition (H-1) and let the assumptions (A-1), (A-2), (A-6) - (A-8) be satisfied. Then there exists a constant $c_E > 0$ depending on the material parameters formulated in the above mentioned assumptions such that for every time step $t_n = n\Delta t$ with $1 \leq n \leq N$ the following estimate holds*

$$E(t_n, c^n, \boldsymbol{u}^n) \geq c_E \left(\|c^n\|^2_{H^1(\Omega)} + \int_\Omega \psi(c^n)\, d\boldsymbol{x} - 1 \right).$$

Proof. We consider the minimiser $c^n \in X_m(\Omega)$ and $\boldsymbol{u}^n \in \boldsymbol{X}(\Omega)$ at time $t_n = n\Delta t$ and take into account the assumptions (A-1), (A-2), (A-6) - (A-8) as well as the a-priori estimate (2.8) for $\boldsymbol{u}^n$. With the Poincaré inequality and the trace theorem 2.2 we calculate

$$\begin{aligned}
E(t_n, c^n, \boldsymbol{u}^n) &= \int_\Omega \frac{1}{2}\boldsymbol{\Gamma}\nabla_{\boldsymbol{x}} c^n \cdot \nabla_{\boldsymbol{x}} c^n + \psi(c^n) + W(c^n, \boldsymbol{\varepsilon}(\boldsymbol{u}^n))\, d\boldsymbol{x} - \int_{\Gamma_N} \boldsymbol{g}^n \cdot \boldsymbol{u}^n \, d\boldsymbol{a}_{\boldsymbol{x}} \\
&\geq \frac{c_\Gamma}{2c_p}\|c^n\|^2_{H^1(\Omega)} - \frac{c_\Gamma}{2}m^2 + \int_\Omega \psi(c^n)\, d\boldsymbol{x} - c_\gamma \|\boldsymbol{g}\|_{C^0(0,T;H^{-\frac{1}{2}}(\Gamma_N))} \|\boldsymbol{u}^n\|_{\boldsymbol{H}^1(\Omega)} \\
&\geq c_E \left(\|c^n\|^2_{H^1(\Omega)} + \int_\Omega \psi(c^n)\, d\boldsymbol{x} - 1 \right),
\end{aligned}$$

with a constant $c_E = c_E(C_{\boldsymbol{u}}, c_\Gamma, c_p, \boldsymbol{g}, m)$. □

We have to remark that in both lemma 2.25 and lemma 2.26 the constants C_E and c_E are independent of the friction coefficient γ and therefore these estimates also hold for the non-viscous Cahn-Larché system.

Lemma 2.27 (A-priori estimates). *Let $\Omega \subset \mathbb{R}^d$ be a domain satisfying condition (H-1) and let the assumptions (A-1) - (A-8) be satisfied. Then for the discrete weak solution c_N, $\bar{c}_N$, μ_N and $\boldsymbol{u}_N$ exist constants C_c, $C_{\bar{c}}$, $C_{\bar{c}'}$, C_μ, $C_{\boldsymbol{u}}$ and $C_\psi > 0$, depending on the material parameters, the boundary loading $\boldsymbol{g}$, the initial condition c_0, time T and* meas(Ω)*, such that the following uniform a-priori estimates hold*

(1) $\|\boldsymbol{u}_N\|_{L_\infty(0,T;\boldsymbol{H}^1(\Omega))} \leq C_{\boldsymbol{u}}$,

(2) $\|c_N\|_{L_\infty(0,T;H^1(\Omega))} \leq C_c$,

(3) $\|\bar{c}_N\|_{L_\infty(0,T;H^1(\Omega))} \leq C_{\bar{c}}$,

(4) $\sup_{t\in[0,T]} \int_\Omega \psi(c_N)\, d\boldsymbol{x} \leq C_\psi$,

(5) $\|\mu_N\|_{L_2(0,T;H^1(\Omega))} \leq C_\mu$,

(6) $\|\dot{\bar{c}}_N\|_{L_2(\Omega_T)} \leq C_{\bar{c}'}$, *if* $\gamma \gneqq 0$.

Proof. Statement *(1)* follows directly from the a-priori estimate (2.8). The statements *(2)*, *(3)* and *(4)* are deduced from the Lyapunov property formulated in lemma 2.24 and from the estimates in lemma 2.25 and 2.26.

In order to prove statement *(5)* we calculate a lower estimate for the chemical potential by using again the Lyapunov property lemma 2.24 and the estimates deduced from lemma 2.25 and 2.26. Applying Poincaré's inequality (2.1) together with (A-3) and the Lagrangian multiplier (2.30) we deduce

$$\begin{aligned}\int_0^T \int_\Omega \boldsymbol{M}(c_N(t-\Delta t,\boldsymbol{x})\nabla_{\boldsymbol{x}}\mu_N \cdot \nabla_{\boldsymbol{x}}\mu_N \, d\boldsymbol{x}dt &\geq c_M \int_0^T \int_\Omega |\nabla_{\boldsymbol{x}}\mu|^2 \, d\boldsymbol{x}dt \\ \geq \frac{c_M}{c_p}\|\mu\|^2_{L_2(0,T;H^1(\Omega))} - c_M \int_0^T \lambda^n dt &\geq \frac{c_M}{c_p}\|\mu\|^2_{L_2(0,T;H^1(\Omega))} - C.\end{aligned}$$

Due to equation (2.30) together with statement *(1)* and *(2)*, there exists a uniform bound C for $c_M \int_0^T \lambda^n dt$. This argument yields statement *(5)*.

Finally, statement *(6)* follows directly from the Lyapunov property lemma 2.24, from the uniform boundedness of c_N and from lemma 2.25 respectively 2.26,

$$\frac{\gamma}{2}\|\dot{\bar{c}}_N\|_{L_2(\Omega_T)} \leq E(c_0,\boldsymbol{u}_0) - E(c^N,\boldsymbol{u}^N) + C.$$

We remark that except $C_{\bar{c}'}$ all other constants in lemma 2.27 are independent of the friction coefficient γ. □

2.2.4 Existence proof

In this section we extract convergent subsequences of the sequences $(c_N)_{N\in\mathbb{N}}$, $(\bar{c}_N)_{N\in\mathbb{N}}$, $(\mu_N)_{N\in\mathbb{N}}$ and $(\boldsymbol{u}_N)_{n\in\mathbb{N}}$ and show that their limits generate a weak solution of the viscous Cahn-Larché equation system in the sense of definition 2.15.

Lemma 2.28. *Let $\Omega \subset \mathbb{R}^d$ be a domain satisfying condition (H-1) and let the assumptions (A-1)-(A-8) be satisfied. Then there exist at least one $c \in L_\infty(0,T;H^1(\Omega))$ and subsequences denoted without loss of generality with the same index $(c_N)_N$, $(\bar{c}_N)_N \subset L_\infty(0,T;H^1(\Omega))$, such that*

$$\bar{c}_N \longrightarrow c \qquad \text{in} \quad C([0,T];L_2(\Omega)), \tag{2.32}$$

$$c_N \longrightarrow c \qquad \text{in} \quad L_\infty(0,T;L_2(\Omega)), \tag{2.33}$$

$$c_N(t,\boldsymbol{x}) \longrightarrow c(t,\boldsymbol{x}) \qquad \text{almost everywhere in } \Omega_T, \tag{2.34}$$

$$c_N \overset{*}{\rightharpoonup} c \qquad \text{in} \quad L_\infty(0,T;X_m(\Omega)), \tag{2.35}$$

Proof. We consider $t_1, t_2 \in (0,T)$ with $t_1 < t_2$ and choose the test function in (2.5) as $\zeta(\boldsymbol{x}) = \bar{c}_N(t_2,\boldsymbol{x}) - \bar{c}_N(t_1,\boldsymbol{x})$. After integration over (t_1,t_2), we apply integration by parts with respect to time, use assumption (A-3) and lemma 2.27 in order to estimate

$$\begin{aligned}
&\|\bar{c}_N(t_2,\cdot) - \bar{c}_N(t_1,\cdot)\|^2_{L_2(\Omega)} \\
&\quad \le \left| \int_{t_1}^{t_2} \int_\Omega \boldsymbol{M}(c_N(t-\Delta t,\boldsymbol{x}))\nabla_{\boldsymbol{x}}\mu_N \cdot \nabla_{\boldsymbol{x}}(\bar{c}_N(t_2,\cdot) - \bar{c}_N(t_1,\cdot))\, d\boldsymbol{x}dt \right| \\
&\quad \le C_M \int_{t_1}^{t_2} \|\mu_N(t,\cdot)\|_{H^1(\Omega)} \|\bar{c}_N(t_2,\cdot) - \bar{c}_N(t_1,\cdot)\|_{H^1(\Omega)} dt \\
&\quad \le 2C_M C_c \int_{t_1}^{t_2} \|\mu_N(t,\cdot)\|_{H^1(\Omega)} dt \le 2C_M C_c C_\mu |t_2 - t_1|^{\frac{1}{2}}.
\end{aligned}$$

This estimate shows, that c_N is equi-continuous. From Rellich-Kondrachov's theorem, we know $X_m(\Omega) \Subset L_2(\Omega)$ and therefore we apply the theorem of Arzelà-Ascoli 2.9 and deduce (2.32).

In order to prove (2.33), we consider an arbitrary but fixed time $t \in (0,T)$ and choose $1 \le n \le N$ as well as $\beta \in [0,1]$, such that $t = \beta n\Delta t + (1-\beta)(n-1)\Delta t$, then we obtain

$$\begin{aligned}
\|\bar{c}_N(t,\cdot) - c_N(t,\cdot)\|_{L_2(\Omega)} &= \|(1-\beta)c^{n-1} + \beta c^n - c^n\|_{L_2(\Omega)} \\
&= (1-\beta)\|c^{n-1} - c^n\|_{L_2(\Omega)} = (1-\beta)\|\bar{c}_N((n-1)\Delta t,\cdot) - \bar{c}_N(n\Delta t,\cdot)\|_{L_2(\Omega)} \\
&= C(\Delta t)^{\frac{1}{4}}.
\end{aligned}$$

In view of (2.32) and the triangle inequality statement (2.33) follows directly. From Weyl's corollary we get an almost everywhere convergent subsequence $(c_N)_{N\in\mathbb{N}}$, which proves (2.34). From lemma 2.27 we directly deduce (2.35). □

Lemma 2.29. *Let $\Omega \subset \mathbb{R}^d$ be a domain satisfying condition (H-1) and let the assumptions (A-1) - (A-8) be satisfied. Then for all times $t \in (0,T)$ holds*

$$c_N(t-\Delta t,\cdot) \longrightarrow c(t,\cdot) \quad \text{in } L_2(\Omega). \tag{2.36}$$

Proof. We consider an arbitrary but fixed time $t \in (0,T)$ and choose $1 \leq n \leq N$ such that $t \in ((n-1)\Delta t, n\Delta t]$. Furthermore, we take into account the equicontinuity of $\bar{c}_N$ and calculate

$$\begin{aligned}\|c_N(t-\Delta t,\cdot) - c_N(t,\cdot)\|_{L_2(\Omega)} &= \|c^{n-1} - c^n\|_{L_2(\Omega)} \\ &= \|\bar{c}_N((n-1)\Delta t,\cdot) - \bar{c}_N(n\Delta t,\cdot)\|_{L_2(\Omega)} \\ &\leq C\Delta t^{\frac{1}{4}}.\end{aligned}$$

In view of this calculation and (2.33) we get the statement of this lemma. □

From (2.36) and Weyl's corollary we deduce, that there exists a subsequence, denoted with the same index N, such that $c_N(t-\Delta t, \boldsymbol{x})$ tends to $c(t,\boldsymbol{x})$ almost everywhere in Ω_T. From lemma 2.27 statement *(6)* we follow that there exists a weak convergent subsequence without loss of generality denoted with the same index

$$\dot{\bar{c}}_N \rightharpoonup \dot{c}_1 \qquad \text{in } L_2(\Omega_T). \tag{2.37}$$

Lemma 2.30. *Let $\Omega \subset \mathbb{R}^d$ be a domain satisfying condition (H-1) and let the assumptions (A-1) - (A-8) be satisfied and additional we assume $\gamma \gneqq 0$. Let $c \in C([0,T];L_2(\Omega))$ the limit of c_N respectively $\bar{c}_N$ obtained in lemma 2.28. Then in the distributional sense holds*

$$\dot{c}_1 = \dot{c}.$$

Proof. Let $\xi \in \mathscr{D}(0,T;L_2(\Omega))$ with $\xi(T,\cdot) = 0$ be arbitrary but fixed and let $\varepsilon > 0$ be arbitrary. Then we calculate form (2.32) and (2.37)

$$\begin{aligned}\int_{\Omega_T} (\dot{c} - \dot{c}_1)\xi \, d\boldsymbol{x}dt &= \int_{\Omega_T} (\dot{c} - \dot{\bar{c}}_N + \dot{\bar{c}}_N - \dot{c}_1)\xi \, d\boldsymbol{x}dt \\ &= \int_\Omega (c - \bar{c}_N)\xi \, d\boldsymbol{x}\Big|_0^T + \int_{\Omega_T} (\bar{c}_N - c)\dot{\xi} \, d\boldsymbol{x}dt + \int_{\Omega_T} (\dot{\bar{c}}_N - \dot{c}_1)\xi \, d\boldsymbol{x}dt \\ &= \int_{\Omega_T} (\bar{c}_N - c)\dot{\xi} \, d\boldsymbol{x}dt + \int_{\Omega_T} (\dot{\bar{c}}_N - \dot{c}_1)\xi \, d\boldsymbol{x}dt \leq \varepsilon.\end{aligned}$$

□

Remark 2.31. If c provides a solution of the viscous Cahn-Larché system with a friction coefficient $\gamma \gneqq 0$, then the concentration field c is smoother with respect to time. It holds

$$c \in \{v \in L_\infty(0,T;X_m(\Omega)) \cap C([0,T];L_2(\Omega)) \ : \ \dot{v} \in L_2(\Omega_T)\}. \tag{2.38}$$

Up to now we know that there exists a concentration field $c \in L_\infty(0,T;X_m(\Omega))$, which possesses a limit of the subsequence $(c_N)_{N\in\mathbb{N}}$. Corresponding to the concentration field $c \in L_\infty(0,T;X_m(\Omega))$ we define a displacement in the whole time space cylinder Ω_T by the following weak problem.

Problem 2.32. Find $\boldsymbol{u} \in L_2(0,T;\boldsymbol{X}(\Omega))$, such that holds

$$\int_{\Omega_T} \boldsymbol{C}(c)\boldsymbol{\varepsilon}(\boldsymbol{u}) : \boldsymbol{\varepsilon}(\boldsymbol{u})\, d\boldsymbol{x}dt = \int_{\Omega_T} \boldsymbol{C}(c)\overline{\boldsymbol{\varepsilon}}(c) : \boldsymbol{\varepsilon}(\boldsymbol{u})\, d\boldsymbol{x}dt + \int_{\Gamma_T^N} \boldsymbol{g}\cdot\boldsymbol{\eta}\, d\boldsymbol{a}_{\boldsymbol{x}}dt$$
$$\forall \boldsymbol{\eta} \in L_2(0,T;\boldsymbol{X}(\Omega)).$$

Similar to lemma 2.14 we calculate the following estimates in the time space cylinder:

Lemma 2.33. *Let $\Omega \subset \mathbb{R}^d$ be a domain satisfying condition (H-1). Furthermore let the assumptions (A-6) - (A-8) be satisfied, then the following estimates hold*

(1) $$\left|\int_{\Omega_T} \boldsymbol{C}(c)\boldsymbol{\varepsilon}(\boldsymbol{u}) : \boldsymbol{\varepsilon}(\boldsymbol{u})\, d\boldsymbol{x}dt\right| \le C_C \|\boldsymbol{u}\|_{L_2(0,T;\boldsymbol{H}^1(\Omega))}\|\boldsymbol{\eta}\|_{L_2(0,T;\boldsymbol{H}^1(\Omega))},$$

(2) $$\int_{\Omega_T} \boldsymbol{C}(c)\boldsymbol{\varepsilon}(\boldsymbol{\eta}) : \boldsymbol{\varepsilon}(\boldsymbol{\eta})\, d\boldsymbol{x}dt \ge \frac{c_C}{c_k}\|\boldsymbol{\eta}\|^2_{L_2(0,T;\boldsymbol{H}^1(\Omega))},$$

(3) $$\left|\int_{\Omega_T} \boldsymbol{C}(c)\overline{\boldsymbol{\varepsilon}}(c) : \boldsymbol{\varepsilon}(\boldsymbol{\eta})\, d\boldsymbol{x}dt + \int_{\Gamma_T^N} \boldsymbol{g}\cdot\boldsymbol{\eta}\, d\boldsymbol{a}_{\boldsymbol{x}}dt\right|$$
$$\le CT^{\frac{1}{2}}\left(\mathrm{meas}^{\frac{1}{2}}(\Omega) + \|\boldsymbol{g}\|_{C^0(0,T;\boldsymbol{H}^{-\frac{1}{2}}(\Gamma_N))}\right).$$

Proof. Statement *(1)* follows directly from assumption (A-6) together with Hölder's inequality. Statement *(2)* is a consequence of the assumption (A-6) and Korn's inequality applied in every time $t \in (0,T)$. Taking into account assumption (A-6) - (A-8), Hölder's inequality and the trace theorem statement *(3)* is proved. □

Corollary 2.34. *Let $\Omega \subset \mathbb{R}^d$ be a domain satisfying condition (H-1) and let the assumptions (A-6) - (A-8) be satisfied, then there exists a unique solution $\boldsymbol{u} \in L_2(0,T;\boldsymbol{X}(\Omega))$ of problem 2.32, satisfying the a-priori estimate*

$$\|\boldsymbol{u}\|_{L_2(0,T;\boldsymbol{H}^1(\Omega))} \le C_{\boldsymbol{u}}T^{\frac{1}{2}}.$$

Proof. Since $L_2(0,T;\boldsymbol{X}(\Omega))$ is a Hilbert space we follow from lemma 2.33 and from Lax-Milgram's theorem the existence and uniqueness of a solution $\boldsymbol{u} \in L_2(0,T;\boldsymbol{X}(\Omega))$ satisfying the uniform a-priori estimate. □

Moreover, we have to show that the subsequence of displacement $(\boldsymbol{u}_N)_{N\in\mathbb{N}} \subset L_2(0,T;\boldsymbol{X}(\Omega))$ corresponding to the subsequence of concentration $(c_N)_{N\in\mathbb{N}} \subset L_\infty(0,T;H^1(\Omega))$ converges to $\boldsymbol{u} \in L_2(0,T;\boldsymbol{X}(\Omega))$ if c_N tends to c.

Lemma 2.35. *Let $\Omega \subset \mathbb{R}^d$ be a domain satisfying condition (H-1) and let the assumptions (A-1) - (A-8) be satisfied, then it holds*

$$\boldsymbol{u}_N \to \boldsymbol{u} \qquad \text{in} \quad L_2(0,T;\boldsymbol{H}^1(\Omega)).$$

Proof. We integrate the semi-weak momentum balance (2.7) over $(0,T)$ and subtract it from the weak formulation of problem 2.32. By inserting $\int_{\Omega_T}(\boldsymbol{C}(c_N)\boldsymbol{\varepsilon}(\boldsymbol{u}) - \boldsymbol{C}(c_N)\boldsymbol{\varepsilon}(\boldsymbol{u})) : \boldsymbol{\varepsilon}(\boldsymbol{\eta})\, d\boldsymbol{x}dt$ we deduce for the left hand side

$$\begin{aligned}\int_{\Omega_T} &(\boldsymbol{C}(c)\boldsymbol{\varepsilon}(\boldsymbol{u}) - \boldsymbol{C}(c_N)\boldsymbol{\varepsilon}(\boldsymbol{u}_N)) : \boldsymbol{\varepsilon}(\boldsymbol{\eta})\, d\boldsymbol{x}dt \\ &= \int_{\Omega_T} \boldsymbol{C}(c_N)\boldsymbol{\varepsilon}(\boldsymbol{u}-\boldsymbol{u}_N) : \boldsymbol{\varepsilon}(\boldsymbol{\eta}) + (\boldsymbol{C}(c) - \boldsymbol{C}(c_N))\boldsymbol{\varepsilon}(\boldsymbol{u}) : \boldsymbol{\varepsilon}(\boldsymbol{\eta})\, d\boldsymbol{x}dt.\end{aligned}$$

The test function is chosen by $\boldsymbol{\eta} = \boldsymbol{u} - \boldsymbol{u}_N$ and we calculate under assumption (A-6), Korn's and Hölder's inequality and with the above calculation

$$\begin{aligned}&\frac{c_C}{c_k}\|\boldsymbol{u}-\boldsymbol{u}_N\|^2_{L_2(0,T;\boldsymbol{H}^1(\Omega))} \\ &\quad\le \left|\int_{\Omega_T} (\boldsymbol{C}(c) - \boldsymbol{C}(c_N))\boldsymbol{\varepsilon}(\boldsymbol{u}) : \boldsymbol{\varepsilon}(\boldsymbol{u}-\boldsymbol{u}_N)\, d\boldsymbol{x}dt\right| \\ &\qquad + \left|\int_{\Omega_T} (\boldsymbol{C}(c)\overline{\boldsymbol{\varepsilon}}(c) - \boldsymbol{C}(c_N)\overline{\boldsymbol{\varepsilon}}(c_N)) : \boldsymbol{\varepsilon}(\boldsymbol{u}-\boldsymbol{u}_N)\, d\boldsymbol{x}dt\right| \\ &\qquad + \left|\int_{\Gamma_T^N} (\boldsymbol{g}-\boldsymbol{g}_N)\cdot(\boldsymbol{u}-\boldsymbol{u}_N)\, d\boldsymbol{a}_{\boldsymbol{x}}dt\right| \\ &\quad\le \|(\boldsymbol{C}(c) - \boldsymbol{C}(c_N))\boldsymbol{\varepsilon}(\boldsymbol{u})\|_{\boldsymbol{L}_2(\Omega_T)}\|\boldsymbol{u}-\boldsymbol{u}_N\|_{L_2(0,T;\boldsymbol{H}^1(\Omega))} \\ &\qquad + \|\boldsymbol{C}(c)\overline{\boldsymbol{\varepsilon}}(c) - \boldsymbol{C}(c_N)\overline{\boldsymbol{\varepsilon}}(c_N)\|_{\boldsymbol{L}_2(\Omega_T)}\|\boldsymbol{u}-\boldsymbol{u}_N\|_{L_2(0,T;\boldsymbol{H}^1(\Omega))} \\ &\qquad + c_\gamma\|\boldsymbol{g}-\boldsymbol{g}_N\|_{C^0(0,T;\boldsymbol{H}^{-\frac{1}{2}}(\Gamma_N))}\|\boldsymbol{u}-\boldsymbol{u}_N\|_{L_2(0,T;\boldsymbol{H}^1(\Omega))}\end{aligned}$$

The convergence follows from the almost everywhere convergence of the concentration field, see lemma 2.28, together with Lebesgue's convergence theorem and from the Lipschitz continuity of the boundary loading, see assumption (A-8). □

We remark, that due to lemma 2.35 and Weyl's corollary we extract an almost everywhere convergent subsequence denoted with the same index

$$\boldsymbol{\varepsilon}(\boldsymbol{u}_N(t,\boldsymbol{x})) \to \boldsymbol{\varepsilon}(\boldsymbol{u}(t,\boldsymbol{x})) \qquad \text{almost everywhere in } \Omega_T. \tag{2.39}$$

Furthermore we remark that due to the uniform a-priori estimates in lemma 2.27 there exists a weak convergent subsequence denoted without loss of generality with the same index

$$\mu_N \rightharpoonup \mu \qquad \text{in} \qquad L_2(0,T;H^1(\Omega)). \tag{2.40}$$

Now we are able to prove, that the above obtained limits $c \in L_\infty(0,T;X_m(\Omega))$, $\mu \in L_2(0,T;H^1(\Omega))$ and $\boldsymbol{u} \in L_2(0,T;\boldsymbol{X}(\Omega))$ generate a weak solution of the viscous Cahn-Larché equation system in the sense of definition 2.15.

Proof of theorem 2.16. **Step 1**: At first we consider the discrete semi-weak diffusion equation (2.31). We integrate over $(0,T)$, apply integration by parts with respect to time and use (2.32) to deduce for the first term of (2.31)

$$\lim_{N\to\infty} \left| \int_{\Omega_T} \dot{\zeta}(c - \bar{c}_N) \, d\boldsymbol{x}dt \right| = 0.$$

In the second term of (2.31) we insert zero and use the fact, that $(\mu_N)_{N\in\mathbb{N}}$ is uniformly bounded and $(c_N(t-\Delta t,\boldsymbol{x}))_{N\in\mathbb{N}}$ converges almost everywhere, together with assumption (A-3) and Lebesgue's convergence theorem. Furthermore, we apply the weak convergence of $(\mu_N)_{N\in\mathbb{N}}$ and obtain

$$\begin{aligned}
&\lim_{N\to\infty} \left| \int_{\Omega_T} \boldsymbol{M}(c_N(t-\Delta t,\cdot))\nabla_{\boldsymbol{x}}\mu_N \cdot \nabla_{\boldsymbol{x}}\zeta - \boldsymbol{M}(c(t,\cdot))\nabla_{\boldsymbol{x}}\mu \cdot \nabla_{\boldsymbol{x}}\zeta \, d\boldsymbol{x}dt \right| \\
&\quad \leq \lim_{N\to\infty} \left(\left| \int_{\Omega_T} (\boldsymbol{M}(c_N(t-\Delta t,\cdot)) - \boldsymbol{M}(c(t,\cdot)))\nabla_{\boldsymbol{x}}\mu_N \cdot \nabla_{\boldsymbol{x}}\zeta \, d\boldsymbol{x}dt \right| \right. \\
&\qquad \left. + \left| \int_{\Omega_T} \boldsymbol{M}(c)(\nabla_{\boldsymbol{x}}\mu_N - \nabla_{\boldsymbol{x}}\mu) \cdot \nabla_{\boldsymbol{x}}\zeta \, d\boldsymbol{x}dt \right| \right) = 0.
\end{aligned}$$

Step 2: In the next step, we consider the discrete semi-weak equation of the chemical potential (2.19), integrate over $(0,T)$ and deduce from the weak convergence of $(\mu_N)_{N\in\mathbb{N}}$ for the left hand side

$$\lim_{N\to\infty} \left| \int_{\Omega_T} (\mu_N - \mu)\xi \, d\boldsymbol{x}dt \right| = 0.$$

For the right hand side of (2.19), we observe at first the surface energy. From the weak-$\star$ convergence of the mass concentration $(c_N)_{N\in\mathbb{N}}$ we directly get

$$\lim_{N\to\infty} \left| \int_{\Omega_T} \boldsymbol{\Gamma}(\nabla_{\boldsymbol{x}}c_N - \nabla_{\boldsymbol{x}}c) \cdot \nabla_{\boldsymbol{x}}\xi \, d\boldsymbol{x}dt \right| = 0.$$

Moreover, we consider the convex part ψ^+ of the Gibbs free energy ψ. By assumption (A-2) we have $\psi^+ \in C^1(\mathbb{R},\mathbb{R})$ together with the almost everywhere convergence of $(c_N)_{N\in\mathbb{N}}$ we get

$$\psi^+_{,c}(c_N(t,\boldsymbol{x})) \to \psi^+_{,c}(c(t,\boldsymbol{x})) \quad \text{almost everywhere} \quad N \to \infty.$$

Furthermore, let $\epsilon > 0$ be arbitrary, we choose a set $\mathcal{E} \in \Omega_T$ with the property $\text{meas}(\mathcal{E}) \leq \epsilon$, use assumption (A-2) with $\delta = \epsilon$ and apply lemma 2.27 statement *(4)*,

from which we calculate

$$\int_{\mathcal{E}} \left|\psi^+_{,c}(c_N)\right| \, d\boldsymbol{x}dt \leq \int_{\mathcal{E}} \delta\psi^+(c_N) + C_\delta \, d\boldsymbol{x}dt$$
$$\leq \delta \sup_{t\in[0,T]} \int_\Omega \psi^+(c_N) \, d\boldsymbol{x} + C_\delta \, \mathrm{meas}(\mathcal{E}) \leq C\epsilon.$$

In view of Vitali's convergence theorem 2.11, we conclude

$$\lim_{N\to\infty} \left| \int_{\Omega_T} \psi^+_{,c}(c_N)\xi - \psi^+_{,c}(c)\xi \, d\boldsymbol{x}dt \right| = 0.$$

The concave part of the Gibbs free energy ψ^- is polynomial bounded due to assumption (A-2) and we get by the generalised Lebesgue convergence theorem 2.10

$$\lim_{N\to\infty} \left| \int_{\Omega_T} \psi^-_{,c}(c_N)\xi - \psi^-_{,c}(c)\xi \, d\boldsymbol{x}dt \right| = 0.$$

Next, we observe the mechanical contribution to the chemical potential and we get from assumption (A-6) and (A-7) the estimate $|W_{,c}(c, \boldsymbol{\varepsilon}(\boldsymbol{u}))| \leq C(|\boldsymbol{\varepsilon}(\boldsymbol{u})|^2 + 1)$. Therefore we apply the generalised Lebesgue's convergence theorem 2.10 together with the strong convergence of the displacement $\boldsymbol{u}_N$, which is proved in lemma 2.35. The almost everywhere convergence of c_N finally yields

$$\lim_{N\to\infty} \left| \int_{\Omega_T} (W_{,c}(c_N, \boldsymbol{\varepsilon}(\boldsymbol{u}_N)) - W_{,c}(c, \boldsymbol{\varepsilon}(\boldsymbol{u})))\xi \, d\boldsymbol{x}dt \right| = 0.$$

For the friction term we use the strong convergence of $\bar{c}_N$ in order to follow directly

$$\lim_{N\to\infty} \left| \int_{\Omega_T} \gamma(c - \bar{c}_N)\dot{\xi} \, d\boldsymbol{x}dt \right| = 0.$$

Step 3: Finally, we consider the discrete semi-weak formulation of the balance of momentum (2.20) and follow directly from lemma 2.35

$$\lim_{N\to\infty} \int_{\Omega_T} W_{,\boldsymbol{\varepsilon}}(c_N, \boldsymbol{\varepsilon}(\boldsymbol{u}_N)) : \boldsymbol{\varepsilon}(\boldsymbol{\eta}) - W_{,\boldsymbol{\varepsilon}}(c, \boldsymbol{\varepsilon}(\boldsymbol{u})) : \boldsymbol{\varepsilon}(\boldsymbol{\eta}) \, d\boldsymbol{x}dt = 0.$$

This argument finishes the whole existence proof of weak solutions of the viscous Cahn-Larché equation system. □

Chapter 3

Numerical basics

In this chapter the numerical basics are prepared, which are necessary to derive and analyse Faedo-Galerkin methods for the Cahn-Larché system.

First of all we introduce the decomposition $\mathscr{T}_h(\Omega)$ of the reference domain Ω in a finite number of simplices. In two space dimensions the decomposition consists of triangles, in contrast to three space dimensions, where $\mathscr{T}_h(\Omega)$ contains tetrahedrons. Nevertheless, in both cases we use the synonym triangulation for the decomposition of the domain. The properties assumed for the triangulation are taken from classical textbooks, e.g. [18, 25, 85].

The second section of this chapter treats with the Clement quasi-interpolation operator, which in detail is discussed in [26]. The aim of this section is to develop an approximation theory of functions in the Sobolev space $H^1(\Omega)$ without classical interpolation techniques. From [26] we take a-priori estimates and approximation results in $L_2(\Omega)$ and $H^1(\Omega)$. Moreover, we use a special type of the Clement quasi-interpolation operator from [16, 92] in order to prove an a-priori estimate in $L_\infty(\Omega)$. Finally, an approximation result for functions in the whole time-space cylinder is proved.

The Cahn-Larché system describes a time dependent problem. Therefore we have to construct the discrete initial data at time $t = 0$. In the third section of this chapter we analyse the $L_2(\Omega)$-projection of the initial data c_0 onto the finite element space. We outline classical a-priori estimates and convergence results in $L_2(\Omega)$ and $H^1(\Omega)$ taken from [18, 85]. Additionally we prove an a-priori estimate in $L_\infty(\Omega)$, which is necessary for the a-priori estimates of the discrete solutions calculated by the approximation methods for the Cahn-Larché system in the following chapters.

In the final section of this chapter we compute the initial displacement corresponding to the initial concentration field c_0. Here we have to solve a linear elasticity problem, for which the a-priori estimates and convergence results are known, see [15, 25]. Nevertheless, we additionally have to analyse the influence of the concentration field c_0 on the material parameters.

3.1 Triangulation

In section 2.2.1 we have introduced a uniform time discretisation of the concentration field c, the chemical potential μ and the displacement $\boldsymbol{u}$. Additional to this time discretisation, a discretisation with respect to space must be developed in order to get an approximation method which can be implemented directly.

We apply a finite element discretisation for the numerical approximation of the time discrete fields c^n, μ^n and $\boldsymbol{u}^n$ in each time step $t = n\Delta t$ with $0 \leq n \leq N$. Both approximation techniques together are called Faedo-Galerkin method, see [96].

The finite element method needs essentially a decomposition $\mathscr{T}_h(\Omega)$ of the reference domain Ω. Let $\mathscr{T}_h(\Omega)$ be a partition of the domain Ω into a finite number of simplices. We remark that in two space dimensions the reference domain Ω is decomposed into triangles, in three space dimensions the decomposition contains tetrahedrons. In both cases we denote the decomposition $\mathscr{T}_h(\Omega)$ as triangulation. We point out that in every time step $t = n\Delta t$ with $0 \leq n \leq N$ the same triangulation $\mathscr{T}_h(\Omega)$ is used. We consider an exact triangulation, because Ω is assumed to be a polygonal respectively polyhedral bounded domain as mentioned in section 2.1. Furthermore $\mathscr{N}_h(\Omega)$ is the set of all nodes of the triangulation $\mathscr{T}_h(\Omega)$ and $\mathscr{E}_h(\Omega)$ denotes the set of all edges of the triangulation $\mathscr{T}_h(\Omega)$. In three space dimensions $\mathscr{F}_h(\Omega)$ denotes the set of all faces of the decomposition.

The triangulation has to satisfy the usual admissibility condition formulated in [18, 25, 85]: any two elements share at most a vertex, or a whole edge, or a whole face. For two simplices $\tau_i, \tau_j \in \mathscr{T}_h(\Omega)$ with $i \neq j$ holds

$$\text{if } d = 2 : \tau_i \cap \tau_j = \begin{cases} \exists! \boldsymbol{z} \in \mathscr{N}_h(\Omega), \\ \exists! \boldsymbol{e} \in \mathscr{E}_h(\Omega), \end{cases} \qquad \text{if } d = 3 : \tau_i \cap \tau_j = \begin{cases} \exists! \boldsymbol{z} \in \mathscr{N}_h(\Omega), \\ \exists! \boldsymbol{e} \in \mathscr{E}_h(\Omega), \\ \exists! \boldsymbol{f} \in \mathscr{F}_h(\Omega). \end{cases}$$

In other words, we do not allow hanging nodes. An important mesh parameter in finite element theory is the mesh size.

Definition 3.1 (Mesh size). The local mesh size of the triangulation $\mathscr{T}_h(\Omega)$ is given by

$$h_\tau := \sqrt[d]{\text{meas}(\tau)} \qquad \text{for all } \tau \in \mathscr{T}_h(\Omega)$$

and the global mesh size is defined by

$$h := \max_{\tau \in \mathscr{T}_h(\Omega)} h_\tau.$$

Definition 3.2 (Shape regularity). The triangulation $\mathscr{T}_h(\Omega)$ of the domain Ω is called shape regular, if there exists a constant $\kappa > 0$ independent of the mesh size, such that for all simplices $\tau \in \mathscr{T}_h(\Omega)$ with a ball $B_{r_\tau} \subset \tau$ of radius r_τ holds

$$\frac{h_\tau}{r_\tau} \leq \kappa.$$

An alternative to the shape regularity condition in two space dimensions is the angle condition. Furthermore, for the introduction of the Clement quasi-interpolation operator we need some local domains corresponding to a basis function $\varphi_{\boldsymbol{z}}$ at node $\boldsymbol{z} \in \mathscr{N}_h(\Omega)$. We define

$$\omega_{\boldsymbol{z}} := \operatorname{supp}(\varphi_{\boldsymbol{z}}), \qquad \omega_\tau := \bigcup_{\boldsymbol{z} \in \mathscr{N}_h(\tau)} \omega_{\boldsymbol{z}}.$$

Fig. 3.1 shows an illustration of both domains $\omega_{\boldsymbol{z}}$ and ω_τ, if $\varphi_{\boldsymbol{z}}$ is a piecewise linear basis function. Using the domain $\omega_{\boldsymbol{z}}$ an averaged local mesh size is introduced. In general $\sharp$ denotes the cardinality of a set. Let $\sharp\mathscr{T}_h(\omega_{\boldsymbol{z}})$ be the number of simplices in a triangulation $\mathscr{T}_h(\omega_{\boldsymbol{z}})$, then we define

$$h_{\boldsymbol{z}} := \frac{1}{\sharp\mathscr{T}_h(\omega_{\boldsymbol{z}})} \sum_{\tau \in \mathscr{T}_h(\omega_{\boldsymbol{z}})} h_\tau.$$

From [16] we take the definition of a locally quasi-uniform mesh.

Definition 3.3. The finite element triangulation $\mathscr{T}_h(\Omega)$ is called locally quasi-uniform, if there exists a constant $q > 0$ independent of the mesh size such that for all $\tau \in \mathscr{T}_h(\Omega)$ holds

$$\frac{1}{q} h_\tau \leq h_{\boldsymbol{z}} \leq q h_\tau.$$

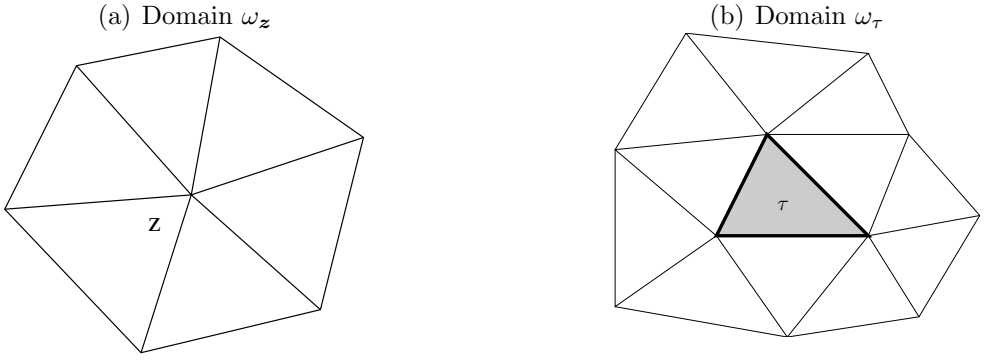

Fig. 3.1: Subdomains of the triangulation in 2D

We denote by $\mathscr{P}_1(\tau)$ the space of continuous linear functions on a simplex $\tau \in \mathscr{T}_h(\Omega)$ and set

$$X_h(\Omega) := \{v_h \in C^0(\overline{\Omega}) \ : \ \forall \tau \in \mathscr{T}_h(\Omega)\ v_{h|\tau} \in \mathscr{P}_1(\tau)\}. \tag{3.1}$$

$X_h(\Omega)$ is a nodal conform trial space with $X_h(\Omega) \subset H^1(\Omega)$, where $\varphi_{\boldsymbol{z}} \in X_h(\Omega)$ is a piecewise linear continuous basis function at node $\boldsymbol{z} \in \mathscr{N}_h(\Omega)$. This trial space is used to approximate the time discrete fields c^n and μ^n for all time steps $0 \leq n \leq N$. The discrete fields $c_h^n, \mu_h^n \in X_h(\Omega)$ are represented by the basis functions using the approach

$$c_h^n(\boldsymbol{x}) = \sum_{\boldsymbol{z} \in \mathscr{N}_h(\Omega)} c_{\boldsymbol{z}}^n \varphi_{\boldsymbol{z}}(\boldsymbol{x}); \qquad \mu_h^n(\boldsymbol{x}) = \sum_{\boldsymbol{z} \in \mathscr{N}_h(\Omega)} \mu_{\boldsymbol{z}}^n \varphi_{\boldsymbol{z}}(\boldsymbol{x}).$$

Naturally, we identify coefficient vectors with this representation defined by $\underline{\boldsymbol{c}}^n := (c_{\boldsymbol{z}}^n)_{\boldsymbol{z} \in \mathscr{N}_h(\Omega)}$ and $\underline{\boldsymbol{\mu}}^n := (\mu_{\boldsymbol{z}}^n)_{\boldsymbol{z} \in \mathscr{N}_h(\Omega)}$.

For theoretical reasons only we introduce a trial space satisfying the mass conservation (1.17). This trial space is given by

$$X_{m,h}(\Omega) := \left\{ v_h \in X_h(\Omega) : \int_\Omega v_h \, d\boldsymbol{x} = m \geq 0 \right\}. \tag{3.2}$$

The space $X_{m,h}(\Omega)$ is also a conform trial space such that holds $X_{m,h}(\Omega) \subset X_m(\Omega)$. Note that the space $X_{m,h}(\Omega)$ is only used for theoretical reasons, all computation are implemented using the trial space $X_h(\Omega)$.

In order to approximate the time discrete displacement $\boldsymbol{u}^n$ a trial space of vector valued functions is necessary. We define

$$\boldsymbol{X}_h(\Omega) := \left\{ \boldsymbol{v}_h \in C^0(\overline{\Omega}, \mathbb{R}^d) : \forall \tau \in \mathscr{T}_h(\Omega), \boldsymbol{v}_{|\tau} \in [\mathscr{P}_1(\tau)]^d, \gamma_{|\Gamma_D} \boldsymbol{v}_h \equiv 0 \right\}. \tag{3.3}$$

Obviously $\boldsymbol{X}_h(\Omega)$ is a nodal conform trial space $\boldsymbol{X}_h(\Omega) \subset \boldsymbol{X}(\Omega)$ satisfying the Dirichlet boundary condition (1.56). Moreover, the approximation of the time discrete displacement $\boldsymbol{u}^n$ leads to the representation of the displacement $\boldsymbol{u}_h^n \in \boldsymbol{X}_h(\Omega)$ by basis functions $\boldsymbol{\varphi}_{\boldsymbol{z},i}$ for each component of the vector valued function,

$$\boldsymbol{u}_h^n(\boldsymbol{x}) = \sum_{\boldsymbol{z} \in \mathscr{N}_h(\Omega \setminus \Gamma_D)} \sum_{i=1}^{d} u_{\boldsymbol{z},i}^n \boldsymbol{\varphi}_{\boldsymbol{z},i}(\boldsymbol{x}).$$

Corresponding to this approach a coefficient vector is observed, which is introduced by $\underline{\boldsymbol{u}}^n := (u_{\boldsymbol{z},i}^n)_{(\boldsymbol{z} \in \mathscr{N}_h(\Omega \setminus \Gamma_D), 1 \leq i \leq d)}$.

Similar as in section 2.2.1 we formulate a piecewise constant expansion of the time discrete fields c_h^n, μ_h^n and $\boldsymbol{u}_h^n$ with respect to time and define for all time steps $1 \leq n \leq N$ at time $t \in ((n-1)\Delta t, n\Delta t]$

$$c_{\Delta t,h}(t, \boldsymbol{x}) := c_h^n(\boldsymbol{x}), \quad \mu_{\Delta t,h}(t, \boldsymbol{x}) := \mu_h^n(\boldsymbol{x}), \quad \boldsymbol{u}_{\Delta t,h}(t, \boldsymbol{x}) := \boldsymbol{u}_h^n(\boldsymbol{x}).$$

The time derivative of the concentration field $c_{\Delta t,h}$ will be approximated by an implicit Eulerian scheme. We get for all time steps $t = n\Delta t$ with $1 \leq n \leq N$

$$\dot{c}_{\Delta t,h}(n\Delta t, \boldsymbol{x}) \approx \frac{c_h^n(\boldsymbol{x}) - c_h^{n-1}(\boldsymbol{x})}{\Delta t} =: \partial_{\Delta t} c_h^n(\boldsymbol{x}).$$

Additionally to the piecewise constant expansion of the concentration field with respect to time we need a piecewise linear interpolant of the concentration. For all time steps $1 \leq n \leq N$ we define at time $t \in ((n-1)\Delta t, n\Delta t]$

$$\begin{aligned}
\overline{c}_{\Delta t,h}(t, \boldsymbol{x}) &:= c_h^n(\boldsymbol{x}) \left(\frac{t - (n-1)\Delta t}{\Delta t} \right) - c_h^{n-1}(\boldsymbol{x}) \left(\frac{t - n\Delta t}{\Delta t} \right), \\
\dot{\overline{c}}_{\Delta t,h}(t, \boldsymbol{x}) &:= \frac{c_h^n(\boldsymbol{x}) - c_h^{n-1}(\boldsymbol{x})}{\Delta t}.
\end{aligned}$$

The nonlinearity in the mobility tensor $\boldsymbol{M}$ is linearised analogous to section 2.2.1, however on a discrete level. We define for $c_h^{n-1} \in X_h(\Omega)$ the linearised mobility tensor

$$\boldsymbol{M}_h^{n-1}(\boldsymbol{x}) := \boldsymbol{M}(c_h^{n-1}(\boldsymbol{x})). \tag{3.4}$$

Additionally we need further mesh conditions taken form [16] in order to formulate appropriate properties of the $L_2(\Omega)$-projection. For each finite element $\tau \in \mathscr{T}_h(\Omega)$ we define the following local matrices $\underline{\boldsymbol{G}}_\tau$, $\underline{\boldsymbol{D}}_\tau$ and $\underline{\boldsymbol{H}}_\tau$ for all nodes $\boldsymbol{x}, \boldsymbol{z} \in \mathscr{N}_h(\tau)$

$$\underline{\boldsymbol{G}}_\tau[\boldsymbol{x}, \boldsymbol{z}] := \langle \varphi_{\boldsymbol{x}}, \varphi_{\boldsymbol{z}} \rangle_{L_2(\tau)}, \quad \underline{\boldsymbol{D}}_\tau := \operatorname{diag}(\|\varphi_{\boldsymbol{z}}\|^2_{L_2(\tau)}), \quad \underline{\boldsymbol{H}}_\tau := \operatorname{diag}(h_{\boldsymbol{z}}).$$

Similar as above $\varphi_{\boldsymbol{z}}$ denotes the piecewise linear basis function corresponding to the node $\boldsymbol{z} \in \mathscr{N}_h(\Omega)$ of the triangulation $\mathscr{T}_h(\Omega)$. For the triangulation $\mathscr{T}_h(\Omega)$ we assume in view of [16] that there exists a constant c independent of the mesh size such that

$$(\underline{\boldsymbol{H}}_\tau^{-1} \underline{\boldsymbol{G}}_\tau \underline{\boldsymbol{H}}_\tau \underline{\boldsymbol{x}}_\tau, \underline{\boldsymbol{x}}_\tau) \geq c(\underline{\boldsymbol{D}}_\tau \underline{\boldsymbol{x}}_\tau, \underline{\boldsymbol{x}}_\tau), \quad \forall \underline{\boldsymbol{x}} \in \mathbb{R}^{\sharp \mathscr{N}_h(\tau)}. \tag{3.5}$$

Finally we deal with the inverse inequality taken from [18, 93]:

Lemma 3.4 (Inverse inequality). *Let $\mathscr{T}_h(\Omega)$ be an admissible triangulation satisfying the shape regularity condition. Then there exists a constant C independent of the mesh size such that for an arbitrary function $v_h \in X_h(\Omega)$ on any simplex $\tau \in \mathscr{T}_h(\Omega)$ the following local inverse inequality holds*

$$\|v_h\|_{L_\infty(\tau)} \leq C h_\tau^{-\frac{d}{2}} \|v_h\|_{L_2(\tau)}.$$

Moreover, let the triangulation $\mathscr{T}_h(\Omega)$ additionally be uniform, then a global inverse inequality holds

$$\|v_h\|_{L_\infty(\Omega)} \leq C h^{-\frac{d}{2}} \|v_h\|_{L_2(\Omega)}.$$

Proof. These statements are proved in [93], corollary 9.1 and lemma 9.4. □

3.2 Clement quasi-interpolation operator

The aim of this section is to give an approximation theorem of functions in Sobolev spaces $H^1(\Omega)$ by finite element functions in $X_h(\Omega)$ without classical interpolation, which is investigated in [18, 85]. In order to achieve this we introduce the Clement quasi-interpolation operator from [26], which is additionally used to derive stability estimates even in $L_\infty(\Omega)$.

Clement formulated this operator in a very general way. In this subsection we introduce a Clement type quasi-interpolation operator taken from [92]. First of all, we define the local $L_2(\omega_{\boldsymbol{z}})$-projection in the following way:

Definition 3.5. For all nodes $\boldsymbol{z} \in \mathcal{N}_h(\Omega)$ of an admissible triangulation $\mathcal{T}_h(\Omega)$ the local $L_2(\omega_{\boldsymbol{z}})$-projection on the local trial space $X_h(\omega_{\boldsymbol{z}})$ is defined by

$$\begin{aligned} \mathcal{Q}_h^{\omega_{\boldsymbol{z}}} : L_2(\omega_{\boldsymbol{z}}) &\longrightarrow X_h(\omega_{\boldsymbol{z}}), \\ v &\longmapsto v_h := \mathcal{Q}_h^{\omega_{\boldsymbol{z}}} v, \end{aligned}$$

where v_h is defined by the following weak problem: Find $v_h \in L_2(\Omega)$ such that holds

$$\int_{\omega_{\boldsymbol{z}}} v_h \xi_h \, d\boldsymbol{x} = \int_{\omega_{\boldsymbol{z}}} v \xi_h \, d\boldsymbol{x} \qquad \xi_h \in X_h(\omega_{\boldsymbol{z}}).$$

It is a classical result that the local $L_2(\omega_{\boldsymbol{z}})$-projection has a unique solution and satisfies an uniform a-priori estimate in the norm of $L_2(\omega_{\boldsymbol{z}})$. The local $L_2(\omega_{\boldsymbol{z}})$-projection is used to calculate the interpolation weights of the global Clement quasi-interpolation operator.

Definition 3.6 (Clement quasi-interpolation operator). For an admissible triangulation $\mathcal{T}_h(\Omega)$ the global Clement quasi-interpolation operator $\mathcal{R}_h$ is defined by

$$\begin{aligned} \mathcal{R}_h : L_2(\Omega) &\longrightarrow X_h(\Omega), \\ v &\longmapsto v_h = \mathcal{R}_h v := \sum_{\boldsymbol{z} \in \mathcal{N}_h(\Omega)} (\mathcal{Q}_h^{\omega_{\boldsymbol{z}}} v)(\boldsymbol{z}) \varphi_{\boldsymbol{z}}. \end{aligned}$$

Lemma 3.7 (A-priori estimate). *Let $\mathcal{T}_h(\Omega)$ be an admissible, exact and locally quasi-uniform triangulation, satisfying the shape regularity condition. Let $v \in H^1(\Omega) \cap L_\infty(\Omega)$ be arbitrary. Then there exists a constant C independent of the mesh size, such that holds:*

(1) $\|\mathcal{R}_h v\|_{L_2(\Omega)} \leq \|v\|_{L_2(\Omega)}$

(2) $\|\mathcal{R}_h v\|_{H^1(\Omega)} \leq C \|v\|_{H^1(\Omega)}$

(3) $\|\mathcal{R}_h v\|_{L_\infty(\Omega)} \leq C \|v\|_{L_\infty(\Omega)}$

Proof. The a-priori estimate in $L_2(\Omega)$ is a result proved in [26]. In [16] the a-priori estimate in $H^1(\Omega)$ is proved by using the fact that the mesh is locally quasi-uniform.

It remains to show the a-priori estimate in $L_\infty(\Omega)$. Let $v \in H^1(\Omega) \cap L_\infty(\Omega)$ be arbitrary, then there exists a node $\boldsymbol{y} \in \mathscr{N}_h(\Omega)$ where the maximum of $\mathcal{R}_h v$ is achieved. Using the local inverse inequality from lemma 3.4 and taking into account that $\mathscr{T}_h(\Omega)$ is locally quasi-uniform, then we calculate

$$\begin{aligned}\|\mathcal{R}_h v\|_{L_\infty(\Omega)} = |(\mathcal{Q}_h^{\omega_{\boldsymbol{y}}} v)(\boldsymbol{y})| &\leq \sum_{\tau \in \mathscr{T}_h(\omega_{\boldsymbol{y}})} \|\mathcal{Q}_h^{\omega_{\boldsymbol{y}}} v\|_{L_\infty(\tau)} \\ &\leq C \sum_{\tau \in \mathscr{T}_h(\omega_{\boldsymbol{y}})} h_\tau^{-\frac{d}{2}} \|\mathcal{Q}_h^{\omega_{\boldsymbol{y}}} v\|_{L_2(\tau)} \leq \tilde{C} h_{\boldsymbol{y}}^{-\frac{d}{2}} \|\mathcal{Q}_h^{\omega_{\boldsymbol{y}}} v\|_{L_2(\omega_{\boldsymbol{y}})} \\ &\leq \tilde{C} h_{\boldsymbol{y}}^{-\frac{d}{2}} \|v\|_{L_2(\omega_{\boldsymbol{y}})} \leq \hat{C} h_{\boldsymbol{y}}^{-\frac{d}{2}} \operatorname{meas}(\omega_{\boldsymbol{y}})^{\frac{1}{2}} \|v\|_{L_\infty(\omega_{\boldsymbol{y}})}.\end{aligned}$$

Finally, we have to take into account the shape regularity condition and the fact that $\mathscr{T}_h(\Omega)$ is locally quasi-uniform in order to calculate

$$\operatorname{meas}(\omega_{\boldsymbol{y}})^{\frac{1}{2}} \leq \sum_{\tau \in \mathscr{T}_h(\omega_{\boldsymbol{y}})} h_\tau^{\frac{d}{2}} \leq \sharp \mathscr{T}_h(\omega_{\boldsymbol{y}}) q h_{\boldsymbol{y}}^{\frac{d}{2}} \leq C h_{\boldsymbol{y}}^{\frac{d}{2}}$$

This calculation leads directly to the statement of this lemma. □

Lemma 3.8 (Approximation property). *Let $\mathscr{T}_h(\Omega)$ be an admissible, exact and locally quasi-uniform triangulation, which satisfies the shape regularity condition and let $v \in H^1(\Omega)$ be arbitrary. Then there exists a constant C independent of the mesh size, such that the following convergence results hold:*

(1) $\|v - \mathcal{R}_h v\|_{L_2(\tau)} \leq C h_\tau |v|_{H^1(\omega_\tau)}$

(2) $\|v - \mathcal{R}_h v\|_{H^1(\Omega)} \longrightarrow 0$ *if* $h \longrightarrow 0$

Proof. Statement *(1)* is proved in [16] taking into account that the mesh is locally quasi-uniform. A global convergence result in $L_2(\Omega)$ is available even for global uniform meshes in [26]. Statement *(2)* follows from [26]. □

Moreover, we have to consider quasi-interpolation with respect to space and time. Let $v \in L_2(0,T;H^1(\Omega))$, then it must be remarked that for almost all $t \in (0,T)$ the Clement quasi-interpolation operator formulated in definition 3.6 is well defined,

$$v_h(t,\cdot) := \mathcal{R}_h v(t,\cdot).$$

Consequently, the a-priori estimates from lemma 3.7 and the convergence results formulated in lemma 3.8 hold for almost all times $t \in (0,T)$.

Lemma 3.9 (Approximation property). *Let $\mathscr{T}_h(\Omega)$ be an admissible, exact and locally quasi-uniform triangulation satisfying the shape regularity condition. Furthermore, let $v \in L_2(0,T;H^1(\Omega))$ be arbitrary, then the following convergence result holds*

$$\|v - \mathcal{R}_h v\|_{L_2(0,T;H^1(\Omega))} \longrightarrow 0 \qquad \text{if} \quad h \longrightarrow 0.$$

Proof. Let $v \in L_2(0,T;H^1(\Omega))$ be arbitrary, then we consider

$$\|v - \mathcal{R}_h v\|^2_{L_2(0,T;H^1(\Omega))} = \int_0^T \|v(t,\cdot) - \mathcal{R}_h v(t,\cdot)\|^2_{H^1(\Omega)} dt.$$

Since for almost all $t \in (0,T)$ holds $\|v(t,\cdot) - \mathcal{R}_h v(t,\cdot)\|^2_{H^1(\Omega)} \to 0$ if $h \to 0$ and $\|v(t,\cdot) - \mathcal{R}_h v(t,\cdot)\|^2_{H^1(\Omega)} \leq 2\|v(t,\cdot)\|_{H^1(\Omega)}$, the convergence follows from Lebesgue's convergence theorem. □

3.3 Preprocessing

Due to the fact that the Cahn-Larché system describes a time dependent problem, we have to compute initial quantities. First of all, we have to project the initial data c_0 onto the trial space $X_h(\Omega)$. Furthermore, the initial displacement $\boldsymbol{u}_h^0$, which corresponds to the initial concentration field c_h^0, has to be computed.

3.3.1 Projection of the initial data

The projection of the initial data c_0 onto the trial space $X_h(\Omega)$ is done by applying a $L_2(\Omega)$-projection, which is possible, because we assume in (A-5) that $c_0 \in H^1(\Omega) \cap L_\infty(\Omega)$.

Definition 3.10. Let $\Omega \subset \mathbb{R}^d$ be a domain satisfying condition (H-1). The triangulation is assumed to be exact and admissible. Then the $L_2(\Omega)$-projection is denoted by the following operator

$$\begin{aligned} \mathcal{Q}_h : L_2(\Omega) &\longrightarrow X_h(\Omega), \\ c_0 &\longmapsto c_h^0 := \mathcal{Q}_h c_0, \end{aligned}$$

and defined by the following weak problem: Find $c_h^0 \in X_h(\Omega)$ such that holds

$$\int_\Omega c_h^0 \xi_h \, d\boldsymbol{x} = \int_\Omega c_0 \xi_h \, d\boldsymbol{x} \qquad \forall \xi_h \in X_h(\Omega).$$

Corollary 3.11 (Existence of a solution). *Let $\Omega \subset \mathbb{R}^d$ be a domain satisfying condition (H-1). Moreover, we assume that the initial data c_0 satisfy the assumption (A-5) and $\mathscr{T}_h(\Omega)$ is an admissible and exact triangulation. Then there exists a unique solution $c_h^0 \in X_h(\Omega)$ of the $L_2(\Omega)$-projection. Moreover, it holds $c_h^0 \in X_{m,h}(\Omega)$.*

Proof. The existence of a unique solution follows from classical textbooks, e.g. [18, 85]. We have to show that $c_h^0 \in X_{m,h}(\Omega)$ holds. By using the test function $\xi_h \equiv 1 \in X_h(\Omega)$, we deduce directly from assumption (A-5)

$$\int_\Omega c_h^0 \, d\boldsymbol{x} = \int_\Omega c_0 \, d\boldsymbol{x} = m.$$

This means that the $L_2(\Omega)$-projection is mass conserving. □

Lemma 3.12 (Convergence). *Let $\Omega \subset \mathbb{R}^d$ be a domain satisfying condition (H-1). We assume that the initial data c_0 satisfy assumption (A-5) and that the triangulation $\mathscr{T}_h(\Omega)$ is exact, admissible, uniform and satisfies the shape regularity condition. Then there exists a constant $C > 0$ independent of the mesh size, such that for the $L_2(\Omega)$-projection c_h^0 the following convergence result holds*

$$\|c_0 - c_h^0\|_{L_2(\Omega)} \leq Ch\|c_0\|_{H^1(\Omega)}.$$

Proof. This statement is proved in classical textbooks like [18, 85]. □

Lemma 3.13 (A-priori estimate). *Let $\Omega \subset \mathbb{R}^d$ be a domain satisfying condition (H-1). We assume that the initial data c_0 satisfy assumption (A-5) and that the triangulation $\mathscr{T}_h(\Omega)$ is exact, admissible, uniform and satisfies the mesh property* (3.5)*. Then there exists a constant C independent of the mesh size, such that for the $L_2(\Omega)$-projection c_h^0 holds*

(1) $\|c_h^0\|_{L_2(\Omega)} \leq \|c_0\|_{L_2(\Omega)}$

(2) $\|c_h^0\|_{H^1(\Omega)} \leq C\|c_0\|_{H^1(\Omega)}$

(3) $\|c_h^0\|_{L_\infty(\Omega)} \leq C(\|c_0\|_{H^1(\Omega)} + \|c_0\|_{L_\infty(\Omega)})$

Proof. Statement *(1)* is proved in classical textbooks, e.g. [18, 85]. Statement *(2)* also holds for locally quasi-uniform meshes, which is proved in [16] by using the Clement quasi-interpolation operator $\mathcal{R}_h$ and taking into account the mesh condition (3.5).

It remains to show the stability in $L_\infty(\Omega)$ of the $L_2(\Omega)$-projection. Statement *(3)* is proved by applying the $L_\infty(\Omega)$ stability of the Clement quasi-interpolation operator $\mathcal{R}_h$ proved in lemma 3.7. We yield

$$\|c_h^0\|_{L_\infty(\Omega)} = \|c_h^0 - \mathcal{R}_h c_0 + \mathcal{R}_h c_0\|_{L_\infty(\Omega)} \leq \|c_h^0 - \mathcal{R}_h c_0\|_{L_\infty(\Omega)} + C\|c_0\|_{L_\infty(\Omega)}$$

Considering the first term in this calculation we use the inverse inequality, the convergence of the $L_2(\Omega)$-projection, see lemma 3.12, and the convergence of the Clement

quasi-interpolation operator, see lemma 3.8, in order to deduce

$$\begin{aligned}\|c_h^0 - \mathcal{R}_h c_0\|_{L_\infty(\Omega)} &\leq Ch^{-1}\|c_h^0 - \mathcal{R}_h c_0\|_{L_2(\Omega)} \\ &\leq Ch^{-1}\left(\|c_h^0 - c_0\|_{L_2(\Omega)} + \|c_0 - \mathcal{R}_h c_0\|_{L_2(\Omega)}\right) \\ &\leq C\|c_0\|_{H^1(\Omega)}.\end{aligned}$$

Summing up both estimates this yields $\|c_h^0\|_{L_\infty(\Omega)} \leq C(\|c_0\|_{H^1(\Omega)} + \|c_0\|_{L_\infty(\Omega)})$. □

The $L_2(\Omega)$-projection leads to a linear equation system (LES), which has to be solved at the beginning of the simulation process. This LES is given by the weak problem in definition 3.10 in the following form: For all nodes $\boldsymbol{y}, \boldsymbol{z} \in \mathcal{N}_h(\Omega)$ we have

$$\underline{\boldsymbol{A}}\underline{\boldsymbol{c}}^0 = \underline{\boldsymbol{f}}, \quad \underline{\boldsymbol{A}}[\boldsymbol{y}, \boldsymbol{z}] := \int_\Omega \varphi_{\boldsymbol{y}}\varphi_{\boldsymbol{x}}\, d\boldsymbol{x}, \quad \underline{\boldsymbol{f}}[\boldsymbol{z}] := \int_\Omega c_0\varphi_{\boldsymbol{z}}\, d\boldsymbol{x}.$$

Obviously the matrix $\underline{\boldsymbol{A}}$ is a symmetric positive definite matrix and due to this fact the LES has a unique solution. Within the numerical simulation this LES is solved iteratively by using the conjugated gradient method (CG) developed in [58]. The precondition of the LES is done by applying the diagonal matrix $\underline{\boldsymbol{B}} = \mathrm{diag}(\underline{\boldsymbol{A}})$. From [93] follows that $\underline{\boldsymbol{B}}$ and $\underline{\boldsymbol{A}}$ are spectral equivalent and due to this fact $\underline{\boldsymbol{B}}$ is an appropriate choice for a precondition matrix and can be fastly applied.

During numerical simulation the entries of the matrix $\underline{\boldsymbol{A}}$ are computed by an explicit formula, in contrast to the computation of the vector $\underline{\boldsymbol{f}}$, which is done by a quadrature formula. On a triangle $\tau \in \mathscr{T}_h(\Omega)$ the seven point formula of Radon [1, 27, 86] is applied, in three dimensions we refer to [60] for a quadrature formula on a tetrahedron.

3.3.2 Solution of the initial elasticity problem

The second task in the preprocessing procedure is the numerical solution of the initial elasticity problem corresponding to the initial concentration field c_0. From definition 2.13 of a semi-weak solution of the Cahn-Larché system we take (2.7) and get the following discrete problem of the initial displacement.

Problem 3.14. Find $\boldsymbol{u}_h^0 \in \boldsymbol{X}(\Omega)$, such that holds

$$\int_\Omega \boldsymbol{C}(c_h^0)\boldsymbol{\varepsilon}(\boldsymbol{u}_h^0) : \boldsymbol{\varepsilon}(\boldsymbol{\eta}_h)\, d\boldsymbol{x} = \int_\Omega \boldsymbol{C}(c_h^0)\overline{\boldsymbol{\varepsilon}}(c_h^0) : \boldsymbol{\varepsilon}(\boldsymbol{\eta}_h)\, d\boldsymbol{x} + \int_{\Gamma_N} \boldsymbol{g}^0 \cdot \boldsymbol{\eta}_h\, d\boldsymbol{a}_{\boldsymbol{x}} \qquad \forall \boldsymbol{\eta}_h \in \boldsymbol{X}_h(\Omega).$$

Note that within this problem $\boldsymbol{u}_h^0$ is the unknown quantity, whereas c_h^0 is known from the above considered $L_2(\Omega)$-projection of the initial data c_0. Due to the assumptions (A-6) - (A-8) all integrals exist and problem 3.14 is well defined. We have

to remark that the analysis of the discrete weak problem 3.14 is well known from [15, 25], because for a fixed concentration field c_h^0, it is a linear problem for the unknown displacement $\boldsymbol{u}_h^0$. But in context of the Cahn-Larché system we additionally have to consider the dependence of the material parameter from the concentration field c_h^0.

Lemma 3.15 (A-priori estimate). *Let $\Omega \subset \mathbb{R}^d$ be a domain satisfying condition (H-1). Let the assumptions (A-6) - (A-8) be satisfied and let $\mathscr{T}_h(\Omega)$ be an exact and admissible triangulation, then there exists a unique solution $\boldsymbol{u}_h^0 \in \boldsymbol{X}_h(\Omega)$ of problem 3.14, which satisfies the a-priori estimate*

$$\|\boldsymbol{u}_h^0\|_{\boldsymbol{H}^1(\Omega)} \leq C_{\boldsymbol{u}}.$$

Proof. The estimates calculated in lemma 2.14 are obviously valid for problem 3.14 and the Lax-Milgram theorem leads to the unique solution of problem 3.14 with the same a-priori estimate as in (2.8). □

In order to show convergence of the discrete solution $\boldsymbol{u}_h^0$ of the initial elasticity problem, we derive an error estimate similar to the Strang lemma. For this reason we observe the following auxiliary problem:

Problem 3.16. Find $\tilde{\boldsymbol{u}}_0 \in \boldsymbol{X}(\Omega)$ such that holds

$$\int_\Omega \boldsymbol{C}(c_h^0)\boldsymbol{\varepsilon}(\tilde{\boldsymbol{u}}_0) : \boldsymbol{\varepsilon}(\boldsymbol{\eta})\, d\boldsymbol{x} = \int_\Omega \boldsymbol{C}(c_h^0)\overline{\boldsymbol{\varepsilon}}(c_h^0) : \boldsymbol{\varepsilon}(\boldsymbol{\eta})\, d\boldsymbol{x} + \int_{\Gamma_N} \boldsymbol{g}^0 \cdot \boldsymbol{\eta}\, d\boldsymbol{a}_{\boldsymbol{x}} \qquad \forall \boldsymbol{\eta} \in \boldsymbol{X}(\Omega).$$

In view of assumption (A-6) - (A-8), Hölder's and Korn's inequality together with the trace theorem the same estimates as in lemma 2.14 hold. Due to this fact and Lax-Milgram's theorem there exists a unique solution $\tilde{\boldsymbol{u}}_0 \in \boldsymbol{X}(\Omega)$ of problem 3.16.

Corollary 3.17 (Galerkin orthogonality). *Let $\boldsymbol{u}_h^0 \in \boldsymbol{X}_h(\Omega)$ be the unique solution of the discrete problem 3.14 and let $\tilde{\boldsymbol{u}}_0 \in \boldsymbol{X}(\Omega)$ be the unique solution of the auxiliary problem 3.16. Then the Galerkin orthogonality holds*

$$\int_\Omega \boldsymbol{C}(c_h^0)(\boldsymbol{\varepsilon}(\boldsymbol{u}_h^0) - \boldsymbol{\varepsilon}(\tilde{\boldsymbol{u}}_0)) : \boldsymbol{\varepsilon}(\boldsymbol{\eta}_h)\, d\boldsymbol{x} = \boldsymbol{0} \qquad \forall \boldsymbol{\eta}_h \in \boldsymbol{X}_h(\Omega).$$

Proof. This relation follows directly from the weak formulation in problem 3.16 by choosing $\boldsymbol{\eta} = \boldsymbol{\eta}_h$ and subtracting this equation from the discrete weak formulation in problem 3.14. □

Lemma 3.18 (Cea's lemma). *Let $\Omega \subset \mathbb{R}^d$ be a domain satisfying condition (H-1) and let the assumptions (A-6) - (A-8) be satisfied. Let $\mathscr{T}_h(\Omega)$ be an exact and*

admissible triangulation of the reference domain Ω. Furthermore, let $\boldsymbol{u}_h^0 \in \boldsymbol{X}_h(\Omega)$ be the unique solution of the discrete problem 3.14 and let $\tilde{\boldsymbol{u}}_0 \in \boldsymbol{X}(\Omega)$ be the unique solution of the auxiliary problem 3.16. Then the following a-priori error estimate holds

$$\|\boldsymbol{u}_h^0 - \tilde{\boldsymbol{u}}_0\|_{\boldsymbol{H}^1(\Omega)} \leq \frac{C_C c_k}{c_C} \inf_{\boldsymbol{\eta}_h \in \boldsymbol{X}_h(\Omega)} \|\tilde{\boldsymbol{u}}_0 - \boldsymbol{\eta}_h\|_{\boldsymbol{H}^1(\Omega)}.$$

Proof. By using assumption (A-6), Korn's inequality (2.3), Hölder's inequality and the above mentioned Galerkin orthogonality formulated in corollary 3.17, we derive

$$\begin{aligned}
\frac{c_C}{c_k}\|\boldsymbol{u}_h^0 - \tilde{\boldsymbol{u}}_0\|_{H^1(\Omega)}^2 &\leq \int_\Omega \boldsymbol{C}(c_h^0)(\boldsymbol{\varepsilon}(\boldsymbol{u}_h^0) - \boldsymbol{\varepsilon}(\tilde{\boldsymbol{u}}_0)) : (\boldsymbol{\varepsilon}(\boldsymbol{u}_h^0) - \boldsymbol{\varepsilon}(\tilde{\boldsymbol{u}}_0))\, d\boldsymbol{x} \\
&\quad + \int_\Omega \boldsymbol{C}(c_h^0)(\boldsymbol{\varepsilon}(\boldsymbol{u}_h^0) - \boldsymbol{\varepsilon}(\tilde{\boldsymbol{u}}_0)) : (\boldsymbol{\varepsilon}(\boldsymbol{\eta}_h) - \boldsymbol{\varepsilon}(\boldsymbol{u}_h^0))\, d\boldsymbol{x} \\
&= \int_\Omega \boldsymbol{C}(c_h^0)(\boldsymbol{\varepsilon}(\boldsymbol{u}_h^0) - \boldsymbol{\varepsilon}(\tilde{\boldsymbol{u}}_0)) : (\boldsymbol{\varepsilon}(\boldsymbol{\eta}_h) - \boldsymbol{\varepsilon}(\tilde{\boldsymbol{u}}_0))\, d\boldsymbol{x} \\
&\leq C_C \|\boldsymbol{u}_h^0 - \tilde{\boldsymbol{u}}_0\|_{\boldsymbol{H}^1(\Omega)} \|\tilde{\boldsymbol{u}}_0 - \boldsymbol{\eta}_h\|_{\boldsymbol{H}^1(\Omega)}.
\end{aligned}$$

Due to the fact that $\boldsymbol{\eta}_h \in \boldsymbol{X}_h(\Omega)$ is chosen arbitrary the statement of this lemma is proved. □

Lemma 3.19 (Error estimate). *Let $\Omega \subset \mathbb{R}^d$ be a domain satisfying condition (H-1) and let the assumptions (A-6) - (A-8) be satisfied. Let $\mathscr{T}_h(\Omega)$ be an exact and admissible triangulation of the reference domain Ω. Furthermore, let $\tilde{\boldsymbol{u}}_0 \in \boldsymbol{X}(\Omega)$ be the unique solution of the problem 3.16 and let $\boldsymbol{u}_0 \in \boldsymbol{X}(\Omega)$ be the unique solution of the semi-weak problem* (2.7)*. Then the following error estimate holds*

$$\begin{aligned}
\|\tilde{\boldsymbol{u}}_0 - \boldsymbol{u}_0\|_{\boldsymbol{H}^1(\Omega)} \leq \frac{c_k}{c_C} \big(&\|(\boldsymbol{C}(c_h^0) - \boldsymbol{C}(c_0))\boldsymbol{\varepsilon}(\boldsymbol{u}_0)\|_{\boldsymbol{L}_2(\Omega)} \\
&+ \|\boldsymbol{C}(c_h^0)\overline{\boldsymbol{\varepsilon}}(c_h^0) - \boldsymbol{C}(c_0)\overline{\boldsymbol{\varepsilon}}(c_0)\|_{\boldsymbol{L}_2(\Omega)} \big).
\end{aligned}$$

Proof. Subtracting the weak formulation (2.7) from the discrete weak formulation in problem 3.16 and inserting $\int_\Omega \boldsymbol{C}(c_h^0)\boldsymbol{\varepsilon}(\boldsymbol{u}_0) : \boldsymbol{\varepsilon}(\boldsymbol{\eta}) - \boldsymbol{C}(c_h^0)\boldsymbol{\varepsilon}(\boldsymbol{u}_0) : \boldsymbol{\varepsilon}(\boldsymbol{\eta})\, d\boldsymbol{x}$ on the left hand side, we get

$$\begin{aligned}
&\int_\Omega (\boldsymbol{C}(c_h^0)\boldsymbol{\varepsilon}(\tilde{\boldsymbol{u}}_0) - \boldsymbol{C}(c_0)\boldsymbol{\varepsilon}(\boldsymbol{u}_0)) : \boldsymbol{\varepsilon}(\boldsymbol{\eta})\, d\boldsymbol{x} \\
&= \int_\Omega (\boldsymbol{C}(c_h^0) - \boldsymbol{C}(c_0))\boldsymbol{\varepsilon}(\boldsymbol{u}_0) : \boldsymbol{\varepsilon}(\boldsymbol{\eta})\, d\boldsymbol{x} + \int_\Omega \boldsymbol{C}(c_h^0)(\boldsymbol{\varepsilon}(\tilde{\boldsymbol{u}}_0) - \boldsymbol{\varepsilon}(\boldsymbol{u}_0)) : \boldsymbol{\varepsilon}(\boldsymbol{\eta})\, d\boldsymbol{x}.
\end{aligned}$$

Finally we choose $\boldsymbol{\eta} = \tilde{\boldsymbol{u}}_0 - \boldsymbol{u}_0$ and take into account assumption (A-6) together

with Hölder's and Korn's inequality, then we calculate

$$\begin{aligned}\frac{c_C}{c_k}\|\tilde{\boldsymbol{u}}_0-\boldsymbol{u}_0\|^2_{\boldsymbol{H}^1(\Omega)} &\leq \int_\Omega \boldsymbol{C}(c_h^0)\boldsymbol{\varepsilon}(\tilde{\boldsymbol{u}}_0-\boldsymbol{u}_0):\boldsymbol{\varepsilon}(\tilde{\boldsymbol{u}}_0-\boldsymbol{u}_0)\,d\boldsymbol{x}\\ &\leq \left|\int_\Omega (\boldsymbol{C}(c_h^0)-\boldsymbol{C}(c_0))\boldsymbol{\varepsilon}(\boldsymbol{u}_0):\boldsymbol{\varepsilon}(\tilde{\boldsymbol{u}}_0-\boldsymbol{u}_0)\,d\boldsymbol{x}\right|\\ &\quad+\left|\int_\Omega (\boldsymbol{C}(c_h^0)\overline{\boldsymbol{\varepsilon}}(c_h^0)-\boldsymbol{C}(c_0)\overline{\boldsymbol{\varepsilon}}(c_0)):\boldsymbol{\varepsilon}(\tilde{\boldsymbol{u}}_0-\boldsymbol{u}_0)\,d\boldsymbol{x}\right|\\ &\leq \|(\boldsymbol{C}(c_h^0)-\boldsymbol{C}(c_0))\overline{\boldsymbol{\varepsilon}}(\boldsymbol{u}_0)\|_{\boldsymbol{L}_2(\Omega)}\|\tilde{\boldsymbol{u}}_0-\boldsymbol{u}_0\|_{\boldsymbol{H}^1(\Omega)}\\ &\quad+\|\boldsymbol{C}(c_h^0)\overline{\boldsymbol{\varepsilon}}(c_h^0)-\boldsymbol{C}(c_0)\overline{\boldsymbol{\varepsilon}}(c_0)\|_{\boldsymbol{L}_2(\Omega)}\|\tilde{\boldsymbol{u}}_0-\boldsymbol{u}_0\|_{\boldsymbol{H}^1(\Omega)}.\end{aligned}$$

□

From lemma 3.13 we extract by applying Weyl's corollary 2.12 an almost everywhere convergent subsequence

$$c_h^0(\boldsymbol{x})\longrightarrow c_0(\boldsymbol{x})\quad\text{if}\quad h\longrightarrow 0.$$

Lemma 3.20 (Convergence). *Let $\Omega\subset\mathbb{R}^d$ be a domain satisfying condition (H-1) and let the assumptions (A-6) - (A-8) be satisfied. The triangulation $\mathscr{T}_h(\Omega)$ is assumed to be exact, admissible and satisfies the shape regularity condition. Furthermore let $\boldsymbol{u}_h^0\in\boldsymbol{X}_h(\Omega)$ be the unique solution of the discrete weak problem 3.14 and let $\boldsymbol{u}_0\in\boldsymbol{X}(\Omega)$ be the unique solution of the semi-weak problem* (2.7)*. Then it holds*

$$\boldsymbol{u}_h^0\longrightarrow\boldsymbol{u}_0\quad in\quad \boldsymbol{H}^1(\Omega)\quad if\quad h\longrightarrow 0.$$

Proof. In view of Cea's lemma 3.18 and the error estimate formulated in lemma 3.19 we derive by using the Clement operator

$$\begin{aligned}\|\boldsymbol{u}_h^0-\boldsymbol{u}_0\|_{\boldsymbol{H}^1(\Omega)} &\leq \|\boldsymbol{u}_h^0-\tilde{\boldsymbol{u}}_0\|_{\boldsymbol{H}^1(\Omega)}+\|\tilde{\boldsymbol{u}}_0-\boldsymbol{u}_0\|_{\boldsymbol{H}^1(\Omega)}\\ &\leq \frac{C_{\boldsymbol{u}}c_k}{c_{\boldsymbol{u}}}\|\tilde{\boldsymbol{u}}_0-\mathcal{R}_h\tilde{\boldsymbol{u}}_0\|_{\boldsymbol{H}^1(\Omega)}+\frac{c_k}{c_{\boldsymbol{u}}}\left(\|(\boldsymbol{C}(c_h^0)-\boldsymbol{C}(c_0))\boldsymbol{\varepsilon}(\tilde{\boldsymbol{u}}_0)\|_{\boldsymbol{L}_2(\Omega)}\right.\\ &\qquad\left.+\|\boldsymbol{C}(c_h^0)\overline{\boldsymbol{\varepsilon}}(c_h^0)-\boldsymbol{C}(c_0)\overline{\boldsymbol{\varepsilon}}(c_0)\|_{\boldsymbol{L}_2(\Omega)}\right).\end{aligned}$$

The convergence follows from the convergence result formulated in lemma 3.8 and from the almost everywhere convergence of c_h^0 together with the Lebesgue convergence theorem. □

Problem 3.14 corresponds to a LES for the displacement $\boldsymbol{u}_h^0$, which must be solved in the beginning of the numerical simulation. This LES is given for all nodes

$\boldsymbol{y}, \boldsymbol{z} \in \mathscr{N}_h(\Omega)$ by

$$\begin{aligned} \underline{\boldsymbol{L}}\underline{\boldsymbol{u}}^0 &= \underline{\boldsymbol{f}}, \\ \underline{\boldsymbol{L}}[\boldsymbol{z}, \boldsymbol{y}] &:= \int_\Omega \boldsymbol{C}(c_h^0)\boldsymbol{\varepsilon}(\boldsymbol{\eta}_{\boldsymbol{y}}) : \boldsymbol{\varepsilon}(\boldsymbol{\eta}_{\boldsymbol{z}})\, d\boldsymbol{x}, \\ \underline{\boldsymbol{f}}[\boldsymbol{z}] &:= \int_\Omega \boldsymbol{C}(c_h^0)\overline{\boldsymbol{\varepsilon}}(c_h^0) : \boldsymbol{\varepsilon}(\boldsymbol{\eta}_{\boldsymbol{z}})\, d\boldsymbol{x} + \int_{\Gamma_N} \boldsymbol{g}^0 \cdot \boldsymbol{\eta}_{\boldsymbol{z}}\, d\boldsymbol{a}_{\boldsymbol{x}}. \end{aligned} \tag{3.6}$$

The stiffness matrix $\underline{\boldsymbol{L}}$ is symmetric and positive definite, due to the fact that the elasticity tensor satisfies the symmetry property formulated in assumption (A-6). The positive definiteness of the matrix $\underline{\boldsymbol{L}}$ implies that the LES has a unique solution.

We remark that during numerical simulation the matrix $\underline{\boldsymbol{L}}$ respectively the vector $\underline{\boldsymbol{f}}$ are computed by using a quadrature formula. On a triangle $\tau \in \mathscr{T}_h(\Omega)$ the seven point formula of Radon [1, 86] is applied and in three space dimensions we refer to [60] for quadrature formulas on a tetrahedron. On the Neumann boundary Γ_N the integration of the boundary loading in two space dimensions is done by a five point quadrature formula of Gauß-Legendre, derived e.g. in [88]. In the three dimensional case, the integration takes place over a triangle, where Radon's seven point formula is used.

Within the numerical simulation the LES (3.6) is solved iteratively by using the CG method, see [58]. It is a known problem that the LES is ill conditioned. We have to construct a precondition matrix $\underline{\boldsymbol{B}}$, which is spectral equivalent to the stiffness matrix $\underline{\boldsymbol{L}}$ in order to solve the LES by the CG method efficiently.

The semi-weak elasticity problem (2.7) corresponds to a $\boldsymbol{X}(\Omega)$-elliptic selfadjoint operator $\boldsymbol{\mathcal{L}} : \boldsymbol{X}(\Omega) \longrightarrow \boldsymbol{X}'(\Omega)$. For this case Bramble, Pasciak and Xu [17, 105] developed a multilevel preconditioner (BPX), which is spectral equivalent to $\boldsymbol{\mathcal{L}}$ and also simple to apply.

We consider a hierarchy of global uniform triangulations $\mathscr{T}_{h_l}(\Omega)$ of the reference domain Ω. Corresponding to this mesh hierarchy we observe a hierarchy of conform nodal trial space

$$\boldsymbol{X}_{h_0}(\Omega) \subset \boldsymbol{X}_{h_1}(\Omega) \subset \ldots \subset \boldsymbol{X}_{h_L}(\Omega) \subset \ldots \subset \boldsymbol{X}(\Omega).$$

By using the global $L_2(\Omega)$-projection given by definition 3.10 we introduce the BPX-preconditioner in the following form

$$\begin{aligned} &\boldsymbol{\mathcal{B}} : \boldsymbol{X}(\Omega) \longrightarrow \boldsymbol{X}'(\Omega), \\ &\qquad \boldsymbol{v} \longmapsto \boldsymbol{z} = \boldsymbol{\mathcal{B}}\boldsymbol{v} := \sum_{l=0}^{\infty} h_l^{-2}(\boldsymbol{\mathcal{Q}}_{h_l} - \boldsymbol{\mathcal{Q}}_{h_{l-1}})\boldsymbol{v}. \end{aligned}$$

In [17, 93, 105] it is proved that $\boldsymbol{\mathcal{B}}$ is a bounded and $\boldsymbol{X}(\Omega)$-elliptic operator. Moreover, from [17, 93, 105] follows that the inverse Operator $\boldsymbol{\mathcal{B}}^{-1} : \boldsymbol{X}'(\Omega) \longrightarrow \boldsymbol{X}(\Omega)$ exists and it is also a bounded and $\boldsymbol{X}'(\Omega)$-elliptic operator. Therefore $\boldsymbol{\mathcal{B}}$ and $\boldsymbol{\mathcal{L}}$ are spectral equivalent. The inverse precondition operator $\boldsymbol{\mathcal{B}}^{-1}$ satisfies also a multilevel representation,

$$\boldsymbol{\mathcal{B}}^{-1} : \boldsymbol{X}'(\Omega) \longrightarrow \boldsymbol{X}(\Omega),$$
$$\boldsymbol{v} \longmapsto \boldsymbol{z} = \boldsymbol{\mathcal{B}}^{-1}\boldsymbol{v} := \sum_{l=0}^{\infty} h_l^2 (\boldsymbol{\mathcal{Q}}_{h_l} - \boldsymbol{\mathcal{Q}}_{h_{l-1}})\boldsymbol{v}.$$

For practical application the inverse precondition operator $\boldsymbol{\mathcal{B}}^{-1}$ must be efficiently implemented. Let $\boldsymbol{v}_h \in \boldsymbol{X}_{h_L}(\Omega)$, then it holds

$$\boldsymbol{z}_h = \boldsymbol{\mathcal{B}}^{-1}\boldsymbol{v}_h = \sum_{l=0}^{L} h_l^2 (\boldsymbol{\mathcal{Q}}_{h_l} - \boldsymbol{\mathcal{Q}}_{h_{l-1}})\boldsymbol{v}_h.$$

In iterative solution methods like CG we work with the corresponding coefficient vector $\underline{\boldsymbol{z}}$ and $\underline{\boldsymbol{v}}$. From [93] we take the following spectral equivalent application of the BPX precondition

$$\underline{\boldsymbol{z}} = \sum_{l=0}^{L} h_l^2 \underline{\boldsymbol{R}}_l \operatorname{diag}(\underline{\boldsymbol{A}}_l)^{-1} \underline{\boldsymbol{R}}_l^T \underline{\boldsymbol{v}}.$$

In this representation $\underline{\boldsymbol{R}}_l^T$ denotes the restriction operator from $X_{h_L}(\Omega)$ onto $X_{h_l}(\Omega)$, in contrast to $\underline{\boldsymbol{R}}_l$, which indicates the prolongation from $X_{h_l}(\Omega)$ onto $X_{h_L}(\Omega)$. The matrix $\underline{\boldsymbol{A}}_l$ represents the $L_2(\Omega)$-projection on the l-th grid level within the mesh hierarchy.

Chapter 4

Faedo-Galerkin methods for the viscous Cahn-Larché system

The fourth chapter deals with the numerical simulation of the spinodal decomposition under elastic loadings. These numerical simulations are done by applying a discretisation of the viscous Cahn-Larché system (1.51) - (1.53).

We remark that many authors before dealed with the simulation of spinodal decomposition. Spectral methods are used for solving the non-viscous Cahn-Larché system with periodic boundary conditions by Dreyer and Müller in [33] and Leo and Lowengrub in [59]. Due to the strong nonlinearities of the Cahn-Larché system, which appear in the mobility, elasticity and eigenstrain tensor and furthermore in the Gibbs free energy density, spectral methods lose their efficiency.

Three fast numerical methods for the non-viscous Cahn-Larché system are developed by Weikard in [102]. In general in [102] a finite difference method with respect to time and a finite element discretisation with respect to space are applied to the non-linear partial differential equation system. These techniques lead to Faedo-Galerkin methods, see [96], for the concentration field c_h^n, for the chemical potential μ_h^n and for the displacement $\boldsymbol{u}_h^n$ in every time step $0 \leq n \leq N$.

The first approximation technique in [102] contains a classical implicit Eulerian time discretisation and a finite element method with respect to space of the Cahn-Larché system. Within these methods the concentration field c_h^n, the chemical potential μ_h^n and the displacement $\boldsymbol{u}_h^n$ are computed simultaneously in every time step $1 \leq n \leq N$. This fact makes the complexity of the method extremely large. Nevertheless, the analysis of this approximation method is done for constant elasticity tensors in [50] and with concentration depending elasticity tensors in [51, 102].

Moreover, Weikard proposed in [102] a further Faedo-Galerkin scheme which decouples diffusion and elasticity. A decoupling of the elasticity from the diffusion reduces the computational complexity essentially, because only the concentration

field c_h^n and the chemical potential μ_h^n are computed simultaneously in every time step. The displacement $\boldsymbol{u}_h^n$ is determined in a postprocessing in every time step. In [102] Weikard proves the existence of a discrete solution of the numerical method, which decouples diffusion and elasticity. Furthermore, uniform a-priori estimates and the convergence of this method are shown.

Finally in [102] an operator splitting method is recommended, which is the most efficient method, but the analysis is still an open problem. Originally this splitting method was proposed in [94] and applied to the Navier-Stokes equations in [78]. We have to remark that in [50] also a Crank-Nicholson scheme is analysed.

For practical applications the surface stress tensor $\boldsymbol{\Gamma}$ is extremely small and the spinodal decomposition is mainly dominated by the non-convex part of the Gibbs free energy density and by the elastic contributions. In this situation phase separation is characterised by significant high frequency contributions to the concentration field, which are visible along phase interfaces. These oscillations are observed in terms of large overshoots and undershoots, a behaviour, which is known as Gibbs phenomena.

Fig.4.1 shows the development of the Sn concentration within a Sn-Pb alloy. Red coloured regions indicate the Sn-rich phase in contrast to the blue coloured areas, which indicate the Pb-rich phase. At time $t = 0$, see fig. 4.1(a), it is obvious to see that the diffusive interfaces between the Sn- and Pb-rich phase are smooth. The following time steps are computed with a Faedo-Galerkin discretisation of the non-viscous Cahn-Larché system, which decouples diffusion and elasticity. In both time steps we see high overshoots and undershoots along all phase interfaces making the diffusive phase interface more and more rougher.

(a) c_h^0 at $t = 0$ (b) c_h^1 at $t = 1.5 \times 10^{-5}s$ (c) c_h^2 at $t = 3.0 \times 10^{-5}s$

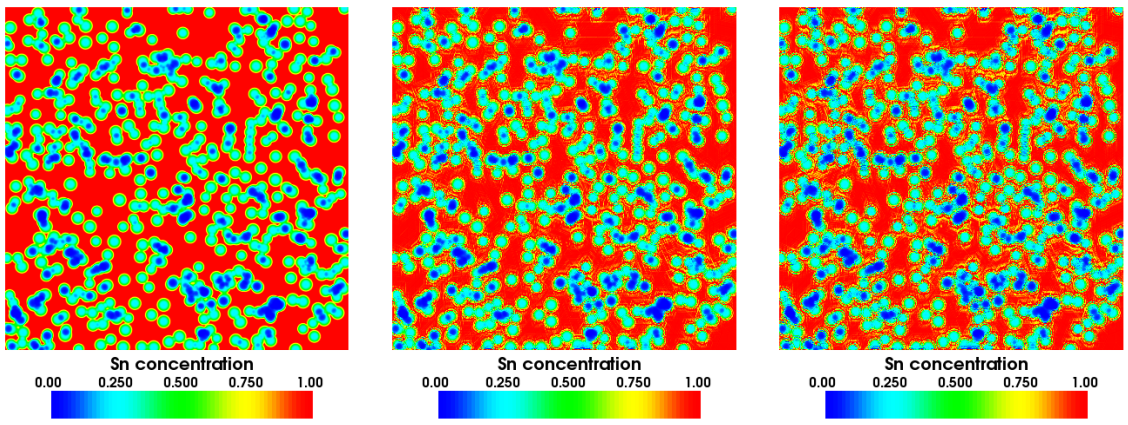

Fig. 4.1: High frequency contributions to the Sn concentration

We show this phenomena more precisely. In fig. 4.2 a cross section cut in y-direction through a particle from fig. 4.1 is demonstrated. At time $t = 0$ we see

in fig. 4.2(a) that there exists a smooth diffusive interface from the Sn-rich phase ($c \approx 1.0$) to the Pb-rich phase ($c \approx 0.0$). In the following figures it is outlined that heavy oscillations appear within the interface indicating Gibbs phenomena.

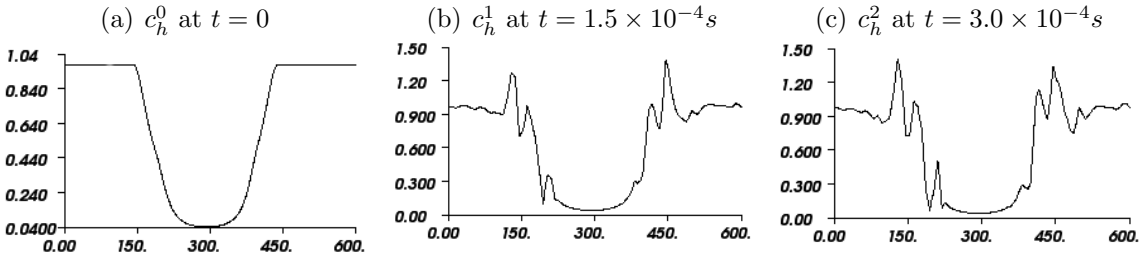

Fig. 4.2: Cross section cut through a particle

Moreover, these oscillations enlarge the gradient of the concentration field. But in diffusive phase interface models the gradient of the concentration field describes the interface and determines the interfacial energy. If the solution starts to oscillate, then the interfacial energy increases, which contradicts to the Lyapunov property, see lemma 2.24, where it is proved that the system goes into an energetic favourable state.

In this chapter a new scientific contribution is made by developing numerical approximation methods, which avoid the Gibbs phenomena.

- The numerical method, which decouples diffusion and elasticity, proposed by Weikard in [102], is extended to the Cahn-Larché system with concentration depending mobilities, viscosity and mixed boundary conditions for the displacement.

- Two different formulations of viscosity are observed for which equivalence is proved. On the one hand viscosity is considered by a dynamical formulation similar to the previous chapters, on the other hand viscosity is observed by driving forces.

- The viscous terms are used as a stabilisation for the non-viscous Cahn-Larché system in order to avoid overshoots and undershoots along phase interfaces.

In the following we denote a numerical method unstable, if it is producing an oscillating solution as described above. The main part of this work is to develop a numerical approximation method for the Cahn-Larché system, which is stable in the above mentioned sense, even for extreme small surface stress tensors $\mathbf{\Gamma}$.

This chapter is organised as follows: In the first section of this chapter we consider a Faedo-Galerkin method of the viscous Cahn-Larché system (1.51) - (1.53). The approximation method consists of an implicit Eulerian discretisation with respect to

time and a finite element approximation with respect to space. In order to reduce the computational complexity we decouple diffusion and elasticity.

Furthermore we show the existence of a discrete solution c_h^n and μ_h^n by minimising the energy corresponding to the structural composition of the alloy and maximising the dissipation. The uniqueness of the discrete solution is proved by formulating a relation between the time discretisation Δt, the mesh size h and the friction coefficient γ. Uniform a-priori estimates are derived for all fields. We emphasise that these a-priori estimates are independent of the friction coefficient, except the estimate of $\dot{\bar{c}}_{\Delta t,h}$.

This observation leads to the idea exploiting the discretisation of the viscous Cahn-Larché system in order to get a stabilised approximation method for the non-viscous Cahn-Larché equations. In the following we prove the convergence of the discrete concentration field $c_{\Delta t,h}$, chemical potential $\mu_{\Delta t,h}$ and displacement $\boldsymbol{u}_{\Delta t,h}$ to a solution of the non-viscous Cahn-Larché system, if Δt, h and γ go to zero.

In the second section of this chapter we extend the idea of stabilisation by viscous terms. The discretisation of the viscous Cahn-Larché system (1.51) - (1.53) contains viscosity by the dynamic term $\gamma\dot{c}$. In the second section we introduce viscosity by driving forces. The driving force of the diffusion process is given by the gradient of the chemical potential μ, which is obvious in view of the flux equation $\boldsymbol{J} = -\boldsymbol{M}\nabla_{\boldsymbol{x}}\mu$ derived from thermodynamical investigations in (1.45).

Here we prove essentially the equivalence of both methods, which results from the flow gradient structure of the Cahn-Larché system. This chapter ends with the convergence analysis of the method and the solution of the Euler-Lagrange equations.

Finally, we enforce assumption (A-2) in order to guarantee uniqueness of the discrete solution under sufficiently strong conditions for the discretisation. Additionally to (A-2) we assume the following constraint:

(A′-2) **Concave part of the Gibbs free energy density**: Let $\psi^- \in C^2(\mathbb{R},\mathbb{R})$ be a polynomial of second order. Consequently we have the additional estimate

$$|\psi^-_{,cc}(c)| \leq C_{\psi^-_{,cc}}.$$

If in the following we refer to (A-2) than the extension (A′-2) is always included.

4.1 Stabilisation by dynamic friction

In this section we present a numerical approximation method for the viscous Cahn-Larché system (1.51) - (1.53). We call the discretised viscosity term dynamic, because friction is formulated in terms of $\gamma\dot{c}$. In the following the discretisation of the viscous Cahn-Larché system (1.51) - (1.53) is considered as a stabilised approximation

method of the non-viscous Cahn-Larché system (1.60) - (1.62) in order to avoid high frequency contributions to the concentration field. For that reason the convergence analysis is done for Δt, h and γ going to zero.

4.1.1 Numerical approximation method

Problem 4.1. For all discrete time steps $t = n\Delta t$ with $1 \leq n \leq N$ we have to find $c_h^n \in X_h(\Omega)$, $\mu_h^n \in X_h(\Omega)$ and $\boldsymbol{u}_h^n \in \boldsymbol{X}_h(\Omega)$, such that holds

$$\int_\Omega \partial_{\Delta t} c_h^n \zeta_h \, d\boldsymbol{x} + \int_\Omega \boldsymbol{M}_h^{n-1} \nabla_{\boldsymbol{x}} \mu_h^n \cdot \nabla_{\boldsymbol{x}} \zeta_h \, d\boldsymbol{x} = 0 \qquad \forall \zeta_h \in X_h(\Omega), \quad (4.1)$$

$$\int_\Omega \mu_h^n \xi_h \, d\boldsymbol{x} = \int_\Omega \boldsymbol{\Gamma} \nabla_{\boldsymbol{x}} c_h^n \cdot \nabla_{\boldsymbol{x}} \xi_h + \psi_{,c}(c_h^n)\xi_h + W_{,c}(c_h^n, \boldsymbol{\varepsilon}(\boldsymbol{u}_h^{n-1}))\xi_h + \gamma \partial_{\Delta t} c_h^n \xi_h \, d\boldsymbol{x} \qquad \forall \xi_h \in X_h(\Omega), \quad (4.2)$$

$$\int_\Omega \boldsymbol{C}(c_h^n)\boldsymbol{\varepsilon}(\boldsymbol{u}_h^n) : \boldsymbol{\varepsilon}(\boldsymbol{\eta}_h) \, d\boldsymbol{x} = \int_\Omega \boldsymbol{C}(c_h^n)\overline{\boldsymbol{\varepsilon}}(c_h^n) : \boldsymbol{\varepsilon}(\boldsymbol{\eta}_h) \, d\boldsymbol{x} + \int_{\Gamma_N} \boldsymbol{g}^n \cdot \boldsymbol{\eta}_h \, d\boldsymbol{a}_{\boldsymbol{x}} \qquad \forall \boldsymbol{\eta}_h \in \boldsymbol{X}_h(\Omega). \quad (4.3)$$

We get this numerical scheme by inserting the discrete functions c_h^n, μ_h^n and $\boldsymbol{u}_h^n$ into the definition of a semi-weak solution, definition 2.13. We remark that all integrals in problem 4.1 exist due to the assumptions (A-1) - (A-8) and the fact that the discrete test functions are almost everywhere bounded. Due to the fact that we use $\boldsymbol{u}_h^{n-1}$ in the equation of the chemical potential (4.2), diffusion and elasticity are decoupled. This decomposition of the problem reduces the computational complexity essentially, because only the concentration field c_h^n and the chemical potential μ_h^n must be computed simultaneously in every time step. The displacement is determined within a preprocessing in every time step.

Numerical approximation methods of the non-viscous Cahn-Larché system, which do not decouple diffusion and elasticity, are proposed in [51, 102]. We have to point out that the approximation method formulated by problem 4.1 is also mass conserving:

Corollary 4.2. *Let $\Omega \subset \mathbb{R}^d$ be a domain satisfying condition (H-1). Assuming that the initial data c_0 satisfy assumption (A-5) and that the triangulation $\mathscr{T}_h(\Omega)$ is admissible. Then for every time $t = n\Delta t$ with $0 \leq n \leq N$ holds*

$$\int_\Omega c_h^n \, d\boldsymbol{x} = m.$$

Proof. This corollary is proved by using complete induction. Due to corollary 3.11 we know that the $L_2(\Omega)$-projection c_h^0 of the initial data c_0 preserves the mass. Assuming that c_h^{n-1} is mass preserving, we take the test function $\zeta_h \equiv 1 \in X_h(\Omega)$ and calculate from the discrete diffusion equation (4.1)

$$\int_\Omega \partial_{\Delta t} c_h^n \, d\boldsymbol{x} = \int_\Omega \frac{c_h^n - c_h^{n-1}}{\Delta t} \, d\boldsymbol{x} = 0.$$

This calculation shows the statement of this corollary. □

Finally it is clear that for all time steps $t = n\Delta t$ with $0 \leq n \leq N$ holds $c_h^n \in X_{m,h}(\Omega)$.

Time dependent problems like the Cahn-Larché system need some preprocessing tasks, which are discussed in section 3.3. The initial data c_0 are projected on the trial space $X_h(\Omega)$ by a $L_2(\Omega)$-projection, see section 3.3.1 and the corresponding displacement $\boldsymbol{u}_h^0$ is computed by solving an elasticity problem, see section 3.3.2. Moreover, we have to calculate an initial chemical potential $\mu_h^0 \in X_h(\Omega)$ corresponding to the initial concentration $c_h^0 \in X_{m,h}(\Omega)$ and the initial displacement $\boldsymbol{u}_h^0 \in \boldsymbol{X}_h(\Omega)$.

Problem 4.3. Find the initial chemical potential $\mu_h^0 \in X_h(\Omega)$ such that holds

$$\int_\Omega \mu_h^0 \xi_h \, d\boldsymbol{x} = \int_\Omega \boldsymbol{\Gamma} \nabla_{\boldsymbol{x}} c_h^0 \cdot \nabla_{\boldsymbol{x}} \xi_h + \psi_{,c}(c_h^0)\xi_h + W_{,c}(c_h^0, \boldsymbol{u}_h^0)\xi_h \, d\boldsymbol{x} \qquad \forall \xi_h \in X_h(\Omega).$$

We remark, that all integrals in problem 4.3 exist due to the assumptions (A-1) - (A-8) and the fact that the test functions $\xi_h \in X_h(\Omega)$ are almost everywhere bounded. Problem 4.3 corresponds to a LES which must be solved in the beginning of the numerical simulation.

$$\begin{aligned} \underline{\boldsymbol{A}} \, \underline{\boldsymbol{\mu}}^0 &= \underline{\boldsymbol{f}}, \qquad (4.4) \\ \underline{\boldsymbol{A}}[\boldsymbol{z}, \boldsymbol{y}] &:= \int_\Omega \varphi_{\boldsymbol{y}} \varphi_{\boldsymbol{z}} \, d\boldsymbol{x}, \\ \underline{\boldsymbol{f}}[\boldsymbol{z}] &:= \int_\Omega \boldsymbol{\Gamma} \nabla_{\boldsymbol{x}} c_h^0 \cdot \nabla_{\boldsymbol{x}} \varphi_{\boldsymbol{z}} + \psi_{,c}(c_h^0)\varphi_{\boldsymbol{z}} + W_{,c}(c_h^0, \boldsymbol{u}_h^0)\varphi_{\boldsymbol{z}} \, d\boldsymbol{x}. \end{aligned}$$

Obviously the projection matrix $\underline{\boldsymbol{A}}$ is computed by an explicit formula, in contrast to the right hand side $\underline{\boldsymbol{f}}$, which is computed by a quadrature formula. On a triangle we use the seven point formula of Radon derived in [1, 86] and on a tetrahedron we refer to [60] for quadrature formulas. The LES (4.4) is solved iteratively by using the preconditioned CG method [58]. As a precondition the matrix $\underline{\boldsymbol{B}} := \mathrm{diag}(\underline{\boldsymbol{A}})$ is applied, which is an appropriate choice due to the fact that $\underline{\boldsymbol{A}}$ and $\underline{\boldsymbol{B}}$ are spectral equivalent, see [93].

4.1.2 Existence of the discrete weak solution

The existence of a solution of the discrete elasticity problem (4.3) is clear due to the analysis of problem 3.14. It remains to show the existence of a solution of the discrete diffusion problem (4.1) and (4.2). The existence proof works in an analogous way as the existence proof for a solution of the continuous Cahn-Larché equations.

Elimination of the diffusion equation

We eliminate the discrete diffusion equation (4.1) by calculating a relation between the diffusion and the dissipation for the discrete formulation. Therefore we introduce the operator $\mathcal{M}_h^n$ similar to definition 2.18.

Definition 4.4. Let $\Omega \subset \mathbb{R}^d$ be a domain satisfying condition (H-1), then the operator $\mathcal{M}_h^n$ is defined by

$$\begin{aligned} &\mathcal{M}_h^n : X_0(\Omega) \longrightarrow Y_0(\Omega), \\ &\langle \mathcal{M}_h^n \mu, \zeta \rangle := \int_\Omega \boldsymbol{M}_h^{n-1} \nabla_{\boldsymbol{x}} \mu \cdot \nabla_{\boldsymbol{x}} \zeta \, d\boldsymbol{x} \qquad\qquad \forall \zeta \in X_0(\Omega). \end{aligned}$$

The operator $\mathcal{M}_h^n$ corresponds to a Laplace operator with a discrete material tensor $\boldsymbol{M}_h^{n-1}$ and homogeneous Neumann boundary conditions.

Corollary 4.5. *Let $\Omega \subset \mathbb{R}^d$ be a domain satisfying condition (H-1). Furthermore let assumption (A-3) be satisfied, then for the operator $\mathcal{M}_h^n$ holds:*

(1) $|\langle \mathcal{M}_h^n \mu, \zeta \rangle| \leq C_M \|\mu\|_{H^1(\Omega)} \|\zeta\|_{H^1(\Omega)} \qquad \forall \mu, \zeta \in X_0(\Omega),$

(2) $\langle \mathcal{M}_h^n \zeta, \zeta \rangle \geq \dfrac{c_M}{c_p} \|\zeta\|^2_{H^1(\Omega)} \qquad \forall \zeta \in X_0(\Omega).$

Proof. This corollary follows directly from lemma 2.19, taking into account Hölder's and Korn's inequality. □

In view of the Lax-Milgram theorem the inverse operator exists and is denoted by $(\mathcal{M}_h^n)^{-1}$. Using the inverse operator $(\mathcal{M}_h^n)^{-1}$ a dissipative inner product on the space $Y_0(\Omega)$ is introduced.

Definition 4.6. Let $f, g \in Y_0(\Omega)$, then the dissipative inner product with respect to the operator $(\mathcal{M}_h^n)^{-1}$ is defined by

$$\langle f, g \rangle_{\mathcal{M}_h^n} := \int_\Omega \boldsymbol{M}_h^{n-1} \nabla_{\boldsymbol{x}} (\mathcal{M}_h^n)^{-1} f \cdot \nabla_{\boldsymbol{x}} (\mathcal{M}_h^n)^{-1} g \, d\boldsymbol{x}$$

and the corresponding norm is given by

$$\|f\|^2_{\mathcal{M}_h^n} := \langle f, f \rangle_{\mathcal{M}_h^n}.$$

Lemma 4.7 (Young's inequality). *Let $\Omega \subset \mathbb{R}^d$ be a domain satisfying condition (H-1). Furthermore, let assumption (A-3) be satisfied. Then for any $\delta \in (0,1)$ and any $\zeta \in X_0(\Omega)$ the following inequality holds*

$$\|\zeta\|^2_{L_2(\Omega)} \leq \frac{C_M}{\delta}\|\zeta\|^2_{\mathcal{M}_h^n} + \delta|\zeta|^2_{H^1(\Omega)}.$$

Proof. We identify a function $\zeta \in X_0(\Omega)$ with a functional in $Y_0(\Omega)$ by the shift operator $\mathcal{S}$ introduced in (2.21), and apply definition 2.18. Furthermore, the mobility tensor is symmetric and positive definite, therefore we calculate the square root and estimate by using the classical Young's inequality

$$\begin{aligned}
\|\zeta\|^2_{L_2(\Omega)} &= \int_\Omega \xi^2 \, d\boldsymbol{x} = \big\langle \mathcal{M}_h^n(\mathcal{M}_h^n)^{-1}\zeta, \zeta\big\rangle = \int_\Omega \boldsymbol{M}_h^{n-1}\nabla_{\boldsymbol{x}}(\mathcal{M}_h^n)^{-1}\zeta \cdot \nabla_{\boldsymbol{x}}\zeta \, d\boldsymbol{x} \\
&= \int_\Omega (\boldsymbol{M}_h^{n-1})^{\frac{1}{2}}\nabla_{\boldsymbol{x}}(\mathcal{M}_h^n)^{-1}\zeta \cdot (\boldsymbol{M}_h^{n-1})^{\frac{1}{2}}\nabla_{\boldsymbol{x}}\zeta \, d\boldsymbol{x} \\
&\leq C_M^{\frac{1}{2}}\|\zeta\|_{\mathcal{M}_h^n}|\zeta|_{H^1(\Omega)} \leq \frac{C_M}{\delta}\|\zeta\|^2_{\mathcal{M}_h^n} + \delta|\zeta|^2_{H^1(\Omega)}.
\end{aligned}$$

□

Finally we eliminate the discrete diffusion equation (4.1) by applying the operator $(\mathcal{M}_h^n)^{-1}$. Therefore the function $\partial_{\Delta t}c_h^n \in X_{0,h}(\Omega)$ is identified with a functional in $Y_0(\Omega)$ by using the shift operator $\mathcal{S}$ from (2.21). We get the representation

$$\mu_h^n = -(\mathcal{M}_h^n)^{-1}\partial_{\Delta t}c_h^n \in X_{0,h}(\Omega). \tag{4.5}$$

Note that for any Lagrangian multiplier $\lambda_h^n \in \ker(\mathcal{M}_h^n) = \mathbb{R}$ additionally holds

$$\mu_h^n = -(\mathcal{M}_h^n)^{-1}\partial_{\Delta t}c_h^n + \lambda_h^n \in X_h(\Omega), \tag{4.6}$$

which is also a solution of the discrete diffusion equation (4.1).

Let $\xi_h \in X_{0,h}(\Omega)$ be a test function, then we use assumption (A-3), the symmetry of $\boldsymbol{M}_h^n$, and calculate in the same way as in (2.23) for the discrete fields

$$\begin{aligned}
\int_\Omega \mu_h^n\xi_h \, d\boldsymbol{x} &= -\int_\Omega (\mathcal{M}_h^n)^{-1}\partial_{\Delta t}c_h^n\xi_h \, d\boldsymbol{x} = -\big\langle (\mathcal{M}_h^n)^{-1}\partial_{\Delta t}c_h^n, \mathcal{M}_h(\mathcal{M}_h^n)^{-1}\xi_h\big\rangle \\
&= -\int_\Omega \boldsymbol{M}_h^{n-1}\nabla_{\boldsymbol{x}}(\mathcal{M}_h^n)^{-1}\partial_{\Delta t}c_h^n \cdot \nabla_{\boldsymbol{x}}(\mathcal{M}_h^n)^{-1}\xi_h \, d\boldsymbol{x} \\
&= -\langle \partial_{\Delta t}c_h^n, \xi_h\rangle_{\mathcal{M}_h^n}.
\end{aligned} \tag{4.7}$$

In view of this calculation we restrict problem 4.1 to two equations only for the discrete concentration field c_h^n and for the discrete displacement $\boldsymbol{u}_h^n$.

Problem 4.8. Find at each discrete time $t = n\Delta t$ for $1 \leq n \leq N$ a function $c_h^n \in X_{m,h}(\Omega)$ and $\boldsymbol{u}_h^n \in \boldsymbol{X}_h(\Omega)$ such that holds

$$\int_\Omega \boldsymbol{\Gamma}\nabla_{\boldsymbol{x}} c_h^n \cdot \nabla_{\boldsymbol{x}}\xi_h + \psi_{,c}(c_h^n)\xi_h + W_{,c}(c_h^n, \boldsymbol{\varepsilon}(\boldsymbol{u}_h^{n-1}))\xi_h + \gamma\partial_{\Delta t} c_h^n \xi_h \, d\boldsymbol{x} + \langle \partial_{\Delta t} c_h^n, \xi_h\rangle_{\mathcal{M}_h^n} = 0 \qquad \forall \xi_h \in X_h(\Omega),$$

$$\int_\Omega \boldsymbol{C}(c_h^n)\boldsymbol{\varepsilon}(\boldsymbol{u}_h^n) : \boldsymbol{\varepsilon}(\boldsymbol{\eta}_h) \, d\boldsymbol{x} = \int_\Omega \boldsymbol{C}(c_h^n)\overline{\boldsymbol{\varepsilon}}(c_h^n) : \boldsymbol{\varepsilon}(\boldsymbol{\eta}_h) \, d\boldsymbol{x} + \int_{\Gamma_N} \boldsymbol{g}^n \cdot \boldsymbol{\eta}_h \, d\boldsymbol{a}_{\boldsymbol{x}} \qquad \forall \boldsymbol{\eta}_h \in \boldsymbol{X}_h(\Omega).$$

Keeping in mind that the discretisation method decouples diffusion and elasticity, we have to formulate two corresponding energy functionals: a configurational energy $E_{h,config}^n$ related to the diffusion and a strain energy $E_{h,mech}^n$ related to the mechanical equilibrium

$$\begin{aligned} E_{h,config}^n(d_h) &:= \int_\Omega \frac{1}{2}\boldsymbol{\Gamma}\nabla_{\boldsymbol{x}} d_h \cdot \nabla_{\boldsymbol{x}} d_h + \psi(d_h) + W(d_h, \boldsymbol{\varepsilon}(\boldsymbol{u}_h^{n-1})) \, d\boldsymbol{x} \\ &\quad + \frac{1}{2\Delta t}\|d_h - c_h^{n-1}\|_{\mathcal{M}_h^n}^2 + \frac{\gamma}{2\Delta t}\|d_h - c_h^{n-1}\|_{L_2(\Omega)}^2, \\ E_{h,mech}^n(\boldsymbol{v}_h) &:= \int_\Omega W(c_h^n, \boldsymbol{\varepsilon}(\boldsymbol{v}_h)) \, d\boldsymbol{x} - \int_{\Gamma_N} \boldsymbol{g}^n \cdot \boldsymbol{v}_h. \end{aligned}$$

The mechanical equilibrium belongs to a $\boldsymbol{X}(\Omega)$-elliptic problem as recommended in lemma 2.14. Due to this property the unique solution $\boldsymbol{u}_h^n$ provides the minimiser of the strain energy functional and therefore it holds

$$E_{h,mech}^n(\boldsymbol{u}_h^n) = \min_{\boldsymbol{v}_h \in \boldsymbol{X}_h(\Omega)} E_{h,mech}^n(\boldsymbol{v}_h).$$

We remark that also for the discretisation the flow gradient structure of the problem is satisfied with respect to the inner product $\langle\cdot,\cdot\rangle_{\mathcal{M}_h^n}$ and $\langle\cdot,\cdot\rangle_{L_2(\Omega)}$. From (2.26) follows for the discrete fields c_h^n and μ_h^n that the dissipation is represented by

$$\frac{1}{2\Delta t}\|c_h^n - c_h^{n-1}\|_{\mathcal{M}_n}^2 + \frac{\gamma}{2\Delta t}\|c_h^n - c_h^{n-1}\|_{L_2(\Omega)}^2 = -\Delta t D_\gamma(c_h^{n-1}, \dot{\bar{c}}_h^n, \mu_h^n) \tag{4.8}$$

From a physical point of view, minimising $E_{h,config}^n(d_h)$ means minimising the configurational energy and maximising the dissipation.

Energy minimisation

In this section we will minimise the configurational energy $E_{h,config}^n(d_h)$. The proof is organised analogous to the continuous case, in fact even simpler because we work on a finite dimensional space $X_{m,h}(\Omega)$.

Lemma 4.9. *Let $\Omega \subset \mathbb{R}^d$ be a domain satisfying condition (H-1). Furthermore, let the assumptions (A-1) - (A-8) be satisfied. Furthermore, $\mathscr{T}_h(\Omega)$ is assumed to be an admissible and exact triangulation. Then there exists at least one $c_h^n \in X_{m,h}(\Omega)$ such that holds*

$$E_{h,config}^n(c_h^n) = \min_{d_h \in X_{m,h}(\Omega)} E_{h,config}^n(d_h).$$

Proof. For the proof of this lemma, we argue similarly as in the proof of lemma 2.22. **Step 1:** At first we show that the energy is coercive. For the surface energy we conclude by using assumption (A-1) together with Poincaré's inequality (2.1)

$$\int_\Omega \frac{1}{2}\mathbf{\Gamma}\nabla_{\boldsymbol{x}} d_h \cdot \nabla_{\boldsymbol{x}} d_h \, d\boldsymbol{x} \geq \frac{c_{\mathbf{\Gamma}}}{2c_p}\|d_h\|_{H^1(\Omega)}^2 - \frac{c_{\mathbf{\Gamma}}}{2}m^2.$$

The Gibbs free energy can be bounded below by applying assumption (A-2) and we yield

$$\int_\Omega \psi(d_h) \, d\boldsymbol{x} \geq -c_\psi \operatorname{meas}(\Omega).$$

The elastic contribution to the configurational energy and the dissipative terms are bounded below by zero by using assumption (A-6) and (A-7). Finally we get

$$E_{h,config}^n(d_h) \geq \frac{c_{\mathbf{\Gamma}}}{2c_p}\|d_h\|_{H^1(\Omega)}^2 - C.$$

Step 2: The density of the configurational energy is continuous with respect to $\nabla_{\boldsymbol{x}} d_h$ and d_h, convex with respect to $\nabla_{\boldsymbol{x}} d_h$ and bounded below by (A-2). Theorem 2.6 yields

$$E_{h,config}^n(d_h) \leq \lim_{k\to\infty} E_{h,config}^n(d_{h,k}).$$

The existence of a minimiser $c_h^n \in X_{m,h}(\Omega)$ follows directly from theorem 2.7. □

Lemma 4.10. *Let $\Omega \subset \mathbb{R}^d$ be a domain satisfying condition (H-1). Furthermore, let the assumptions (A-1) - (A-8) be satisfied. Let the triangulation $\mathscr{T}_h(\Omega)$ be admissible and exact, then for any test function $\xi_h \in X_h(\Omega)$ the Gâteaux derivative of $E_{\Delta t,config}^n$ exists and it holds*

$$\begin{aligned}\lim_{\delta\to 0} &\frac{E_{h,config}^n(d_h + \delta\xi_h) - E_{h,config}^n(d_h)}{\delta} \\ &= \int_\Omega \mathbf{\Gamma}\nabla_{\boldsymbol{x}} d_h \cdot \nabla_{\boldsymbol{x}}\xi_h + \psi_{,c}(d_h)\xi_h + W_{,c}(d_h, \boldsymbol{\varepsilon}(\boldsymbol{u}_h^{n-1}))\xi_h \, d\boldsymbol{x} \\ &\qquad + \frac{1}{\Delta t}\big\langle d_h - c_h^{n-1}, \xi_h\big\rangle_{\mathcal{M}_h^n} + \frac{\gamma}{\Delta t}\big\langle d_h - c_h^{n-1}, \xi_h\big\rangle_{L_2(\Omega)}. \quad (4.9)\end{aligned}$$

Proof. This result follows with the same arguments as in the proof of lemma 2.23. The surface energy is quadratic with respect to $\nabla_{\boldsymbol{x}} d_h$ and this leads directly to

$$\begin{aligned}&\lim_{\delta\to 0}\frac{1}{\delta}\int_\Omega \frac{1}{2}\boldsymbol{\Gamma}\nabla_{\boldsymbol{x}}(d_h+\delta\xi_h)\cdot\nabla_{\boldsymbol{x}}(d_h+\delta\xi_h)-\frac{1}{2}\boldsymbol{\Gamma}\nabla_{\boldsymbol{x}}d_h\cdot\nabla_{\boldsymbol{x}}d_h\,d\boldsymbol{x}\\&\quad=\int_\Omega \boldsymbol{\Gamma}\nabla_{\boldsymbol{x}}d_h\cdot\nabla_{\boldsymbol{x}}\xi_h\,d\boldsymbol{x}.\end{aligned}$$

We consider a decomposition of the Gibbs free energy density into a convex and a concave part. We get for the convex part ψ^+ similar to lemma 2.23 by using the assumption (A-2) that the difference quotient is uniformly bounded

$$\left|\frac{\psi^+(d_h+\delta\xi_h)-\psi^+(d_h)}{\delta}\right|\leq 2(\psi^+(d_h)+C).$$

This uniform bound and the fact that $\psi^+\in C^2(\mathbb{R},\mathbb{R})$ yields with Lebesgue's convergence theorem

$$\lim_{\delta\to 0}\int_\Omega \frac{\psi^+(d_h+\delta\xi_h)-\psi^+(d_h)}{\delta}\,d\boldsymbol{x}=\int_\Omega \psi^+_{,c}(d_h)\xi_h\,d\boldsymbol{x}.$$

The concave part ψ^- of the Gibbs free energy density satisfies a polynomial boundedness and therefore the generalised Lebesgue convergence theorem yields

$$\lim_{\delta\to 0}\int_\Omega \frac{\psi^-(d_h+\delta\xi_h)-\psi^-(d_h)}{\delta}\,d\boldsymbol{x}=\int_\Omega \psi^-_{,c}(d_h)\xi_h\,d\boldsymbol{x}.$$

Furthermore, the elastic contribution to the chemical potential is treated by applying the mean value theorem with assumption (A-6), (A-7) and the Lebesgue convergence theorem

$$\begin{aligned}&\lim_{\delta\to 0}\frac{1}{\delta}\int_\Omega W(d_h+\delta\xi_h,\boldsymbol{\varepsilon}(\boldsymbol{u}_h^{n-1}))\,d\boldsymbol{x}-\int_\Omega W(d_h,\boldsymbol{\varepsilon}(\boldsymbol{u}_h^{n-1}))\,d\boldsymbol{x}\\&\quad=\lim_{\delta\to 0}\int_\Omega W_{,c}(d_h+\nu(\delta)\xi_h,\boldsymbol{\varepsilon}(\boldsymbol{u}_h^{n-1}))\xi_h\,d\boldsymbol{x}=\int_\Omega W_{,c}(d_h,\boldsymbol{\varepsilon}(\boldsymbol{u}_h^{n-1}))\xi_h\,d\boldsymbol{x}.\end{aligned}$$

Finally, the dissipative terms are quadratic and we get by direct calculations

$$\begin{aligned}&\lim_{\delta\to 0}\frac{\gamma}{2\Delta t\delta}(\|d_h+\delta\xi_h-c_h^{n-1}\|^2_{L_2(\Omega)}-\|d_h-c_h^{n-1}\|^2_{L_2(\Omega)})\\&\quad=\frac{\gamma}{\Delta t}\big\langle d_h-c_h^{n-1},\xi_h\big\rangle_{L_2(\Omega)},\\&\lim_{\delta\to 0}\frac{1}{2\Delta t\delta}(\|d_h+\delta\xi_h-c_h^{n-1}\|^2_{\mathcal{M}_h^n}-\|d_h-c_h^{n-1}\|^2_{\mathcal{M}_h^n}\\&\quad=\frac{1}{\Delta t}\big\langle d_h-c_h^{n-1},\xi_h\big\rangle_{\mathcal{M}_h^n}.\end{aligned}$$

□

For a minimiser $c_h^n \in X_h(\Omega)$ holds due to theorem 2.8 that the Gâteaux derivative is equal to zero, this means for any test function $\xi_h \in X_h(\Omega)$ holds

$$\int_\Omega \mathbf{\Gamma}\nabla_{\boldsymbol{x}} d_h \cdot \nabla_{\boldsymbol{x}}\xi_h + \psi_{,c}(d_h)\xi_h + W_{,c}(d_h, \boldsymbol{\varepsilon}(\boldsymbol{u}_h^{n-1}))\xi_h \, d\boldsymbol{x} \\ + \langle \partial_{\Delta t} c_h^n, \xi_h\rangle_{\mathcal{M}_h^n} + \gamma \langle \partial_{\Delta t} c_h^n, \xi_h\rangle_{L_2(\Omega)} = 0.$$

Furthermore, a minimiser $c_h^n \in X_h(\Omega)$, $\boldsymbol{u}_h^n \in \boldsymbol{X}_h(\Omega)$ and the chemical potential $\mu_h^n \in X_h(\Omega)$ given by (4.6) generate a discrete weak solution of the approximation scheme formulated in problem 4.1. The Lagrangian multiplier has to be chosen in the following form

$$\lambda_h^n = \frac{1}{\operatorname{meas}(\Omega)} \int_\Omega \psi_{,c}(c_h^n) + W_{,c}(c_h^n, \boldsymbol{\varepsilon}(\boldsymbol{u}_h^{n-1})) \, d\boldsymbol{x}. \tag{4.10}$$

Obviously we have calculated a piecewise constant interpolants of the concentration field $c_{\Delta t,h,\gamma}$, of the chemical potential $\mu_{\Delta t,h,\gamma}$ and of the displacement $\boldsymbol{u}_{\Delta t,h,\gamma}$. Moreover a piecewise linear interpolant $\overline{c}_{\Delta t,h,\gamma}$ is also known. We indicate all these fields with γ additionally, because friction is used for stabilisation and finally we are interested in the case Δt, h and γ going to zero.

4.1.3 Uniqueness of the discrete solution

In this section we discuss relations between the time discretisation Δt, the mesh size h and the friction parameter γ in order to get a unique solution. We remark that the uniqueness is only proved for the discrete solution of the Cahn-Larché system. The uniqueness of the discrete solution does not imply the uniqueness of the continuous solution of the Cahn-Larché system.

Lemma 4.11 (Uniqueness). *Let $\Omega \subset \mathbb{R}^d$ be a domain satisfying condition (H-1). Moreover let the assumptions (A-1) - (A-8) be satisfied. The triangulation $\mathscr{T}_h(\Omega)$ is assumed to be admissible, exact and uniform. Then there exists a constant $C_{W,cc} > 0$ depending on the elasticity parameters such that in the case of time discretisation Δt, mesh size h and friction parameter γ satisfying the following condition*

$$\Delta t \leq \min\left(\frac{c_\Gamma}{2(C_{\psi,cc}^-)^2 C_M}, \frac{h^d \gamma}{C_{W,cc}}\right),$$

the discrete problem 4.1 has a unique solution for every time step $t = n\Delta t$ with $0 \leq n \leq N$.

Proof. We show this lemma by complete induction.

Step 1: At initial time $t = 0$ the $L_2(\Omega)$-projection of the initial data c_0 is unique due to lemma 3.11. Corresponding to the unique discrete initial data c_h^0 the discrete displacement $\boldsymbol{u}_h^0$ is also unique due to lemma 3.15 and Lax-Milgram's theorem.

We assume that for time $t = (n-1)\Delta t$ the concentration field c_h^{n-1} and the displacement $\boldsymbol{u}_h^{n-1}$ are unique and conclude the uniqueness of the concentration field c_h^n and of the displacement $\boldsymbol{u}_h^n$.

Step2: First we prove the Lipschitz continuity of the elastic contribution $W_{,c}$ to the chemical potential. For any two concentration fields c_1 and c_2 we conclude by using the mean value theorem and assumption (A-6), (A-7) with the mean value $\tilde{c} := \nu c_1 + (1-\nu)c2$ and $\nu \in (0,1)$ the estimate

$$\begin{aligned}
|W_{,c}(c_1,\boldsymbol{\varepsilon}) - W_{,c}(c_2,\boldsymbol{\varepsilon})| &\leq |W_{,cc}(\tilde{c},\boldsymbol{\varepsilon})||(c_1-c_2)| \\
&\leq \Big(\Big|\frac{1}{2}\boldsymbol{C}_{,cc}(\tilde{c})(\boldsymbol{\varepsilon}-\overline{\boldsymbol{\varepsilon}}(\tilde{c})) : (\boldsymbol{\varepsilon}-\overline{\boldsymbol{\varepsilon}}(\tilde{c}))\Big| + \Big|2\boldsymbol{C}_{,c}(\tilde{c})(\boldsymbol{\varepsilon}-\overline{\boldsymbol{\varepsilon}}(\tilde{c})) : \overline{\boldsymbol{\varepsilon}}_{,c}(\tilde{c}))\Big| \\
&\quad + \Big|\boldsymbol{C}(\tilde{c})\overline{\boldsymbol{\varepsilon}}_{,c}(\tilde{c}) : \overline{\boldsymbol{\varepsilon}}_{,c}(\tilde{c})\Big| + \Big|\boldsymbol{C}(\tilde{c})(\boldsymbol{\varepsilon}-\overline{\boldsymbol{\varepsilon}}(\tilde{c})) : \overline{\boldsymbol{\varepsilon}}_{,cc}(\tilde{c})\Big|\Big)\Big|c_1-c_2\Big| \\
&\leq C(|\boldsymbol{\varepsilon}|^2+1)|c_1-c_2|.
\end{aligned}$$

In view of this estimate we define $\int_\Omega C(|\boldsymbol{\varepsilon}|^2+1)\,d\boldsymbol{x} \leq C(C_{\boldsymbol{u}}^2+1) =: C_{W,cc}$.

Step 3: Finally, we assume that there exist two concentration fields $c_{1,h}^n$ and $c_{2,h}^n$ at time $t = n\Delta t$, which are solutions of the reduced problem 4.8. By subtracting the weak formulation in problem 4.8 with solution $c_{1,h}^n$ and $c_{2,h}^n$ from each other, we get

$$\begin{aligned}
\int_\Omega \boldsymbol{\Gamma}\nabla_{\boldsymbol{x}}(c_{1,h}^n - c_{2,h}^n)\cdot\nabla_{\boldsymbol{x}}\xi_h + (\psi_{,c}(c_{1,h}^n) - \psi_{,c}(c_{2,h}^n))\xi_h \\
+ (W_{,c}(c_{1,h}^n, \boldsymbol{\varepsilon}(\boldsymbol{u}_h^{n-1})) - W_{,c}(c_{2,h}^n, \boldsymbol{\varepsilon}(\boldsymbol{u}_h^{n-1})))(c_{1,h}^n - c_{2,h}^n)\,d\boldsymbol{x} \\
+ \frac{1}{\Delta t}\langle c_{1,h}^n - c_{2,h}^n, \xi_h\rangle_{\mathcal{M}_h^n} + \frac{\gamma}{\Delta t}\langle c_{1,h}^n - c_{2,h}^n, \xi_h\rangle_{L_2(\Omega)} = 0.
\end{aligned}$$

The convex terms are estimated below by assumption (A-1) and using the fact that $\psi_{,c}^+$ is a monotone function, thus the corresponding term is bounded below by zero. For the concave parts we apply the uniform a-priori estimates of the displacement $\boldsymbol{u}_h^{n-1}$, the inverse inequality from lemma (3.4) and Young's inequality (4.7). Then it follows

$$\begin{aligned}
c_\Gamma|c_{1,h}^n - c_{2,h}^n|_{H^1(\Omega)}^2 + \frac{1}{\Delta t}\|c_{1,h}^n - c_{2,h}^n\|_{\mathcal{M}_h^n}^2 + \frac{\gamma}{\Delta t}\|c_{1,h}^n - c_{2,h}^n\|_{L_2(\Omega)}^2 \\
\leq C_{\psi_{,cc}^-}\|c_{1,h}^n - c_{2,h}^n\|_{L_2(\Omega)}^2 + C_{W,cc}\frac{1}{h^d}\|c_{1,h}^n - c_{2,h}^n\|_{L_2(\Omega)}^2 \\
\leq C_{\psi_{,cc}^-}\delta|c_{1,h}^n - c_{2,h}^n|_{H^1(\Omega)}^2 + \frac{C_{\psi_{,cc}^-}C_M}{\delta}\|c_{1,h}^n - c_{2,h}^n\|_{\mathcal{M}_h^n}^2 \\
+ C_{W,cc}\frac{1}{h^d}\|c_{1,h}^n - c_{2,h}^n\|_{L_2(\Omega)}^2.
\end{aligned}$$

From this estimate we calculate for the difference of both solutions $c_{1,h}^n$ and $c_{2,h}^n$ the relation

$$\left(c_\Gamma - C_{\psi,cc}^- \delta\right) |c_{1,h}^n - c_{2,h}^n|_{H^1(\Omega)}^2 + \left(\frac{1}{\Delta t} - \frac{C_{\psi,cc}^- C_M}{\delta}\right) \|c_{1,h}^n - c_{2,h}^n\|_{\mathcal{M}_h^n}^2 + \left(\frac{\gamma}{\Delta t} - \frac{C_{W,cc}}{h^d}\right) \|c_{1,h}^n - c_{2,h}^n\|_{L_2(\Omega)}^2 \leq 0.$$

By choosing $\delta = \frac{c_\Gamma}{2C_{\psi,cc}^-}$ we get for the time discretisation the condition

$$\Delta t \leq \min\left(\frac{c_\Gamma}{2(C_{\psi,cc}^-)^2 C_M}, \frac{h^d \gamma}{C_{W,cc}}\right).$$

The above estimate yields directly the uniqueness of the concentration field c_h^n. Furthermore, the uniqueness of the displacement follows from the uniqueness of the concentration field c_h^n and from Lax-Milgram's theorem. Finally, the uniqueness of the chemical potential μ_h^n is obvious due to the uniqueness of the concentration field c_h^n and the displacement $\boldsymbol{u}_h^n$ by taking into account the representation formula (4.6). □

Remark 4.12. If the elasticity tensor does not depend on the concentration field this means $\boldsymbol{C} = \text{const}$, then the uniqueness of the solution is obtained by a weaker condition on the time discretisation

$$\Delta t \leq \min\left(\frac{c_\Gamma}{(C_{\psi,cc}^-)^2 C_M}, \frac{h^{\frac{d}{2}} \gamma}{2C_{W,cc}}\right).$$

Proof. We argue in a similar way as in the proof of lemma 4.11, but the important difference to lemma 4.11 consists in the Lipschitz continuity of the elastic contribution to the chemical potential. The same calculation as in the proof of lemma 4.11 step 2 yields the estimate

$$|W_{,c}(c_1, \boldsymbol{\varepsilon}) - W_{,c}(c_2, \boldsymbol{\varepsilon})| \leq C(|\boldsymbol{\varepsilon}| + 1).$$

The strain $\boldsymbol{\varepsilon}$ enters this estimate only linear and this fact leads to a different estimate as in lemma 4.11 step 3. We get for a constant elasticity tensor $\boldsymbol{C}$ the following estimate

$$\begin{aligned} c_\Gamma |c_{1,h}^n - c_{2,h}^n|_{H^2(\Omega)}^2 + \frac{1}{\Delta t}\|c_{1,h}^n - c_{2,h}^n\|_{\mathcal{M}_h^n}^2 + \frac{\gamma}{\Delta t}\|c_{1,h}^n - c_{2,h}^n\|_{L_2(\Omega)}^2 \\ \leq C_{\psi,cc}^- \|c_{1,h}^n - c_{2,h}^n\|_{L_2(\Omega)}^2 + C_{W,cc} \frac{1}{h^{\frac{d}{2}}} \|c_{1,h}^n - c_{2,h}^n\|_{L_2(\Omega)}^2 \end{aligned}$$

The same argumentation leads to the statement of this remark. □

Remark 4.13. The existence of a discrete solution of problem 4.1 was proved by minimising the configurational energy and following that the Euler-Lagrange equations are equal to zero in the minimiser.

In contrast to this theoretical argumentation, we solve the Euler-Lagrange equations in the numerical simulation. In general it is not true that a solution of the Euler-Lagrange equations minimises the corresponding energy functional. But for the case of the solution of the Euler-Lagrange equation being unique a global minimum of the energy is achieved, see [29].

4.1.4 A-priori estimates

In this section we derive uniform a-priori estimates of a discrete weak solution of problem 4.1. The Lyapunov property of the system is again the key issue to derive a-priori estimates. Also for the discrete fields, the system goes into an energetic stable state. Due to the decoupling of diffusion and elasticity we have to argue in a different way in comparison to the continuous Cahn-Larché system.

Lemma 4.14 (Lyapunov property). *Let $\Omega \subset \mathbb{R}^d$ be a domain satisfying condition (H-1). Let $c_{\Delta t,h,\gamma}$, $\overline{c}_{\Delta t,h,\gamma}$, $\mu_{\Delta t,h,\gamma}$ and $\boldsymbol{u}_{\Delta t,h,\gamma}$ be the discrete solution of problem 4.1. Furthermore let the assumptions (A-1) - (A-8) be satisfied, then for the discrete time $t_n = n\Delta t$, with $1 \leq n \leq N$ the Lyapunov property holds*

$$E(t_n, c_h^n, \boldsymbol{u}_h^n) + \frac{1}{2}\int_0^{t_n}\int_\Omega \boldsymbol{M}(c_{\Delta t,h,\gamma}(t-\Delta t,\cdot))\nabla_{\boldsymbol{x}}\mu_{\Delta t,h,\gamma}\cdot\nabla_{\boldsymbol{x}}\mu_{\Delta t,h,\gamma}\,d\boldsymbol{x}dt + \frac{\gamma}{2}\int_0^{t_n}\int_\Omega(\dot{\overline{c}}_{\Delta t,h,\gamma})^2\,d\boldsymbol{x}dt \leq E(0,c_h^0,\boldsymbol{u}_h^0) + CT \quad (4.11)$$

with a constant $C = C(C_C, c_C, C_{\overline{\boldsymbol{\varepsilon}}}, \boldsymbol{g}, \mathrm{meas}(\Omega))$.

Proof. We observe the configurational energy $E^n_{h,config}$ at time $t_n = n\Delta t$ with $1 \leq n \leq N$ and use a minimiser $c_h^n \in X_{m,h}(\Omega)$ with a comparison function $c_h^{n-1} \in X_{m,h}(\Omega)$. Then we calculate

$$\begin{aligned}
&E^n_{h,config}(c_h^n) - \int_{\Gamma_N}\boldsymbol{g}^n\cdot\boldsymbol{u}_h^{n-1}\,d\boldsymbol{a}_{\boldsymbol{x}}\\
&\quad= \int_\Omega \frac{1}{2}\boldsymbol{\Gamma}\nabla_{\boldsymbol{x}}c_h^n\cdot\nabla_{\boldsymbol{x}}c_h^n + \psi(c_h^n) + W(c_h^n,\boldsymbol{\varepsilon}(\boldsymbol{u}_h^{n-1}))\,d\boldsymbol{x} - \int_{\Gamma_N}\boldsymbol{g}^n\cdot\boldsymbol{u}_h^{n-1}\,d\boldsymbol{a}_{\boldsymbol{x}}\\
&\qquad+ \frac{1}{2\Delta t}\|c_h^n - c_h^{n-1}\|^2_{\mathcal{M}_h^n} + \frac{\gamma}{2\Delta t}\|c_h^n - c_h^{n-1}\|^2_{L_2(\Omega)}\\
&\quad\leq \int_\Omega \frac{1}{2}\boldsymbol{\Gamma}\nabla_{\boldsymbol{x}}c_h^{n-1}\cdot\nabla_{\boldsymbol{x}}c_h^{n-1} + \psi(c_h^{n-1}) + W(c_h^{n-1},\boldsymbol{\varepsilon}(\boldsymbol{u}_h^{n-1}))\,d\boldsymbol{x}\\
&\qquad- \int_{\Gamma_N}\boldsymbol{g}^n\cdot\boldsymbol{u}_h^{n-1}\,d\boldsymbol{a}_{\boldsymbol{x}}
\end{aligned}$$

$$
\begin{aligned}
&= E(t_n, c_h^{n-1}, \boldsymbol{u}_h^{n-1}) + \int_\Omega (\boldsymbol{g}^{n-1} - \boldsymbol{g}^n) \cdot \boldsymbol{u}_h^{n-1} \, d\boldsymbol{a}_{\boldsymbol{x}} \\
&\leq E(t_{n-1}, c_h^{n-1}, \boldsymbol{u}_h^{n-1}) + C\Delta t.
\end{aligned}
$$

For the lower bound we remark that $\boldsymbol{u}_h^n$ minimises the strain energy $E_{h,mech}^n(\boldsymbol{u}_h^n)$ and we take into account (4.8) in order to conclude

$$
\begin{aligned}
E_{h,config}^n(c_h^n) - \int_{\Gamma_N} \boldsymbol{g}^n \cdot \boldsymbol{u}_h^{n-1} \, d\boldsymbol{a}_{\boldsymbol{x}} &\geq E(t_n, c_h^n, \boldsymbol{u}_h^n) \\
&+ \frac{1}{2} \int_{t_{(n-1)}}^{t_n} \int_\Omega \boldsymbol{M}_h^{n-1} \nabla_{\boldsymbol{x}} \mu_h^n \cdot \nabla_{\boldsymbol{x}} \mu_h^n \, d\boldsymbol{x} dt + \frac{\gamma}{2} \int_{t_{(n-1)}}^{t_n} \int_\Omega (\dot{\bar{c}}_{\Delta t,h,\gamma})^2 \, d\boldsymbol{x} dt.
\end{aligned}
$$

Both estimates together and their recursive application yield the statement of this lemma. □

Lemma 4.15. *Let $\Omega \subset \mathbb{R}^d$ be a domain satisfying condition (H-1) and let the assumptions (A-1), (A-2), (A-6) - (A-8) be satisfied. Let $\mathscr{T}_h(\Omega)$ be an admissible, exact and locally quasi-uniform mesh satisfying condition* (3.5)*. Then there exists a constant $C_E > 0$ depending on the material parameters formulated in the above mentioned assumptions, on the initial condition c_0 and on the boundary loading $\boldsymbol{g}$, but independent of the mesh size h and of the friction coefficient γ such that holds*

$$E(0, c_h^0, \boldsymbol{u}_h^0) \leq C_E.$$

Proof. We observe the energy at initial time $t = 0$ and apply the assumptions (A-1), (A-2), (A-6) - (A-8). Furthermore, we take into account the a-priori estimate (3.15) of the initial displacement $\boldsymbol{u}_h^0$ and calculate similarly as in lemma 2.25

$$E(0, c_h^0, \boldsymbol{u}_h^0) \leq \overline{C}(\|c_h^0\|_{H^1(\Omega)}^2 + \|\psi(c_h^0)\|_{L_1(\Omega)} + \mathrm{meas}(\Omega)),$$

where $\overline{C}$ is independent of the mesh size. The $H^1(\Omega)$-stability of the $L_2(\Omega)$-projection proved in lemma 3.13 shows that $\|c_h^0\|_{H^1(\Omega)} \leq C\|c_0\|_{H^1(\Omega)}$. Therefore it remains to show that the initial Gibbs free energy is bounded independent of the mesh size,

$$\|\psi(c_h^0)\|_{L_1(\Omega)} \leq \|\psi^+(c_h^0)\|_{L_1(\Omega)} + \|\psi^-(c_h^0)\|_{L_1(\Omega)}.$$

At first we consider the convex part of the Gibbs free energy density and calculate

$$\psi^+(c_0) \geq \psi^+(c_h^0) + \psi_{,c}^+(c_h^0)(c_0 - c_h^0).$$

Using assumption (A-2) and the $L_\infty(\Omega)$-stability of the $L_2(\Omega)$-projection we get

$$
\begin{aligned}
\psi^+(c_h^0) &\leq \psi^+(c_0) + |\psi_{,c}^+(c_h^0)||c_0 - c_h^0| \\
&\leq \psi^+(c_0) + (\delta\psi^+(c_h^0) + C_\delta)\|c_0 - c_h^0\|_{L_\infty(\Omega)} \\
&\leq \psi^+(c_0) + C(\delta\psi^+(c_h^0) + C_\delta)(\|c_0\|_{H^1(\Omega)} + \|c_0\|_{L_\infty(\Omega)}).
\end{aligned}
$$

By choosing $\delta = (2C(\|c_0\|_{H^1(\Omega)} + \|c_0\|_{L_\infty(\Omega)}))^{-1}$ we get the estimate

$$|\psi^+(c_h^0)| \leq C(|\psi^+(c_0)| + \|c_0\|_{H^1(\Omega)} + \|c_0\|_{L_\infty(\Omega)}),$$

which proves the statement for the convex term. For the non-convex part ψ^- we apply the polynomial boundedness by assumption (A-2), Rellich-Kondrachov embedding theorem 2.4 and the $H^1(\Omega)$-stability of the $L_2(\Omega)$-projection formulated in lemma 3.13. Then we calculate

$$\begin{aligned}\|\psi^-(c_h^0)\|_{L_1(\Omega)} &\leq C_\psi(\|c_h^0\|_{L_q(\Omega)}^q + \operatorname{meas}(\Omega)) \leq C_\psi(c_e^q\|c_h^0\|_{H^1(\Omega)}^q + \operatorname{meas}(\Omega)) \\ &\leq C(\|c_0\|_{H^1(\Omega)}^q + 1).\end{aligned}$$

This calculation finally shows the statement of this lemma. □

Lemma 4.16. *Let $\Omega \subset \mathbb{R}^d$ be a domain satisfying condition (H-1) and let the assumptions (A-1), (A-2), (A-6) - (A-8) be satisfied. Then there exists a constant $c_E > 0$ independent of the mesh size h and of the friction coefficient γ such that for every time step $t_n = n\Delta t$ with $1 \leq n \leq N$ the following estimate holds*

$$E(t_n, c_h^n, \boldsymbol{u}_h^n) \geq c_E \left(\|c_h^n\|_{H^1(\Omega)}^2 + \int_\Omega \psi(c_h^n)\, d\boldsymbol{x} - 1 \right).$$

Proof. The proof of this lemma follows basically from the Poincaré inequality. See lemma 2.26 for details. □

Lemma 4.17 (A-priori estimates). *Let $\Omega \subset \mathbb{R}^d$ be a domain satisfying condition (H-1) and let the assumptions (A-1) - (A-8) be satisfied. Let $\mathscr{T}_h(\Omega)$ be an admissible locally quasi-uniform mesh satisfying condition* (3.5)*. Then for the discrete weak solution c_N, $\overline{c}_{\Delta t,h,\gamma}$, $\mu_{\Delta t,h,\gamma}$ and $\boldsymbol{u}_{\Delta t,h,\gamma}$ there exists constants C_c, $C_{\overline{c}}$, $C_{\dot{\overline{c}}}$, C_μ, $C_{\boldsymbol{u}}$ and $C_\psi > 0$, depending on the material parameters, the boundary loading $\boldsymbol{g}$, the initial condition c_0, time T and* meas(Ω)*, such that the following uniform a-priori estimates hold*

(1) $\|\boldsymbol{u}_{\Delta t,h,\gamma}\|_{L_\infty(0,T;\boldsymbol{H}^1(\Omega))} \leq C_{\boldsymbol{u}}$,

(2) $\|c_{\Delta t,h,\gamma}\|_{L_\infty(0,T;H^1(\Omega))} \leq C_c$,

(3) $\|\overline{c}_{\Delta t,h\gamma}\|_{L_\infty(0,T;H^1(\Omega))} \leq C_{\overline{c}}$,

(4) $\sup_{t\in[0,T]} \int_\Omega \psi(c_{\Delta t,h,\gamma})\, d\boldsymbol{x} \leq C_\psi$,

(5) $\|\mu_{\Delta t,h,\gamma}\|_{L_2(0,T;H^1(\Omega))} \leq C_\mu$,

(6) $\|\dot{\overline{c}}_{\Delta t,h,\gamma}\|_{L_2(\Omega_T)} \leq C_{\overline{c}'}$, *if* $\gamma \gneqq 0$.

Proof. Using the Lyapunov property formulated in lemma 4.14 together with the upper estimates from lemma 4.15 and the lower estimate from lemma 4.16 the results follow by arguing analogously as in lemma 4.17. We remark that except $C_{\overline{c}'}$ all constants are independent of the mesh size h and of the friction coefficient γ. □

4.1.5 Convergence of the method

In this subsection we show that the finite element solutions $c_{\Delta t,h,\gamma}$, $\mu_{\Delta t,h,\gamma}$ and $\boldsymbol{u}_{\Delta t,h,\gamma}$ converge to a solution of the non-viscous Cahn-Larché system if Δt, h and γ go to zero. Note that the piecewise linear interpolant $\overline{c}_{\Delta t,h,\gamma}$ satisfies the discrete diffusion equation in the following way

$$\int_\Omega \dot{\overline{c}}_{\Delta t,h,\gamma}\zeta_h \, d\boldsymbol{x} + \int_\Omega \boldsymbol{M}(c_{\Delta t,h,\gamma}(t-\Delta t,\cdot))\nabla_{\boldsymbol{x}}\mu_{\Delta t,h,\gamma}\cdot\nabla_{\boldsymbol{x}}\zeta_h \, d\boldsymbol{x} = 0 \qquad \forall \zeta_h \in X_0(\Omega). \quad (4.12)$$

Lemma 4.18. *Let $\Omega \subset \mathbb{R}^d$ be a domain satisfying condition (H-1). Moreover, let the assumptions (A-1) - (A-8) be satisfied. Furthermore the triangulation is assumed to be exact, admissible, locally quasi-uniform and satisfies the mesh condition* (3.5). *Then there exist at least one $c \in L_\infty(0,T;H^1(\Omega))$ and subsequences denoted without loss of generality with the same index $(c_{\Delta t,h,\gamma})_{\Delta t,h,\gamma}$, $(\bar{c}_{\Delta t,h,\gamma})_{\Delta t,h,\gamma} \subset L_\infty(0,T;H^1(\Omega))$, such that for Δt, h, $\gamma \to 0$ holds*

$$\overline{c}_{\Delta t,h,\gamma} \longrightarrow c \qquad \text{in} \quad C([0,T];L_2(\Omega)), \quad (4.13)$$

$$c_{\Delta t,h,\gamma} \longrightarrow c \qquad \text{in} \quad L_\infty(0,T;L_2(\Omega)), \quad (4.14)$$

$$c_{\Delta t,h,\gamma}(t,\boldsymbol{x}) \longrightarrow c(t,\boldsymbol{x}) \qquad \text{almost everywhere in } \Omega_T, \quad (4.15)$$

$$c_{\Delta t,h,\gamma} \overset{*}{\rightharpoonup} c \qquad \text{in} \quad L_\infty(0,T;X_m(\Omega)), \quad (4.16)$$

Proof. The proof of this lemma follows directly by arguing analogously as in the proof of lemma 2.28. □

Lemma 4.19. *Let $\Omega \subset \mathbb{R}^d$ be a domain satisfying condition (H-1). Furthermore, let the assumptions (A-1) - (A-8) be satisfied. Moreover, the triangulation $\mathscr{T}_h(\Omega)$ is assumed to be exact, admissible, locally quasi-uniform and satisfies the mesh condition* (3.5). *Then for all times $t \in (0,T)$ holds*

$$c_{\Delta t,h,\gamma}(t-\Delta t,\cdot) \longrightarrow c(t,\cdot) \quad \text{in } L_2(\Omega) \text{ if } \Delta t, h, \gamma \to 0. \quad (4.17)$$

Proof. The same arguments as in the proof of lemma 2.29 yield the statement of this lemma. □

Up to now we know that there exists at least one concentration field $c \in L_\infty(0,T;X_m(\Omega))$, which is a limit of the approximation $c_{\Delta t,h,\gamma}$. We define a displacement $\boldsymbol{u} \in L_2(0,T;\boldsymbol{X}(\Omega))$ corresponding to $c \in L_\infty(0,T;X_m(\Omega))$ via the following problem.

Problem 4.20. Find $\boldsymbol{u} \in L_2(0,T;\boldsymbol{X}(\Omega))$ such that

$$\int_{\Omega_T} \boldsymbol{C}(c)\boldsymbol{\varepsilon}(\boldsymbol{u}) : \boldsymbol{\varepsilon}(\boldsymbol{\eta})\, d\boldsymbol{x}dt = \int_{\Omega_T} \boldsymbol{C}(c)\overline{\boldsymbol{\varepsilon}}(c) : \boldsymbol{\varepsilon}(\boldsymbol{\eta})\, d\boldsymbol{x}dt + \int_{\Gamma_T^N} \boldsymbol{g}\cdot\boldsymbol{\eta}\, d\boldsymbol{a}_{\boldsymbol{x}}dt$$
$$\boldsymbol{\eta} \in L_2(0,T;\boldsymbol{X}(\Omega)).$$

Lemma 4.21. *Let $\Omega \subset \mathbb{R}^d$ be a domain satisfying condition (H-1). Furthermore, let the assumptions (A-6) - (A-8) be satisfied. Then the following estimates in the time space cylinder hold*

(1) $$\left|\int_{\Omega_T} \boldsymbol{C}(c)\boldsymbol{\varepsilon}(\boldsymbol{u}) : \boldsymbol{\varepsilon}(\boldsymbol{\eta})\, d\boldsymbol{x}dt\right| \le C_c \|\boldsymbol{u}\|_{L_2(0,T;\boldsymbol{H}^1(\Omega))}\|\boldsymbol{\eta}\|_{L_2(0,T;\boldsymbol{H}^1(\Omega))},$$

(2) $$\int_{\Omega_T} \boldsymbol{C}(c)\boldsymbol{\varepsilon}(\boldsymbol{\eta}) : \boldsymbol{\varepsilon}(\boldsymbol{\eta})\, d\boldsymbol{x}dt \ge \frac{c_c}{c_k}\|\boldsymbol{\eta}\|^2_{L_2(0,T;\boldsymbol{H}^1(\Omega))},$$

(3) $$\left|\int_{\Omega_T} \boldsymbol{C}(c)\overline{\boldsymbol{\varepsilon}}(c) : \boldsymbol{\varepsilon}(\boldsymbol{\eta})\, d\boldsymbol{x}dt + \int_{\Gamma_T^N} \boldsymbol{g}\cdot\boldsymbol{\eta}\, d\boldsymbol{a}_{\boldsymbol{x}}dt\right|$$
$$\le CT^{\frac{1}{2}}\Big(\operatorname{meas}^{\frac{1}{2}}(\Omega) + \|\boldsymbol{g}\|_{C^0(0,T;H^{-\frac{1}{2}}(\Gamma_N))}\Big).$$

Proof. Statement *(1)* follows from assumption (A-6) and Hölder's inequality. Statement *(2)* is a direct consequence of (A-6) and Korn's inequality for any time $t \in (0,T)$. Statement *(3)* is proved by using the assumptions (A-6) - (A-8) and Hölder's inequality. □

Corollary 4.22. *Let $\Omega \subset \mathbb{R}^d$ be an open bounded domain with a Lipschitz boundary and let the assumptions (A-6) - (A-8) be satisfied. Then there exists a unique solution $\boldsymbol{u} \in L_2(0,T;\boldsymbol{X}(\Omega))$ with the a-priori estimate*

$$\|\boldsymbol{u}\|_{L_2(0,T;\boldsymbol{H}^1(\Omega))} \le T^{\frac{1}{2}} C_{\boldsymbol{u}}.$$

Proof. Since $L_2(0,T;\boldsymbol{X}(\Omega))$ is a Hilbert space the statement of the corollary follows from Lax-Milgram's theorem under consideration of lemma 4.21. □

Finally we have to show that the numerical approximation of the displacement $\boldsymbol{u}_{\Delta t,h,\gamma}$ converges strongly to $\boldsymbol{u} \in L_2(0,T;\boldsymbol{X}(\Omega))$ if $c_{\Delta t,h,\gamma} \longrightarrow c$. In order to get this result, we consider the following auxiliary problem.

Problem 4.23. Find $\tilde{\boldsymbol{u}} \in L_2(0,T;\boldsymbol{X}(\Omega))$ such that holds

$$\int_{\Omega_T} \boldsymbol{C}(c_{\Delta t,h,\gamma})\boldsymbol{\varepsilon}(\tilde{\boldsymbol{u}}) : \boldsymbol{\varepsilon}(\boldsymbol{\eta})\, d\boldsymbol{x}dt = \int_{\Omega_T} \boldsymbol{C}(c_{\Delta t,h,\gamma})\overline{\boldsymbol{\varepsilon}}(c_{\Delta t,h,\gamma}) : \boldsymbol{\varepsilon}(\boldsymbol{\eta})\, d\boldsymbol{x}dt$$
$$+ \int_{\Gamma_T^N} \boldsymbol{g}_{\Delta t}\cdot\boldsymbol{\eta}\, d\boldsymbol{a}_{\boldsymbol{x}}dt \qquad \forall \boldsymbol{\eta} \in L_2(0,T;\boldsymbol{X}(\Omega)).$$

We remark that the estimates from lemma 4.21 are still valid for the auxiliary problem 4.23 due to the assumptions (A-6) - (A-8). Therefore by using Lax-Milgram's theorem we deduce the existence of a unique solution $\tilde{\boldsymbol{u}} \in L_2(0,T;\boldsymbol{X}(\Omega))$.

Corollary 4.24 (Galerkin orthogonality). *For all discrete test functions $\boldsymbol{\eta}_h = \mathcal{R}_h\boldsymbol{\eta}$ with an arbitrary $\eta \in L_2(0,T;\boldsymbol{X}(\Omega))$ holds*

$$\int_{\Omega_T} \boldsymbol{C}(c_{\Delta t,h,\gamma})\boldsymbol{\varepsilon}(\tilde{\boldsymbol{u}} - \boldsymbol{u}_{\Delta t,h,\gamma}) : \boldsymbol{\varepsilon}(\boldsymbol{\eta}_h)\, d\boldsymbol{x}dt = 0.$$

Proof. The Galerkin orthogonality follows by integrating the discrete semi-weak formulation (4.3) in problem 4.1 with respect to time $(0,T)$ and subtracting it from the weak formulation in the auxiliary problem 4.23. □

Lemma 4.25 (Cea's lemma). *Let $\Omega \subset \mathbb{R}^d$ be a domain satisfying condition (H-1). Furthermore, let the assumptions (A-6) - (A-8) be satisfied. Let $\tilde{\boldsymbol{u}} \in L_2(0,T;\boldsymbol{X}(\Omega))$ be a unique solution of the auxiliary problem 4.23 and let $\boldsymbol{u}_{\Delta t,h,\gamma}$ be the piecewise constant interpolant of the discrete solution of problem 4.1. Then it holds*

$$\|\tilde{\boldsymbol{u}} - \boldsymbol{u}_{\Delta t,h,\gamma}\|_{L_2(0,T;H^1(\Omega))} \leq \frac{C_C c_k}{c_C} \inf_{\boldsymbol{\eta}_h} \|\tilde{\boldsymbol{u}} - \boldsymbol{\eta}_h\|_{L_2(0,T;\boldsymbol{H}^1(\Omega))}.$$

Proof. By using assumption (A-6), Korn's inequality, the Galerkin inequality and Hölder's inequality, we calculate

$$\begin{aligned}
&\frac{c_c}{c_k}\|\tilde{\boldsymbol{u}} - \boldsymbol{u}_{\Delta t,h,\gamma}\|^2_{L_2(0,T;\boldsymbol{H}^1(\Omega))} \\
&\quad\leq \int_{\Omega_T} \boldsymbol{C}(c_{\Delta t,h,\gamma})\boldsymbol{\varepsilon}(\tilde{\boldsymbol{u}} - \boldsymbol{u}_{\Delta t,h,\gamma}) : \boldsymbol{\varepsilon}(\tilde{\boldsymbol{u}} - \boldsymbol{u}_{\Delta t,h,\gamma})\, d\boldsymbol{x}dt \\
&\qquad+ \int_{\Omega_T} \boldsymbol{C}(c_{\Delta t,h,\gamma})\boldsymbol{\varepsilon}(\tilde{\boldsymbol{u}} - \boldsymbol{u}_{\Delta t,h,\gamma}) : \boldsymbol{\varepsilon}(\boldsymbol{u}_{\Delta t,h,\gamma} - \boldsymbol{\eta}_h)\, d\boldsymbol{x}dt \\
&\quad\leq C_c\|\tilde{\boldsymbol{u}} - \boldsymbol{u}_{\Delta t,h\gamma}\|_{L_2(0,T;\boldsymbol{H}^1(\Omega))}\|\tilde{\boldsymbol{u}} - \boldsymbol{\eta}_h\|_{L_2(0,T;\boldsymbol{H}^1(\Omega))}.
\end{aligned}$$

Since $\boldsymbol{\eta}_h$ is chosen arbitrary the statement of this lemma follows. □

Lemma 4.26 (Error estimate). *Let $\Omega \subset \mathbb{R}^d$ be a domain satisfying condition (H-1). Furthermore, let the assumptions (A-6) - (A-8) be satisfied. Let $\boldsymbol{u} \in L_2(0,T;\boldsymbol{X}(\Omega))$ be the unique solution of problem 4.20 and let $\tilde{\boldsymbol{u}} \in L_2(0,T;\boldsymbol{X}(\Omega))$ be the unique solution of the auxiliary problem 4.23. Then it holds*

$$\begin{aligned}
\|\boldsymbol{u} - \tilde{\boldsymbol{u}}\|_{L_2(0,T;\boldsymbol{H}^1(\Omega))} \leq C\Big(&\|\boldsymbol{C}(c)\overline{\boldsymbol{\varepsilon}}(c) - \boldsymbol{C}(c_{\Delta t,h,\gamma})\overline{\boldsymbol{\varepsilon}}(c_{\Delta t,h,\gamma})\|_{L_2(\Omega_T)} \\
&+ \|(\boldsymbol{C}(c) - \boldsymbol{C}(c_{\Delta t,h,\gamma}))\boldsymbol{\varepsilon}(\tilde{\boldsymbol{u}})\|_{L_2(\Omega_T)} \\
&+ T^{\frac{1}{2}}\|\boldsymbol{g} - \boldsymbol{g}_{\Delta t}\|_{C^0(0,T;H^{-\frac{1}{2}}(\Gamma_N))}\Big).
\end{aligned}$$

Proof. Subtracting the weak formulation of problem 4.20 from the weak formulation of problem 4.23 and inserting $\int_{\Omega_T}(\boldsymbol{C}(c_{\Delta t,h,\gamma})\boldsymbol{\varepsilon}(\boldsymbol{u})-\boldsymbol{C}(c_{\Delta t,h,\gamma})\boldsymbol{\varepsilon}(\boldsymbol{u})):\boldsymbol{\varepsilon}(\boldsymbol{\eta})\,d\boldsymbol{x}dt$, this yields for the left hand side

$$\begin{aligned}
&\int_{\Omega_T}(\boldsymbol{C}(c_{\Delta t,h,\gamma})\boldsymbol{\varepsilon}(\tilde{\boldsymbol{u}})-\boldsymbol{C}(c)\boldsymbol{\varepsilon}(\boldsymbol{u})):\boldsymbol{\eta}\,d\boldsymbol{x}dt\\
&\quad=\int_{\Omega_T}\boldsymbol{C}(c_{\Delta t,h,\gamma})\boldsymbol{\varepsilon}(\tilde{\boldsymbol{u}}-\boldsymbol{u}):\boldsymbol{\varepsilon}(\boldsymbol{\eta})\,d\boldsymbol{x}dt\\
&\qquad+\int_{\Omega_T}(\boldsymbol{C}(c_{\Delta t,h,\gamma})-\boldsymbol{C}(c))\boldsymbol{\varepsilon}(\boldsymbol{u}):\boldsymbol{\varepsilon}(\boldsymbol{\eta})\,d\boldsymbol{x}dt.
\end{aligned}$$

We choose $\boldsymbol{\eta}=\boldsymbol{u}-\tilde{\boldsymbol{u}}$ and deduce in view of Korn's inequality (2.3) and the trace theorem 2.2 the following estimate

$$\begin{aligned}
\frac{c_C}{c_k}\|\boldsymbol{u}-\tilde{\boldsymbol{u}}\|^2_{L_2(0,T;\boldsymbol{H}^1(\Omega))}&\le\int_{\Omega_T}\boldsymbol{C}(c_{\Delta t,h,\gamma})\boldsymbol{\varepsilon}(\boldsymbol{u}-\tilde{\boldsymbol{u}}):\boldsymbol{\varepsilon}(\boldsymbol{u}-\tilde{\boldsymbol{u}})\,d\boldsymbol{x}dt\\
&\le\left|\int_{\Omega_T}(\boldsymbol{C}(c)-\boldsymbol{C}(c_{\Delta t,h,\gamma}))\boldsymbol{\varepsilon}(\boldsymbol{u}):\boldsymbol{\varepsilon}(\boldsymbol{u}-\tilde{\boldsymbol{u}})\,d\boldsymbol{x}dt\right|\\
&\quad+\left|\int_{\Omega_T}(\boldsymbol{C}(c)\overline{\boldsymbol{\varepsilon}}(c)-\boldsymbol{C}(c_{\Delta t,h,\gamma})\overline{\boldsymbol{\varepsilon}}(c_{\Delta t,h,\gamma})):\boldsymbol{\varepsilon}(\boldsymbol{u}-\tilde{\boldsymbol{u}})\,d\boldsymbol{x}dt\right|\\
&\quad+\left|\int_{\Gamma_T^N}(\boldsymbol{g}-\boldsymbol{g}_{\Delta t})\cdot(\tilde{\boldsymbol{u}}-\boldsymbol{u})\,d\boldsymbol{a}_{\boldsymbol{x}}dt\right|\\
&\le\|(\boldsymbol{C}(c)-\boldsymbol{C}(c_{\Delta t,h,\gamma}))\boldsymbol{\varepsilon}(\boldsymbol{u})\|_{L_2(\Omega_T)}\|\boldsymbol{u}-\tilde{\boldsymbol{u}}\|_{L_2(0,T;\boldsymbol{H}^1(\Omega))}\\
&\quad+\|\boldsymbol{C}(c)\overline{\boldsymbol{\varepsilon}}(c)-\boldsymbol{C}(c_{\Delta t,h,\gamma})\overline{\boldsymbol{\varepsilon}}(c_{\Delta t,h,\gamma})\|_{L_2(\Omega_T)}\|\boldsymbol{u}-\tilde{\boldsymbol{u}}\|_{L_2(0,T;\boldsymbol{H}^1(\Omega))}\\
&\quad+CT^{\frac{1}{2}}\|\boldsymbol{g}-\boldsymbol{g}_{\Delta t}\|_{C^0(0,T;H^{-\frac{1}{2}}(\Gamma_N))}\|\boldsymbol{u}-\tilde{\boldsymbol{u}}\|_{L_2(0,T;\boldsymbol{H}^1(\Omega))}.
\end{aligned}$$

□

Remark 4.27. Under the same hypotheses as in lemma 4.26, we get by arguing similarly as in the proof of lemma 4.26 the following estimate

$$\begin{aligned}
&\|\boldsymbol{u}-\tilde{\boldsymbol{u}}(t-\Delta t,\cdot)\|_{L_2(0,T;\boldsymbol{H}^1(\Omega))}\\
&\quad\le C\Big(\|\boldsymbol{C}(c)\overline{\boldsymbol{\varepsilon}}(c)-\boldsymbol{C}(c_{\Delta t,h,\gamma}(t-\Delta t,\cdot))\overline{\boldsymbol{\varepsilon}}(c_{\Delta t,h,\gamma}(t-\Delta t,\cdot))\|_{L_2(\Omega_T)}\\
&\qquad+\|(\boldsymbol{C}(c)-\boldsymbol{C}(c_{\Delta t,h,\gamma}(t-\Delta t,\cdot)))\boldsymbol{\varepsilon}(\tilde{\boldsymbol{u}}(t-\Delta t,\cdot))\|_{L_2(\Omega_T)}\\
&\qquad+T^{\frac{1}{2}}\|\boldsymbol{g}-\boldsymbol{g}_{\Delta t}(t-\Delta t,\cdot)\|_{C^0(0,T;H^{-\frac{1}{2}}(\Gamma_N))}\Big).
\end{aligned}$$

Lemma 4.28 (Convergence). *Let $\Omega\subset\mathbb{R}^d$ be a domain satisfying condition (H-1). Furthermore, let the assumptions (A-6) - (A-8) be satisfied. Let $\boldsymbol{u}\in L_2(0,T;\boldsymbol{X}(\Omega))$ be the unique solution of problem 4.20 and let $\boldsymbol{u}_{\Delta t,h,\gamma}\in L_2(0,T;\boldsymbol{X}_h(\Omega))$ be the piecewise constant interpolant of discrete weak solutions of problem* (4.1)*. Then it holds for Δt, h, $\gamma\to 0$*

$$\begin{aligned}
\boldsymbol{u}_{\Delta t,h,\gamma}&\longrightarrow\boldsymbol{u}&&\text{in}\quad L_2(0,T;\boldsymbol{H}^1(\Omega)),\\
\boldsymbol{u}_{\Delta t,h,\gamma}(t-\Delta t,\cdot)&\longrightarrow\boldsymbol{u}&&\text{in}\quad L_2(0,T;\boldsymbol{H}^1(\Omega)).
\end{aligned}$$

Proof. Taking into account Cea's lemma 4.25 and the error estimate of lemma 4.26, it follows by using the Clement operator

$$\begin{aligned}
&\|\boldsymbol{u}-\boldsymbol{u}_{\Delta t,h,\gamma}\|_{L_2(0,T;\boldsymbol{H}^1(\Omega))}\\
&\quad\leq \|\boldsymbol{u}-\tilde{\boldsymbol{u}}\|_{L_2(0,T;\boldsymbol{H}^1(\Omega))}+\|\tilde{\boldsymbol{u}}-\boldsymbol{u}_{\Delta t,h,\gamma}\|_{L_2(0,T;\boldsymbol{H}^1(\Omega))}\\
&\quad\leq C\Big(\|\boldsymbol{C}(c)\overline{\boldsymbol{\varepsilon}}(c)-\boldsymbol{C}(c_{\Delta t,h,\gamma})\overline{\boldsymbol{\varepsilon}}(c_{\Delta t,h,\gamma})\|_{L_2(\Omega_T)}\\
&\qquad+\|(\boldsymbol{C}(c)-\boldsymbol{C}(c_{\Delta t,h,\gamma}))\boldsymbol{\varepsilon}(\tilde{\boldsymbol{u}})\|_{L_2(\Omega_T)}+T^{\frac{1}{2}}\|\boldsymbol{g}-\boldsymbol{g}_{\Delta t}\|_{C^0(0,T;H^{-\frac{1}{2}}(\Gamma_N))}\Big)\\
&\qquad+\frac{C_C c_k}{c_C}\|\boldsymbol{u}-\mathcal{R}_h\boldsymbol{u}\|_{L_2(0,T;\boldsymbol{H}^1(\Omega))}.
\end{aligned}$$

The convergence follows from the convergence of the Clement quasi-interpolation, see lemma 3.9, from the almost everywhere convergence of the concentration field together with Lebesgue's convergence theorem and from the Lipschitz continuity with respect to time of the boundary loading, see assumption (A-8). The second statement follows from remark 4.27 and from the continuity of the concentration field shown in lemma 4.18. □

Due to the uniform a-priori estimate for the chemical potential $\mu_{\Delta t,h,\gamma}$ calculated in lemma 4.17 statement *(5)* we extract a weak convergent subsequence without loss of generality indicated with the same index

$$\mu_{\Delta t,h,\gamma}\rightharpoonup\mu\quad\text{in } L_2(0,T;H^1(\Omega))\quad\text{if } \Delta t,h,\gamma\longrightarrow 0.$$

Theorem 4.29 (Convergence of the method). *Let $\Omega\subset\mathbb{R}^d$ be a domain satisfying condition (H-1). Furthermore, $\mathscr{T}_h(\Omega)$ is assumed to be an exact, admissible and locally quasi-uniform triangulation satisfying the shape regularity condition. Let the assumptions (A-1) - (A-8) be satisfied, then $c_{\Delta t,h,\gamma}$, $\mu_{\Delta t,h,\gamma}$ and $\boldsymbol{u}_{\Delta t,h,\gamma}$ converge to a weak solution of the non-viscous Cahn-Larché system, if Δt, h, γ go to zero.*

Proof. **Step 1**: As a test function we use $\zeta_h=\mathcal{R}_h\zeta$ with $\zeta\in\{v\in L_2(0,T;H^1(\Omega))$ with $\dot{v}\in L_2(\Omega_T)\}$ in the discrete diffusion equation (4.1), integrate over $(0,T)$ and apply integration by parts with respect to time. After subtraction from the weak formulation of the non-viscous Cahn-Larché system, we deduce for the first term

$$\begin{aligned}
&\left|\int_{\Omega_T}(\bar{c}_{\Delta t,h,\gamma}-c_h^0)\mathcal{R}_h\dot{\zeta}-(c-c_0)\dot{\zeta}\;d\boldsymbol{x}dt\right|\\
&=\left|\int_{\Omega_T}(\bar{c}_{\Delta t,h,\gamma}-c_h^0)(\mathcal{R}_h\dot{\zeta}-\dot{\zeta})+(\bar{c}_{\Delta t,h,\gamma}-c)\dot{\zeta}+(c_0-c_h^0)\dot{\zeta}\;d\boldsymbol{x}dt\right|\\
&\leq\|\bar{c}_{\Delta t,h,\gamma}-c_h^0\|_{L_2(\Omega_T)}\|\mathcal{R}_h\dot{\zeta}-\dot{\zeta}\|_{L_2(\Omega_T)}+\|\bar{c}_{\Delta t,h,\gamma}-c\|_{L_2(\Omega_T)}\|\dot{\zeta}\|_{L_2(\Omega_T)}\\
&\qquad+T^{\frac{1}{2}}\|c_0-c_h^0\|_{L_2(\Omega)}\|\dot{\zeta}\|_{L_2(\Omega_T)}.
\end{aligned}$$

The convergence of this term follows from the a-priori estimates in lemma 4.17 statement *(3)*, from the convergence of the concentration formulated in lemma 4.18 and from the approximation property in lemma 3.9.

For the second term of the discrete diffusion equation (4.1) we use the same test function $\zeta_h = \mathcal{R}_h\zeta$ and insert zero in order to derive

$$\begin{aligned}
&\left|\int_{\Omega_T} \boldsymbol{M}(c_{\Delta t,h,\gamma}(t-\Delta t,\cdot))\nabla_{\boldsymbol{x}}\mu_{\Delta t,h,\gamma}\cdot\nabla_{\boldsymbol{x}}\mathcal{R}_h\zeta - \boldsymbol{M}(c)\nabla_{\boldsymbol{x}}\mu\cdot\nabla_{\boldsymbol{x}}\zeta\; d\boldsymbol{x}dt\right| \\
&= \left|\int_{\Omega_T} \boldsymbol{M}(c_{\Delta t,h,\gamma}(t-\Delta t))\nabla_{\boldsymbol{x}}\mu_{\Delta t,h,\gamma}\cdot\nabla_{\boldsymbol{x}}\mathcal{R}_h\zeta - \boldsymbol{M}(c)\nabla_{\boldsymbol{x}}\mu_{\Delta t,h,\gamma}\cdot\nabla_{\boldsymbol{x}}\mathcal{R}_h\zeta\; d\boldsymbol{x}dt\right| \\
&\quad + \left|\int_{\Omega_T} \boldsymbol{M}(c)\nabla_{\boldsymbol{x}}\mu_{\Delta t,h,\gamma}\cdot\nabla_{\boldsymbol{x}}\mathcal{R}_h\zeta - \boldsymbol{M}(c)\nabla_{\boldsymbol{x}}\mu_{\Delta t,h,\gamma}\cdot\nabla_{\boldsymbol{x}}\zeta\; d\boldsymbol{x}dt\right| \\
&\quad + \left|\int_{\Omega_T} \boldsymbol{M}(c)\nabla_{\boldsymbol{x}}\mu_{\Delta t,h,\gamma}\cdot\nabla_{\boldsymbol{x}}\zeta - \boldsymbol{M}(c)\nabla_{\boldsymbol{x}}\mu\cdot\nabla_{\boldsymbol{x}}\zeta\; d\boldsymbol{x}dt\right| \\
&\leq \left|\int_{\Omega_T} (\boldsymbol{M}(c_{\Delta t,h,\gamma}(t-\Delta t,\cdot)) - \boldsymbol{M}(c))\nabla_{\boldsymbol{x}}\mu_{\Delta t,h,\gamma}\cdot\nabla_{\boldsymbol{x}}\mathcal{R}_h\zeta\; d\boldsymbol{x}dt\right| \\
&\quad + c_M\|\mu_{\Delta t,h,\gamma}\|_{L_2(0,T;H^1(\Omega))}\|\mathcal{R}_h\zeta-\zeta\|_{L_2(0,T;H^1(\Omega))} \\
&\quad + \left|\int_{\Omega_T} \boldsymbol{M}(c)(\nabla_{\boldsymbol{x}}\mu_{\Delta t,h,\gamma} - \nabla_{\boldsymbol{x}}\mu)\cdot\nabla_{\boldsymbol{x}}\zeta\; d\boldsymbol{x}dt\right|
\end{aligned}$$

The continuity of the concentration field with respect to time in lemma 4.19 together with Lebesgue's convergence theorem, the approximation property from lemma 3.9 and the weak convergence of the chemical potential yield the convergence.

Step 2: In the next step, we consider the discrete semi-weak equation of the chemical potential (4.2). We choose as a test function $\xi_h = \mathcal{R}_h\xi$ with $\xi \in \{v \in L_2(0,T;H^1(\Omega)) \cap L_\infty(\Omega_T) \;:\; \dot{v} \in L_2(\Omega_T)\}$. After integrating (4.2) over $(0,T)$ and subtraction from the weak formulation of the non-viscous Cahn-Larché system, we deduce for the left hand side

$$\begin{aligned}
\left|\int_{\Omega_T} \mu_{\Delta t,h,\gamma}\mathcal{R}_h\xi - \mu\xi\; d\boldsymbol{x}dt\right| &= \left|\int_{\Omega_T} \mu_{\Delta t,h,\gamma}(\mathcal{R}_h\xi-\xi) + (\mu_{\Delta t,h,\gamma}-\mu)\xi\; d\boldsymbol{x}dt\right| \\
&\leq \|\mu_{\Delta t,h,\gamma}\|_{L_2(0,T;H^1(\Omega))}\|\mathcal{R}_h\xi-\xi\|_{L_2(0,T;H^1(\Omega))} + \left|\int_{\Omega_T} (\mu_{\Delta t,h,\gamma}-\mu)\xi\; d\boldsymbol{x}dt\right|.
\end{aligned}$$

The uniform boundedness of the chemical potential from lemma 4.17 statement *(5)*, the approximation property lemma 3.9 and the weak convergence of the chemical potential yield the convergence of this term.

For the right hand side we first consider the surface energy and insert zero in

order to calculate

$$\begin{aligned}
&\left| \int_{\Omega_T} \mathbf{\Gamma} \nabla_{\boldsymbol{x}} c_{\Delta t,h,\gamma} \cdot \nabla_{\boldsymbol{x}} \mathcal{R}_h \xi - \mathbf{\Gamma} \nabla_{\boldsymbol{x}} c \cdot \nabla_{\boldsymbol{x}} \xi \; d\boldsymbol{x}dt \right| \\
&= \left| \int_{\Omega_T} \mathbf{\Gamma} \nabla_{\boldsymbol{x}} c_{\Delta t,h,\gamma} \cdot \nabla_{\boldsymbol{x}} (\mathcal{R}_h \xi - \xi) + \mathbf{\Gamma} \nabla_{\boldsymbol{x}} (c_{\Delta t,h,\gamma} - c) \cdot \nabla_{\boldsymbol{x}} \xi \; d\boldsymbol{x}dt \right| \\
&\leq C_\Gamma \| c_{\Delta t,h,\gamma} \|_{L_2(0,T;H^1(\Omega))} \| \mathcal{R}_h \xi - \xi \|_{L_2(0,T;H^1(\Omega))} \\
&\quad + \left| \int_{\Omega_T} \mathbf{\Gamma} \nabla_{\boldsymbol{x}} (c_{\Delta t,h,\gamma} - c) \cdot \nabla_{\boldsymbol{x}} \xi \; d\boldsymbol{x}dt \right|.
\end{aligned}$$

The uniform boundedness of the concentration field, see lemma 4.17, the approximation property in lemma 3.9 and the weak-$\star$ convergence of the concentration field imply the convergence of this term.

Moreover, we consider the first part ψ^+ of the Gibbs free energy density ψ. By assumption (A-2) we know $\psi^+ \in C^1(\mathbb{R}, \mathbb{R})$. Together with the almost everywhere convergence of $c_{\Delta t,h,\gamma}$ and $\xi_h = \mathcal{R}_h \xi$ we get

$$\psi^+_{,c}(c_{\Delta t,h,\gamma}(t,\boldsymbol{x}))\xi_h(t,\boldsymbol{x}) \longrightarrow \psi^+_{,c}(c(t,\boldsymbol{x}))\xi(t,\boldsymbol{x}) \qquad \text{if} \qquad \Delta t, h \longrightarrow 0.$$

Furthermore, let $\epsilon > 0$ be arbitrary, we choose $\mathscr{E} \subset \Omega_T$ with the property $\operatorname{meas}(\mathscr{E}) \leq \epsilon$ use assumption (A-2) with $\delta = \epsilon$ and take into account lemma 4.17 statement *(4)* together with the $L_\infty(\Omega)$- stability of the Clement operator in order to calculate

$$\begin{aligned}
&\int_{\mathscr{E}} \psi^+_{,c}(c_{\Delta t,h,\gamma}) \mathcal{R}_h \xi \; d\boldsymbol{x}dt \leq \int_{\mathscr{E}} (\delta \psi^+(c_{\Delta t,h,\gamma}) + C_\delta) \mathcal{R}_h \xi \; d\boldsymbol{x}dt \\
&\leq \left(\delta \sup_{t \in (0,T)} \int_\Omega \psi^+(c_{\Delta t,h,\gamma}) \; d\boldsymbol{x} + C_\delta \operatorname{meas}(\mathscr{E}) \right) \| \xi \|_{L_\infty(\Omega)} \leq C\epsilon.
\end{aligned}$$

In view of Vitali's convergence theorem 2.11 the convergence of this term follows.

The second part of the Gibbs free energy density is polynomially bounded due to assumption (A-2). By inserting zero, we calculate

$$\begin{aligned}
&\left| \int_{\Omega_T} \psi^-_{,c}(c_{\Delta t,h,\gamma}) \mathcal{R}_h \xi - \psi^-_{,c}(c) \xi \; d\boldsymbol{x}dt \right| \\
&= \left| \int_{\Omega_T} \psi^-_{,c}(c_{\Delta t,h,\gamma})(\mathcal{R}_h \xi - \xi) + (\psi^-_{,c}(c_{\Delta t,h,\gamma}) - \psi^-_{,c}(c)) \xi \; d\boldsymbol{x}dt \right| \\
&\leq C(\| c_{\Delta t,h,\gamma} \|^{q-1}_{L_q(\Omega)} + 1) \| \mathcal{R}_h \xi - \xi \|_{H^1(\Omega)} + \left| \int_{\Omega_T} (\psi^-_{,c}(c_{\Delta t,h}) - \psi^-_{,c}(c)) \xi \; d\boldsymbol{x}dt \right|.
\end{aligned}$$

The uniform boundedness of the concentration in lemma 4.17 together with the approximation property in lemma 3.9, the almost everywhere convergence of the concentration field and generalised Lebesgue's convergence theorem yield the convergence of this term.

For the mechanical contribution to the chemical potential we first remark that due to the almost everywhere convergence of the concentration field and the continuity of the deformation with respect to time follows

$$W_{,c}(c_{\Delta t,h,\gamma}(t,\boldsymbol{x}),\boldsymbol{\varepsilon}(\boldsymbol{u}_{\Delta t,h,\gamma}(t-\Delta t,\boldsymbol{x})))\mathcal{R}_h\xi \longrightarrow W_{,c}(c(t,\boldsymbol{x}),\boldsymbol{\varepsilon}(\boldsymbol{u}(t,\boldsymbol{x})))\xi \quad \text{if} \quad \Delta t,h,\gamma \longrightarrow 0.$$

Taking into account the assumptions (A-6), (A-7) and the a-priori estimates of the Clement operator in $L_\infty(\Omega)$, see lemma 3.7, we estimate the elastic contribution of the chemical potential by

$$\begin{aligned} &W_{,c}(c_{\Delta t,h,\gamma}(t,\boldsymbol{x}),\boldsymbol{\varepsilon}(\boldsymbol{u}_{\Delta t,h,\gamma}(t-\Delta t,\boldsymbol{x})))\mathcal{R}_h\xi \\ &\quad\le C(|\boldsymbol{\varepsilon}(\boldsymbol{u}_{\Delta t,h,\gamma}(t-\Delta t,\boldsymbol{x}))|^2+1)\|\mathcal{R}_h\xi\|_{L_\infty(\Omega)} \\ &\quad\le C(|\boldsymbol{\varepsilon}(\boldsymbol{u}_{\Delta t,h,\gamma}(t-\Delta t,\boldsymbol{x}))|^2+1)\|\xi\|_{L_\infty(\Omega)}. \end{aligned}$$

The strong convergence of the displacement proved in lemma 4.28 together with the generalised Lebesgue convergence theorem 2.10 yields the convergence of the mechanical contribution to the chemical potential.

For the stabilisation term we calculate

$$\left|\gamma\int_{\Omega_T}(\bar{c}_{\Delta t,h,\gamma}-c_0)\mathcal{R}_h\dot{\xi}\,d\boldsymbol{x}dt\right| \le \gamma\|\bar{c}_{\Delta t,h,\gamma}-c_0\|_{L_2(0,T;H^1(\Omega))}\|\mathcal{R}_h\dot{\xi}\|_{L_2(\Omega_T)}.$$

Since the concentration field is uniformly bounded and the Clement operator is obviously bounded in $L_2(\Omega_T)$, the stabilisation term vanishes if the friction coefficient γ goes to zero.

Step 3: Finally, the convergence of the displacement $\boldsymbol{u}_{\Delta t,h,\gamma}$ follows from lemma 2.35. This argument finishes the whole convergence proof of the viscous approximation method. □

4.1.6 Numerical solution of the Euler-Lagrange equations

The numerical approximation method introduced by problem 4.1 leads to a non-linear equation system, which must be solved in every time step $t = n\Delta t$ with $1 \le n \le N$. This non-linear equation system follows from (4.1) and (4.2) having the form

$$\underline{\boldsymbol{A}}(\underline{\boldsymbol{c}}^n-\underline{\boldsymbol{c}}^{n-1})+\Delta t\underline{\boldsymbol{M}}^n\underline{\boldsymbol{\mu}}^n=\underline{\boldsymbol{0}}, \tag{4.18}$$

$$-\underline{\boldsymbol{G}}_\gamma(\underline{\boldsymbol{c}}^n,\underline{\boldsymbol{u}}^{n-1})+\underline{\boldsymbol{A}}\underline{\boldsymbol{\mu}}^n=\underline{\boldsymbol{0}}. \tag{4.19}$$

In this system $\underline{\boldsymbol{c}}^n$ and $\underline{\boldsymbol{\mu}}^n$ are the unknown quantities, whereas $\underline{\boldsymbol{c}}^{n-1}$ and $\underline{\boldsymbol{\mu}}^{n-1}$ are known from the previous time step. The matrices $\underline{\boldsymbol{A}}$ and $\underline{\boldsymbol{M}}^n$ as well as the vector

valued function $\underline{\boldsymbol{G}}_\gamma$ are calculated by the formula

$$\begin{aligned}
\underline{\boldsymbol{A}}[\boldsymbol{y},\boldsymbol{z}] &:= \int_\Omega \varphi_{\boldsymbol{y}}\varphi_{\boldsymbol{z}}\, d\boldsymbol{x},\\
\underline{\boldsymbol{M}}^n[\boldsymbol{y},\boldsymbol{z}] &:= \int_\Omega \boldsymbol{M}(c_h^{n-1})\nabla_{\boldsymbol{x}}\varphi_{\boldsymbol{y}}\cdot\nabla_{\boldsymbol{x}}\varphi_{\boldsymbol{z}}\, d\boldsymbol{x},\\
\underline{\boldsymbol{G}}_\gamma(\underline{\boldsymbol{c}}^n,\underline{\boldsymbol{u}}^{n-1})[\boldsymbol{z}] &:= \int_\Omega \boldsymbol{\Gamma}\nabla_{\boldsymbol{x}}c_h^n\cdot\nabla_{\boldsymbol{x}}\varphi_{\boldsymbol{z}} + \psi_{,c}(c_h^n)\varphi_{\boldsymbol{z}} + W_{,c}(c_h^n,\boldsymbol{\varepsilon}(\boldsymbol{u}_h^{n-1}))\varphi_{\boldsymbol{z}}\\
&\qquad + \frac{\gamma}{\Delta t}(c_h^n - c_h^{n-1})\varphi_{\boldsymbol{z}}\, d\boldsymbol{x}.
\end{aligned}$$

We remark that all integrals in this equation system exist due to the assumptions (A-1) - (A-8). Obviously the algebraic non-linearity appears only in the vector valued function $\underline{\boldsymbol{G}}_\gamma$ in the concentration field $\underline{\boldsymbol{c}}^n$.

This non-linear equation system is solved iteratively by using the Newton method, see e.g. [88]. For the equation system (4.18), (4.19) the Newton method is given by the following algorithm.

Algorithm 4.30 (Newton method).

// Initial vectors:
$\underline{\boldsymbol{c}}_0^n = \underline{\boldsymbol{c}}^{n-1}$
$\underline{\boldsymbol{\mu}}_0^n = \underline{\boldsymbol{\mu}}^{n-1}$

// Initial residuum:
$\underline{\boldsymbol{q}}_0 = -\Delta t\underline{\boldsymbol{M}}^n\underline{\boldsymbol{\mu}}_0^n$
$\underline{\boldsymbol{r}}_0 = \underline{\boldsymbol{G}}_\gamma(\underline{\boldsymbol{c}}_0^n,\underline{\boldsymbol{u}}^{n-1}) - \underline{\boldsymbol{A}}\underline{\boldsymbol{\mu}}_0^n$
if $\sqrt{\|\underline{\boldsymbol{q}}_0\|^2 + \|\underline{\boldsymbol{r}}_0\|^2} \le TOL$ ***then***
  $\underline{\boldsymbol{c}}^n = \underline{\boldsymbol{c}}_0^n$
  $\underline{\boldsymbol{\mu}}^n = \underline{\boldsymbol{\mu}}_0^n$
  return
end if

// Newton iteration:
for $k = 1$ *to* $MaxIterations$ ***do***
  Solve*:*

$$\underline{\boldsymbol{A}}\underline{\boldsymbol{z}}_k + \Delta t\underline{\boldsymbol{M}}^n\underline{\boldsymbol{w}}_k = \underline{\boldsymbol{q}}_{k-1} \tag{4.20}$$

$$-\mathrm{D}_c\,\underline{\boldsymbol{G}}_\gamma(\underline{\boldsymbol{c}}_{k-1}^n,\underline{\boldsymbol{u}}^{n-1})\underline{\boldsymbol{z}}_k + \underline{\boldsymbol{A}}\underline{\boldsymbol{w}}_k = \underline{\boldsymbol{r}}_{k-1} \tag{4.21}$$

// Update:
$\underline{\boldsymbol{c}}_k^n = \underline{\boldsymbol{c}}_{k-1}^n + \underline{\boldsymbol{z}}_k$
$\underline{\boldsymbol{\mu}}_k^n = \underline{\boldsymbol{\mu}}_{k-1}^n + \underline{\boldsymbol{w}}_k$

// Compute residuum:
$\underline{\boldsymbol{q}}_k = \underline{\boldsymbol{A}}(\underline{\boldsymbol{c}}^{n-1} - \underline{\boldsymbol{c}}_k^n) - \Delta t \underline{\boldsymbol{M}}^n \underline{\boldsymbol{\mu}}_k^n$
$\underline{\boldsymbol{r}}_k = \underline{\boldsymbol{G}}_\gamma(\underline{\boldsymbol{c}}_k^n, \underline{\boldsymbol{u}}^{n-1}) - \underline{\boldsymbol{A}}\underline{\boldsymbol{\mu}}_k^n$

if $\sqrt{\|\underline{\boldsymbol{q}}_k\|^2 + \|\underline{\boldsymbol{r}}_k\|^2} / \sqrt{\|\underline{\boldsymbol{q}}_0\|^2 + \|\underline{\boldsymbol{r}}_0\|^2} \leq TOL$ ***then***
$\underline{\boldsymbol{c}}^n = \underline{\boldsymbol{c}}_k^n$
$\underline{\boldsymbol{\mu}}^n = \underline{\boldsymbol{\mu}}_k^n$
return
end if
end for

In order to apply this algorithm we have to ensure that the LES (4.20) and (4.21) in each Newton step has an unique solution.

Lemma 4.31. *Let $\Omega \subset \mathbb{R}^d$ be a domain satisfying condition (H-1). Furthermore, let the assumptions (A-1) - (A-8) be satisfied. Moreover let $\mathscr{T}_h(\Omega)$ be an admissible, exact and uniform triangulation of the reference domain Ω. If the time discretisation satisfies the following condition*

$$\Delta t \leq \min\left(\frac{c_\Gamma}{2(C_{\psi,cc}^-)^2 C_M}, \frac{h^d \gamma}{C_{W,cc}}\right),$$

then LES (4.20) *and* (4.21) *in the Newton method has a unique solution $\underline{\boldsymbol{z}}_k$ and $\underline{\boldsymbol{w}}_k$.*

Proof. We show the uniqueness of a solution by eliminating the first equation. The matrix $\underline{\boldsymbol{M}}^n$ corresponds to a discretisation of the operator $\mathcal{M}_h^n$, which is $X_0(\Omega)$-elliptic in view of corollary 4.5. Due to this fact $\underline{\boldsymbol{M}}^n$ is invertible and we deduce

$$\underline{\boldsymbol{w}}_k = -\frac{1}{\Delta t}(\underline{\boldsymbol{M}}^n)^{-1}\underline{\boldsymbol{A}}\underline{\boldsymbol{z}}_k + \frac{1}{\Delta t}(\underline{\boldsymbol{M}}^n)^{-1}\underline{\boldsymbol{q}}_{k-1}$$

By inserting this relation into the second equation, we get a LES for the update vector $\underline{\boldsymbol{z}}_k$

$$\left(\mathrm{D}_c\, \underline{\boldsymbol{G}}_\gamma(\underline{\boldsymbol{c}}_{k-1}^n, \underline{\boldsymbol{u}}^{n-1}) + \frac{1}{\Delta t}\underline{\boldsymbol{A}}(\underline{\boldsymbol{M}}^n)^{-1}\underline{\boldsymbol{A}}\right)\underline{\boldsymbol{z}}_k = \frac{1}{\Delta t}(\underline{\boldsymbol{M}}^n)^{-1}\underline{\boldsymbol{q}}_{k-1} - \underline{\boldsymbol{r}}_{k-1}$$

Finally, we have to show that the remaining LES has a unique solution. This is done by proving the statement, that the matrix $\mathrm{D}_c\, \underline{\boldsymbol{G}}_\gamma(\underline{\boldsymbol{c}}_{k-1}^n, \underline{\boldsymbol{u}}^{n-1}) + \frac{1}{\Delta t}\underline{\boldsymbol{A}}(\underline{\boldsymbol{M}}^n)^{-1}\underline{\boldsymbol{A}}$ is positive definite. In order to do this, we get for any coefficient vector $\underline{\boldsymbol{\xi}} \in \mathbb{R}^{\sharp\mathscr{N}_h(\Omega)}$

the following integral formulation

$$\begin{aligned}
&\left(\mathrm{D}_c \underline{\boldsymbol{G}}_\gamma(\underline{\boldsymbol{c}}_{k-1}^n, \underline{\boldsymbol{u}}^{n-1}) + \frac{1}{\Delta t}\underline{\boldsymbol{A}}(\underline{\boldsymbol{M}}^n)^{-1}\underline{\boldsymbol{A}}\right)\underline{\boldsymbol{\xi}}\cdot\underline{\boldsymbol{\xi}} \\
&= \int_\Omega \boldsymbol{\Gamma}\nabla_{\boldsymbol{x}}\xi_h\cdot\nabla_{\boldsymbol{x}}\xi_h + \psi_{,cc}(c_{k,h}^n)\xi_h^2 + W_{,cc}(c_{k,h}^n, \boldsymbol{\varepsilon}(\boldsymbol{u}_h^{n-1}))\xi_h^2\, d\boldsymbol{x} \\
&\qquad + \frac{\gamma}{\Delta t}\|\xi_h\|_{L_2(\Omega)}^2 + \frac{1}{\Delta t}\|\xi_h\|_{\mathcal{M}_h^n}^2.
\end{aligned}$$

The convex terms of this formulation are estimated below by using assumption (A-1) and the property $\psi_{,cc}^+ \geq 0$. We apply the assumptions (A-2) - (A-7) with Young's inequality (4.7) to the non-convex terms and choose $\delta = \frac{c_\Gamma}{2C_{\psi_{,cc}^-}}$. This leads to the following calculations

$$\begin{aligned}
&\int_\Omega \boldsymbol{\Gamma}\nabla_{\boldsymbol{x}}\xi_h\cdot\nabla_{\boldsymbol{x}}\xi_h + \psi_{,cc}(c_{k,h}^n)\xi_h^2 + W_{,cc}(c_{k,h}^n, \boldsymbol{\varepsilon}(\boldsymbol{u}_h^{n-1}))\xi_h^2\, d\boldsymbol{x} \\
&\quad + \frac{\gamma}{\Delta t}\|\xi_h\|_{L_2(\Omega)}^2 + \frac{1}{\Delta t}\|\xi_h\|_{\mathcal{M}_h^n}^2 \\
&\geq c_\Gamma|\xi_h|_{H^1(\Omega)}^2 - C_{\psi_{,cc}^-}\|\xi_h\|_{L_2(\Omega)}^2 - C(\|\boldsymbol{u}_h^{n-1}\|_{H^1(\Omega)}^2 + 1)\|\xi_h\|_{L_\infty(\Omega)}^2 \\
&\quad + \frac{\gamma}{\Delta t}\|\xi_h\|_{L_2(\Omega)}^2 + \frac{1}{\Delta t}\|\xi_h\|_{\mathcal{M}_h^n}^2 \\
&\geq c_\Gamma|\xi_h|_{H^1(\Omega)}^2 - C_{\psi_{,cc}^-}\delta|\xi|_{H^1(\Omega)}^2 - \frac{C_{\psi_{,cc}^-}C_M}{\delta}\|\xi_h\|_{L_2(\Omega)}^2 \\
&\quad - C_{W,cc}\frac{1}{h^2}\|\xi_h\|_{L_2(\Omega)}^2 + \frac{\gamma}{\Delta t}\|\xi_h\|_{L_2(\Omega)}^2 + \frac{1}{\Delta t}\|\xi_h\|_{\mathcal{M}_h^n}^2 \\
&\geq \frac{c_\Gamma}{2c_p}\|\xi_h\|_{H^1(\Omega)}^2.
\end{aligned}$$

This estimate shows that the remaining matrix $\mathrm{D}_c \underline{\boldsymbol{G}}_\gamma(\underline{\boldsymbol{c}}_{k-1}^n, \underline{\boldsymbol{u}}^{n-1}) + \frac{1}{\Delta t}\underline{\boldsymbol{A}}(\underline{\boldsymbol{M}}^n)^{-1}\underline{\boldsymbol{A}}$ is positive definite. The uniqueness of the update vector $\underline{\boldsymbol{w}}_k$ follows from the positive definiteness of the matrix $\underline{\boldsymbol{M}}^n$. □

Remark 4.32. The same constraint on the time discretisation leads to a unique solution of the approximation method as it is formulated in section 3.2.5. If the elasticity tensor is constant, then a unique solution of the LES in the Newton method is guaranteed under a weaker condition

$$\Delta t \leq \min\left(\frac{c_\Gamma}{2(C_{\psi_{,cc}^-})^2 C_M}, \frac{h^{\frac{d}{2}}\gamma}{C_{W,cc}}\right).$$

Within the numerical simulation the LES is solved iteratively. We use either the BiCGStab method derived in [98] or the GMRes algorithm explained in [87] in order to determine the unique solution of the LES. For both methods it is proved that

they find a solution of a positive definite but non-symmetric LES. We observed no significant difference between both methods throughout our computations.

Precondition for a LES of this type is indeed a difficult problem. We apply for $\underline{\boldsymbol{z}}_k$ and $\underline{\boldsymbol{w}}_k$ a BPX precondition, see [17]. This technique works quite well, but it is not clear if it is the right choice.

4.2 Stabilisation by driving forces

In section 4.1 we analysed a Faedo-Galerkin method for the viscous Cahn-Larché system (1.51) - (1.53). The main idea in the previous section was to use the dynamic friction $\gamma\dot{c}$ in order to get a stabilised numerical approximation method for the non-viscous Cahn-Larché system. In section 4.2 we extend the idea of stabilising by friction. Here, friction is not observed by the dynamic term $\gamma\dot{c}$. Instead by using the flow gradient structure friction is introduced in terms of driving forces $-\gamma \boldsymbol{M}\nabla_{\boldsymbol{x}}\mu$. The observation of this new method is mainly motivated by the intention of getting a method, which has a better condition than the method of the previous section.

This section is organised as follows: First we formulate the new approximation method with friction in terms of driving forces and make some remarks to the pre-processing procedure, which differs from the previous method.

By eliminating the discrete diffusion equation taking into account the operator $\mathcal{M}_h^n$, we show that both approximation methods are equal, since they are reduced to the same auxiliary problem 4.8. Due to this fact existence, uniqueness and a-priori estimates of the solution follow directly from the previous section.

It remains to show the convergence of the discrete solution to a solution of the non-viscous Cahn-Larché system, if Δt, h and γ go to zero. The section ends with the analysis of the Newton method corresponding to the method stabilised by driving forces.

4.2.1 Numerical approximation method

Problem 4.33. For all discrete time steps $t = n\Delta t$ with $1 \leq n \leq N$ we have to find $c_h^n \in X_h(\Omega)$, $\mu_h^n \in X_h(\Omega)$ and $\boldsymbol{u}_h^n \in \boldsymbol{X}_h(\Omega)$, such that for the stabilised numerical scheme holds

$$\int_\Omega \partial_{\Delta t} c_h^n \zeta_h \, d\boldsymbol{x} + \int_\Omega \boldsymbol{M}_h^{n-1} \nabla_{\boldsymbol{x}} \mu_h^n \cdot \nabla_{\boldsymbol{x}} \zeta_h \, d\boldsymbol{x} = 0 \qquad \forall \zeta_h \in X_h(\Omega), \quad (4.22)$$

$$\begin{aligned} &\int_\Omega \mu_h^n \xi_h \, d\boldsymbol{x} + \gamma \int_\Omega \boldsymbol{M}_h^{n-1} \nabla_{\boldsymbol{x}} \mu_h^n \cdot \nabla_{\boldsymbol{x}} \xi_h \, d\boldsymbol{x} \\ &= \int_\Omega \boldsymbol{\Gamma} \nabla_{\boldsymbol{x}} c_h^n \cdot \nabla_{\boldsymbol{x}} \xi_h + \psi_{,c}(c_h^n)\xi_h + W_{,c}(c_h^n, \boldsymbol{\varepsilon}(\boldsymbol{u}_h^{n-1}))\xi_h \qquad \forall \xi_h \in X_h(\Omega), \quad (4.23) \end{aligned}$$

$$\int_\Omega \boldsymbol{C}(c_h^n)\boldsymbol{\varepsilon}(\boldsymbol{u}_h^n) : \boldsymbol{\varepsilon}(\boldsymbol{\eta}_h) \, d\boldsymbol{x} = \int_\Omega \boldsymbol{C}(c_h^n)\overline{\boldsymbol{\varepsilon}}(c_h^n) : \boldsymbol{\varepsilon}(\boldsymbol{\eta}_h) \, d\boldsymbol{x} + \int_{\Gamma_N} \boldsymbol{g}^n \cdot \boldsymbol{\eta}_h \, d\boldsymbol{a}_{\boldsymbol{x}}$$
$$\forall \boldsymbol{\eta}_h \in \boldsymbol{X}_h(\Omega). \quad (4.24)$$

We get this numerical scheme by inserting the discrete functions c_h^n, μ_h^n and $\boldsymbol{u}_h^n$ into the definition of a non-viscous semi-weak solution of the Cahn-Larché system and adding the stabilisation term $\gamma \int_\Omega \boldsymbol{M}_h^{n-1} \nabla_{\boldsymbol{x}} \mu_h^n \cdot \nabla_{\boldsymbol{x}} \xi_h \, d\boldsymbol{x}$. We remark that all integrals in problem 4.33 exist due to the assumptions (A-1) - (A-8) and the fact that the discrete test functions are almost everywhere bounded.

Due to the fact that we use $\boldsymbol{u}_h^{n-1}$ in the equation of the chemical potential (4.23), diffusion and elasticity are decoupled. Obviously for any $c_h^n \in X_h(\Omega)$ there exists a unique solution $\boldsymbol{u}_h^n \in \boldsymbol{X}_h(\Omega)$ satisfying the uniform a-priori estimate (2.8).

Since the Cahn-Larché system is a time dependent problem we have to calculate some tasks in advance. In order to apply the numerical approximation method given by problem 4.33 we first have to project the initial data c_0 on the trial space $X_h(\Omega)$. This is done similarly as in section 3.2.1 by using the $L_2(\Omega)$-projection introduced by definition 3.10.

Obviously this projection satisfies various estimates in different norms proved in lemma 3.13 and the convergence is investigated in lemma 3.12. We remember that the $L_2(\Omega)$-projection is mass conserving, see lemma 3.11, which means $c_h^0 \in X_{m,h}(\Omega)$. Due to this fact and by observing the discrete diffusion equation (4.22), corollary 4.2 also holds for the discrete solution of problem 4.33. This means that stabilisation by driving forces also conserves the mass and we have $c_h^n \in X_{m,h}(\Omega)$.

The second initial task is the computation of an initial displacement $\boldsymbol{u}_h^0 \in \boldsymbol{X}_h(\Omega)$. This is done analogously as in problem 3.14. The existence, stability and convergence of the initial displacement $\boldsymbol{u}_h^0 \in \boldsymbol{X}(\Omega)$ are still valid as formulated in lemma 3.15 and lemma 3.20.

The only difference to the previous approximation method is the computation of an initial chemical potential.

Problem 4.34. Find $\mu_h^0 \in X_h(\Omega)$ such that holds

$$\begin{aligned}\int_\Omega \mu_h^0 \xi_h \, d\boldsymbol{x} + \gamma \int_\Omega \boldsymbol{M}(c_h^0) \nabla_{\boldsymbol{x}} \mu_h^0 \cdot \nabla_{\boldsymbol{x}} \xi_h \, d\boldsymbol{x} \\ = \int_\Omega \boldsymbol{\Gamma} \nabla_{\boldsymbol{x}} c_h^0 \cdot \nabla_{\boldsymbol{x}} \xi_h + \psi_{,c}(c_h^0) \xi_h + W_{,c}(c_h^0, \boldsymbol{\varepsilon}(\boldsymbol{u}_h^0)) \xi_h \qquad \forall \xi_h \in X_h(\Omega).\end{aligned}$$

We remark that in this problem μ_h^0 is unknown, whereas $c_h^0 \in X_{m,h}(\Omega)$ and $\boldsymbol{u}_h^0 \in \boldsymbol{X}(\Omega)$ are known from the previous computations in the initial procedure.

Problem 4.34 corresponds to a LES, which is given in the following form

$$\underline{\boldsymbol{H}}_\gamma \underline{\boldsymbol{\mu}}^0 = \underline{\boldsymbol{f}}, \tag{4.25}$$

$$\underline{\boldsymbol{H}}_\gamma[\boldsymbol{z}, \boldsymbol{y}] := \int_\Omega \varphi_{\boldsymbol{y}} \varphi_{\boldsymbol{z}} + \gamma \boldsymbol{M}(c_h^0) \nabla_{\boldsymbol{x}} \varphi_{\boldsymbol{y}} \cdot \nabla_{\boldsymbol{x}} \varphi_{\boldsymbol{z}} \, d\boldsymbol{x},$$

$$\underline{\boldsymbol{f}}[\boldsymbol{z}] := \int_\Omega \boldsymbol{\Gamma} \nabla_{\boldsymbol{x}} c_h^0 \cdot \nabla_{\boldsymbol{x}} \varphi_{\boldsymbol{z}} + \psi_{,c}(c_h^0) \varphi_{\boldsymbol{z}} + W_{,c}(c_h^0, \boldsymbol{\varepsilon}(\boldsymbol{u}_h^0)) \varphi_{\boldsymbol{z}} \, d\boldsymbol{x}.$$

The matrix $\underline{\boldsymbol{H}}_\gamma$ is symmetric and positive definite due to the properties of the mobility tensor formulated in assumption (A-3). We compute the matrix $\underline{\boldsymbol{H}}_\gamma$ and the vector $\underline{\boldsymbol{f}}$ by using a quadrature formula. On a triangle $\tau \in \mathscr{T}_h(\Omega)$ Radon's seven point formula from [86] is applied.

Since the matrix $\underline{\boldsymbol{H}}_\gamma$ is symmetric and positive definite the LES (4.25) is solved iteratively by the preconditioned CG method taken from [58]. In order to take care about the stabilisation parameter γ we employ a scaled BPX preconditioner.

4.2.2 Equivalence of the methods

In this section we have to show that problem 4.33 has a solution $c_h^n \in X_h(\Omega)$ and $\mu_h^n \in X_h(\Omega)$ for any time step $1 \leq n \leq N$. The existence of a corresponding displacement $\boldsymbol{u}_h^n \in \boldsymbol{X}_h(\Omega)$ is obvious due to the decoupling of diffusion and strain by taking into account the calculations and results of section 3.1.

In order to show the existence of a concentration field $c_h^n \in X_h(\Omega)$ and of a chemical potential $\mu_h^n \in X_h(\Omega)$, we show that problem 4.1 and problem 4.33 are equivalent. Therefore we reformulate the problem by eliminating the diffusion equation (4.22). This is done by calculating a relation between diffusion and dissipation, which uses the flow gradient structure of the problem.

From definition 4.4 we take the operator $\mathcal{M}_h^n : X_0(\Omega) \longrightarrow Y_0(\Omega)$, which is in view of corollary 4.5 a linear, $X_0(\Omega)$-elliptic and bounded operator. By applying the Lax-Milgram theorem the inverse operator $(\mathcal{M}_h^n)^{-1} : Y_0(\Omega) \longrightarrow X_0(\Omega)$ exists. In order to eliminate the discrete diffusion equation (4.22) we apply the inverse operator $(\mathcal{M}_h^n)^{-1}$ to the diffusion equation and deduce analogous to (4.6) the following representation of the chemical potential

$$\mu_h^n = -(\mathcal{M}_h^n)^{-1}\partial_{\Delta t} c_h^n + \lambda_h^n.$$

Note, that we have to choose the Lagrangian multiplier by $\lambda_h^n \in \ker(\mathcal{M}_h^n) = \mathbb{R}$.

Furthermore we insert this representation of the chemical potential into (4.23) and calculate for the left hand side

$$\begin{aligned}
&\int_\Omega \mu_h^n \xi_h \, d\boldsymbol{x} + \gamma \int_\Omega \boldsymbol{M}_h^n \nabla_{\boldsymbol{x}} \mu_h^n \cdot \nabla_{\boldsymbol{x}} \xi_h \, d\boldsymbol{x} && (4.26)\\
&\quad = -\int_\Omega (\mathcal{M}_h^n)^{-1} \partial_{\Delta t} c_h^n \xi_h \, d\boldsymbol{x} - \gamma \int_\Omega \partial_{\Delta t} c_h^n \xi_h && (4.27)\\
&\quad = -\int_\Omega (\mathcal{M}_h^n)^{-1} \mathcal{M}_h (\mathcal{M}_h^n)^{-1} \partial_{\Delta t} c_h^n \xi_h \, d\boldsymbol{x} - \gamma \int_\Omega \partial_{\Delta t} c_h^n \xi_h \, d\boldsymbol{x} && (4.28)\\
&\quad = -\int_\Omega \mathcal{M}_h (\mathcal{M}_h^n)^{-1} \partial_{\Delta t} c_h^n (\mathcal{M}_h^n)^{-1} \xi_h \, d\boldsymbol{x} - \gamma \int_\Omega \partial_{\Delta t} c_h^n \xi_h \, d\boldsymbol{x} && (4.29)\\
&\quad = -\langle \partial_{\Delta t} c_h^n, \xi_h \rangle_{\mathcal{M}_h} - \gamma \langle \partial_{\Delta t} c_h^n, \xi_h \rangle_{L_2(\Omega)}. && (4.30)
\end{aligned}$$

By using this calculation we restrict problem 4.33 from three equations to a system of two equations for the unknown concentration field $c_h^n \in X_h(\Omega)$ and the unknown displacement $\boldsymbol{u}_h^n \in \boldsymbol{X}_h(\Omega)$.

Problem 4.35. Find for each discrete time $t = n\Delta t$ for $1 \leq n \leq N$ a function $c_h^n \in X_{0,h}(\Omega)$ and $\boldsymbol{u}_h^n \in \boldsymbol{X}_h(\Omega)$ such that holds

$$\int_\Omega \boldsymbol{\Gamma}\nabla_{\boldsymbol{x}} c_h^n \cdot \nabla_{\boldsymbol{x}}\xi_h + \psi_{,c}(c_h^n)\xi_h + W_{,c}(c_h^n, \boldsymbol{\varepsilon}(\boldsymbol{u}_h^{n-1}))\xi_h + \gamma\partial_{\Delta t} c_h^n \xi_h \, d\boldsymbol{x} + \langle \partial_{\Delta t} c_h^n, \xi_h\rangle_{\mathcal{M}_h^n} = 0 \qquad \forall \xi_h \in X_h(\Omega),$$

$$\int_\Omega \boldsymbol{C}(c_h^n)\boldsymbol{\varepsilon}(\boldsymbol{u}_h^n) : \boldsymbol{\varepsilon}(\boldsymbol{\eta}_h) \, d\boldsymbol{x} = \int_\Omega \boldsymbol{C}(c_h^n)\overline{\boldsymbol{\varepsilon}}(c_h^n) : \boldsymbol{\varepsilon}(\boldsymbol{\eta}_h) \, d\boldsymbol{x} + \int_{\Gamma_N} \boldsymbol{g}^n \cdot \boldsymbol{\eta}_h \, d\boldsymbol{a}_{\boldsymbol{x}} \qquad \forall \boldsymbol{\eta}_h \in \boldsymbol{X}_h(\Omega).$$

Obviously problem 4.35 and problem 4.8 are the same and due to this fact both approximation methods lead to the same discrete solution $c_h^n \in X_h(\Omega)$ and $\boldsymbol{u}_h^n \in \boldsymbol{X}_h(\Omega)$. Keeping in mind that the discretisation method decouples diffusion and elasticity, we have to formulate two corresponding energy functionals. A configurational energy $E_{h,config}^n$ relating to the diffusion and a strain energy $E_{h,mech}^n$ related to the mechanical equilibrium:

$$\begin{aligned} E_{h,config}^n(d_h) &:= \int_\Omega \frac{1}{2}\boldsymbol{\Gamma}\nabla_{\boldsymbol{x}} d_h \cdot \nabla_{\boldsymbol{x}} d_h + \psi(d_h) + W(d_h, \boldsymbol{\varepsilon}(\boldsymbol{u}_h^{n-1})) \, d\boldsymbol{x} \\ &\quad + \frac{1}{2\Delta t}\|d_h - c_h^{n-1}\|_{\mathcal{M}_h^n}^2 + \frac{\gamma}{2\Delta t}\|d_h - c_h^{n-1}\|_{L_2(\Omega)}^2, \\ E_{h,mech}^n(\boldsymbol{v}_h) &:= \int_\Omega W(c_h^n, \boldsymbol{\varepsilon}(\boldsymbol{v}_h)) \, d\boldsymbol{x} - \int_{\Gamma_N} \boldsymbol{g}^n \cdot \boldsymbol{v}_h. \end{aligned}$$

Obviously, these energy functionals are equivalent to the configurational energy function and to the strain energy functional of the previous section.

Lemma 4.36 (Existence). *Let $\Omega \subset \mathbb{R}^d$ be a domain satisfying condition (H-1). Furthermore, let the assumptions (A-1) - (A-8) be satisfied. The triangulation $\mathscr{T}_h(\Omega)$ is assumed to be admissible, exact and uniform. Then in every time step $1 \leq n \leq N$ there exists at least one discrete solution $c_h^n \in X_{m,h}(\Omega)$, $\mu_h^n \in X_h(\Omega)$ and $\boldsymbol{u}_h^n \in \boldsymbol{X}_h(\Omega)$ of problem 4.33. If the time discretisation additionally satisfies the constraint*

$$\Delta t \leq \min\left(\frac{c_\Gamma}{2(C_{\psi,cc}^-)^2 C_M}, \frac{h^d\gamma}{C_{W,cc}}\right),$$

then the discrete solution is unique.

Proof. The existence proof of a solution of the approximation method stabilised by driving forces is the same as in section 3.2.3, because the reformulated problems of problem 4.1 and problem 4.33 are the same. In fact, the existence of a discrete concentration field follows by minimising the configurational energy $E^n_{h,config}$, see lemma 4.9. The existence of a discrete displacement $\boldsymbol{u}^n_h$ is a direct conclusion from lemma 2.14 and we remember, that $\boldsymbol{u}^n_h$ provides a minimiser of the strain energy $E^n_{h,mech}$. The derivation of the Gâteaux derivative, lemma 4.10 and the calculation in (4.30) lead to the existence of a solution. The uniqueness follows from lemma 4.11, because there we prove the uniqueness of the solution of the reformulated problem. □

Lemma 4.37 (A-priori estimates). *Let $\Omega \subset \mathbb{R}^d$ be a domain satisfying condition (H-1). Furthermore let the assumptions (A-1) - (A-8) be satisfied. $\mathscr{T}_h(\Omega)$ is assumed to be an admissible, exact and locally quasi-uniform mesh satisfying condition* (3.5)*. Then for the discrete weak solution $c_{\Delta t,h,\gamma}$, $\bar{c}_{\Delta t,h,\gamma}$, $\mu_{\Delta t,h,\gamma}$ and $\boldsymbol{u}_{\Delta t,h,\gamma}$ there exist constants C_c, $C_{\bar{c}}$, C_μ, $C_{\boldsymbol{u}}$ and $C_{\dot{\bar{c}}} > 0$ depending on the material parameters, the boundary loading g, the initial condition c_0, time T and* meas(Ω)*, such that the following uniform a-priori estimates hold*

(1) $\|\boldsymbol{u}_{\Delta t,h,\gamma}\|_{L_\infty(0,T;\boldsymbol{H}^1(\Omega))} \leq C_{\boldsymbol{u}}$,

(2) $\|c_{\Delta t,h,\gamma}\|_{L_\infty(0,T;H^1(\Omega))} \leq C_c$,

(3) $\|\bar{c}_{\Delta t,h\gamma}\|_{L_\infty(0,T;H^1(\Omega))} \leq C_{\bar{c}}$,

(4) $\sup\limits_{t\in[0,T]} \int_\Omega \psi(c_{\Delta t,h,\gamma})\, d\boldsymbol{x} \leq C_\psi$,

(5) $\|\mu_{\Delta t,h,\gamma}\|_{L_2(0,T;H^1(\Omega))} \leq C_\mu$,

(6) $\|\dot{\bar{c}}_{\Delta t,h,\gamma}\|_{L_2(\Omega_T)} \leq C_{\bar{c}'}$, *if* $\gamma \gneqq 0$.

Proof. Since we have to minimise the same energy functional $E^n_{h,config}$, the Lyapunov property formulated in lemma 4.14 holds for the approximation method stabilised by driving forces. Moreover the upper bound of the initial energy in lemma 4.15 and the lower bound of the energy in lemma 4.16 are also satisfied for the discrete solution of problem 4.33 and by arguing similarly to lemma 4.17 the a-priori estimates follow. □

Lemma 4.38 (Convergence of the method). *Let $\Omega \subset \mathbb{R}^d$ be a domain satisfying condition (H-1). Moreover, the triangulation $\mathscr{T}_h(\Omega)$ is assumed to be exact, admissible, locally quasi-uniform and satisfies the shape regularity condition. Let the assumptions (A-1) - (A-8) be satisfied, then $c_{\Delta t,h,\gamma}$, $\mu_{\Delta t,h,\gamma}$ and $\boldsymbol{u}_{\Delta t,h,\gamma}$ converge to a weak solution of the non-viscous Cahn-Larché system.*

Proof. We remark, that the convergence results for the concentration formulated in lemma 4.18 also hold for the concentration computed by problem 4.33 and the same result is valid for the displacement. The convergence follows by the same arguments

as in theorem 4.29 except the stabilisation term. We calculate by using Hölder's inequality

$$\gamma \left| \int_{\Omega_T} \boldsymbol{M}(c_{\Delta t,h,\gamma}(t-\Delta t,\cdot))\nabla_{\boldsymbol{x}}\mu_{\Delta t,h,\gamma} \cdot \nabla_{\boldsymbol{x}}\mathcal{R}_h\xi \; d\boldsymbol{x}dt \right| \\ \leq \gamma C_M \|\mu_{\Delta t,h,\gamma}\|_{L_2(0,T;H^1(\Omega))} \|\xi\|_{L_2(0,T;H^1(\Omega))}$$

Since the chemical potential is uniformly bounded and the Clement operator is bounded in $L_2(0,T;H^1(\Omega))$ the stabilisation term vanishes if the friction coefficient γ goes to zero. □

4.2.3 Numerical solution of the Euler-Lagrange equations

The approximation method stabilised by driving forces leads to a non-linear equation system, which must be solved in every time step $t_n = n\Delta t$ with $1 \leq n \leq N$. This non-linear equation system results from (4.22) - (4.23) and it is given in the form

$$\underline{\boldsymbol{A}}(\underline{\boldsymbol{c}}^n - \underline{\boldsymbol{c}}^{n-1}) + \Delta t \underline{\boldsymbol{M}}^n \underline{\boldsymbol{\mu}}^n = \underline{\boldsymbol{0}}, \tag{4.31}$$

$$-\underline{\boldsymbol{G}}(c^n, \boldsymbol{u}^{n-1}) + \underline{\boldsymbol{H}}_\gamma \underline{\boldsymbol{\mu}}^n = \underline{\boldsymbol{0}}. \tag{4.32}$$

The unknown quantities are $\underline{\boldsymbol{c}}^n$ and $\underline{\boldsymbol{\mu}}^n$, whereas $\underline{\boldsymbol{c}}^{n-1}$ and $\underline{\boldsymbol{u}}^{n-1}$ are known from the previous time step. We remark that the equation system (4.31) and (4.32) differs slightly from the system (4.18) and (4.19). The matrices $\underline{\boldsymbol{A}}$, $\underline{\boldsymbol{M}}^n$ and $\underline{\boldsymbol{H}}_\gamma$ as well as the vector valued function $\underline{\boldsymbol{G}}(\underline{\boldsymbol{c}}^n, \underline{\boldsymbol{u}}^{n-1})$ are calculated by the following formulas

$$\begin{aligned}
\underline{\boldsymbol{A}}[\boldsymbol{y},\boldsymbol{z}] &:= \int_\Omega \varphi_{\boldsymbol{y}}\varphi_{\boldsymbol{z}} \; d\boldsymbol{x}, \\
\underline{\boldsymbol{M}}^n[\boldsymbol{y},\boldsymbol{z}] &:= \int_\Omega \boldsymbol{M}(c_h^{n-1})\nabla_{\boldsymbol{x}}\varphi_{\boldsymbol{y}} \cdot \nabla_{\boldsymbol{x}}\varphi_{\boldsymbol{z}} \; d\boldsymbol{x}, \\
\underline{\boldsymbol{G}}(\underline{\boldsymbol{c}}^n, \underline{\boldsymbol{u}}^{n-1})[\boldsymbol{z}] &:= \int_\Omega \boldsymbol{\Gamma}\nabla_{\boldsymbol{x}}c_h^n \cdot \nabla_{\boldsymbol{x}}\varphi_{\boldsymbol{z}} + \psi_{,c}(c_h^n)\varphi_{\boldsymbol{z}} + W_{,c}(c_h^n, \boldsymbol{\varepsilon}(\boldsymbol{u}_h^{n-1}))\varphi_{\boldsymbol{z}} \; d\boldsymbol{x}, \\
\underline{\boldsymbol{H}}_\gamma[\boldsymbol{y},\boldsymbol{z}] &:= \int_\Omega \varphi_{\boldsymbol{y}}\varphi_{\boldsymbol{z}} \; d\boldsymbol{x} + \gamma \int_\Omega \boldsymbol{M}(c_h^{n-1})\nabla_{\boldsymbol{x}}\varphi_{\boldsymbol{y}} \cdot \nabla_{\boldsymbol{x}}\varphi_{\boldsymbol{z}} \; d\boldsymbol{x}.
\end{aligned}$$

Obviously all integrals exist in this equation system due to the assumptions (A-1) - (A-8) and the non-linearity appears only in the vector valued function $\underline{\boldsymbol{G}}$ in the concentration field $\underline{\boldsymbol{c}}^n$. We apply Newton's method, see [88], in order to compute a solution of the equation system (4.31) and (4.32), which is different from the Newton method presented in algorithm 4.30.

Algorithm 4.39 (Newton method).

// Initial vectors:
$\underline{\boldsymbol{c}}_0^n = \underline{\boldsymbol{c}}^{n-1}$
$\underline{\boldsymbol{\mu}}_0^n = \underline{\boldsymbol{\mu}}^{n-1}$

// Initial residuum:
$\underline{\boldsymbol{q}}_0 = -\Delta t \underline{\boldsymbol{M}}^n \underline{\boldsymbol{\mu}}_0^n$
$\underline{\boldsymbol{r}}_0 = \underline{\boldsymbol{G}}(\underline{\boldsymbol{c}}_0^n, \underline{\boldsymbol{u}}^{n-1}) - \underline{\boldsymbol{H}}_\gamma \underline{\boldsymbol{\mu}}_0^n$
if $\sqrt{\|\underline{\boldsymbol{q}}_0\|^2 + \|\underline{\boldsymbol{r}}_0\|^2} \leq TOL$ ***then***
$\underline{\boldsymbol{c}}^n = \underline{\boldsymbol{c}}_0^n$
$\underline{\boldsymbol{\mu}}^n = \underline{\boldsymbol{\mu}}_0^n$
return
end if

// Newton iteration:
for $k = 1$ *to* $MaxIterations$ ***do***
Solve*:*

$$\underline{\boldsymbol{A}}\underline{\boldsymbol{z}}_k + \Delta t \underline{\boldsymbol{M}}^n \underline{\boldsymbol{w}}_k = \underline{\boldsymbol{q}}_{k-1} \tag{4.33}$$

$$-\mathrm{D}_c \underline{\boldsymbol{G}}(\underline{\boldsymbol{c}}_{k-1}^n, \underline{\boldsymbol{u}}^{n-1})\underline{\boldsymbol{z}}_k + \underline{\boldsymbol{H}}_\gamma \underline{\boldsymbol{w}}_k = \underline{\boldsymbol{r}}_{k-1} \tag{4.34}$$

// Update:
$\underline{\boldsymbol{c}}_k^n = \underline{\boldsymbol{c}}_{k-1}^n + \underline{\boldsymbol{z}}_k$
$\underline{\boldsymbol{\mu}}_k^n = \underline{\boldsymbol{\mu}}_{k-1}^n + \underline{\boldsymbol{w}}_k$

// Compute residuum:
$\underline{\boldsymbol{q}}_k = \underline{\boldsymbol{A}}(\underline{\boldsymbol{c}}^{n-1} - \underline{\boldsymbol{c}}_k^n) - \Delta t \underline{\boldsymbol{M}}^n \underline{\boldsymbol{\mu}}_k^n$
$\underline{\boldsymbol{r}}_k = \underline{\boldsymbol{G}}(\underline{\boldsymbol{c}}_k^n, \underline{\boldsymbol{u}}^{n-1}) - \underline{\boldsymbol{H}}_\gamma \underline{\boldsymbol{\mu}}_k^n$

if $\sqrt{\|\underline{\boldsymbol{q}}_k\|^2 + \|\underline{\boldsymbol{r}}_k\|^2} / \sqrt{\|\underline{\boldsymbol{q}}_0\|^2 + \|\underline{\boldsymbol{r}}_0\|^2} \leq TOL$ ***then***
$\underline{\boldsymbol{c}}^n = \underline{\boldsymbol{c}}_k^n$
$\underline{\boldsymbol{\mu}}^n = \underline{\boldsymbol{\mu}}_k^n$
return
end if
end for

In the Newton algorithm 4.39 we have to solve a different LES than in algorithm 4.30, although both algorithms lead to the same solution. Nevertheless we have to analyse the existence of a solution $\underline{\boldsymbol{z}}_k$ and $\underline{\boldsymbol{w}}_k$.

Lemma 4.40. *Let $\Omega \subset \mathbb{R}^d$ be a domain satisfying condition (H-1). Furthermore, let the assumptions (A-1) - (A-8) be satisfied. Moreover, let $\mathscr{T}_h(\Omega)$ be an admissible, exact and uniform triangulation of the reference domain Ω. If the time discretisation satisfies the following condition*

$$\Delta t \leq \min\left(\frac{c_\Gamma}{2(C_{\psi,cc}^-)^2 C_M}, \frac{h^d \gamma}{C_{W,cc}}\right),$$

then LES (4.33) *and* (4.34) *in the Newton method has a unique solution $\underline{\boldsymbol{z}}_k$ and $\underline{\boldsymbol{w}}_k$.*

Proof. We eliminate the first equation, since $\underline{\boldsymbol{M}}^n$ is invertible due to the fact that the operator $\mathcal{M}_h^n$ is $X_0(\Omega)$-elliptic, see lemma 4.5. We get for the update vector $\underline{\boldsymbol{w}}_k$ the representation

$$\underline{\boldsymbol{w}}_k = -\frac{1}{\Delta t}(\underline{\boldsymbol{M}}^n)^{-1}\underline{\boldsymbol{A}}\underline{\boldsymbol{z}}_k + \frac{1}{\Delta t}(\underline{\boldsymbol{M}}^n)^{-1}\underline{\boldsymbol{q}}_{k-1}.$$

By inserting this representation of $\underline{\boldsymbol{w}}_k$ into the second equation we get a LES for the update vector $\underline{\boldsymbol{z}}_k$.

$$\left(\mathrm{D}_c\,\underline{\boldsymbol{G}}(\underline{\boldsymbol{c}}_{k-1}^n, \underline{\boldsymbol{u}}^{n-1}) + \frac{1}{\Delta t}\underline{\boldsymbol{H}}_\gamma(\underline{\boldsymbol{M}}^n)^{-1}\underline{\boldsymbol{A}}\right)\underline{\boldsymbol{z}}_k = \frac{1}{\Delta t}(\underline{\boldsymbol{M}}^n)^{-1}\underline{\boldsymbol{q}}_{k-1} - \underline{\boldsymbol{r}}_{k-1}$$

For any coefficient vector $\underline{\boldsymbol{\xi}} \in \mathbb{R}^{\sharp\mathscr{N}_h(\Omega)}$ we get the following integral formulation taking into account (4.30)

$$\begin{aligned}
&\left(\mathrm{D}_c\,\underline{\boldsymbol{G}}(\underline{\boldsymbol{c}}_{k-1}^n, \underline{\boldsymbol{u}}^{n-1}) + \frac{1}{\Delta t}\underline{\boldsymbol{H}}_\gamma(\underline{\boldsymbol{M}}^n)^{-1}\underline{\boldsymbol{A}}\right)\underline{\boldsymbol{\xi}}\cdot\underline{\boldsymbol{\xi}} \\
&= \int_\Omega \boldsymbol{\Gamma}\nabla_{\boldsymbol{x}}\xi_h\cdot\nabla_{\boldsymbol{x}}\xi_h + \psi_{,cc}(c_{k,h}^n)\xi_h^2 + W_{,cc}(c_{k,h}^n, \boldsymbol{\varepsilon}(\boldsymbol{u}_h^{n-1}))\xi_h^2\,d\boldsymbol{x} \\
&\qquad + \frac{\gamma}{\Delta t}\|\xi_h\|_{L_2(\Omega)}^2 + \frac{1}{\Delta t}\|\xi_h\|_{\mathcal{M}_h^n}^2.
\end{aligned}$$

The positive definiteness of the matrix $(\mathrm{D}_c\,\underline{\boldsymbol{G}}(\underline{\boldsymbol{c}}_{k-1}^n, \underline{\boldsymbol{u}}^{n-1}) + \frac{1}{\Delta t}\underline{\boldsymbol{H}}_\gamma\underline{\boldsymbol{M}}^{-1,n}\underline{\boldsymbol{A}})$ follows by the same arguments as in lemma 4.31. □

Remark 4.41. We have to point out that the constraint on the time discretisation in order to get a unique solution of the LES in the Newton algorithm 4.39 is the same as in algorithm 4.30. It is not surprising that for a constant elasticity tensor, a weaker constraint on the time discretisation ensures the unique solvability of the LES in the Newton method,

$$\Delta t \leq \min\left(\frac{c_\Gamma}{2(C_{\psi,cc}^-)^2 C_M}, \frac{h^{\frac{d}{2}}\gamma}{C_{W,cc}}\right).$$

In the numerical simulation the LES (4.33) and (4.34) is solved iteratively either by the BiCGStab method outlined in [98] or the GMRes method taken from [87]. Both methods work quite well for the LES (4.33) and (4.34) and we observe no important differences.

The LES is preconditioned by the BPX method, see [17], which improves the iterative process essentially. Indeed, we observe that the Newton method based on stabilisation with driving forces has a better condition number than the stabilisation by dynamic friction.

Chapter 5

Faedo-Galerkin method with operator-splitting

In the previous chapter we discussed different numerical approximation methods for the viscous Cahn-Larché system. The viscous methods are used in order to get a stabilised approximation scheme for the non-viscous Cahn-Larché system. The smoothness of a solution of the viscous Cahn-Larché equations (2.38) avoids high frequent contributions to the concentration field along phase interfaces and therefore Gibbs phenomena is not observed for this numerical approximation method.

For both Faedo-Galerkin methods stabilised by friction the convergence to a solution of the non-viscous Cahn-Larché system was proved, if the time discretisation Δt, the mesh size h and the friction coefficient γ go to zero. We remark that the convergence was proved in a weak respectively weak-$\star$ sense only.

Unfortunately, we have no classical error estimates for these methods. Therefore it is not clear how large the error is between a discrete solution and a solution of the non-viscous system for a finite time step Δt, a finite mesh size h and a finite friction coefficient γ, used in the computations. Moreover, there is no estimate showing how the rate of coarsening is slowed down due to the artificial friction.

These observations lead to the necessity to develop a stable Faedo-Galerkin method for the non-viscous Cahn-Larché system. Weikard proposed in [102] an operator splitting method for the Cahn-Larché system, which originally was developed for the Navier-Stokes equations in [78]. The numerical analysis of this operator splitting applied to the Cahn-Larché system is still an open problem, but it seems to be the most efficient method remarked in [50, 102].

Operator splitting is a standard technique for the stabilisation of numerical methods. Elliot and Stuart analyse an operator splitting method for semilinear parabolic equations in [41], where the nonlinearity is decomposed into a convex and a concave part. The convex part, which corresponds to the stable state, is discretised implicitly,

in contrast to the concave part, which describes the unstable state and it is treated explicitly. Barrett and Blowey applied in [9, 10] this technique to the Cahn-Hilliard equation by decomposing the Gibbs free energy density. A similar approach for the thin film equation is considered by Rumpf and Grün in [54].

In the fifth chapter of this work a new numerical approximation method for the non-viscous Cahn-Larché system is proposed using the above mentioned splitting ideas. First of all we decouple diffusion and elasticity again, a technique, which can also be understood as an operator splitting. Furthermore the Gibbs free energy density is decomposed into a convex part ψ^+ and a concave part ψ^-. The convex part ψ^+ is discretised implicitly, since it corresponds to the stable state of the system. In contrast the concave part ψ^- is treated explicitly and therefore it describes a volume force driving the spinodal decomposition.

This chapter is organised as follows: We start with a physical motivation of the splitting of the Gibbs free energy density into a convex and a concave part. Although in (A-2) we have assumed the existence of a decomposition of the Gibbs free energy density into a convex and a concave part, such a decomposition must be constructed in general. We outline a technique for doing this and demonstrate the result for the spline interpolation (1.71). By eliminating the discrete diffusion equation and using the flow gradient structure we determine a discrete solution by minimising the energy and maximising the dissipation. Uniqueness of the discrete solution is also proved by formulating a relation between the time discretisation Δt and the mesh size h. We show that the splitting of the Gibbs free energy density fits to the Lyapunov property of the system, from which uniform a-priori estimates are calculated. The chapter ends with a convergence proof of the discrete solution to a solution of the non-viscous Cahn-Larché system. Unfortunately, we get convergence of the concentration field $c_{\Delta t,h}$ and the chemical potential $\mu_{\Delta t,h}$ in a weak respectively weak-$\star$ sense only. A consideration of the used Newton method closes this chapter.

5.1 Splitting of the Gibbs free energy density

In assumption (A-2) we postulate a splitting of the Gibbs free energy density into a convex part ψ^+ and a concave part ψ^-. For a general Gibbs free energy density like the spline interpolation (1.71) a splitting into a convex and a concave part must be constructed. In the next section we formulate a physical motivation of this splitting and construct this decomposition for the spline interpolation given in (1.71).

5.1.1 Construction of a convex density

The numerical approximation method stabilised by splitting the Gibbs free energy density is motivated by the following physical consideration:

We observe that the Gibbs free energy density is given by a spline interpolation (1.71), which is demonstrated in fig.5.1. If the numerical solution of the concentration field $c_h^n \in X_{m,h}(\Omega)$ is locally close to one of both equilibrium concentrations $c^{\alpha/\beta}$ the system is locally in a stable state, because the Gibbs free energy density is convex in a neighbourhood of the equilibrium concentration. Consequently, the numerical approximation method behaves stable near one of both equilibrium concentration $c^{\alpha/\beta}$.

Within an diffusive phase interface the situation is completely different. If the concentration field $c_h^n \in X_{m,h}(\Omega)$ reaches a value between both equilibrium concentrations $c^{\alpha/\beta}$ the Gibbs free energy density is a non-convex function. The spinodal points $s^{\alpha/\beta}$ are defined by $\psi_{,cc}(s^{\alpha/\beta}) = 0$. Especially between both spinodal points $s^{\alpha/\beta}$ the Gibbs free energy density is a concave function. In this range the physical system is in an unstable state, which drives the separation process. Consequently, the numerical approximation method is also unstable in the non-convex region of the Gibbs free energy density, where the driving forces of the diffusion are extreme large. The numerical instability occurs in high frequency contribution to the concentration field, which can be seen as high over- and undershoots in the numerical solution $c_h^n \in X_{m,h}(\Omega)$. This behaviour is denoted as Gibbs phenomena.

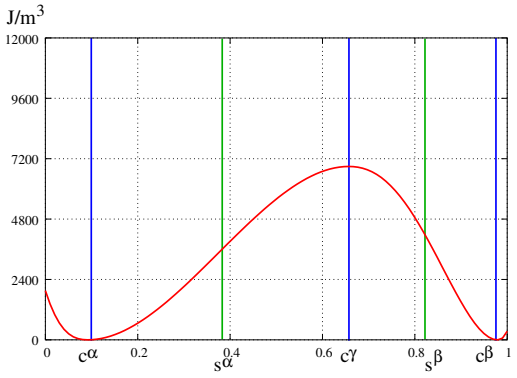

Fig. 5.1: Gibbs free energy density

In order to stabilise the numerical approximation method we take the idea from [54] and split the Gibbs free energy into a convex part ψ^+ and a concave part ψ^-. In the following the convex part of the Gibbs free energy density ψ^+ corresponds to the stable state of the system and is discretised implicitly, in contrast to the concave part of the Gibbs free energy density ψ^-, which corresponds to the unstable state of the system and is discretised explicitly. The concave part ψ^- therefore plays the role of a volume force for the approximation scheme.

We have to outline in which way the decomposition is constructed from a given Gibbs free energy density function $\psi \in C^2(\mathbb{R}, \mathbb{R})$. We introduce the convex part of the Gibbs free energy density ψ^+ in the following way:

$$\psi_{,c}^+(c) := \int_0^c \max(\psi_{,cc}(s), 0) ds, \tag{5.1}$$

$$\psi^+(c) := \int_0^c \psi_{,c}^+(s) ds = \int_0^c \int_0^s \max(\psi_{,cc}(t), 0) dt ds. \tag{5.2}$$

Finally, we define the concave part of the Gibbs free energy density by $\psi^-(c) := \psi(c) - \psi^+(c)$ and obviously we have an additive decomposition of the Gibbs free energy density.

We apply the above formulated decomposition to the spline interpolation of the Gibbs free energy density (1.71) and calculate this decomposition, which is demonstrated in the following figures:

(a) Monotone increasing $\psi^+_{,c}$ at $\theta = 20°C$

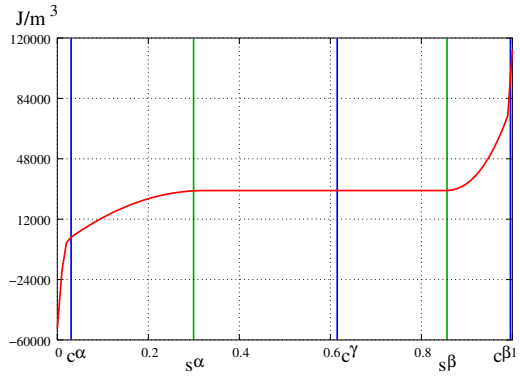

(b) Monotone decreasing $\psi^-_{,c}$ at $\theta = 20°C$

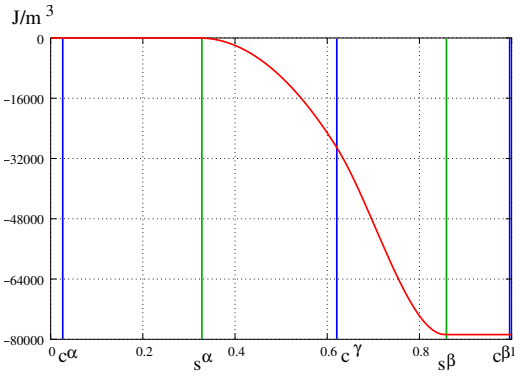

(c) Monotone increasing $\psi^+_{,c}$ at $\theta = 125°C$

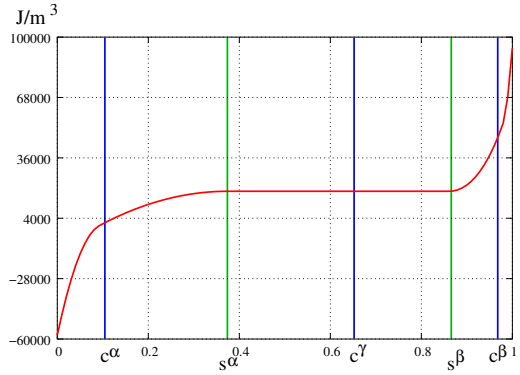

(d) Monotone decreasing $\psi^-_{,c}$ at $\theta = 125°C$

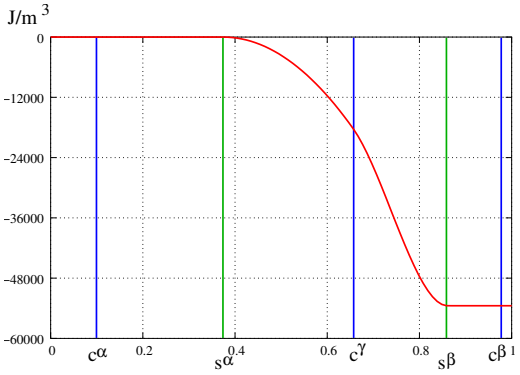

Fig. 5.2: Decomposition of $\psi_{,c}$ at different temperatures

5.1.2 Numerical approximation method

The stabilisation of the numerical approximation method is done by discretising the convex part of the Gibbs free energy density ψ^+ implicitly, in contrast to the concave part ψ^-, which is discretised explicitly.

Problem 5.1. Find for all time steps $1 \leq n \leq N$ a concentration field $c_h^n \in X_{m,h}(\Omega)$, a chemical potential $\mu_h^n \in X_h(\Omega)$ and a displacement $\boldsymbol{u}_h^n \in \boldsymbol{X}_h(\Omega)$, such that holds

$$\int_\Omega \partial_{\Delta t} c_h^n \zeta_h \, d\boldsymbol{x} + \int_\Omega \boldsymbol{M}_h^{n-1} \nabla_{\boldsymbol{x}} \mu_h^n \cdot \nabla_{\boldsymbol{x}} \zeta_h \, d\boldsymbol{x} = 0 \qquad \forall \zeta_h \in X_h(\Omega), \tag{5.3}$$

$$\int_\Omega \mu_h^n \xi_h \, d\boldsymbol{x} = \int_\Omega \boldsymbol{\Gamma} \nabla_{\boldsymbol{x}} c_h^n \cdot \nabla_{\boldsymbol{x}} \xi_h + \psi_{,c}^+(c_h^n)\xi_h + \psi_{,c}^-(c_h^{n-1})\xi_h + W_{,c}(c_h^n, \boldsymbol{\varepsilon}(\boldsymbol{u}_h^{n-1}))\xi_h \, d\boldsymbol{x} \qquad \forall \xi_h \in X_h(\Omega), \tag{5.4}$$

$$\int_\Omega \boldsymbol{C}(c_h^n)\boldsymbol{\varepsilon}(\boldsymbol{u}_h^n) : \boldsymbol{\varepsilon}(\boldsymbol{\eta}_h) \, d\boldsymbol{x} = \int_\Omega \boldsymbol{C}(c_h^n)\overline{\boldsymbol{\varepsilon}}(c_h^n) : \boldsymbol{\varepsilon}(\boldsymbol{\eta}_h) \, d\boldsymbol{x} + \int_{\Gamma_N} \boldsymbol{g}^n \cdot \boldsymbol{\eta}_h \, d\boldsymbol{a}_{\boldsymbol{x}} \qquad \forall \boldsymbol{\eta}_h \in \boldsymbol{X}_h(\Omega). \tag{5.5}$$

We remark that all integrals in problem 5.1 exist due to the assumptions (A-1) - (A-8) and the fact that we use almost everywhere bounded test functions. The decomposition of the Gibbs free energy does not effect this fact.

Since the Cahn-Larché system is a time dependent problem, we have to compute some initial tasks. Analogously to the viscous methods in the previous chapter, we compute a $L_2(\Omega)$-projection of the initial date $c_0 \in X_m(\Omega)$, which is formulated in definition 3.10 and analysed in section 3.2.1. Moreover, the corresponding initial displacement $\boldsymbol{u}_h^0 \in \boldsymbol{X}_h(\Omega)$ is computed by solving the initial elasticity problem 3.14. The solution $\boldsymbol{u}_h^0 \in \boldsymbol{X}_h(\Omega)$ satisfies the stability and convergence properties formulated in section 3.2.1. The initial chemical potential $\mu_h^0 \in X_h(\Omega)$ is computed by solving problem 4.3, which finishes the preprocessing procedure.

5.1.3 Elimination of the diffusion equation

In the same way as in the previous chapter we eliminate the discrete diffusion equation (5.3). This is done by calculating a relation between the diffusion and the dissipation.

The operator $\mathcal{M}_h^n$, introduced in definition 4.4, describes a linear, $X_0(\Omega)$-elliptic and continuous operator due to corollary 4.5. It corresponds to a homogeneous Neumann problem with material parameter $\boldsymbol{M}_h^{n-1}$. Consequently, the inverse operator $(\mathcal{M}_h^n)^{-1}$ exists by applying the Lax-Milgram theorem. In view of the operator $(\mathcal{M}_h^n)^{-1}$ we conclude from the discrete diffusion equation (5.3) similar to (4.6) the following representation of the chemical potential

$$\mu_h^n = -(\mathcal{M}_h^n)^{-1} \partial_{\Delta t} c_h^n + \lambda_h^n \in X_h(\Omega). \tag{5.6}$$

We remark that the Lagrangian multiplier has to be chosen in the kernel of the operator $\mathcal{M}_h^n$, which means $\lambda_h^n \in \ker(\mathcal{M}_h^n) = \mathbb{R}$.

Let $\xi_h \in X_{0,h}(\Omega)$ be an arbitrary test function, then we calculate analogously to (4.7) for the discrete fields

$$\int_\Omega \mu_h^n \xi_h \, d\boldsymbol{x} = -\langle \partial_{\Delta t} c_h^n, \xi_h \rangle_{\mathcal{M}_h^n}.$$

Taking into account this calculation we restrict the discrete weak problem 5.1 to a system of two equations for the unknown concentration field $c_h^n \in X_{m,h}(\Omega)$ and for the unknown displacement $\boldsymbol{u}_h^n \in \boldsymbol{X}_h(\Omega)$.

Problem 5.2. Find at each discrete time $t = n\Delta t$ for $1 \leq n \leq N$ a function $c_h^n \in X_{m,h}(\Omega)$ and $\boldsymbol{u}_h^n \in \boldsymbol{X}_h(\Omega)$ such that holds

$$\begin{aligned}\int_\Omega \boldsymbol{\Gamma} \nabla_{\boldsymbol{x}} c_h^n \cdot \nabla_{\boldsymbol{x}} \xi_h + \psi_{,c}^+(c_h^n)\xi_h + \psi_{,c}^-(c_h^{n-1})\xi_h + W_{,c}(c_h^n, \boldsymbol{\varepsilon}(\boldsymbol{u}_h^{n-1}))\xi_h \, d\boldsymbol{x} \\ + \langle \partial_{\Delta t} c_h^n, \xi_h \rangle_{\mathcal{M}_h^n} = 0 \qquad \forall \xi_h \in X_h(\Omega),\end{aligned}$$

$$\begin{aligned}\int_\Omega \boldsymbol{C}(c_h^n)\boldsymbol{\varepsilon}(\boldsymbol{u}_h^n) : \boldsymbol{\varepsilon}(\boldsymbol{\eta}_h) \, d\boldsymbol{x} = \int_\Omega \boldsymbol{C}(c_h^n)\overline{\boldsymbol{\varepsilon}}(c_h^n) : \boldsymbol{\varepsilon}(\boldsymbol{\eta}_h) \, d\boldsymbol{x} + \int_{\Gamma_N} \boldsymbol{g}^n \cdot \boldsymbol{\eta}_h \, d\boldsymbol{a}_{\boldsymbol{x}} \\ \forall \boldsymbol{\eta}_h \in \boldsymbol{X}_h(\Omega).\end{aligned}$$

This numerical approximation method decouples the convex and concave part of the Gibbs free energy density as well as diffusion and elasticity. Due to this fact we have to formulate two energy functionals. The first functional contains the configurational energy $E_{h,config}^n$ corresponding to the structural composition of the alloy. We point out that the explicitly discretised concave part of the Gibbs free energy presents a linear contribution to the configurational energy $E_{h,config}^n$, corresponding to a volume force. The second functional contains the strain energy $E_{h,mech}^n$ related to the mechanical equilibrium. We get for both functionals

$$\begin{aligned}E_{h,config}^n(d_h) &:= \int_\Omega \frac{1}{2}\boldsymbol{\Gamma}\nabla_{\boldsymbol{x}} d_h \cdot \nabla_{\boldsymbol{x}} d_h + \psi^+(d_h) + \psi_{,c}^-(c_h^{n-1})(d_h - c_h^{n-1}) \\ &\quad + W(d_h, \boldsymbol{\varepsilon}(\boldsymbol{u}_h^{n-1})) \, d\boldsymbol{x} + \frac{1}{2\Delta t}\|d_h - c_h^{n-1}\|_{\mathcal{M}_h^n}^2, \\ E_{h,mech}^n(\boldsymbol{v}_h) &:= \int_\Omega W(c_h^n, \boldsymbol{\varepsilon}(\boldsymbol{v}_h)) \, d\boldsymbol{x} - \int_{\Gamma_N} \boldsymbol{g}^n \cdot \boldsymbol{v}_h \, d\boldsymbol{a}_{\boldsymbol{x}}.\end{aligned}$$

We remark that the mechanical equilibrium (5.5) belongs to a $\boldsymbol{X}(\Omega)$-elliptic problem as outlined in lemma 2.14 and due to this property the solution $\boldsymbol{u}_h^n$ provides a minimiser of the strain energy

$$E_{h,mech}^n(\boldsymbol{u}_h^n) = \min_{\boldsymbol{v}_h \in \boldsymbol{X}_h(\Omega)} E_{h,mech}^n(\boldsymbol{v}_h).$$

In contrast to the discrete problems of the previous section problem 5.1 has a flow gradient structure with respect to the inner product $\langle \cdot, \cdot \rangle_{\mathcal{M}_h^n}$ only. From (2.26) we deduce the relation between diffusion and dissipation of the non-viscous Cahn-Larché system

$$\frac{1}{2\Delta t}\|c_h^n - c_h^{n-1}\|_{\mathcal{M}_h^n}^2 = -\Delta t D(c_h^{n-1}, \mu_h^n). \tag{5.7}$$

For problem 5.1 the dissipation contains diffusion only, but no friction. Obviously minimising the configurational energy means minimising the Helmholtz free energy and maximising the dissipation.

5.2 Existence of a discrete solution

In this section we prove the existence of a discrete solution of problem 5.1. Furthermore, we show uniform a-priori estimates of the discrete solution of problem 5.1 by using energy estimates based on the Lyapunov property.

5.2.1 Energy minimisation

The existence of a solution is proved by minimising the configurational energy $E_{h,config}^n$ in order to calculate a physical state of minimal Helmholtz free energy and maximal dissipation.

Lemma 5.3. *Let $\Omega \subset \mathbb{R}^d$ be a domain satisfying condition (H-1). Furthermore, let the assumptions (A-1) - (A-8) be satisfied. Then there exists at least one $c_h^n \in X_{m,h}(\Omega)$ such that holds*

$$E_{h,config}^n(c_h^n) = \min_{d_h \in X_{m,h}(\Omega)} E_{h,config}^n(d_h).$$

Proof. The proof is organised in two steps.
Step 1: In the first step we show that the configurational energy is described by a coercive functional. Clearly, the surface energy is coercive due to assumption (A-1) and due to the Poincaré inequality (2.1). We get

$$\int_\Omega \frac{1}{2}\mathbf{\Gamma}\nabla_{\boldsymbol{x}} d_h \cdot \nabla_{\boldsymbol{x}} d_h \, d\boldsymbol{x} \geq \frac{c_{\mathbf{\Gamma}}}{2c_p}\|d_h\|_{H^1(\Omega)}^2 - \frac{c_{\mathbf{\Gamma}}}{2}m^2.$$

The Gibbs free energy is bounded below by a constant depending on the concentration field of the previous time step c_h^{n-1}. Taking into account that ψ^- is concave and

by applying assumption (A-2) we calculate

$$\begin{aligned}
&\int_\Omega \psi^+(d_h) + \psi^-_{,c}(c_h^{n-1})(d_h - c_h^{n-1})\, d\boldsymbol{x} \\
&\quad \geq \int_\Omega \psi^+(d_h) + \psi^-(d_h) - \psi^-(c_h^{n-1})\, d\boldsymbol{x} = \int_\Omega \psi(d_h) - \psi^-(c_h^{n-1})\, d\boldsymbol{x} \\
&\quad \geq -c_\psi \operatorname{meas}(\Omega) - \int_\Omega \psi^-(c_h^{n-1})\, d\boldsymbol{x} = -\tilde{C}.
\end{aligned}$$

The elastic contribution to the configurational energy and the dissipative term are obviously bounded below by zero. Summing up the above calculations the coercivity of the configurational energy functional is proved and it holds

$$E^n_{h,config}(d_h) \geq \frac{c_{\mathbf{\Gamma}}}{2c_p}\|d_h\|^2_{H^1(\Omega)} - C.$$

Step 2: The density of the configurational energy is continuous with respect to $\nabla_{\boldsymbol{x}} d_h$ and d_h. Moreover, the density is convex with respect to $\nabla_{\boldsymbol{x}} d_h$ and bounded below. The non-convex term of the Gibbs free energy density plays the role of a volume force. Finally, for a minimising sequence $(d_{h,k})_{k\in\mathbb{N}}$ theorem 2.6 yields for a weak convergent sequence $(d_{h,k})_{k\in\mathbb{N}} \subset X_{m,h}(\Omega)$

$$E^n_{h,config}(d_h) \leq \lim_{k\to\infty} E^n_{h,config}(d_{h,k}).$$

The existence of a minimiser $c_h^n \in X_{m,h}(\Omega)$ follows from theorem 2.7. □

Lemma 5.4. *Let $\Omega \subset \mathbb{R}^d$ be a domain satisfying condition (H-1). Furthermore, let the assumptions (A-1) - (A-8) be satisfied. Then, the Gâteaux derivative of the configurational energy $E^n_{h,config}$ exists for any test function $\xi_h \in X_h(\Omega)$ and it holds*

$$\begin{aligned}
&\lim_{\delta\to 0} \frac{E^n_{h,config}(d_h + \delta\xi_h) - E^n_{h,config}(d_h)}{\delta} \\
&= \int_\Omega \mathbf{\Gamma}\nabla_{\boldsymbol{x}} d_h \cdot \nabla_{\boldsymbol{x}}\xi_h + \psi^+_{,c}(d_h)\xi_h + \psi^-_{,c}(c_h^{n-1})\xi_h + W_{,c}(d_h, \boldsymbol{\varepsilon}(\boldsymbol{u}_h^{n-1}))\xi_h\, d\boldsymbol{x} \\
&\qquad + \frac{1}{\Delta t}\big\langle d_h - c_h^{n-1}, \xi_h\big\rangle_{\mathcal{M}_h^n}. \qquad (5.8)
\end{aligned}$$

Proof. This result follows by arguing in the same way as in the proof of lemma 2.23. The surface energy is quadratic with respect to $\nabla_{\boldsymbol{x}} d_h$ and this leads directly to

$$\begin{aligned}
&\lim_{\delta\to 0} \frac{1}{\delta}\int_\Omega \frac{1}{2}\mathbf{\Gamma}\nabla_{\boldsymbol{x}}(d_h + \delta\xi_h)\cdot\nabla_{\boldsymbol{x}}(d_h + \delta\xi_h) - \frac{1}{2}\mathbf{\Gamma}\nabla_{\boldsymbol{x}} d_h \cdot \nabla_{\boldsymbol{x}} d_h\, d\boldsymbol{x} \\
&\quad = \int_\Omega \mathbf{\Gamma}\nabla_{\boldsymbol{x}} d_h \cdot \nabla_{\boldsymbol{x}}\xi_h\, d\boldsymbol{x}.
\end{aligned}$$

The convex part of the Gibbs free energy density ψ^+, which is implicitly discretised, is treated analogously to the proof of lemma 2.23. The difference quotient of the convex function ψ^+ is uniformly bounded by using the assumption (A-2). We get

$$\left|\frac{\psi^+(d_h+\delta\xi_h)-\psi^+(d_h)}{\delta}\right| \leq 2(\psi^+(d_h)+C).$$

This uniform bound and the fact that $\psi^+ \in C^2(\mathbb{R},\mathbb{R})$ yields with Lebesgue's convergence theorem

$$\lim_{\delta\to 0}\int_\Omega \frac{\psi^+(d_h+\delta\xi_h)-\psi^+(d_h)}{\delta}\,d\boldsymbol{x} = \int_\Omega \psi^+_{,c}(d_h)\xi_h\,d\boldsymbol{x}.$$

The concave part ψ^- of the Gibbs free energy density, which is explicitly discretised, is linear with respect to d_h. Therefore it directly follows

$$\begin{aligned}\lim_{\delta\to 0}\int_\Omega \frac{\psi^-_{,c}(c_h^{n-1})(d_h+\delta\xi_h-c_h^{n-1})-\psi^-_{,c}(c_h^{n-1})(d_h-c_h^{n-1})}{\delta}\,d\boldsymbol{x}\\ = \int_\Omega \psi^-_{,c}(c_h^{n-1})\xi_h\,d\boldsymbol{x}.\end{aligned}$$

Furthermore, the elastic contribution to the chemical potential is treated by applying the mean value theorem together with the assumptions (A-6), (A-7) and the Lebesgue convergence theorem

$$\begin{aligned}&\lim_{\delta\to 0}\frac{1}{\delta}\left(\int_\Omega W(d_h+\delta\xi_h,\boldsymbol{\varepsilon}(\boldsymbol{u}_h^{n-1}))\,d\boldsymbol{x}-\int_\Omega W(d_h,\boldsymbol{\varepsilon}(\boldsymbol{u}_h^{n-1}))\,d\boldsymbol{x}\right)\\ &\quad=\lim_{\delta\to 0}\int_\Omega W_{,c}(d_h+\nu(\delta)\xi_h,\boldsymbol{\varepsilon}(\boldsymbol{u}_h^{n-1}))\xi_h\,d\boldsymbol{x}=\int_\Omega W_{,c}(d_h,\boldsymbol{\varepsilon}(\boldsymbol{u}_h^{n-1}))\xi_h\,d\boldsymbol{x}.\end{aligned}$$

Finally, the dissipative term is quadratic and we get by direct calculations

$$\begin{aligned}&\lim_{\delta\to 0}\frac{1}{2\Delta t\delta}\left(\|d_h+\delta\xi_h-c_h^{n-1}\|^2_{\mathcal{M}_h^n}-\|d_h-c_h^{n-1}\|^2_{\mathcal{M}_h^n}\right)\\ &\quad=\frac{1}{\Delta t}\langle d_h-c_h^{n-1},\xi_h\rangle_{\mathcal{M}_h^n}.\end{aligned}$$

Summing up all calculations the statement of this lemma is proved. □

For the minimiser $c_h^n \in X_h(\Omega)$ holds due to theorem 2.8 that the Gâteaux derivative is equal to zero, this means for any test function $\xi_h \in X_h(\Omega)$ holds

$$\begin{aligned}\int_\Omega \boldsymbol{\Gamma}\nabla_{\boldsymbol{x}} d_h\cdot\nabla_{\boldsymbol{x}}\xi_h+\psi^+_{,c}(d_h)\xi_h+\psi^-_{,c}(c_h^{n-1})\xi_h\\ +W_{,c}(d_h,\boldsymbol{\varepsilon}(\boldsymbol{u}_h^{n-1}))\xi_h\,d\boldsymbol{x}+\langle\partial_{\Delta t}c_h^n,\xi_h\rangle_{\mathcal{M}_h^n}=0.\end{aligned}$$

Furthermore, the minimiser $c_h^n \in X_h(\Omega)$, the discrete displacement $\boldsymbol{u}_h^n \in \boldsymbol{X}_h(\Omega)$ and the discrete chemical potential $\mu_h^n \in X_h(\Omega)$ given by (5.6) generate a discrete solution of problem 5.2. The Lagrangian multiplier has to be chosen in the following form

$$\lambda_h^n = \frac{1}{\text{meas}(\Omega)} \int_\Omega \psi_{,c}^+(c_h^n) + \psi_{,c}^-(c_h^{n-1}) + W_{,c}(c_h^n, \boldsymbol{\varepsilon}(\boldsymbol{u}_h^{n-1}))\, d\boldsymbol{x}. \tag{5.9}$$

Naturally, the piecewise constant interpolants of the concentration field $c_{\Delta t,h}$, of the chemical potential $\mu_{\Delta t,h}$ and of the displacement $\boldsymbol{u}_{\Delta t,h}$ are computed. Furthermore the piecewise linear interpolant $\overline{c}_{\Delta t,h}$ is also determined.

5.2.2 Uniqueness of the discrete solution

In this section we derive relations between the time discretisation Δt and the mesh size h in order to get a unique solution of the approximation method.

Lemma 5.5 (Uniqueness). *Let $\Omega \subset \mathbb{R}^d$ be a domain satisfying condition (H-1). Moreover let the assumptions (A-1) - (A-8) be satisfied. The triangulation $\mathscr{T}_h(\Omega)$ is assumed to be admissible, exact and uniform. If the time discretisation Δt and the mesh size h satisfy the following condition*

$$\Delta t \leq \frac{c_\Gamma h^{2d}}{2C_M(C_{W,cc})^2},$$

then for every time step $t = n\Delta t$ with $0 \leq n \leq N$ the discrete problem 5.1 has a unique solution.

Proof. We show this lemma by complete induction. At initial time $t = 0$ the $L_2(\Omega)$-projection of the initial data c_0 has a unique solution due to lemma 3.11 and the corresponding discrete displacement $\boldsymbol{u}_h^0$ is also unique. We assume that for time $t = (n-1)\Delta t$ the concentration field c_h^{n-1} and the displacement $\boldsymbol{u}_h^{n-1}$ is unique. Therfore the uniqueness of the concentration field c_h^n and of the displacement $\boldsymbol{u}_h^n$ is given. In order to derive this conclusion, we use the Lipschitz continuity of $W_{,c}$ derived in lemma 4.11,

$$|W_{,c}(c_1, \boldsymbol{\varepsilon}) - W_{,c}(c_2, \boldsymbol{\varepsilon})| \leq C(|\boldsymbol{\varepsilon}|^2 + 1).$$

Finally, we assume that at time $t = n\Delta t$ there exist two concentration fields $c_{1,h}^n$ and $c_{2,h}^n$, which are solutions of the reformulated problem 5.2. By subtracting the weak formulation in problem 5.2 with solutions $c_{1,h}^n$ and $c_{2,h}^n$ from each other, we get

$$\begin{aligned}\int_\Omega \boldsymbol{\Gamma}\nabla_{\boldsymbol{x}}(c_{1,h}^n - c_{2,h}^n) \cdot \nabla_{\boldsymbol{x}}\xi_h + (\psi_{,c}^+(c_{1,h}^n) - \psi_{,c}^+(c_{2,h}^n))\xi_h \\ + (W_{,c}(c_{1,h}^n, \boldsymbol{\varepsilon}(\boldsymbol{u}_h^{n-1})) - W_{,c}(c_{2,h}^n, \boldsymbol{\varepsilon}(\boldsymbol{u}_h^{n-1})))(c_{1,h}^n - c_{2,h}^n)\, d\boldsymbol{x} \\ + \frac{1}{\Delta t}\langle c_{1,h}^n - c_{2,h}^n, \xi_h\rangle_{\mathcal{M}_h^n} = 0.\end{aligned}$$

In the following the test function is chosen to be $\xi_h = c^n_{1,h} - c^n_{2,h}$. The convex terms are estimated below by assumption (A-1) and using the fact that $\psi^+_{,c}$ is a monotone function, thus the corresponding term is bounded below by zero. The Lipschitz continuity of $W_{,c}$ and the uniform a-priori estimates of the displacement $\boldsymbol{u}^{n-1}_h$are applied with the inverse inequality from lemma 3.4 and Young's inequality (4.7) to the non-convex term. Then it follows

$$\begin{aligned} c_\Gamma |c^n_{1,h} - c^n_{2,h}|^2_{H^1(\Omega)} + \frac{1}{\Delta t}\|c^n_{1,h} - c^n_{2,h}\|^2_{\mathcal{M}^n_h} &\leq C_{W,cc}\frac{1}{h^d}\|c^n_{1,h} - c^n_{2,h}\|^2_{L_2(\Omega)} \\ &\leq C_{W,cc}\frac{1}{h^d}\left(\delta|c^n_{1,h} - c^n_{2,h}|^2_{H^1(\Omega)} + \frac{C_M}{\delta}\|c^n_{1,h} - c^n_{2,h}\|^2_{\mathcal{M}^n_h}\right). \end{aligned}$$

In this estimate we define $\int_\Omega C(|\boldsymbol{\varepsilon}|^2 + 1)\, d\boldsymbol{x} \leq C(C^2_{\boldsymbol{u}} + \mathrm{meas}(\Omega)) =: C_{W,cc}$. From this estimate we deduce for the difference of both solutions $c^n_{1,h}$ and $c^n_{2,h}$ the relation

$$\left(c_\Gamma - \frac{C_{W,cc}}{h^d}\delta\right)|c^n_{1,h} - c^n_{2,h}|^2_{H^1(\Omega)} + \left(\frac{1}{\Delta t} - \frac{C_M}{C}_{W,cc}\, h^d\delta\right)\|c^n_{1,h} - c^n_{2,h}\|^2_{\mathcal{M}^n_h} \leq 0.$$

By choosing $\delta = \frac{c_\Gamma h^d}{2C_{W,cc}}$ we get for the time discretisation the condition

$$\Delta t \leq \frac{c_\Gamma h^{2d}}{2C_M(C_{W,cc})^2}.$$

The above estimate directly yields the uniqueness of the concentration field c^n_h. Consequently, the uniqueness of the displacement $\boldsymbol{u}^n_h$ follows from the Lax-Milgram theorem and the representation formula (5.6) shows the uniqueness of the chemical potential $\mu^n_h \in X_h(\Omega)$. □

Remark 5.6. If the elasticity tensor is constant, the uniqueness of the discrete concentration field $c^n_h \in X_{m,h}(\Omega)$ is obtained by a weaker condition on the time discretisation

$$\Delta t \leq \frac{c_\Gamma h^d}{2C_M(C_{W,cc})^2}.$$

Proof. This result follows in a similar way as in the proof of lemma 5.5. The significant difference to lemma 5.5 is the Lipschitz continuity of the elastic contribution to the chemical potential. The strain $\boldsymbol{\varepsilon}$ enters this estimate only linear

$$|W_{,c}(c_1, \boldsymbol{\varepsilon}) - W_{,c}(c_2, \boldsymbol{\varepsilon})| \leq C(|\boldsymbol{\varepsilon}| + 1)|c_1 - c_2|.$$

The same argumentation as above leads to the statement of this remark. □

Remark 5.7. The existence of a discrete solution of problem 5.1 was proved by minimising the configurational energy and showing that the Euler-Lagrange equations are zero within the minimiser.

In the numerical simulation the Euler-Lagrange equations are solved in order to derive a discrete solution of the problem. In general it is not true that a solution of the Euler-Lagrange equations minimises the corresponding energy functional. But for the case of the solution of the Euler-Lagrange equation being unique, a global minimum of the energy is achieved, see [29].

5.2.3 A-priori estimates

In this section we calculate a-priori estimates of a discrete solution of problem 5.1. The key of this proof is again the Lyapunov property of the system, which means that also the discretised system leads to an energetic stable state. The proof of the Lyapunov property for the operator splitting method differs from the techniques shown in the previous sections due to the decoupling of the diffusion and elasticity and due to the splitting of the Gibbs free energy density.

Lemma 5.8 (Lyapunov property). *Let $\Omega \subset \mathbb{R}^d$ be a domain satisfying condition (H-1). Let $c_{\Delta t,h}$, $\mu_{\Delta t,h}$ and $\boldsymbol{u}_{\Delta t,h}$ be a discrete solution of problem 5.1. Furthermore, let the assumptions (A-1) - (A-8) be satisfied. Then the Lyapunov property holds*

$$E(c_h^n, \boldsymbol{u}_h^n) + \frac{1}{2}\int_0^t \int_\Omega \boldsymbol{M}(c_{\Delta t,h}(t-\Delta t,\cdot))\nabla_{\boldsymbol{x}}\mu_{\Delta t,h} \cdot \nabla_{\boldsymbol{x}}\mu_{\Delta t,h}\, d\boldsymbol{x}dt \leq E(c_h^0, \boldsymbol{u}_h^0) + CT$$

with a constant $C = C(C_C, c_C, C_{\overline{\boldsymbol{\varepsilon}}}, \boldsymbol{g}, \mathrm{meas}(\Omega))$.

Proof. Analogous to the previous section we observe the configurational energy $E^n_{h,config}$ at time $t = n\Delta t$ with $1 \leq n \leq N$ and use the minimiser $c_h^n \in X_{m,h}(\Omega)$ together with the comparison function $c_h^{n-1} \in X_{m,h}(\Omega)$. Then we calculate an above estimate from

$$\begin{aligned}
&E^n_{h,config}(c_h^n) - \int_{\Gamma_N} \boldsymbol{g}^n \cdot \boldsymbol{u}_h^{n-1}\, d\boldsymbol{a}_{\boldsymbol{x}} \\
&\quad = \int_\Omega \frac{1}{2}\boldsymbol{\Gamma}\nabla_{\boldsymbol{x}}c_h^n \cdot \nabla_{\boldsymbol{x}}c_h^n + \psi^+(c_h^n) + \psi^-_{,c}(c_h^{n-1})(c_h^n - c_h^{n-1}) \\
&\qquad + W(c_h^n, \boldsymbol{\varepsilon}(\boldsymbol{u}_h^{n-1}))\, d\boldsymbol{x} - \int_{\Gamma_N} \boldsymbol{g}^n \cdot \boldsymbol{u}_h^{n-1}\, d\boldsymbol{a}_{\boldsymbol{x}} + \frac{1}{2\Delta t}\|c_h^n - c_h^{n-1}\|^2_{\mathcal{M}_h^n} \\
&\quad \leq \int_\Omega \frac{1}{2}\boldsymbol{\Gamma}\nabla_{\boldsymbol{x}}c_h^{n-1} \cdot \nabla_{\boldsymbol{x}}c_h^{n-1} + \psi^+(c_h^{n-1}) + W(c_h^{n-1}, \boldsymbol{\varepsilon}(\boldsymbol{u}_h^{n-1}))\, d\boldsymbol{x} \\
&\qquad - \int_{\Gamma_N} \boldsymbol{g}^{n-1} \cdot \boldsymbol{u}_h^{n-1}\, d\boldsymbol{a}_{\boldsymbol{x}} + \int_{\Gamma_N} (\boldsymbol{g}^{n-1} - \boldsymbol{g}^n) \cdot \boldsymbol{u}_h^{n-1}\, d\boldsymbol{a}_{\boldsymbol{x}}
\end{aligned}$$

An estimate from below is derived by using the fact that the displacement $\boldsymbol{u}_h^n$ minimises the strain energy $E_{h,mech}^n$ and that ψ^- is a concave function. We get

$$\begin{aligned}
&E_{h,config}^n(c_h^n) - \int_{\Gamma_N} \boldsymbol{g}^n \cdot \boldsymbol{u}_h^{n-1}\, d\boldsymbol{a}_{\boldsymbol{x}} \\
&\quad \geq \int_\Omega \frac{1}{2}\boldsymbol{\Gamma}\nabla_{\boldsymbol{x}} c_h^n \cdot \nabla_{\boldsymbol{x}} c_h^n + \psi^+(c_h^n) + \psi_{,c}^-(c_h^{n-1})(c_h^n - c_h^{n-1}) \\
&\qquad + W(c_h^n, \boldsymbol{\varepsilon}(\boldsymbol{u}_h^n))\, d\boldsymbol{x} - \int_{\Gamma_N} \boldsymbol{g}^n \cdot \boldsymbol{u}_h^n\, d\boldsymbol{a}_{\boldsymbol{x}} + \frac{1}{2\Delta t}\|c_h^n - c_h^{n-1}\|_{\mathcal{M}_h^n}^2 \\
&\quad \geq \int_\Omega \frac{1}{2}\boldsymbol{\Gamma}\nabla_{\boldsymbol{x}} c_h^n \cdot \nabla_{\boldsymbol{x}} c_h^n + \psi^+(c_h^n) + \psi^-(c_h^n) - \psi^-(c_h^{n-1}) \\
&\qquad + W(c_h^n, \boldsymbol{\varepsilon}(\boldsymbol{u}_h^n))\, d\boldsymbol{x} - \int_{\Gamma_N} \boldsymbol{g}^n \cdot \boldsymbol{u}_h^n\, d\boldsymbol{a}_{\boldsymbol{x}} + \frac{1}{2\Delta t}\|c_h^n - c_h^{n-1}\|_{\mathcal{M}_h^n}^2
\end{aligned}$$

Summing up both estimates and taking into account the representation of the dissipation in (5.7) it follows

$$\begin{aligned}
&E(c_h^n, \boldsymbol{u}_h^n) + \frac{1}{2}\int_{t_{n-1}}^{t^n}\int_\Omega \boldsymbol{M}_h^n \nabla_{\boldsymbol{x}}\mu_h^n \cdot \nabla_{\boldsymbol{x}}\mu_h^n\, d\boldsymbol{x} \\
&\quad \leq E(c_h^{n-1}, \boldsymbol{u}_h^{n-1}) + \int_{\Gamma_N} (\boldsymbol{g}^n - \boldsymbol{g}^{n-1}) \cdot \boldsymbol{u}_h^{n-1}\, d\boldsymbol{a}_{\boldsymbol{x}} \leq E(c_h^{n-1}, \boldsymbol{u}_h^{n-1}) + C\Delta t.
\end{aligned}$$

The recursive application of the estimate yields the statement of this lemma. □

Lemma 5.9 (A-priori estimates). *Let $\Omega \subset \mathbb{R}^d$ be a domain satisfying condition (H-1). Furthermore, let the assumptions (A-1) - (A-8) be satisfied and $\mathscr{T}_h(\Omega)$ be an exact, admissible and locally quasi-uniform mesh satisfying condition* (3.5)*. Then for the discrete weak solution $c_{\Delta t,h}$, $\bar{c}_{\Delta t,h}$, $\mu_{\Delta t,h}$ and $\boldsymbol{u}_{\Delta t,h}$ there exist constants C_c, $C_{\bar{c}}$, C_μ, $C_{\boldsymbol{u}}$ and $C_{\dot{\bar{c}}} > 0$ depending on the material parameters, the boundary loading g, the initial condition c_0, time T and* meas(Ω)*, such that the following uniform a-priori estimates hold*

(1) $\|\boldsymbol{u}_{\Delta t,h}\|_{L_\infty(0,T;\boldsymbol{H}^1(\Omega))} \leq C_{\boldsymbol{u}}$,

(2) $\|c_{\Delta t,h}\|_{L_\infty(0,T;H^1(\Omega))} \leq C_c$,

(3) $\|\bar{c}_{\Delta t,h}\|_{L_\infty(0,T;H^1(\Omega))} \leq C_{\bar{c}}$,

(4) $\sup_{t\in[0,T]} \int_\Omega \psi(c_{\Delta t,h})\, d\boldsymbol{x} \leq C_\psi$,

(5) $\|\mu_{\Delta t,h}\|_{L_2(0,T;H^1(\Omega))} \leq C_\mu$.

Proof. In addition to the Lyapunov property we need an upper estimate of the energy at initial time $t = 0$. This result is proved in lemma 4.15. Furthermore, a lower estimate of the energy at time $t = n\Delta t$ is necessary, which we take from lemma 4.16. These results together with the Lyapunov property derived in lemma 5.8 yield the statements of this lemma. □

5.3 Convergence of the method

First of all we have to repeat two results from the previous chapter, which obviously hold for the approximation method presented here.

Lemma 5.10. *Let $\Omega \subset \mathbb{R}^d$ be a domain satisfying condition (H-1). Furthermore, let the assumptions (A-1) - (A-8) be satisfied. Furthermore the triangulation is assumed to be an exact, admissible and locally quasi-uniform mesh satisfying condition* (3.5). *Then there exist at least one $c \in L_\infty(0,T;H^1(\Omega))$ and subsequences denoted without loss of generality with the same index $(c_{\Delta t,h})_{\Delta t,h}$, $(\bar{c}_{\Delta t,h})_{\Delta t,h} \subset L_\infty(0,T;H^1(\Omega))$, such that for $\Delta t \to 0$ and $h \to 0$*

$$\bar{c}_{\Delta t,h} \longrightarrow c \qquad \text{in} \quad C([0,T];L_2(\Omega)), \tag{5.10}$$

$$c_{\Delta t,h} \longrightarrow c \qquad \text{in} \quad L_\infty(0,T;L_2(\Omega)), \tag{5.11}$$

$$c_{\Delta t,h}(t,\boldsymbol{x}) \longrightarrow c(t,\boldsymbol{x}) \qquad \text{almost everywhere in } \Omega_T, \tag{5.12}$$

$$c_{\Delta t,h} \overset{*}{\rightharpoonup} c \qquad \text{in} \quad L_\infty(0,T;X_m(\Omega)). \tag{5.13}$$

Proof. The proof of this result is similar to lemma 4.18. Statement (5.10) and (5.11) are derived from the discrete diffusion equation (5.3) and from Arzela-Ascoli's theorem 2.9. In view of (5.11), statement (5.12) follows from Weyl's corollary 2.12 and the uniform a-priori estimate in lemma 5.9 statement *(2)* yields the weak-$\star$ convergence. □

Lemma 5.11 (Convergence). *Let $\Omega \subset \mathbb{R}^d$ be a domain satisfying condition (H-1). Furthermore, let the assumptions (A-6) - (A-8) be satisfied. Let $\boldsymbol{u} \in L_2(0,T;\boldsymbol{X}(\Omega))$ be the unique solution of problem 2.32 and let $\boldsymbol{u}_{\Delta t,h} \in L_2(0,T;\boldsymbol{X}_h(\Omega))$ be the piecewise constant interpolant of discrete weak solutions of* (5.5). *Then it holds for $\Delta t \to 0$ and $h \to 0$*

$$\boldsymbol{u}_{\Delta t,h} \longrightarrow \boldsymbol{u} \qquad \text{in} \quad L_2(0,T;\boldsymbol{H}^1(\Omega)),$$

$$\boldsymbol{u}_{\Delta t,h}(t-\Delta t,\cdot) \longrightarrow \boldsymbol{u} \qquad \text{in} \quad L_2(0,T;\boldsymbol{H}^1(\Omega)).$$

Proof. This result is obviously proved in lemma 4.28 by using the auxiliary problem 4.23. This convergence result bases on the Galerkin orthogonality from lemma 4.24 taking into account Cea's lemma 4.25 and the error estimate outlined in lemma 4.26. □

We have to remark that due to the uniform a-priori estimate of the chemical potential $\mu_{\Delta t,h}$ proved in lemma 5.9 statement (5) a weak convergent subsequence denoted without loss of generality with the same index exists;

$$\mu_{\Delta t,h} \rightharpoonup \mu \quad \text{in } L_2(0,T;H^1(\Omega)) \quad \text{if } \Delta t \to 0,\ h \to 0.$$

Theorem 5.12 (Convergence of the method). *Let $\Omega \subset \mathbb{R}^d$ be a domain satisfying condition (H-1). Furthermore, $\mathscr{T}_h(\Omega)$ is assumed to be an exact, admissible and locally quasi-uniform triangulation satisfying the shape regularity condition. Let the assumptions (A-1) - (A-8) be satisfied, then $c_{\Delta t,h}$, $\mu_{\Delta t,h}$ and $\boldsymbol{u}_{\Delta t,h}$ converge to a weak solution of the non-viscous Cahn-Larché system, if Δt and h go to zero.*

Proof. **Step 1**: The first step of this proof considers the discrete diffusion equation (5.3). The convergence of the discrete concentration field $c_{\Delta t,h}$ and the discrete chemical potential $\mu_{\Delta t,h}$ to a solution of the diffusion equation follows by the same arguments as in the proof of theorem 4.29.

Step 2: In the next step, we consider the discrete semi-weak equation of the chemical potential (5.4). As a test function we choose $\xi \in \{v \in L_2(0,T;H^1(\Omega)) \cap L_\infty(\Omega_T) \ : \ \dot{v} \in L_2(\Omega_T)\}$ and apply the Clement quasi-interpolation operator $\xi_h = \mathcal{R}_h\xi$. By integrating (5.4) over $(0,T)$ and subtracting it from the weak formulation of the non-viscous Cahn-Larché system, we deduce for the left hand side

$$\begin{aligned}\left|\int_{\Omega_T} \mu_{\Delta t,h}\mathcal{R}_h\xi - \mu\xi \, d\boldsymbol{x}dt\right| &= \left|\int_{\Omega_T} \mu_{\Delta t,h}(\mathcal{R}_h\xi - \xi) + (\mu_{\Delta t,h} - \mu)\xi \, d\boldsymbol{x}dt\right| \\ &\leq \|\mu_{\Delta t,h}\|_{L_2(0,T;H^1(\Omega))}\|\mathcal{R}_h\xi - \xi\|_{L_2(0,T;H^1(\Omega))} + \left|\int_{\Omega_T} (\mu_{\Delta t,h} - \mu)\xi \, d\boldsymbol{x}dt\right|.\end{aligned}$$

The uniform a-priori estimates of the chemical potential taken from lemma 5.9 statement *(5)*, the approximation property in lemma 3.9 and the weak convergence of the chemical potential yield the convergence of this term.

We consider first for the right hand side the surface energy and insert zero in order to calculate

$$\begin{aligned}&\left|\int_{\Omega_T} \boldsymbol{\Gamma}\nabla_{\boldsymbol{x}} c_{\Delta t,h} \cdot \nabla_{\boldsymbol{x}}\mathcal{R}_h\xi - \boldsymbol{\Gamma}\nabla_{\boldsymbol{x}} c \cdot \nabla_{\boldsymbol{x}}\xi \, d\boldsymbol{x}dt\right| \\ &\quad= \left|\int_{\Omega_T} \boldsymbol{\Gamma}\nabla_{\boldsymbol{x}} c_{\Delta t,h} \cdot \nabla_{\boldsymbol{x}}(\mathcal{R}_h\xi - \xi) + \boldsymbol{\Gamma}\nabla_{\boldsymbol{x}}(c_{\Delta t,h} - c) \cdot \nabla_{\boldsymbol{x}}\xi \, d\boldsymbol{x}dt\right| \\ &\quad\leq C_\Gamma\|c_{\Delta t,h}\|_{L_2(0,T;H^1(\Omega))}\|\mathcal{R}_h\xi - \xi\|_{L_2(0,T;H^1(\Omega))} \\ &\qquad+ \left|\int_{\Omega_T} \boldsymbol{\Gamma}\nabla_{\boldsymbol{x}}(c_{\Delta t,h} - c) \cdot \nabla_{\boldsymbol{x}}\xi \, d\boldsymbol{x}dt\right|.\end{aligned}$$

The uniform a-priori estimate of the concentration field, see lemma 5.9, the approximation property in lemma 3.9 and the weak-$\star$ convergence of the concentration field imply the convergence of this term.

Moreover, we consider the convex part ψ^+ of the Gibbs free energy density ψ. By assumption (A-2) we have $\psi^+ \in C^2(\mathbb{R},\mathbb{R})$ together with the almost everywhere convergence of $c_{\Delta t,h}$ and $\xi_h = \mathcal{R}_h\xi$ we get

$$\psi^+_{,c}(c_{\Delta t,h}(t,\boldsymbol{x}))\xi_h(t,\boldsymbol{x}) \longrightarrow \psi^+_{,c}(c(t,\boldsymbol{x}))\xi(t,\boldsymbol{x}) \qquad \text{if} \qquad \Delta t, h \longrightarrow 0.$$

Furthermore, let $\epsilon > 0$ be arbitrary, we choose $\mathscr{E} \subset \Omega_T$ with the property $\mathrm{meas}(\mathscr{E}) \leq \epsilon$, use assumption (A-2) with $\delta = \epsilon$ and take into account lemma 5.9 statement *(4)* together with the $L_\infty(\Omega)$- stability of the Clement operator in order to calculate

$$\begin{aligned}\int_{\mathscr{E}} \psi_{,c}^+(c_{\Delta t,h})\mathcal{R}_h\xi \; d\boldsymbol{x}dt &\leq \int_{\mathscr{E}} (\delta\psi^+(c_{\Delta t,h}) + C_\delta)\mathcal{R}_h\xi \; d\boldsymbol{x}dt \\ &\leq \left(\delta \sup_{t\in(0,T)} \int_\Omega \psi^+(c_{\Delta t,h}) \; d\boldsymbol{x} + C_\delta \,\mathrm{meas}(\mathscr{E})\right) \|\xi\|_{L_\infty(\Omega)} \leq C\epsilon.\end{aligned}$$

In view of Vitali's convergence theorem 2.11 the convergence of this term follows.

The concave part ψ^- of the Gibbs free energy density is polynomial bounded due to assumption (A-2). By inserting zero, we calculate

$$\begin{aligned}&\left|\int_{\Omega_T} \psi_{,c}^-(c_{\Delta t,h}(t-\Delta t,\cdot))\mathcal{R}_h\xi - \psi_{,c}^-(c)\xi \; d\boldsymbol{x}dt\right| \\ &\quad\leq \left|\int_{\Omega_T} \psi_{,c}^-(c_{\Delta t,h}(t-\Delta t,\cdot))(\mathcal{R}_h\xi - \xi) \; d\boldsymbol{x}dt\right| \\ &\qquad + \left|\int_{\Omega_T} (\psi_{,c}^-(c_{\Delta t,h}(t-\Delta t,\cdot)) - \psi_{,c}^-(c))\xi \; d\boldsymbol{x}dt\right| \\ &\quad\leq C(\|c_{\Delta t,h}\|_{L_q(\Omega)}^{q-1} + 1)\|\mathcal{R}_h\xi - \xi\|_{H^1(\Omega)} \\ &\qquad + \left|\int_{\Omega_T} (\psi_{,c}^-(c_{\Delta t,h}(t-\Delta t,\cdot)) - \psi_{,c}^-(c))\xi \; d\boldsymbol{x}dt\right|.\end{aligned}$$

The uniform a-priori estimate of the concentration in lemma 5.9 together with the approximation property in lemma 3.9, the almost everywhere continuity of the concentration field with respect to time and Lebesgue's convergence theorem yield the convergence of this term.

For the mechanical contribution to the chemical potential we first remark that due to the almost everywhere convergence of the concentration field and the continuity of the deformation with respect to time it follows

$$W_{,c}(c_{\Delta t,h}(t,\boldsymbol{x}), \boldsymbol{\varepsilon}(\boldsymbol{u}_{\Delta t,h}(t-\Delta t,\boldsymbol{x})))\mathcal{R}_h\xi \longrightarrow W_{,c}(c(t,\boldsymbol{x}), \boldsymbol{\varepsilon}(\boldsymbol{u}(t,\boldsymbol{x})))\xi \qquad \text{if} \quad \Delta t, h \longrightarrow 0.$$

Taking into account the assumptions (A-6), (A-7) and the uniform a-priori estimate of the Clement operator in $L_\infty(\Omega)$, see lemma 3.7, we estimate the elastic contribution of the chemical potential by

$$\begin{aligned}&W_{,c}(c_{\Delta t,h}(t,\boldsymbol{x}), \boldsymbol{\varepsilon}(\boldsymbol{u}_{\Delta t,h}(t-\Delta t,\boldsymbol{x})))\mathcal{R}_h\xi \\ &\quad\leq C(|\boldsymbol{\varepsilon}(\boldsymbol{u}_{\Delta t,h}(t-\Delta t,\boldsymbol{x}))|^2 + 1)\|\mathcal{R}_h\xi\|_{L_\infty(\Omega)} \\ &\quad\leq C(|\boldsymbol{\varepsilon}(\boldsymbol{u}_{\Delta t,h}(t-\Delta t,\boldsymbol{x}))|^2 + 1)\|\xi\|_{L_\infty(\Omega)}.\end{aligned}$$

The strong convergence of the displacement proved in lemma 5.11 together with the generalised Lebesgue convergence theorem 2.10 yield the convergence of the mechanical contribution to the chemical potential.

Step 3: Finally, the convergence of the displacement $\boldsymbol{u}_{\Delta t,h}$ follows from lemma 5.11. This argument finishes the whole convergence proof of the operator-splitting method. □

5.4 Numerical solution of the Euler-Lagrange equations

The approximation method stabilised with a decomposed Gibbs free energy leads to a non-linear equation system, which must be solved in every time step $t_n = n\Delta t$ with $1 \leq n \leq N$. This non-linear equation system follows from (5.3) and (5.4) having the form

$$\underline{\boldsymbol{A}}(\underline{\boldsymbol{c}}^n - \underline{\boldsymbol{c}}^{n-1}) + \Delta t \underline{\boldsymbol{M}}^n \underline{\boldsymbol{\mu}}^n = \underline{\boldsymbol{0}}, \tag{5.14}$$

$$-\underline{\boldsymbol{G}}(\underline{\boldsymbol{c}}^n, \underline{\boldsymbol{c}}^{n-1}, \boldsymbol{u}^{n-1}) + \underline{\boldsymbol{A}}\underline{\boldsymbol{\mu}}^n = \underline{\boldsymbol{0}}. \tag{5.15}$$

In this non-linear equation system the unknown quantities are $\underline{\boldsymbol{c}}^n$ and $\underline{\boldsymbol{\mu}}^n$, whereas the vectors $\underline{\boldsymbol{c}}^{n-1}$ and $\underline{\boldsymbol{u}}^{n-1}$ are known from the previous time step. The matrices $\underline{\boldsymbol{A}}$ and $\underline{\boldsymbol{M}}^n$ as well as the vector valued function $\underline{\boldsymbol{G}}(\underline{\boldsymbol{c}}^n, \underline{\boldsymbol{c}}^{n-1}, \underline{\boldsymbol{u}}^{n-1})$ are calculated by

$$\begin{aligned}
\underline{\boldsymbol{A}}[\boldsymbol{y}, \boldsymbol{z}] &:= \int_\Omega \varphi_{\boldsymbol{y}} \varphi_{\boldsymbol{z}} \, d\boldsymbol{x}, \\
\underline{\boldsymbol{M}}^n[\boldsymbol{y}, \boldsymbol{z}] &:= \int_\Omega \boldsymbol{M}(c_h^{n-1}) \nabla_{\boldsymbol{x}} \varphi_{\boldsymbol{y}} \cdot \nabla_{\boldsymbol{x}} \varphi_{\boldsymbol{z}} \, d\boldsymbol{x}, \\
\underline{\boldsymbol{G}}(\underline{\boldsymbol{c}}^n, \underline{\boldsymbol{c}}^{n-1}, \underline{\boldsymbol{u}}^{n-1})[\boldsymbol{z}] &:= \int_\Omega \boldsymbol{\Gamma} \nabla_{\boldsymbol{x}} c_h^n \cdot \nabla_{\boldsymbol{x}} \varphi_{\boldsymbol{z}} + \psi_{,c}^+(c_h^n) \varphi_{\boldsymbol{z}} + \psi_{,c}^-(c_h^{n-1}) \varphi_{\boldsymbol{z}} \\
&\qquad + W_{,c}(c_h^n, \boldsymbol{\varepsilon}(\boldsymbol{u}_h^{n-1})) \varphi_{\boldsymbol{z}} \, d\boldsymbol{x}.
\end{aligned}$$

Obviously all integrals in this equation system exist due to the assumptions (A-1) - (A-8) and the non-linearity only appears in the vector valued function $\underline{\boldsymbol{G}}$ in the concentration field $\underline{\boldsymbol{c}}$. We apply Newton's method, see [88] in order to compute a solution of the equation system (5.14), (5.15).

Algorithm 5.13 (Newton method).

// Initial vectors:

$\underline{\boldsymbol{c}}_0^n = \underline{\boldsymbol{c}}^{n-1}$

$\underline{\boldsymbol{\mu}}_0^n = \underline{\boldsymbol{\mu}}^{n-1}$

// Initial residuum:
$\underline{\boldsymbol{q}}_0 = -\Delta t \underline{\boldsymbol{M}}^n \underline{\boldsymbol{\mu}}_0^n$
$\underline{\boldsymbol{r}}_0 = \underline{\boldsymbol{G}}(\underline{\boldsymbol{c}}_0^n, \underline{\boldsymbol{c}}^{n-1}, \underline{\boldsymbol{u}}^{n-1}) - \underline{\boldsymbol{A}}\underline{\boldsymbol{\mu}}_0^n$
if $\sqrt{\|\underline{\boldsymbol{q}}_0\|^2 + \|\underline{\boldsymbol{r}}_0\|^2} \leq TOL$ ***then***
  $\underline{\boldsymbol{c}}^n = \underline{\boldsymbol{c}}_0^n$
  $\underline{\boldsymbol{\mu}}^n = \underline{\boldsymbol{\mu}}_0^n$
  return
end if

// Newton iteration:
for $k = 1$ *to* $MaxIterations$ ***do***
  Solve*:*

$$\underline{\boldsymbol{A}}\underline{\boldsymbol{z}}_k + \Delta t \underline{\boldsymbol{M}}^n \underline{\boldsymbol{w}}_k = \underline{\boldsymbol{q}}_{k-1} \tag{5.16}$$

$$-\mathrm{D}_c \underline{\boldsymbol{G}}(\underline{\boldsymbol{c}}_{k-1}^n, \underline{\boldsymbol{c}}^{n-1}, \underline{\boldsymbol{u}}^{n-1})\underline{\boldsymbol{z}}_k + \underline{\boldsymbol{A}}\underline{\boldsymbol{w}}_k = \underline{\boldsymbol{r}}_{k-1} \tag{5.17}$$

  // Update:
  $\underline{\boldsymbol{c}}_k^n = \underline{\boldsymbol{c}}_{k-1}^n + \underline{\boldsymbol{z}}_k$
  $\underline{\boldsymbol{\mu}}_k^n = \underline{\boldsymbol{\mu}}_{k-1}^n + \underline{\boldsymbol{w}}_k$

  // Compute residuum:
  $\underline{\boldsymbol{q}}_k = \underline{\boldsymbol{A}}(\underline{\boldsymbol{c}}^{n-1} - \underline{\boldsymbol{c}}_k^n) - \Delta t \underline{\boldsymbol{M}}^n \underline{\boldsymbol{\mu}}_k^n$
  $\underline{\boldsymbol{r}}_k = \underline{\boldsymbol{G}}(\underline{\boldsymbol{c}}_k^n, \underline{\boldsymbol{c}}^{n-1}, \underline{\boldsymbol{u}}^{n-1}) - \underline{\boldsymbol{A}}\underline{\boldsymbol{\mu}}_k^n$

  if $\sqrt{\|\underline{\boldsymbol{q}}_k\|^2 + \|\underline{\boldsymbol{r}}_k\|^2} / \sqrt{\|\underline{\boldsymbol{q}}_0\|^2 + \|\underline{\boldsymbol{r}}_0\|^2} \leq TOL$ ***then***
    $\underline{\boldsymbol{c}}^n = \underline{\boldsymbol{c}}_k^n$
    $\underline{\boldsymbol{\mu}}^n = \underline{\boldsymbol{\mu}}_k^n$
    return
  end if
end for

In the algorithm 5.13 we have to solve the LES (5.16) and (5.17) corresponding to the linearisation, which is done in Newton's method. We have to analyse this system in order to compute a unique solution.

Lemma 5.14. *Let $\Omega \subset \mathbb{R}^d$ be a domain satisfying condition (H-1). Furthermore, let the assumptions (A-1) - (A-8) be satisfied. Moreover, let $\mathscr{T}_h(\Omega)$ be an admissible, exact and uniform triangulation of the reference domain Ω. If the time discretisation satisfies the condition*

$$\Delta t \leq \frac{c_\Gamma h^{2d}}{2C_M (C_{W,cc})^2},$$

then the LES (5.16) *and* (5.17) *within the Newton method has a unique solution* $\underline{\boldsymbol{z}}_k$ *and* $\underline{\boldsymbol{w}}_k$.

Proof. We eliminate the first equation, since $\underline{\boldsymbol{M}}^n$ is invertible due to the fact that the operator $\mathcal{M}_h^n$ is $X_0(\Omega)$-elliptic, see lemma 4.5. We therefore get

$$\underline{\boldsymbol{w}}_k = -\frac{1}{\Delta t}(\underline{\boldsymbol{M}}^n)^{-1}\underline{\boldsymbol{A}}\underline{\boldsymbol{z}}_k + \frac{1}{\Delta t}(\underline{\boldsymbol{M}}^n)^{-1}\underline{\boldsymbol{q}}_{k-1}).$$

By inserting this representation of $\underline{\boldsymbol{w}}_k$ into the second equation we get a LES for the update vector $\underline{\boldsymbol{z}}_k$.

$$\left(\mathrm{D}_c\,\underline{\boldsymbol{G}}(\underline{\boldsymbol{c}}_{k-1}^n, \underline{\boldsymbol{c}}^{n-1}, \underline{\boldsymbol{u}}^{n-1}) + \frac{1}{\Delta t}\underline{\boldsymbol{A}}(\underline{\boldsymbol{M}}^n)^{-1}\underline{\boldsymbol{A}}\right)\underline{\boldsymbol{z}}_k = \frac{1}{\Delta t}(\underline{\boldsymbol{M}}^n)^{-1}\underline{\boldsymbol{q}}_{k-1} - \underline{\boldsymbol{r}}_{k-1}$$

For any coefficient vector $\underline{\boldsymbol{\xi}} \in \mathbb{R}^{\sharp\mathcal{N}_h(\Omega)}$ we get the following integral formulation in order to prove the positive definiteness by using the Poincaré inequality and the global inverse inequality,

$$\begin{aligned}
&\left(\mathrm{D}_c\,\underline{\boldsymbol{G}}(\underline{\boldsymbol{c}}_{k-1}^n, \underline{\boldsymbol{c}}^{n-1}, \underline{\boldsymbol{u}}^{n-1}) + \frac{1}{\Delta t}\underline{\boldsymbol{A}}(\underline{\boldsymbol{M}}^n)^{-1}\underline{\boldsymbol{A}}\right)\underline{\boldsymbol{\xi}}\cdot\underline{\boldsymbol{\xi}} \\
&\quad= \int_\Omega \boldsymbol{\Gamma}\nabla_{\boldsymbol{x}}\xi_h\cdot\nabla_{\boldsymbol{x}}\xi_h + \psi_{,cc}(c_{k,h}^n)\xi_h^2 + W_{,cc}(c_{k,h}^n, \boldsymbol{\varepsilon}(\boldsymbol{u}_h^{n-1}))\xi_h^2\,d\boldsymbol{x} + \frac{1}{\Delta t}\|\xi_h\|_{\mathcal{M}_h^n}^2 \\
&\quad\geq c_\Gamma|\xi_h|_{H^1(\Omega)}^2 - C_{W,cc}\frac{1}{h^d}\|\xi\|_{L_2(\Omega)}^2 + \frac{1}{\Delta t}\|\xi_h\|_{\mathcal{M}_h^n}^2 \\
&\quad\geq c_\Gamma|\xi_h|_{H^1(\Omega)}^2 - C_{W,cc}\frac{1}{h^d}\left(\delta|\xi_h|_{H^1(\Omega)}^2 + \frac{C_M}{\delta}\|\xi_h\|_{\mathcal{M}_h^n}^2\right) + \frac{1}{\Delta t}\|\xi_h\|_{\mathcal{M}_h^n}^2 \\
&\quad\geq \frac{c_\Gamma}{2}|\xi_h|_{H^1(\Omega)}^2 + \left(\frac{1}{\Delta t} - \frac{2(C_{W,cc})^2C_M}{h^{2d}}\right)\|\xi_h\|_{\mathcal{M}_h^n}^2.
\end{aligned}$$

The positive definiteness of the matrix $(\mathrm{D}_c\,\underline{\boldsymbol{G}}(\underline{\boldsymbol{c}}_{k-1}^n, \underline{\boldsymbol{u}}^{n-1}) + \frac{1}{\Delta t}\underline{\boldsymbol{H}}_\gamma(\underline{\boldsymbol{M}}^n)^{-1}\underline{\boldsymbol{A}})$ follows by the same arguments as in lemma 4.31. □

Remark 5.15. If the elasticity tensor is constant, a weaker constraint on the time discretisation ensures the unique solvability of the LES in the Newton method,

$$\Delta t \leq \frac{c_\Gamma h^d}{2C_M(C_{\psi,cc}^-)^2}.$$

In the numerical simulation the LES is solved iteratively either by the BiCGStab method [98] or the GMRes method [87]. Both methods work quite well in this situation and we observe no important differences. The LES is preconditioned by the BPX method, see [17], which improves the iterative process essentially.

Chapter 6

Numerical simulations and results

In this chapter we focus on the numerical simulation of the spinodal decomposition in eutectic solder. A Sn-Pb alloy is used as an example taking the corresponding material parameter from [33, 73]. The first chapter shows that the surface stress tensor $\mathbf{\Gamma}$ is extremely small in the case of a Sn-Pb alloy. In this situation the Gibbs phenomena is observed, which shows large overshoots and undershoots along diffusive phase interfaces.

In the previous chapters we realised three different numerical approximation methods for the Cahn-Larché system, which are stable, as these methods avoid high frequent contributions to the concentration field along phase interfaces.

The numerical simulation of the spinodal decomposition of eutectic alloys has the following purpose: First of all we want to analyse the influence of changing boundary conditions of the displacement on the development of the Sn-rich and Pb-rich phase. For linear elasticity with a constant elasticity tensor, it is a known result that stress singularities appear in a point with changing boundary conditions. For a detailed theory of calculating stress singularities we refer to [53, 67, 65]. These stress singularities induce locally large contributions to the chemical potential, which directly affect the evolution of the microstructure. The microstructure itself gives information about strength and reliability of the solder joint.

The geometry of the solder joint has an influence on the behaviour of the microstructure. In linear elasticity theory it is also known that stress singularities develop in a reentrant corner. Moreover, if in a reentrant corner additionally the boundary conditions change, the stress singularity becomes much larger, see [53, 67, 65] and the influence on the diffusion process is more significant.

These geometrical influences and changing boundary conditions are simulated under different types of loading. We consider the evolution of the microstructure if the solder joint is subjected to pure pressure, tensile and shear boundary loadings and compare the results with pure temperature loading. We have to emphasise that the temperature enters our model as a parameter only. These loadings are typical

for a solder joint, which is part of a PCB.

The numerical simulations of the spinodal decomposition of an alloy are restricted on a small RVE only. This follows from the fact that we have to resolve the diffusive phase interface properly by the finite element mesh enlarging the computational complexity essentially. Thus we focus on different parts of a solder joint with various boundary loadings.

Since we have to choose the time discretisation in the same range as the mesh size, the simulations cover only a small time range. In order to simulate the long time behaviour of the coarsening within the alloy, other models like sharp interface models must be used. The results of this computations can be used as initial data for long time simulations.

In this chapter we also compare the Cahn-Larché system with a constant and a concentration depending elasticity tensor. Simulations with a constant elasticity tensor are easier to realise and it would be very efficient to apply this model to solder. But an important result of this chapter is, that for solder the Cahn-Larché model with a constant elasticity tensor does not fit with experimental investigations. In contrast to this result, we observe that the Cahn-Larché model with a concentration depending elasticity tensor fits qualitatively well with the experiments.

This chapter is organised as follows: In section 6.1 we discuss some basic concepts of the numerical simulation. The software components and the software environment are discussed, which are used for the following simulations. Additionally we make some remarks about the implementation of the stabilised numerical approximation methods from chapter four and chapter five. The section ends with the presentation of the material data used in the following computations and different domains with the corresponding mesh hierarchies.

The first simulation example is demonstrated in section 6.2. Here we deal with the Cahn-Hilliard equations only, which means that we neglect elastic effects. This example is chosen in order to show the stability of the above mentioned methods. Furthermore the influence of the anisotropy of the surface stress tensor is demonstrated.

The second bundle of numerical simulations deals with the Cahn-Larché system having a constant elasticity tensor. In section 6.3 we only use the viscous method stabilised by driving forces, which is presented in section 4.2. Different types of loading, like heating and pressure are analysed and compared.

In section 6.4 we demonstrate the numerical simulations of the Cahn-Larché system with concentration depending elasticity tensors. We simulate heating, pressure and shear loads of the configuration. Finally, we observe a L-shape domain and consider the influence of a reentrant corner with changing boundary conditions on the microstructure.

6.1 Basic concepts

6.1.1 Remarks to the implementation

In general the numerical simulation of stationary or time dependent processes can be divided into three independent tasks:

- mesh generation and description of boundary loadings
- computation of a discrete solution and of additional physical quantities
- visualisation of all data

We present simulations in two space dimensions only. For that reason we deal with meshes consisting of triangles. The finite element meshes used for the numerical simulation are generated by the command line program *Triangle* written by J. R. Shewchuk. This meshing tool is freely available from [89].

Triangle is a program for two-dimensional mesh generation and construction of Delaunay triangulation, constrained Delaunay triangulation and Voronoï diagrams. Guaranteed-quality meshes, which satisfy the angle condition respectively the shape regularity condition are generated by using Ruppert's Delaunay refinement algorithm. We have to remark that *Triangle* is a fast, memory-efficient and robust meshing tool. For more details about the implementation and the used algorithms, we refer to [90] and the references in there.

Triangle's input is a planar straight line graph (PSLG), which defines the boundary of the computational domain. The PSLG format contains a collection of nodes, laying on the boundary, having a marker, which specifies the boundary condition (Neumann or Dirichlet node). An additional feature is the optional formulation of user-specified attributes, which e.g. describe material parameters and boundary loadings.

The second part of the PSLG format contains the collection of segments, describing the boundary. The segments have a start- and an endpoint, where an additional marker specifies the boundary condition of the segment. In PSLG holes are explicitly marked by an auxiliary point inside the hole. Furthermore user-specified constraints on angles and triangle areas can be formulated.

The second task of the simulation contains the numerical computation of a discrete solution of the Cahn-Larché system. For this purpose we write several command line C++ programs, which compute a numerical solution of the Cahn-Hilliard and Cahn-Larché system using the viscous methods from chapter four and the operator-spitting technique from chapter five.

The simulation programs are written in C++ and base on my personal finite element library *MyFEM++*. This finite element library adapts important administrative tools, which are necessary in finite element simulation. First of all, it manages

the finite element mesh. This means that *MyFEM++* provides an instream for reading meshes generated e.g. by *Triangle* and builds up a mesh hierarchy for using multigrid techniques like BPX.

Moreover, the administrative tasks also contain the scheduling of the degree of freedoms (DoF) for all fields, which are involved in a multifield problem like the Cahn-Larché system. *MyFEM++* provides additional linear algebra classes (LAC), which implement matrix vector computations and different iterative solvers for LES. From the various iterative solvers we use CG, BiCGStab and GMRes. Finally, outstreams to different file formats of visualisation tools are available.

The simulation programs are organised in three parts. After an initialising procedure, where the mesh is read, the multigrid hierarchy is built up and the DoF are distributed, the preprocessing procedure starts. In this program segment the $L_2(\Omega)$-projection of the initial data given by definition 3.10 is computed. Furthermore, by solving the linear problem 3.14 the computations of the initial displacement and the computation of the chemical potential are done.

The main part of the program contains of a loop over all time steps $1 \leq n \leq N$. In this program segment the concentration field c_h^n and the chemical potential μ_h^n are computed by Newton's method corresponding to the respective method, which is either a viscous method from chapter four or an operator-splitting technique from chapter five.

In each time step $1 \leq n \leq N$ there is a postprocessing procedure, where the displacement $\boldsymbol{u}_h^n$ corresponding to the concentration c_h^n is computed by solving the linear problem 3.14. Due to physical reasons, we additionally determine the mechanical stress $\boldsymbol{\sigma}_h^n = \boldsymbol{C}(c_h^n)\boldsymbol{\varepsilon}(\boldsymbol{u}_h^n)$ and the diffusive flux $\boldsymbol{J}_h^n = -\boldsymbol{M}(c_h^{n-1})\nabla_{\boldsymbol{x}}\mu_h^n$ in this part of the program. Moreover, energy and dissipation are also computed here.

At regular intervals the solution is saved in the unstructured grid format (.vtu) of the *Visualisation Toolkit* (VTK). VTK is a freely available C++ library for the visualisation of extremely large data and for the documentation we refer to [8, 64].

The third task of the simulation process is the visualisation of the computed data. For this purpose we apply the program *ParaView*. This tool bases on VTK and provides an excellent access to VTK's visualisation tools and techniques by a graphical users interface. *ParaView* is also freely available from [63].

Naturally, we apply *GNUPlot* in order to visualise scalar valued data like energy and dissipation. *GNUPlot* is free software, which can be downloaded from [103].

6.1.2 General setting of the simulations

The following simulations are performed in a situation where the crystallographic and the laboratory coordinate system are identical. It is not possible to simulate the whole solder joint due to computational complexity. For this reason we perform the

numerical simulations in a RVE, which is part of the solder joint.

Fig. 6.1(a) illustrates a cross-section cut through a solder joint. Here a pin of some electronic device is connected with the PBC by a solder bump. We consider two types of RVEs corresponding to different boundary parts as demonstrated in fig. 6.1(a).

In the first case a quadrangle with side length of $2\mu m$ is considered. If mechanical effects are simulated additionally, this domain is hard clamped at one side, describing the Dirichlet boundary part. The remaining boundary denotes the Neumann part, whereas the different loadings are described later on for the individual examples. The coarse grid of this RVE is shown in fig. 6.1(b) and the corresponding mesh hierarchy is outlined in tab. 6.1, which is used for the BPX preconditioner. In the second

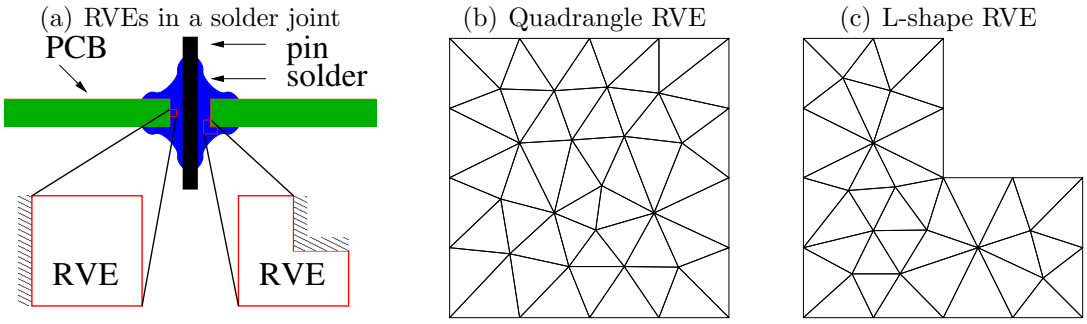

Fig. 6.1: Computational domains

case a RVE is considered having a L-shape form, which is located in the solder joint as demonstrated in fig. 6.1. The Dirichlet boundary is located at the upper right segment of the L-shape and the remaining boundary parts belong to the Neumann boundary. In this situation we have changing boundary conditions in the reentrant corner of the L-shape. In fig. 6.1(c) the coarse grid of the L-shape is outlined and in tab. 6.2 the corresponding mesh hierarchy used for the BPX preconditioner is given.

Level	Nodes	Cells	DoF c_h^n	DoF μ_h^n	DoF $\boldsymbol{u}_h^n$	h
0	33	48	33	33	56	0.365718
1	113	192	113	113	208	0.182859
2	417	768	417	417	800	0.0914296
3	1601	3072	1601	1601	3136	0.0457148
4	6273	12288	6273	6273	12416	0.0228574
5	24833	49152	24833	24833	49408	0.0114287
6	98817	196608	98817	98817	197120	0.00571435
7	394241	786432	394241	394241	787456	0.00285718

Tab. 6.1: Mesh hierarchy of the quadrangle RVE

Level	Nodes	Cells	DoF c_h^n	DoF μ_h^n	DoF $\boldsymbol{u}_h^n$	h
0	28	38	28	28	50	0.353553
1	93	152	93	93	176	0.176777
2	337	608	337	337	656	0.0883883
3	1281	2432	1281	1281	2528	0.0441942
4	4993	9728	4993	4993	9920	0.0220971
5	19713	38912	19713	19713	39296	0.0110485
6	78337	155648	78337	78337	156416	0.00552427
7	312321	622592	312321	312321	624128	0.00276214

Tab. 6.2: Mesh hierarchy of the L-shape RVE

6.2 Cahn-Hilliard example

In this section we present a simulation of the spinodal decomposition without elastic effects. This model is described by the Cahn-Hilliard equation, which simply follows from the Cahn-Larché system neglecting the mechanical contributions.

Setting

The computational domain Ω consists of a quadrangle with side length $2\mu m$. For the unknown fields, concentration $c_{\Delta t,h}$ and chemical potential $\mu_{\Delta t,h}$, we set homogeneous Neumann boundary conditions on all boundary parts of the domain Ω. This means that no material flux across the boundary is observed and the boundary does not affect the phase separation process.

This example is computed with all three numerical methods presented in the previous chapters. The friction coefficient, which is used for stabilisation in the viscous methods of chapter four is chosen to be $\gamma \approx \sqrt{h}$ and the time discretisation takes the value $\Delta t = 2.8s$.

We set the necessary material parameters to the values corresponding the temperature $\theta = 125°C$. The initial data consist of approximately 600 Pb-particles randomisely distributed with a particle diameter of $0.015\mu m$. The first picture of fig.6.3(a) shows the initial condition c_0. Here red coloured regions denote the Sn-rich phase in contrast to blue coloured regions, which denote the Pb-rich phase building the particles in the Sn-matrix.

Results

In fig. 6.3(a)-(d) the computations of the concentration field $c_{\Delta t,h}$ and of the chemical potential $\mu_{\Delta t,h}$ are presented. The evolution of the concentration field $c_{\Delta t,h}$ is demonstrated in fig. 6.3(a)+(b) printed in increasing time. It is obvious to see that the configuration starts to coarsen in order to reduce energy. Small particles with a large interface curvature shrink and blow up the large particle having a small interface curvature. Due to this process the system reduces energy, which can also be seen in fig. 6.2(a), where the energy is plotted over time. In fig. 6.2(a) the energy decreases with respect to time. This fact demonstrates well the Lyapunov property.

In fig. 6.2(b) the dissipation of the system is presented. For the Cahn-Hilliard model dissipation is related to diffusion and in the viscous case additionally to friction. It can be seen that in the beginning of the spinodal decomposition more and more energy is dissipated, which means that a lot of small Pb-particles vanish, see fig. 6.3(a). In a later state of the coarsening process the dissipation goes more and more to zero and we observe in fig. 6.3(b) only a small amount of diffusion. This is clear, because at this time of the process only large particles are left.

The influence of anisotropic surface stress tensor on the spinodal decomposition can also be seen in fig.6.3(a)+(b). The particles grow much faster in y-direction, the marked direction of the anisotropic surface stress tensor.

In fig. 6.3(c)+(d) the diffusive flux $\boldsymbol{J}_{\Delta t,h}$ of the evolution is shown. The visualisation of the diffusive flux is complicated, because it slows down with respect to time and therefore a fix colouring may be not the best choice. In the first picture of fig. 6.3(c) it is obvious to see that the largest diffusive flux occurs in the interface. More precisely it is large in y-direction compared to the x-direction, which is also an influence of the anisotropic surface stress tensor.

6.3 Cahn-Larché equation with constant elasticity tensor

In this section we carry out numerical simulations of the spinodal decomposition considering elastic effects with a constant elasticity tensor. Numerical simulations

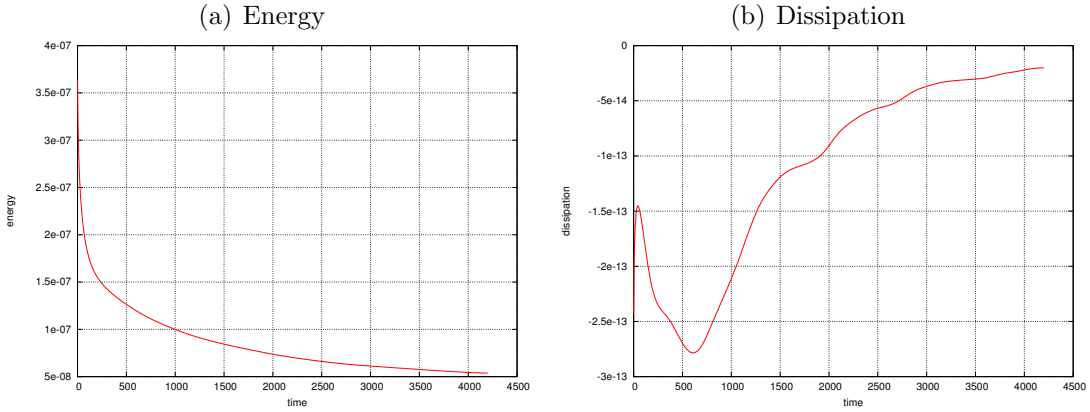

Fig. 6.2: Energy and dissipation of spinodal decomposition without elastic effects

with a constant elasticity tensor are much simpler to realise, compared to those of a concentration depending one. We make these computations in order to compare both material models. Finally, we are able to decide which material model of a solder alloy fits better to experimental observation, at least qualitatively. In section 6.3 we use the following averaged elasticity tensor

$$\boldsymbol{C} := c_{eut}\boldsymbol{C}^{\alpha} + (1 - c_{eut})\boldsymbol{C}^{\beta}.$$

6.3.1 Heating

The first numerical example simulates the heating of an alloy.

Setting

In this computation the unknowns are the concentration field $c_{\Delta t,h}$, the chemical potential $\mu_{\Delta t,h}$ and the displacement $\boldsymbol{u}_{\Delta t,h}$. We take the quadratic domain Ω with side length $2\mu m$. In fig. 6.4 the boundary conditions and the loading of the configuration are outlined. The part of the solder joint is hard clamped at the bottom indicating the Dirichlet boundary of the displacement $\boldsymbol{u}_{\Delta t,h}$ and on the remaining boundary homogeneous Neumann data for the displacement are observed. The loading of the configuration arises from heating by $\Delta\theta = 50°K$. Since the reference temperature is $\theta_{ref} = 20°C$, we have an actual temperature of $\theta = 70°C$ and the material parameters are interpolated to this temperature value.

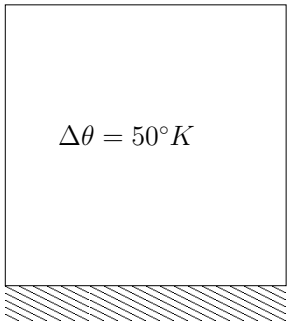

Fig. 6.4: Loading of a RVE

(a) Concentration c_h, at $t = 0.0s$, $t = 840s$ and $t = 1680s$

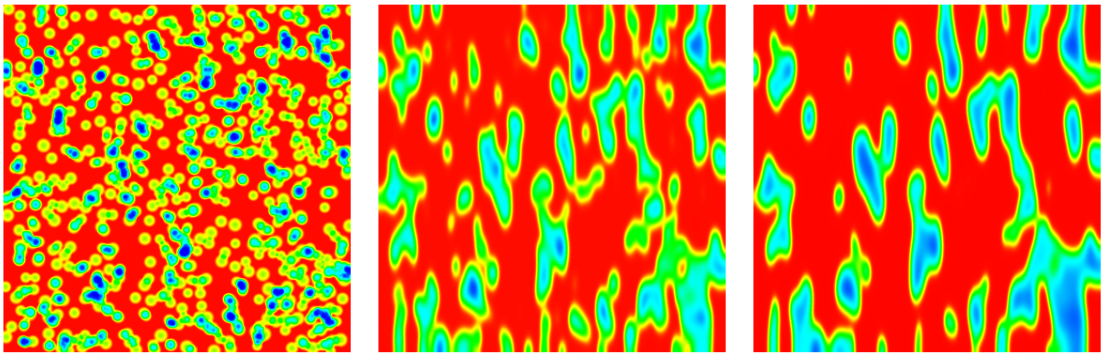

(b) Concentration c_h, at $t = 2520s$, $t = 3360s$ and $t = 4256s$

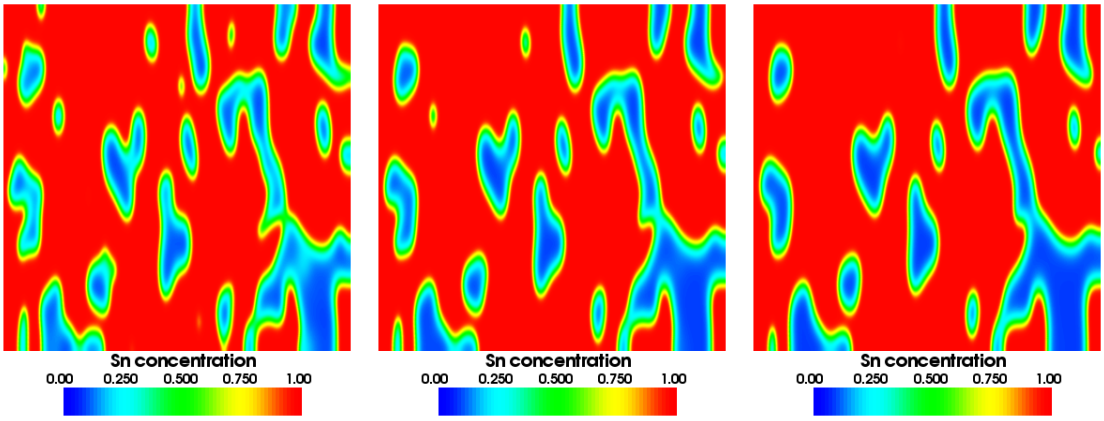

(c) Concentration $\boldsymbol{J}_h$, at $t = 0.0s$, $t = 840s$ and $t = 1680s$

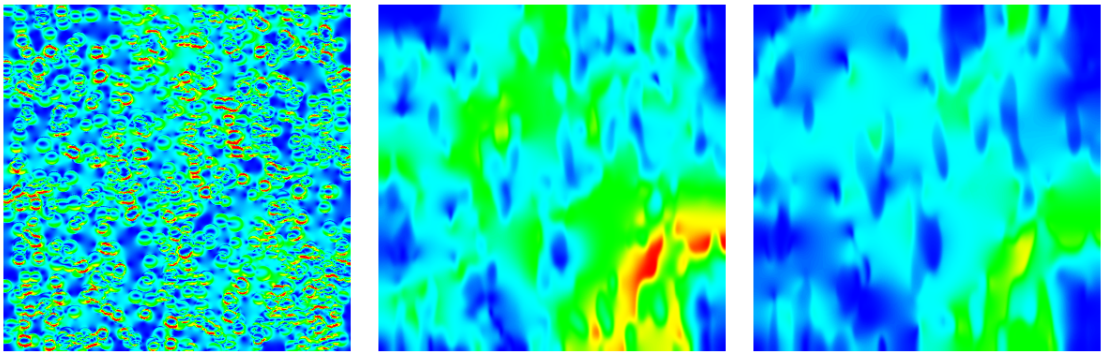

(d) Concentration $\boldsymbol{J}_h$, at $t = 2520s$, $t = 3360s$ and $t = 4256s$

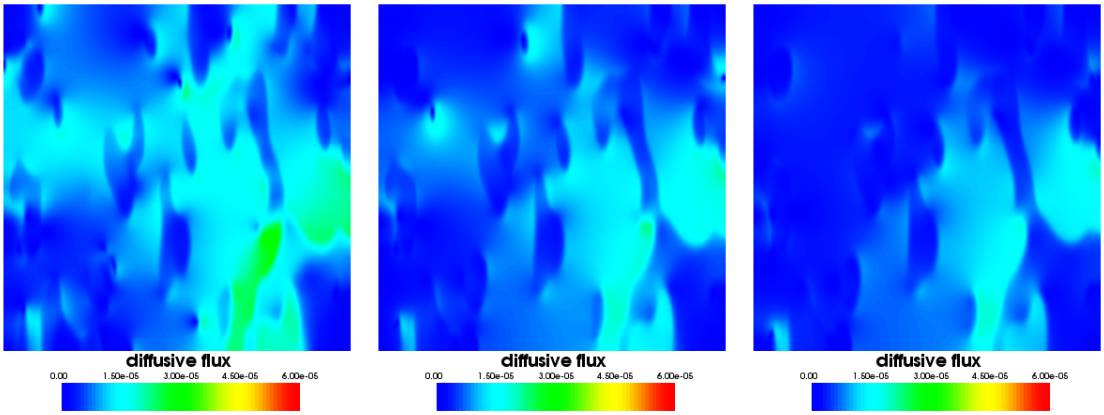

Fig. 6.3: Simulation of the Cahn-Hilliard equation

At the lower left and right corner of the quadrangle we observe changing boundary conditions and due to this fact mechanical stress singularities occur at this points.

The concentration field $c_{\Delta t,h}$ and the chemical potential $\mu_{\Delta t,h}$ undergo homogeneous Neumann conditions on the whole boundary. Therefore no material flux across the boundary is observed and the boundary does not affect the spinodal decomposition. The initial data c_0 consists of approximately 600 Pb-particles in a Sn-matrix, which are randomisely distributed having a diameter of $0.015\mu m$. The initial state c_0 is shown in the first picture of fig. 6.7(a).

Results

The concentration field $c_{\Delta t,h}$, the diffusive flux $\boldsymbol{J}_{\Delta t,h}$ and the mechanical stress $\boldsymbol{\sigma}_{\Delta t,h}$ are shown in fig. 6.7(a)-(d). We see a spinodal decomposition, which is extremely dominated by mechanical contributions to the chemical potential. The Pb-particles near to the hard clamped boundary part, where the mechanical stress is smaller compared to the remaining domain, shrink very fast and diffuse away from the Dirichlet boundary.

A crucial point in this simulation is the fact that in the lower left and right corner points, where mechanical stress singularities occur, a Pb-rich phase develops. This phenomena can be seen in fig. 6.7(a)-(d) by following the development of the concentration in the first picture. Pb is softer than Sn and the evolution of a Pb-rich phase in points with stress singularities reduces these large stresses essentially.

In fig. 6.5(a) the energy of the spinodal decomposition with heating is given over time. It is obvious to see that the energy increases with respect to time and this result demonstrates the Lyapunov property for the Cahn-Larché system with constant elasticity tensor.

In fig. 6.5(b) the dissipation is plotted over time. We observe that with respect to time the dissipation tends to zero, which results in the fact that the diffusion slows down more and more.

The important question is, whether this numerical simulation fits to experimental investigations. In fig. 6.6 we compare the experiment with the numerical simulation at a boundary part, which is hard clamped. Obviously we can see in fig. 6.6 that no particles diffuse away from the Dirichlet boundary in the experiment. This fact demonstrates impressively that the Cahn-Larché system with constant elasticity tensor is not the correct model in order to simulate spinodal decomposition in a Sn-Pb alloy.

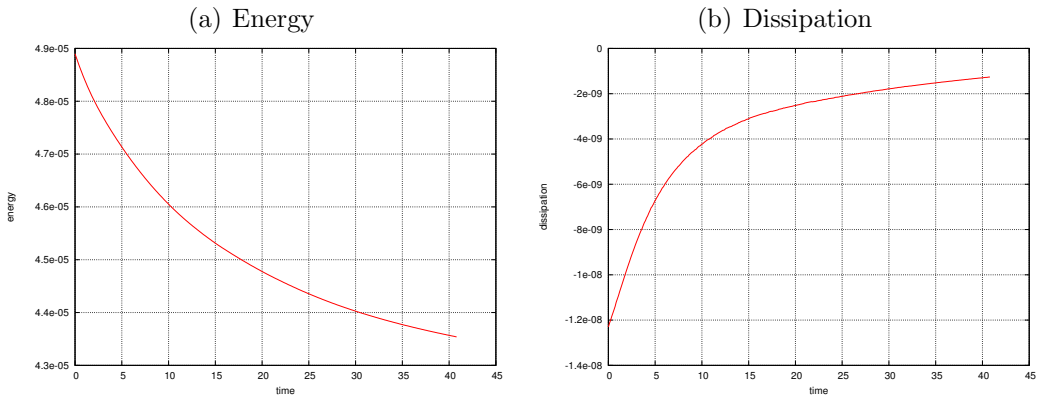

Fig. 6.5: Energy and dissipation of spinodal decomposition with heating

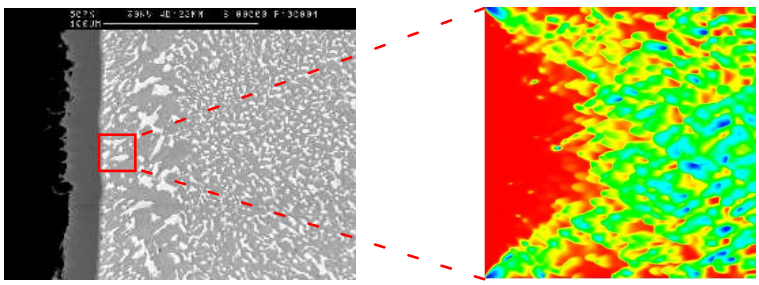

Fig. 6.6: Comparison of experiment and simulation

(a) Concentration c_h, diffusive flux $\boldsymbol{J}_h$ and stress $\boldsymbol{\sigma}_h$ at $t = 0.0s$

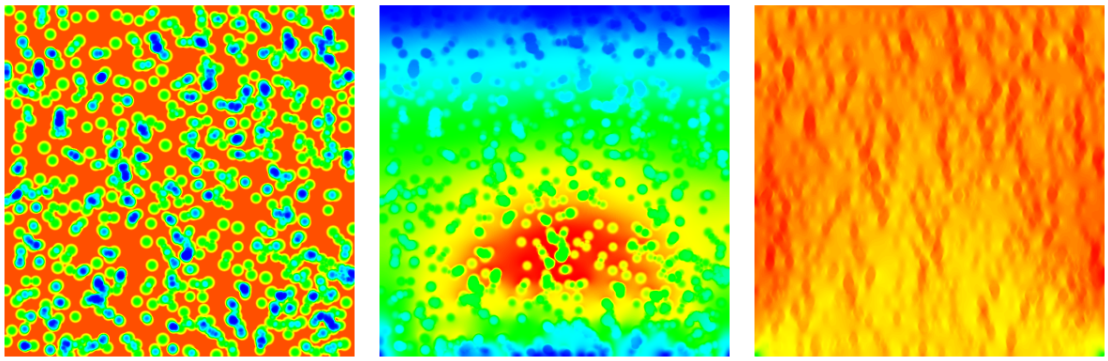

(b) Concentration c_h, diffusive flux $\boldsymbol{J}_h$ and stress $\boldsymbol{\sigma}_h$ at $t = 13.2s$

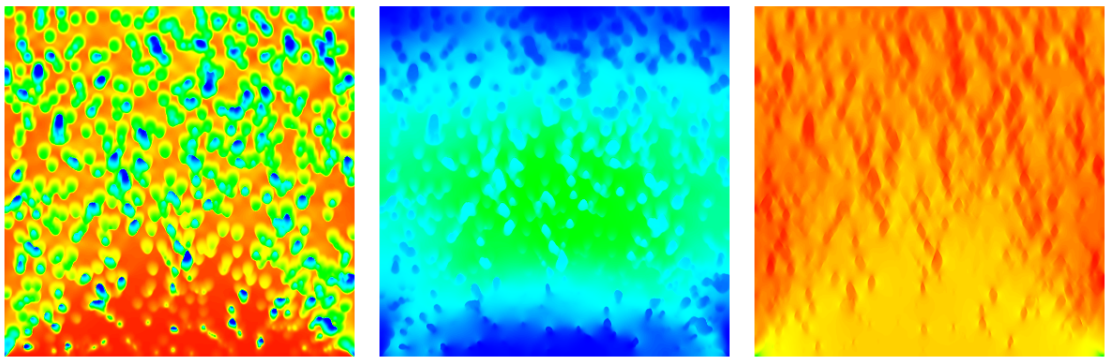

(c) Concentration c_h, diffusive flux $\boldsymbol{J}_h$ and stress $\boldsymbol{\sigma}_h$ at $t = 26.4s$

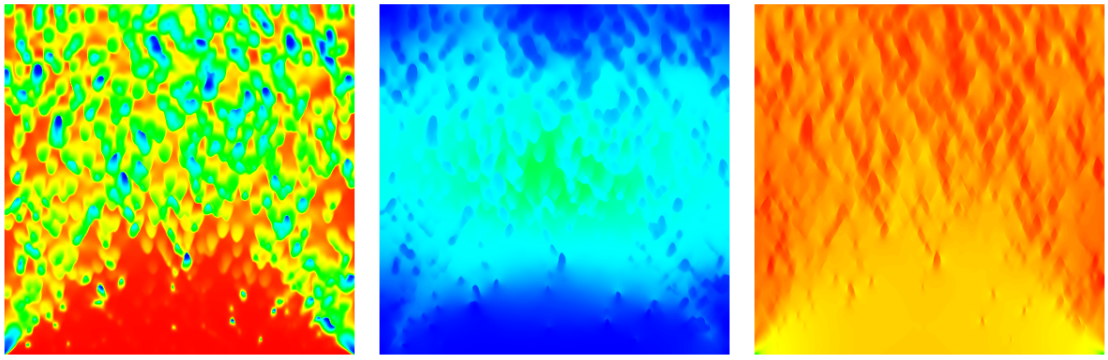

(d) Concentration c_h, diffusive flux $\boldsymbol{J}_h$ and stress $\boldsymbol{\sigma}_h$ at $t = 39.6s$

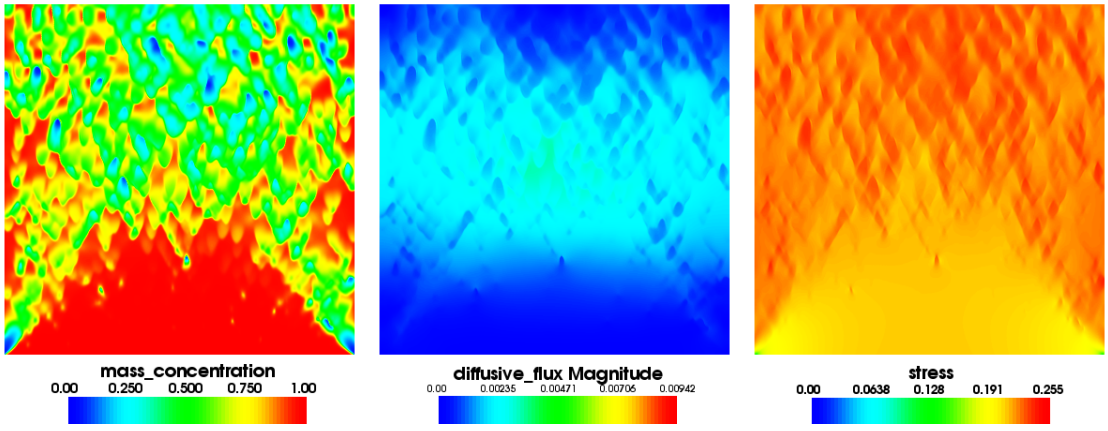

Fig. 6.7: Heating of a RVE about $\Delta\theta = 50°K$

6.3.2 Heating and pressure loading

The second numerical simulation deals with the spinodal decomposition considering elastic effects with a constant elasticity tensor, where heating and additional pressure loading is observed.

Setting

In this simulation the unknown fields are the concentration $c_{\Delta t,h}$, the chemical potential $\mu_{\Delta t,h}$ and the displacement $\boldsymbol{u}_{\Delta t,h}$. Additionally, we compute the diffusive flux $\boldsymbol{J}_{\Delta t,h}$ and the mechanical stress $\boldsymbol{\sigma}_{\Delta t,h}$ for physical reasons only.

We consider a quadratic domain Ω with side length $2\mu m$. This domain is hard clamped at the bottom, on the top a pressure load $\boldsymbol{g}$ is subjected to the configuration and on the left and right side of the domain homogeneous Neumann boundary conditions for the displacement $\boldsymbol{u}_{\Delta t,h}$ are observed. The configuration is demonstrated in fig.6.8. The force on the top of the domain is constant with respect to time and has a value of $\boldsymbol{g} = 5MPa$.

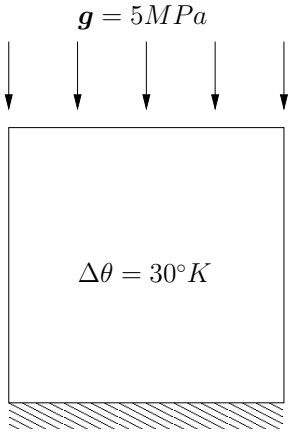

Fig. 6.8: Loading of a RVE

Additionally, the whole configuration is heated about $\Delta\theta = 30°K$. Since the reference temperature is $\theta_{ref} = 20°C$, the simulation is performed at an actual temperature of $\theta = 50°C$, for which the material parameters are interpolated to this temperature value.

Similar as in the previous example stress singularities occur on the lower left and right corner of the quadrangle due to changing boundary conditions.

For the concentration field $c_{\Delta t,h}$ and for the chemical potential $\mu_{\Delta t,h}$ homogeneous Neumann boundary conditions are assumed, which means that no material flux across the boundary takes place and the boundary does not affect the phase separation. The initial data c_0 consists of approximately 600 Pb-particles with a diameter of $0.015\mu m$ randomisely distributed in the Sn-matrix. Fig. 6.10(a) shows the initial state of the configuration.

Results

The results of this numerical simulation are outlined in fig.6.10(a)-(d). The spinodal decomposition of the alloy is once more dominated by mechanical contributions. The Pb-particles close to the Dirichlet boundary shrink very fast and diffuse away from this boundary part.

For this loading of the configuration we have no experiments, thus we can not compare the numerical simulation with experimental investigations. But in view of fig.6.6 the phenomena of Pb-particles diffusing away from the Dirichlet boundary is unnatural.

In contrast to the previous example fig.6.7(a)-(d) the microstructure in fig.6.10(a)-(d) looks different. Comparing both examples we observe that the microstructure in fig. 6.10(d) has much thinner phase interfaces than the microstructure in fig. 6.7(d). We put this phenomena down to the additional pressure loading.

Similar to the previous example, a Pb-rich phase develops in the points where stress singularities occur. This phenomena can be observed by considering the sequence of pictures fig.6.10(a)-(d). By observing the mechanical stress corresponding to the microstructure in fig.6.10(a)-(d), we see again that the development of a Pb-rich phase in the stress singularities reduces them essentially, because Pb is softer than Sn.

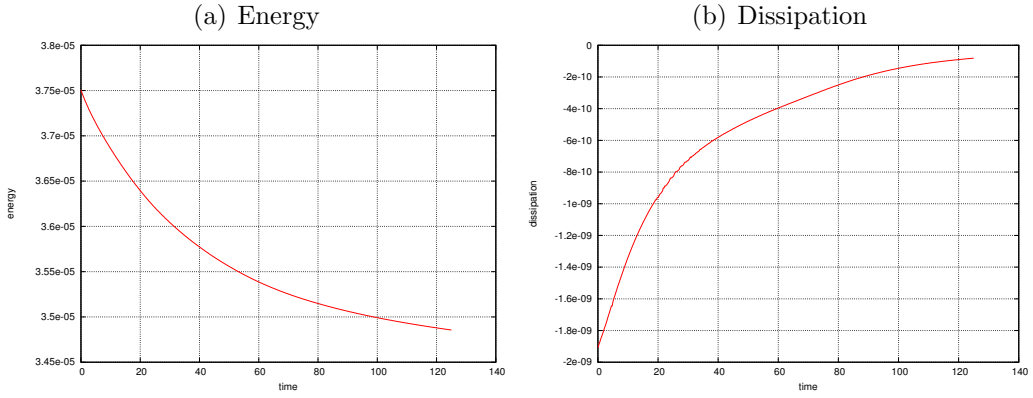

Fig. 6.9: Energy and dissipation

In fig. 6.9(a) the energy of the configuration is plotted with respect to time. Moreover, from this graphics follows that the system reduces the energy essentially, since small Pb-particles having a high surface energy in the beginning diffuse into the larger ones with a small surface energy. The reduction of the mechanical stresses in the lower left and right corner of the domain due to the development of a Pb-rich phase reduces additionally the strain energy. Also in this example the Lyapunov property of the system is demonstrated by the numerical simulations.

The dissipation is plotted in fig. 6.9(b) and we see that it tends more and more to zero. In this model dissipation corresponds to diffusion and therefore we observe that the coarsening process slows down with respect to time.

(a) Concentration c_h, diffusive flux $\boldsymbol{J}_h$ and stress $\boldsymbol{\sigma}_h$ at $t = 0.0s$

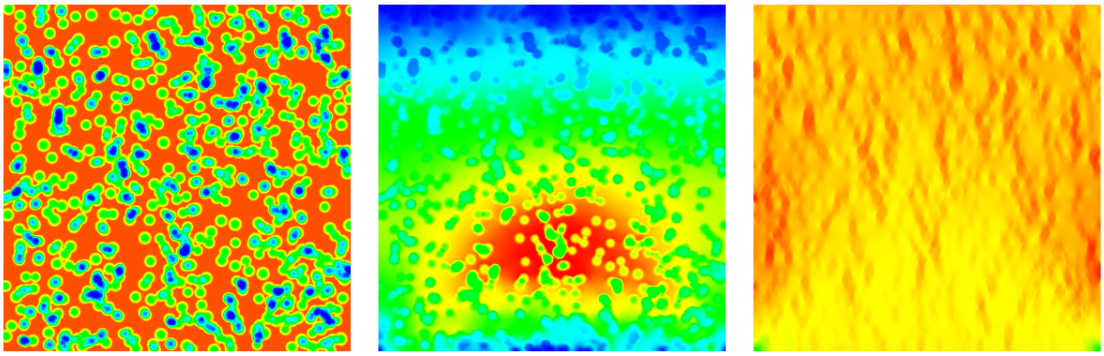

(b) Concentration c_h, diffusive flux $\boldsymbol{J}_h$ and stress $\boldsymbol{\sigma}_h$ at $t = 42.2s$

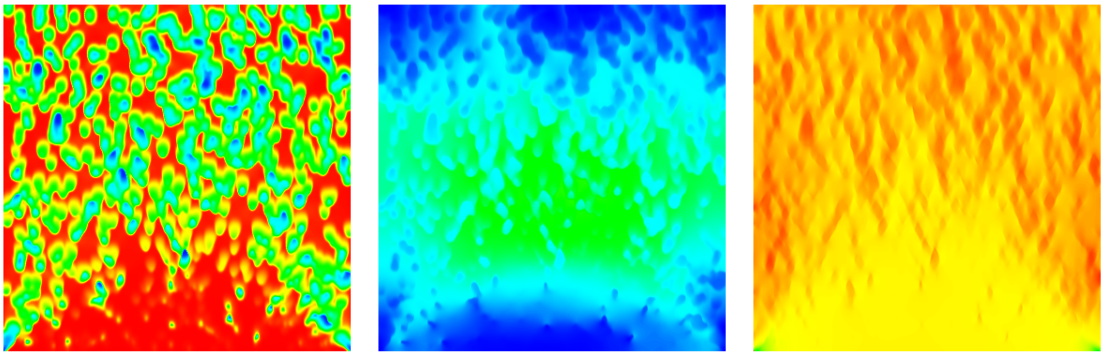

(c) Concentration c_h, diffusive flux $\boldsymbol{J}_h$ and stress $\boldsymbol{\sigma}_h$ at $t = 85.0s$

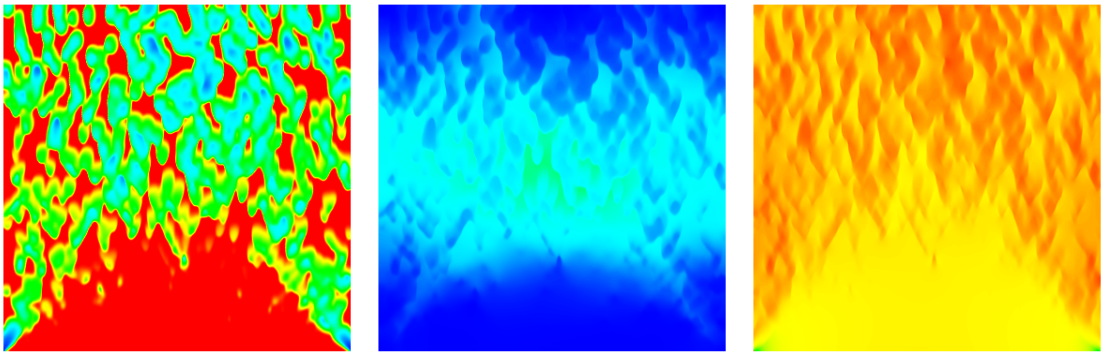

(d) Concentration c_h, diffusive flux $\boldsymbol{J}_h$ and stress $\boldsymbol{\sigma}_h$ at $t = 127.2s$

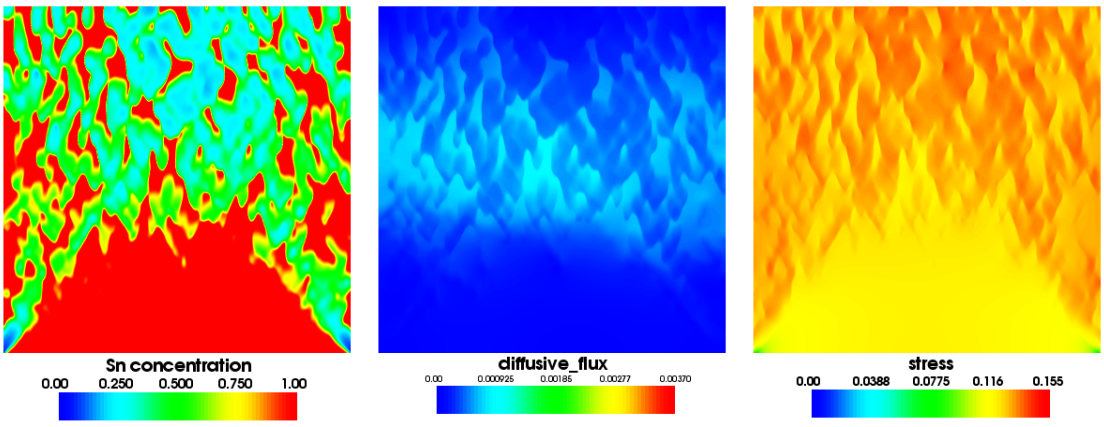

Fig. 6.10: Heating of a RVE about $\Delta\theta = 30°K$ with pressure loading of $\boldsymbol{g} = 5MPa$

6.4 General Cahn-Larché system

In section 6.4 we simulate spinodal decomposition under elastic loadings with a concentration depending elasticity tensor.

6.4.1 Heating

The first numerical example for the general material model contains heating only. For this reason we can compare the results of this simulation with the results of the simulation in section 6.3.1. This comparison is done in order to decide which material model fits qualitatively best to the experimental investigations.

Setting

In this simulation the unknown fields are the concentration $c_{\Delta t,h}$, the chemical potential $\mu_{\Delta t,h}$ and the displacement $\boldsymbol{u}_{\Delta t,h}$. Additionally we determine the diffusive flux $\boldsymbol{J}_{\Delta t,h}$ and the mechanical stress $\boldsymbol{\sigma}_{\Delta t,h}$ for physical reasons.

We observe again the quadratic domain Ω with side length of $2\mu m$. This domain is hard clamped at the bottom and the configuration is heated about $\Delta\theta = 50°K$, see fig. 6.11. The reference temperature is $\theta_{ref} = 20°C$ and due to heating we have an actual temperature of $\theta = 70°C$, where the material parameters are interpolated to this temperature value.

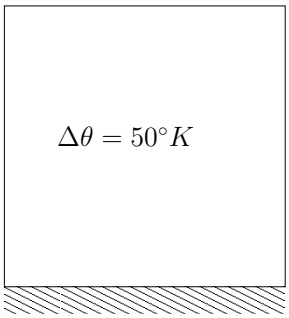

Fig. 6.11: Loading of a RVE

On the remaining boundary homogeneous Neumann boundary condition are assumed for the displacement $\boldsymbol{u}_{\Delta t,h}$. For this loading stress singularities occur in the lower left and right corners of the quadrangle due to changing boundary conditions.

The concentration field $c_{\Delta t,h}$ and the chemical potential $\mu_{\Delta t,h}$ are subjected to homogeneous Neumann boundary conditions on the whole boundary of the domain such that no material flux across the boundary and no influence of the boundary on the spinodal decomposition is observed. The initial data c_0 consists of approximately 600 randomisely distributed Pb-particles with a diameter of $0.015\mu m$ located in the Sn-matrix. In fig. 6.14(a) the initial configuration is shown. This setting is comparable with the setting of the example in section 6.3.1.

Results

The computational results consisting of the concentration field $c_{\Delta t,h}$, the diffusive flux $\boldsymbol{J}_{\Delta t,h}$ and the mechanical stress field $\boldsymbol{\sigma}_{\Delta t,h}$ are presented in fig. 6.14(a)-(d). We see

a spinodal decomposition of the alloy, which is mainly driven by elastic interaction of different elastic material properties of both phases. In contrast to the simulations presented in fig. 6.7(a)-(d) the Pb-particles close to the Dirichlet boundary do not diffuse away from the Dirichlet boundary. They coarsen very fast and build a fixed microstructure, which consists of rectangular Pb-particles with a very thin diffusive phase interface. The microstructure in fig. 6.14(a)-(d) is completely different to the microstructure in fig. 6.7(a)-(d).

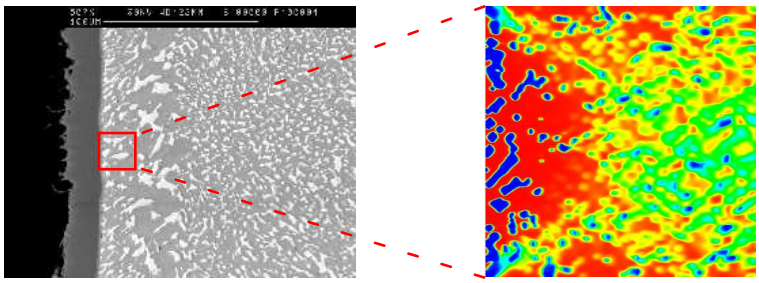

Fig. 6.12: Comparison of experiment and simulation

We compare this numerical simulation with an experimental investigation. In fig. 6.12 we confront the microstructure from fig. 6.14(d) with a hard clamped part of a solder joint. Obviously, in fig. 6.12 it can be seen that rectangular Pb-particles develop along the hard clamped boundary in the experiment. We conclude that at least qualitatively this numerical simulation fits with the experimental investigations, if a concentration depending elasticity tensor is used. Due to this fact the simulation of the spinodal decomposition of a solder alloy must be done with the Cahn-Larché model having a concentration depending elasticity tensor. From a physical point of view this is a comprehensible result, because in our example Sn has a tetragonal lattice structure in contrast to Pb, which has a cubic lattice structure.

In general, the development of rectangular particles was also observed by Weikard in [102]. At least locally our simulation fits the simulation done by Weikard in [102].

By observing the mechanical stress in fig.6.14(a)-(d) we see that the stress within the soft Pb-particles is smaller than the stress in the surrounding Sn-matrix. This is a significant difference between the model with and without a concentration depending elasticity tensor comparing fig. 6.7(a)-(d) and fig. 6.14(a)-(d).

Similar to the simulation in section 6.3.1 a soft Pb-rich phase develops in the stress singularities resulting from changing boundary conditions, which can be seen in fig. 6.14(a)-(d). Moreover, stress singularities develop between the rectangular Pb-particles near to the Dirichlet boundary and the surrounding Sn-matrix, which is clearly observed in fig. 6.14(d). This phenomena is also considered in experiments and indicates the problem that solder joints burst away from the PBC.

In fig. 6.13(a) the energy of the system is plotted over time. Also in this simu-

lation the energy decreases and the system achieves an energetic stable state. For this reason the Lyapunov property of material model is demonstrated well. The dissipation is shown in fig.6.13(b), which becomes smaller and smaller indicating the fact that the diffusion becomes slower.

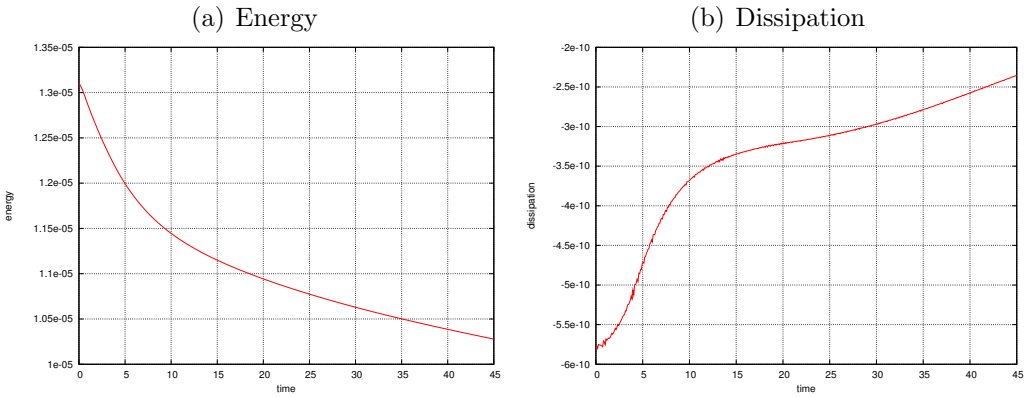

Fig. 6.13: Energy and dissipation

6.4.2 Pressure loading

In section 6.4.2 we investigate a pure pressure loading of the solder alloy.

Setting

The computational domain is given by the usual quadrangle with side length of $2\mu m$. This domain is hard clamped at the bottom and a pressure load $\boldsymbol{g} = 5MPa$ is subjected to the top of the boundary. On the remaining boundaries homogeneous Neumann condition are assumed for the displacement $\boldsymbol{u}_{\Delta t,h}$ and no additional heating is observed, see fig.6.15. This configuration also causes stress singularities at the lower left and right corners due to changing boundary conditions.

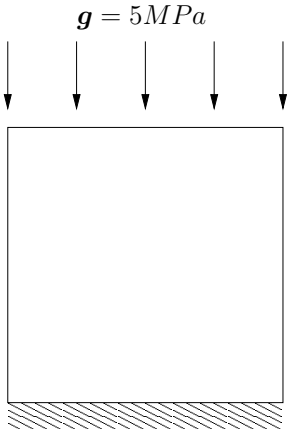

Fig. 6.15: Loading of a RVE

The concentration field $c_{\Delta t,h}$ and the chemical potential $\mu_{\Delta t,h}$ are assumed to satisfy homogeneous Neumann conditions on the whole boundary, such that no material flux occurs across the boundary and the boundary does not affect the coarsening process. We take as initial data c_0 a random distribution of approximately 600 Pb-particles with diameter $0.015\mu m$ in a Sn-matrix.

(a) Concentration c_h, diffusive flux $\boldsymbol{J}_h$ and stress $\boldsymbol{\sigma}_h$ at $t = 0.0s$

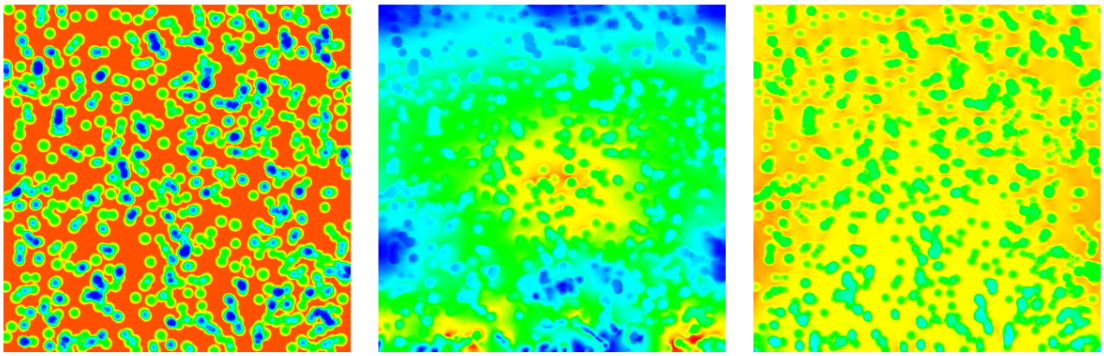

(b) Concentration c_h, diffusive flux $\boldsymbol{J}_h$ and stress $\boldsymbol{\sigma}_h$ at $t = 15.3s$

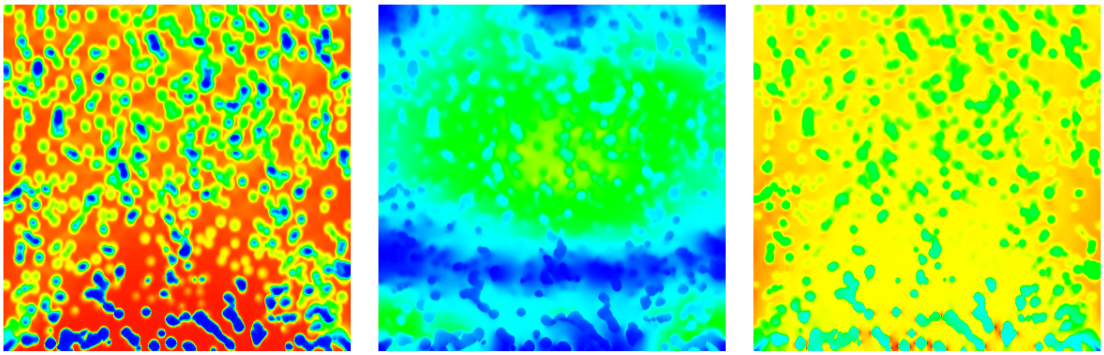

(c) Concentration c_h, diffusive flux $\boldsymbol{J}_h$ and stress $\boldsymbol{\sigma}_h$ at $t = 30.6s$

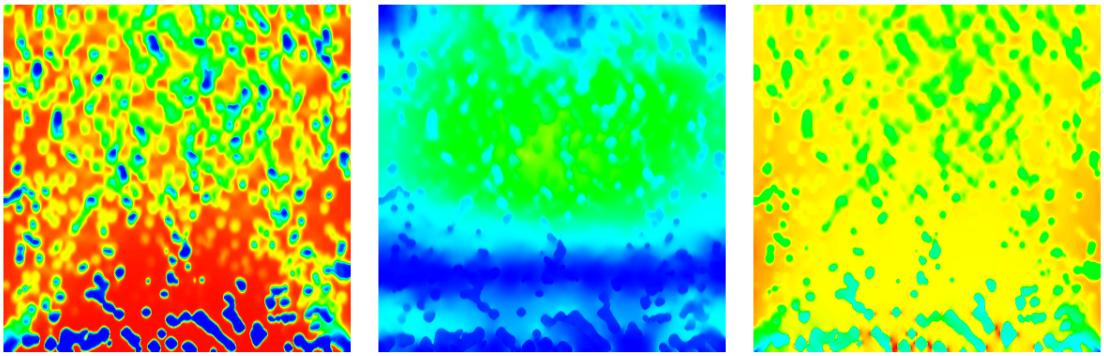

(d) Concentration c_h, diffusive flux $\boldsymbol{J}_h$ and stress $\boldsymbol{\sigma}_h$ at $t = 45.9s$

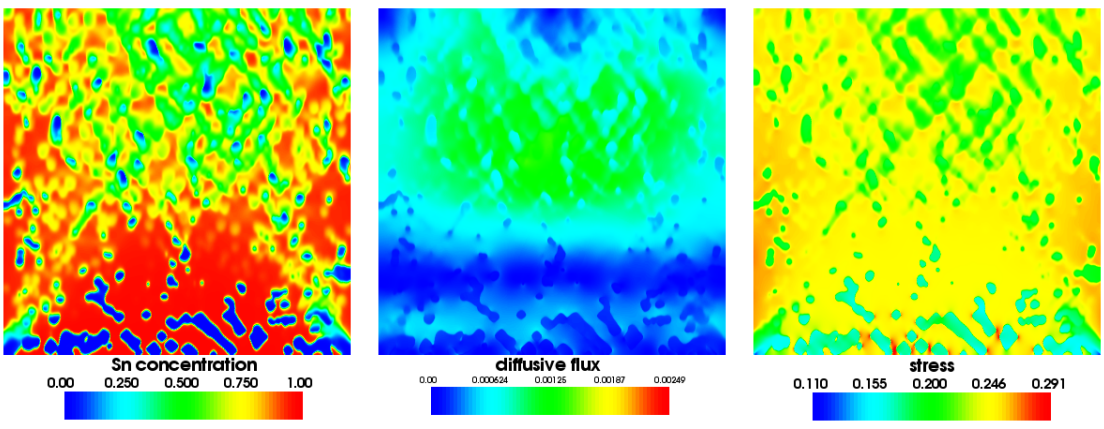

Fig. 6.14: Heating of a RVE about $\Delta\theta = 50°K$

Results

In fig.6.17(a)-(d) the numerical simulations are shown. The spinodal decomposition is mainly driven by mechanical loading. We observe that the initially small Pb-particles shrink and blow up the larger ones. This process is clearly accelerated by the external loading.

Due to the fact that no heating is considered, there is no volume force accelerating the diffusion process. These circumstances lead to a microstructure with thin interfaces. If we compare fig. 6.14(a)-(d) to fig. 6.17(a)-(d) we see a totally different microstructure. The influence of the Dirichlet boundary in fig. 6.14(a)-(d) on the evolution of the microstructure is not observed in the simulation presented in fig.6.17(a)-(d). We conclude that the microstructure extremely depends on the type of loading subjected to the configuration.

The stress singularities in the lower left and right corners of the domain in fig. 6.17(a)-(d) do not affect the spinodal decomposition of the mixture in such a significant way as it is observed in the previous examples plotted in fig.6.14(a)-(d).

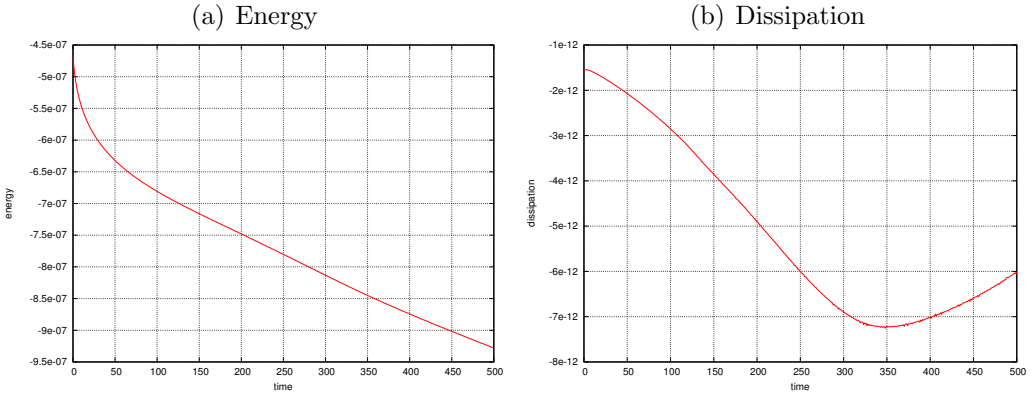

Fig. 6.16: Energy and dissipation

In fig.6.16(a) the energy of the system is plotted over time. We see a decreasing energy of the configuration, which results from the fact that the microstructure coarsens and reduces its interfacial energy. Also for the case of pressure loading Lyapunov's property is obviously observed.

The behaviour of the dissipation plotted in fig.6.16(b) differs from the dissipation in the previous example, which is outlined in fig. 6.14(b). In contrast to fig. 6.14(b) here we observe that more and more energy is dissipated, a property which results from the fact that in the beginning a lot of small Pb-particles with a large interfacial energy vanish. For the development of the microstructure this means that in the beginning a lot of diffusion occurs, which decreases after a certain time.

(a) Concentration c_h, diffusive flux $\boldsymbol{J}_h$ and stress $\boldsymbol{\sigma}_h$ at $t = 0.0s$

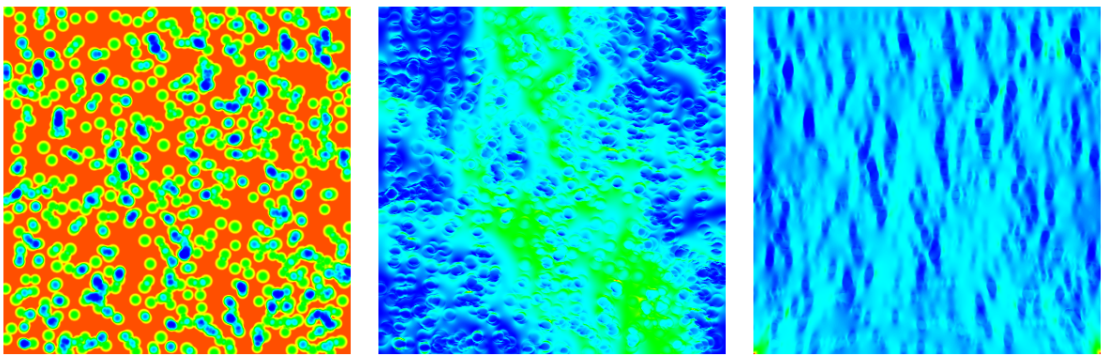

(b) Concentration c_h, diffusive flux $\boldsymbol{J}_h$ and stress $\boldsymbol{\sigma}_h$ at $t = 170s$

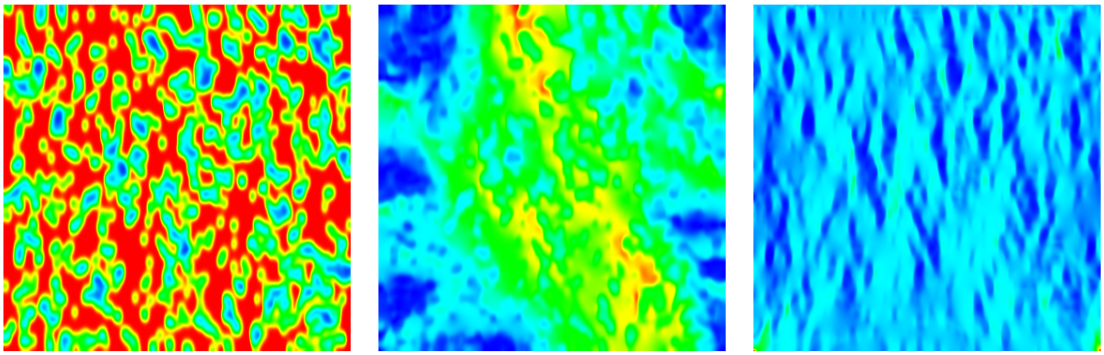

(c) Concentration c_h, diffusive flux $\boldsymbol{J}_h$ and stress $\boldsymbol{\sigma}_h$ at $t = 340s$

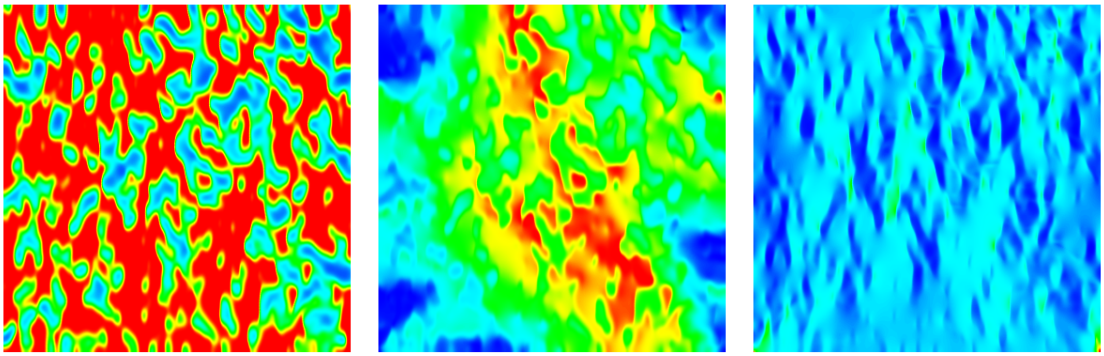

(d) Concentration c_h, diffusive flux $\boldsymbol{J}_h$ and stress $\boldsymbol{\sigma}_h$ at $t = 500s$

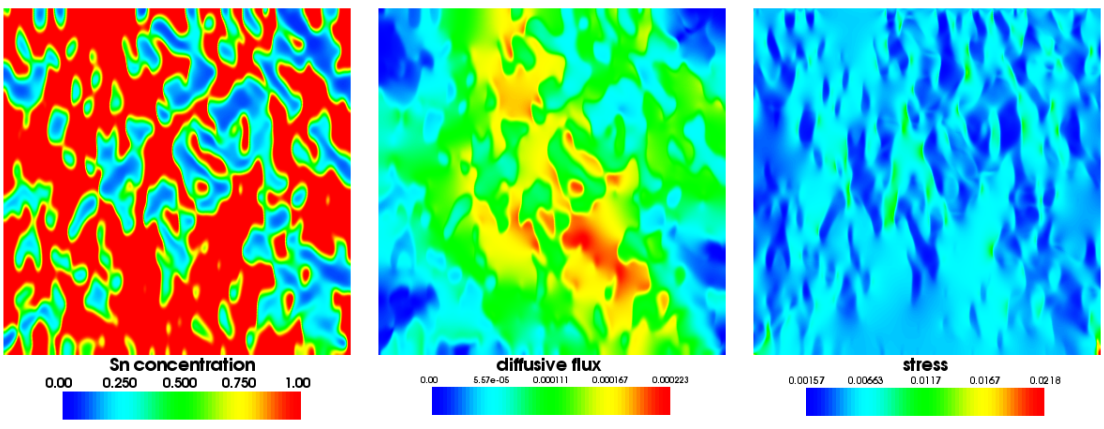

Fig. 6.17: Pressure loading of a RVE with $\boldsymbol{g} = 5MPa$

6.4.3 Shear loading

In this example we analyse the influence of pure shear forces on the coarsening process of an alloy. From experimental investigations it is known that shear stress leads to the most significant damages of a solder joint.

Setting

We use the standard quadratic domain Ω with side length of $2\mu m$ and hold it fixed at the bottom. On the top a shear force $\boldsymbol{g} = 2MPa$ in right direction is subjected to the configuration, see fig. 6.18. On the left and right boundary homogeneous Neumann conditions for the displacement $\boldsymbol{u}_{\Delta t,h}$ are observed. The configuration is not heated, thus we have no volume force accelerating the spinodal decomposition. Again we have stress singularities at the lower left and right corners of the configuration due to changing boundary conditions.

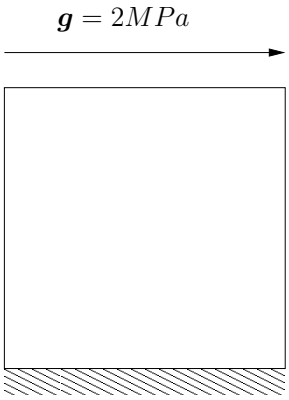

Fig. 6.18: Loading of a RVE

For the concentration field $c_{\Delta t,h}$ and for the chemical potential $\mu_{\Delta t,h}$ homogeneous Neumann boundary conditions are required such that no material flux across the boundary occurs and the spinodal decomposition is not affected by the boundary. The initial data c_0 consists of approximately 600 Pb-particle with a diameter of $0.015\mu m$ randomisely located in a Sn-matrix.

Results

The concentration field $c_{\Delta t,h}$, the diffusive flux $\boldsymbol{J}_{\Delta t,h}$ and the mechanical stress $\boldsymbol{\sigma}_{\Delta t,h}$ resulting from the numerical simulation are shown in fig.6.20(a)-(d). In the beginning we see a typical shear stress profile with a banded structure all over the domain having stress singularities in the lower left and right corners.

The spinodal decomposition is extremely dominated by the shear stress. Almost everywhere in the domain the small Pb-particles shrink. The small Pb-particles diffuse to the lower left and right corner of the domain, where stress singularities appear. Due to this fact, in both corners large Pb-rich phases develop and we observe again the phenomena that the soft material, in this example Pb, reduces the stress singularities essentially. If we compare the microstructure in fig.6.20(a)-(d) with the microstructures of all previous examples, then we conclude that shear stress has the most significant influence on the development of the microstructure.

Finally, we observe the energy, which is plotted over time in fig. 6.19(a). Since the microstructure coarsens, the interfacial energy is reduced and additionally the

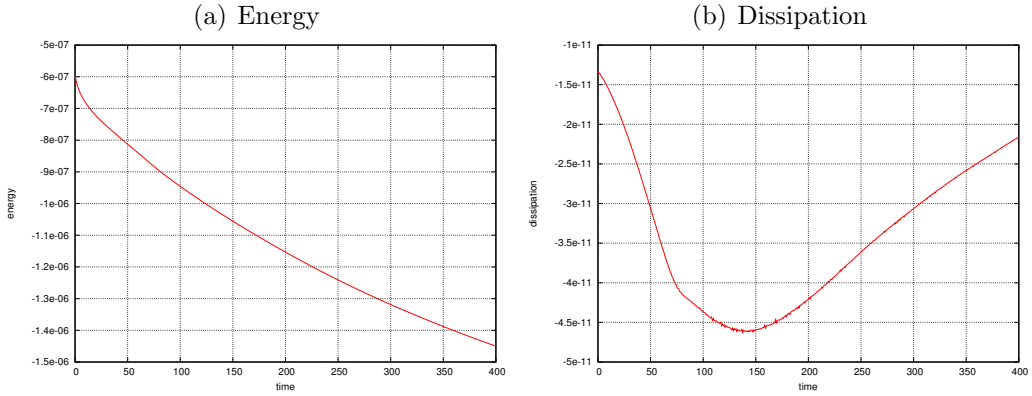

Fig. 6.19: Energy and dissipation

mechanical energy is decreased by the development of Pb-rich phases in points of stress singularities. This leads to a decreasing energy as it is shown in fig. 6.19(a), which again demonstrates the Lyapunov property.

The dissipation of the system is plotted in fig.6.19(b) and we observe qualitatively a similar behaviour of the dissipation as in the example with pure pressure load, see fig. 6.16(b). Clearly, the development of the microstructure in fig. 6.20(a)-(d) shows that in the beginning of the coarsening process a lot of small Pb-particles with a large interfacial energy vanish and therefore a lot of energy is dissipated. This fact causes an increasing dissipation in the beginning of the process and the dissipation decreases when only large particles occur.

6.4.4 Heating of a L-shape with changing boundary conditions

In the last example we investigate the influence of a reentrant corner on the spinodal decomposition.

Setting

In this example we observe a L-shape domain Ω, which is hard clamped at the right top boundary as demonstrated in fig. 6.21. On the remaining boundary parts we require for the displacement $\boldsymbol{u}_{\Delta t,h}$ homogeneous Neumann boundary conditions. The whole body is heated about $\Delta\theta = 50°K$. Since the reference temperature has a value of $\theta_{ref} = 20°C$, the simulation is performed at an actual temperature of $\theta = 70°C$. All material parameters are interpolated to this temperature value. This loading

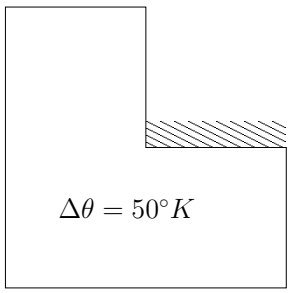

Fig. 6.21: Loading of a L-shape

(a) Concentration c_h, diffusive flux $\boldsymbol{J}_h$ and stress $\boldsymbol{\sigma}_h$ at $t = 0.0s$

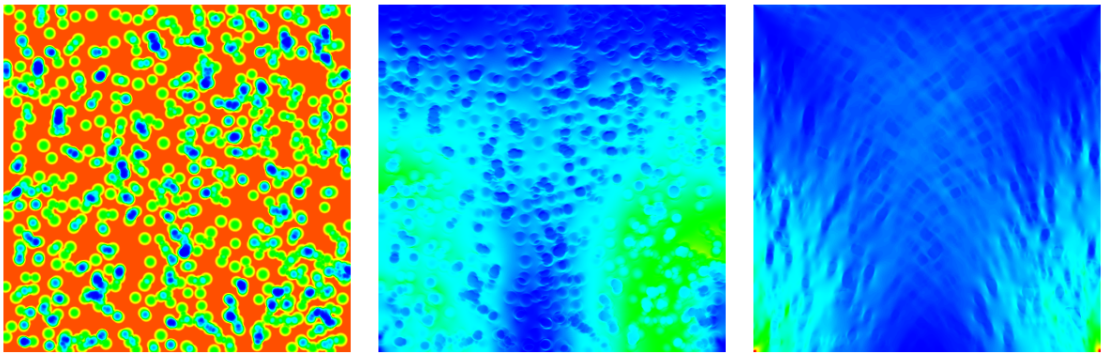

(b) Concentration c_h, diffusive flux $\boldsymbol{J}_h$ and stress $\boldsymbol{\sigma}_h$ at $t = 136s$

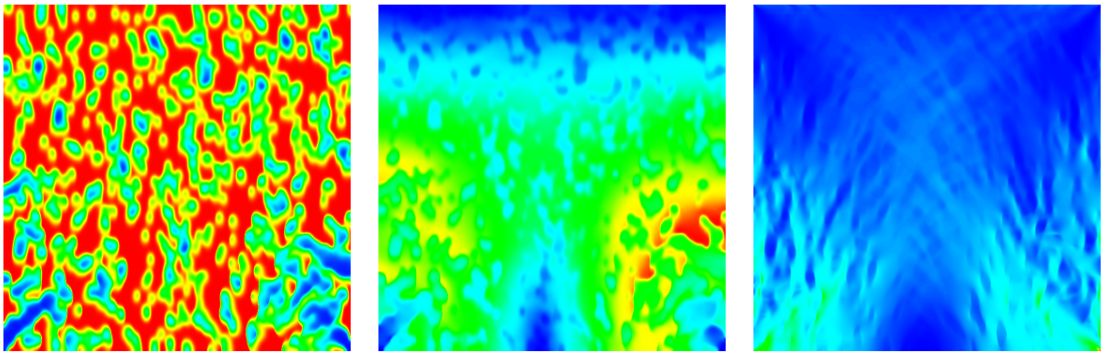

(c) Concentration c_h, diffusive flux $\boldsymbol{J}_h$ and stress $\boldsymbol{\sigma}_h$ at $t = 272s$

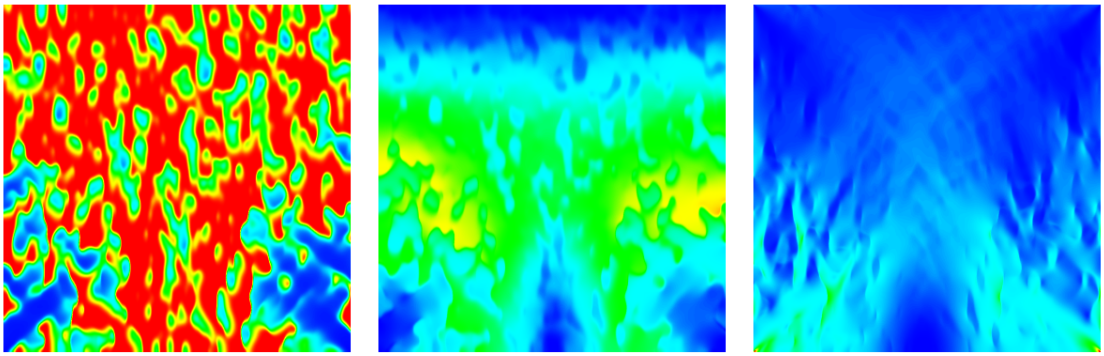

(d) Concentration c_h, diffusive flux $\boldsymbol{J}_h$ and stress $\boldsymbol{\sigma}_h$ at $t = 408s$

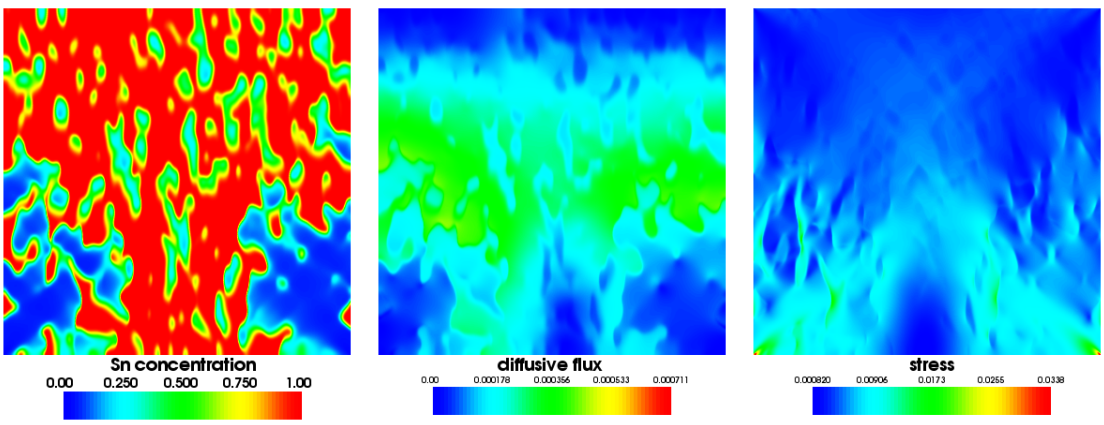

Fig. 6.20: Shear loading of a RVE with $\boldsymbol{g} = 2MPa$

leads to a strong stress singularity at the reentrant corner, since in this point the boundary condition additionally changes.

The concentration field $c_{\Delta t,h}$ and the chemical potential $\mu_{\Delta t,h}$ have to satisfy homogeneous Neumann data on the whole boundary. Due to this fact, no material flux across the boundary occurs and the boundary does not affect the spinodal decomposition.

Finally, the initial data c_0 consists of nearly 450 Pb-particles with a diameter $0.015\mu m$, which are randomisely distributed in the Sn-matrix. The initial state is shown in fig. 6.24(a) and it is organised in such a way that at the reentrant corner the hard material Sn is located.

Results

The evolution of the spinodal decomposition is demonstrated in fig. 6.24(a)-(d). We see at the beginning a clear stress singularity at the reentrant corner, which is large compared with the previous examples, where only the changing boundary conditions cause the stress singularity. The stress singularity in fig. 6.24(a)-(d) locally induces a large diffusive flux at the reentrant corner, which influences the development of the microstructure essentially.

We see in fig. 6.24(a)-(d) that at the reentrant corner a soft Pb-rich phase develops very fast. This phenomena is observed in all previous examples at points, where stress singularities occur. Clearly, the Pb-rich phase at the reentrant corner reduces the mechanical stress singularity essentially, because Pb is softer than Sn. It is of great

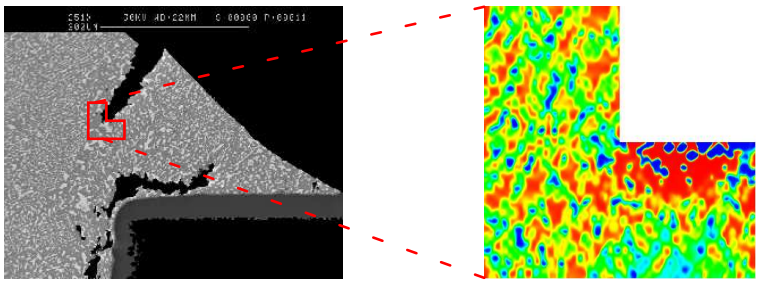

Fig. 6.22: Comparison of experiment and simulation

interest to compare this numerical simulation with experimental investigations. In fig. 6.22 we compare the evolution of the microstructure in a crack tip of a solder joint with the numerical simulation of spinodal decomposition in the L-shape. Obviously, in the crack tip a soft Pb-rich phase develops, similar to the reentrant corner of the L-shape as demonstrated in fig. 6.24(a)-(d). This shows again that the Cahn-Larché system with concentration depending elasticity tensor fits at least qualitatively well to the experimental investigations.

Finally, in fig. 6.23(a) the development of the energy over time is plotted. The energy is decreasing as expected, since the Cahn-Larché system satisfies the Lyapunov property. The dissipation of the configuration decreases, which shows that the diffusion slows down more and more.

(a) Energy

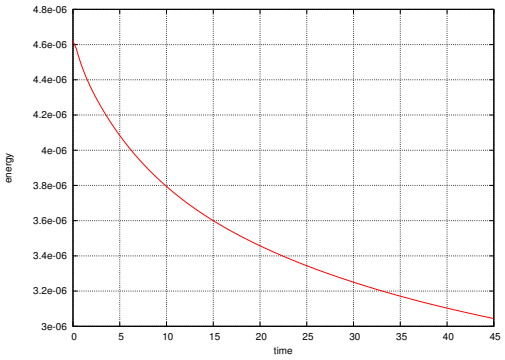

(b) Dissipation

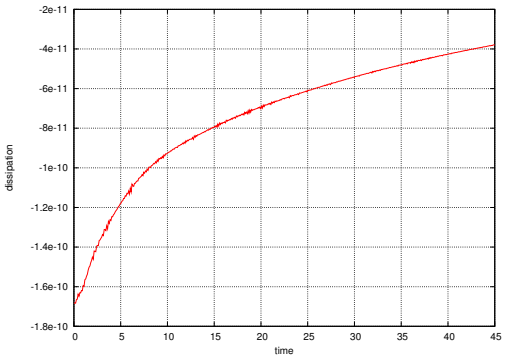

Fig. 6.23: Energy and dissipation

(a) Concentration c_h, diffusive flux $\boldsymbol{J}_h$ and stress $\boldsymbol{\sigma}_h$ at $t = 0.0s$

(b) Concentration c_h, diffusive flux $\boldsymbol{J}_h$ and stress $\boldsymbol{\sigma}_h$ at $t = 15.3s$

(c) Concentration c_h, diffusive flux $\boldsymbol{J}_h$ and stress $\boldsymbol{\sigma}_h$ at $t = 30.6s$

(d) Concentration c_h, diffusive flux $\boldsymbol{J}_h$ and stress $\boldsymbol{\sigma}_h$ at $t = 45.9s$

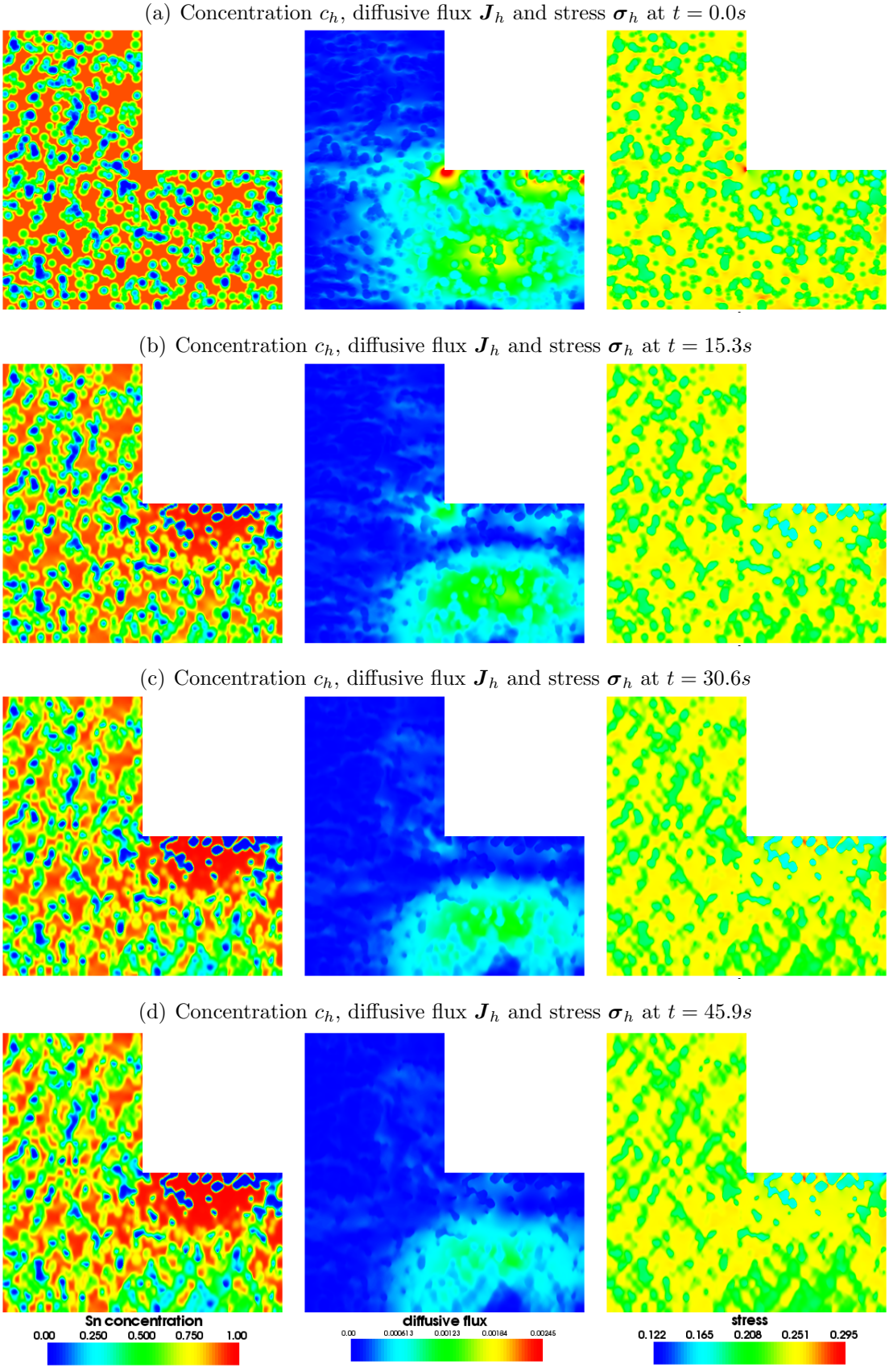

Fig. 6.24: Heating of a L-shape about $\Delta\theta = 50°K$

Chapter 7

Conclusions and open problems

At the end of this thesis we summarise the important results from the previous chapters and specify open problems and questions.

Conclusions

A rigorous mathematical derivation of the Cahn-Larché equations is given in chapter 1, which represents a completion of the classical works [62, 68, 84]. We remark that the influence of external mechanical loadings as well as of viscosity on the spinodal decomposition of an alloy is added to the model. An important aspect of the modelling is the examination of the general entropy principle by Lagrangian multipliers. This method was developed by Liu in [71] and here we apply it to the thermodynamics of phase separation. The thermodynamic Lagrangian multipliers are an alternative to the concept of configurational forces developed by Fried and Gurtin in [46, 47], which is also used for the exploitation of the entropy principle in phase transitions, see [56].

The existence of a weak solution of the viscous Cahn-Larché system with concentration depending mobility and external mechanical forces is proved in chapter 2. In order to prove this, we extend the method derived by Garcke in [48, 49] consisting of a time discretisation, minimising the Helmholtz free energy and maximising the dissipation. We emphasise that the a-priori estimates do not depend on the friction coefficient and for this reason the existence of a weak solution is proved simultaneously for the viscous and non-viscous system. The significant difference between a weak solution of the viscous and non-viscous Cahn-Larché system is that the weak solution of the viscous system is smoother with respect to time.

Numerical approximation methods for the viscous and non-viscous Cahn-Larché system are developed in chapter 4 and 5. We focus on the development of stable methods. In this context, stable means that no overshoots and undershoots occur

within a diffusive interface especially for small surface stress tensors, which appear in practical applications.

In chapter 4 a finite element discretisation is derived for the viscous Cahn-Larché equations, which is based on the time discretisation of chapter 2. The fact that the a-priori estimates does not depend on the friction coefficient is used in order to develop a stable method for the non-viscous system. Here the dynamic friction plays the role of a stabilisation term, whereas the friction coefficient γ is used as a stabilisation parameter and it is $\gamma \approx \sqrt{h}$.

A further stable method is observed, where friction is formulated in terms of driving forces and it is used for stabilisation too. We prove that both viscous methods are equivalent taking into account the flow gradient structure of the system. Both methods are new approximation techniques for the simulation of spinodal decomposition.

An operator-splitting method for the non-viscous Cahn-Larché system is considered in chapter 5. Here the Gibbs free energy density is decomposed into a convex and a concave part, where the convex term is discretised implicitly in contrast to the the concave term, which is treated explicitly. This method is an extension of the technique developed by Rumpf and Grün in [54] for the thin film equation. The result of our investigation is that the operator-splitting method is stable in the above mentioned sense, but the time discretisation must be chosen very small and therefore it is not efficient compared to the viscous methods.

Finally, in chapter 6, various numerical simulations are performed especially using the viscous method stabilised by driving forces. The Cahn-Larché system only models the spinodal decomposition of the alloy immediately after manufacturing the solder joint. The important result of this chapter is the fact that the Cahn-Larché system with concentration dependent elasticity tensor fits qualitatively very well to the experiment. The more simpler model with a constant elasticity tensor, for which the numerical simulation can be performed easier, is unqualified for the simulation of the spinodal decomposition in solder.

Mechanical stress singularities due to changing boundary conditions affect the development of the microstructure essentially. In a local surrounding of a point with a stress singularity a phase with softer material develops in order to reduce the stress. Similar results are observed at reentrant corners, a phenomena, which is also confirmed by the experiment.

Open problems

Using the Cahn-Larché model we simulate the spinodal decomposition in an alloy in a very short time range. This process happens immediately after producing a

solder joint. The simulation results and data can be used in the following in order to compute the long time behaviour of the microstructure in a solder joint. However for the computation of the long time behaviour other models must be derived. One possibility may be the Mullins-Sekerka model, which has in contrast to the Cahn-Larché model a sharp interface. Here only the sharp interface must be discretised and the evolution of the interface can be computed by applying BEM.

Basically, macroscopic material models for solder are of great interest. The macroscopic material behaviour of solder shows visco-plastic effects and creep phenomena. The macroscopic visco-plastic behaviour is mainly influenced by diffusion processes on the micro scale. The numerical results of this thesis could be used on the one hand to derive creep curves and on the other hand they could contribute to a multi scale model.

Furthermore, damage criterias for solder are also an important tool for industrial applications. In contrast to damage criterias for elastic bodies, a damage criteria for solder should also consider the thickness of the diffusive phase interfaces, because extreme thin interfaces make the material fragile. This is demonstrated by the computations in section 6.4. Diffusive interfaces are described by large gradients of the concentration, therefore a damage criteria of solder should take care of both mechanical stress and gradients of the concentrations.

Zusammenfassung

Die elektronische Steuerung von mechanischen Vorgängen insbesondere in der Kraftfahrzeugtechnik wird zunehmend wichtiger für die Automobilindustrie. Steuergeräte übernehmen verantwortungsvolle und sicherheitsrelevante Aufgaben im Fahrzeug, wodurch sie dessen Verhalten stark beeinflussen. Unter all den herausfordernden Problemen, die bei der Entwicklung von Steuergeräten auftreten, befasst sich diese Arbeit mit der Zuverlässigkeit von Lotstellen. In der Aufbau- und Verbindungstechnik wird Lot zur mechanischen und elektrischen Verbindung von elektronischen Bauteilen und der Leiterplatte verwendet.

Aufgrund dieser Entwicklung gewinnt die Zuverlässigkeit und Lebensdauer einer Lotstelle immer mehr an Bedeutung für die Elektronik- und Automobilbranche. Die unterschiedlichen Materialien mit ihren verschieden Eigenschaften, die in ein mikroelektronisches Komposit eingehen, stellen in Verbindung mit hohen thermischen und mechanischen Belastungen den Schlüssel für Zuverlässigkeitsaussagen einer Lotstelle dar. Lot ist im Allgemeinen eine Legierung bestehend aus zwei oder mehreren Bestandteilen. Als Komponenten des Lotes kommen dabei üblicherweise Zinn (Sn), Blei (Pb), Silber (Ag) oder Kupfer (Cu) zum Einsatz.

Experimentelle Untersuchungen von Lotstellen bei denen die Konfiguration vielen Belastungzyklen unterzogen wird, zeigen eine deutlich veränderte Mikrostruktur der Legierung. Z.B. bei Sn-Pb Loten separiert die ursprünglich feine Mischung aus Sn und Pb in Regionen mit hoher Sn und hoher Pb Konzentration. Diese Separation der Mischung in Phasen ist dabei nicht gleichmäßig in der Lotstelle verteilt. Es treten Gebiete mit weitaus gröberer Mikrostruktur auf als andere. Dabei ist zu beobachten, dass Gebiete mit grober Mikrostruktur nicht zufällig in der Lotstelle verteilt sind, sondern sie beginnen z.B. an Spitzkerben oder einspringenden Ecken. Auch wird eine ausgeprägte Vergröberung der Mikrostruktur in einer Umgebung fest eingespannter Randstücke der Lotstelle beobachtet.

All diese Beobachtungen führen zu der Vermutung, dass die Geometrie der Lotstelle, sowie die Art der Belastung den Separationsvorgang stark beeinflussen. Eine genaue Kenntnis der Entwicklung der Mikrostruktur des Lotes ist insbesondere wichtig, da sich Risse und Schädigungen des Materials besonders entlang Regionen mit feiner und grober Mikrostruktur entwickeln. All diese Phänomene zusammen

werden im Allgemeinen als Zerrüttung des Lotes bezeichnet.

Der erste Schritt zum Verständnis der Zerrüttung und Alterung von Lot besteht in der Simulation der Evolution der Mikrostruktur auf einer mesoskopischen Größenskala. Im Allgemein ist die Simulation der Ausbildung einer Mikrostruktur beschränkt auf einen kleinen Bereich des Lotes. Kleine Bereiche sind dabei repräsentative Volumenelemente (RVE), die innerhalb der Lotverbindung liegen. Weitaus interessanter sind jedoch RVEs die sich am Rand des Gebietes befinden und damit dem Einfluss der Geometrie oder wechselnden Randbedingungen unterliegen.

Die Evolution der Mikrostruktur in einer Legierung wird durch einen diffusiven Vorgang beschrieben, dabei ist zwischen einem frühen und einem späten Stadium der Entwicklung zu unterscheiden:

Bei einer Temperatur größer als ein kritischer Wert θ_c besteht die Mischung aus einer homogenen Phase, die sich in einem energetisch stabilen Zustand befindet. Nach Abkühlung unterhalb der kritischen Temperatur θ_c entwickeln sich zwei oder mehr Phasen. Das gesamte System befindet sich dann erneut in einem stabilen Zustand, wobei es seine innere Energie verringert hat. Dieser Vorgang läuft auf einer sehr kleinen Zeitskala ab und wird *spinodale Dekomposition* oder *Phasenseparation* genannt.

Zu einem späteren Stadium der Entwicklung befinden sich in der Mischung eine große Anzahl kleiner Partikel, die sich durch die spinodale Dekomposition gebildet haben. Diese Partikel sind durch Interfaces voneinander getrennt mit denen eine Interface-Energie verbunden wird. Das zweite Stadium der Mikrostruktur-Entwicklung ist dadurch geprägt, dass die Struktur sich zu vergröbern beginnt. Dies bedeutet, dass große Partikel auf Kosten kleiner Partikel wachsen und dadurch die Interface-Energie verkleinert wird. Diesen Teil der Entwicklung nennt man *Gefügevergröberung* oder *Ostwald Reifung*.

Eine Lotlegierung besteht aus vielen verschieden Materialien, die sich in ihren elastischen Materialeigenschaften und in ihrer Gitterstruktur unterscheiden. Diese Tatsache hat großen Einfluss auf die Phasenseparation, sowie auf die Gefügevergröberung und die Gestalt der Partikel. Spannungssingularitäten, die aus Kerben, einspringenden Ecken oder wechselnden Randbedingungen resultieren, lieferen hierzu einen weiteren Beitrag.

Zur Simulation dieser Phänomene sind mindestens drei verschiedene Modelle bekannt. Ein detaillierter Überblick hierzu befindet sich in [44]:

- Atomistische Modelle
- Konzentrationsbasierte Modelle mit diffusivem Interface
- Konzentrationsbasierte Modelle mit scharfem Interface

In dieser Arbeit werden ausschließlich Modelle mit diffusivem Interface betrachtet. Ein diffusives Phasen-Interface-Modell beschreibt ein Interface als eine dünne, aber nicht infinitesimal dünne Region mit einem großen Gradienten des Konzentrationsfeldes. Ein mathematisches Modell diesen Typs wurde von Cahn und Hilliard in [20, 21] hergeleitet, welches als Cahn-Hilliard-Gleichung bezeichnet wird. Die Evolution des Konzentrationsfeldes wird in diesem Modell angetrieben durch den Gradienten des chemischen Potentials der Mischung. Hierbei geht das chemische Potential als Variationsableitung der Energie in Bezug auf die Konzentration in das Modell ein. Aus diesem Grund besitzt das Cahn-Hillard-System eine Fluss-Gradienten-Struktur, was eine wichtige Eigenschaft für die Analysis und Numerik der Gleichung ist. Numerische Simulationen mit Faedo-Galerkin-Verfahren wurden bereits in [36, 37] durchgeführt.

Die Erweiterung dieses Phasen-Separations-Modells im Hinblick auf die Berücksichtigung elastischer Effekte geht zurück auf Cahn [19], Khachaturyan [62], Larché and Cahn [68] sowie Onuki [84]. Numerische Untersuchungen dieser Modelle wurden in [50, 51, 102] durchgeführt.

Die Modellbildung in dieser Arbeit ist motiviert durch die obigen Beobachtungen, so dass folgende neue Aspekte in das Phasenseparationsmodell eingearbeitet wurden:

- Eine mathematisch rigorose Herleitung der Cahn-Larché Gleichungen wird dargestellt, welche zusätzlich zu den bisherigen Modellen in [62, 68, 84] den Einfluss externer mechanischer Kräfte, sowie Viskosität beschreibt.

- Die Auswertung des allgemeinen Entropie-Prinzips für die Phasenseparation erfolgt mit Hilfe Lagranger Multiplikatoren.

Die Methode der Lagrangen Multiplikatoren in der Thermodynamik wurde von Liu in [71] eingeführt. Diese Technik stellt ein alternatives Konzept zur Methode der konfigurierenden Kräfte dar, welches von Fried und Gurtin in [46, 47] hergeleitet und in [56] von Gurtin auf die Cahn-Larché Gleichungen angewandt wurde. Der neue Beitrag zur Analysis des Cahn-Larché Systems ist der folgende:

- Gezeigt wird die Existenz einer schwachen Lösung der viskosen Cahn-Larché Gleichungen unter Einbeziehung eines konzentrationsabhängigen Mobilitätstensors und externer mechanischer Kräfte.

Um dieses Ergebnis zu erzielen, wird die Methode, die von Garcke in [48, 49] entwickelt wurde und aus einer Zeitdiskretisierung mit anschließender Minimierung der inneren Energie und Maximierung der Dissipation besteht, erweitert. Ein interessantes Ergebnis der hier vorgestellten Untersuchungen besteht darin, dass die a-priori Abschätzungen der schwachen Lösung nicht vom Reibungskoeffizienten abhängen.

Durch diese Beobachtung erhält man gleichzeitig die Existenz einer schwachen Lösung der viskosen und nicht-viskosen Cahn-Larché Gleichungen. Eine weiteres entscheidendes Ergebnis der Untersuchungen ist hierbei, dass eine Lösung des viskosen Systems in Bezug auf die Zeit glatter ist, als eine Lösung des nicht-viskosen Systems.

Bei der numerischen Simulation der Phasenseparation ohne Viskosität und mit extrem kleinen Oberflächenspannungen, wie sie bei praktischen Anwendungen vorkommen, beobachtet man das Gibbs Phänomen. Dies bedeutet, dass starke Oszillationen innerhalb eines diffusiven Interfaces auftreten, wodurch die numerischen Simulationsergebnisse unbrauchbar werden.

Diese Effekte motivieren die Entwicklung stabiler numerischer Verfahren zur Approximation der Lösung des Cahn-Larché Systems, wobei stabil in diesem Zusammenhang bedeutet, dass die numerische Lösung keine Oszillationen aufweist. Dieses Ziel wird mit Hilfe folgender Methoden erreicht:

- Ein Faedo-Galerkin Verfahren für die viskosen Cahn-Larché Gleichungen wird hergeleitet. Dabei wird der Reibungsterm als Stabilisierung der Methode für das nicht-viskose System verwendet.

- Ein zweites Approximationsverfahren wird untersucht, bei welchem die Reibung in Form von treibenden Kräften formuliert wird. Hervorzuheben ist, dass die Äquivalenz beider Methoden unter Verwendung der Fluss-Gradienten-Struktur des Modells gezeigt wird.

Beide Methoden stellen ein stabiles Verfahren zur Simulation der spinodalen Dekomposition einer Legierung dar. Dennoch ist es wünschenswert, ein stabiles Verfahren direkt für die nicht-viskosen Gleichungen herzuleiten. Dies erfolgt durch folgendes Vorgehen:

- Für das Cahn-Larché System wird eine Operator-Splitting Methode entwickelt, bei der die Gibbs freie Energie in einen konvexen und in einen konkaven Anteil aufgespaltet wird.

Diese Methode ergibt sich als Erweiterung der Techniken, die von Barrett und Blowey in [9, 10] für die Cahn-Hilliard Gleichung entwickelt wurden. Die Untersuchungen in dieser Arbeit zeigen, dass die Operator-Splitting Methode zwar stabil, aber im Vergleich mit den viskosen Methode nicht so effizient ist, da eine sehr kleine Zeitschrittweite gewählt werden muss.

Die zahlreichen numerischen Simulationen, die in dieser Arbeit hauptsächlich mittels der viskosen Methode stabilisiert durch treibende Kräfte durchgeführt werden, zeigen folgende Ergebnisse:

- Das Cahn-Larché Modell mit konzentrationsabhängigem Elastizitätstensor stimmt qualitativ besser mit dem Experiment überein als das einfachere Modell mit konstantem Elastizitätstensor.

- Mechanische Spannungssingularitäten, die aus wechselnden Randbedingungen resultieren, beeinflussen die Entwicklung der Mikrostruktur wesentlich.
- Ein entsprechendes Resultat ergibt sich für einspringende Ecken und Kerben. In beiden Fällen entwickelt sich in der Umgebung der Spannungssingularität eine Phase bestehend aus dem weicheren Material.

List of Figures

Acronyms and symbols

Acronyms:

Ag	Chemical symbol of silver	1
BEM	Boundary Element Method	4
BiCGStab	Biorthogonal conjugated gradient method	114
BPX	Bramble, Pasciak and Xu multilevel preconditioner	84
CG	Conjugated gradient method	80
Cu	Chemical symbol of copper	1
DoF	Degree of freedoms	148
GMRes	General minimum residual method	114
LAC	Linear algebra classes	148
LES	Linear equation system	80
LSW	Lifshitz, Slyozov and Wagner theory	2
MyFEM++	My personal Finite element library	147
Pb	Chemical symbol of lead	1
PCB	Printed Circuit Board	1
PSLG	Planar straight line graph	147
RVE	Representative Volume Element	2
SMT	Surface Mount Technology	1
Sn	Chemical symbol of tin	1
VTK	Visualisation Toolkit	148

Symbols:

$\underline{\boldsymbol{A}}$	Mass matrix	80
$\boldsymbol{\mathcal{B}}$	BPX operator	84
b_j^i	Spline weights	34
B_i^n	i-th Bernstein polynomial of degree n	34
$\boldsymbol{C}$	Elasticity tensor	34
c	Material mass concentration	16
$C^{k,l}(\Omega)$	Hölder space	41
c_0	Initial concentration	16
$\boldsymbol{C}^{\alpha/\beta}$	Elasticity tensors of the α-/β-phase	36
$c^{\alpha/\beta}$	Equilibrium concentrations of the α-/β-phase	30

ϵ	Material specific internal energy density	20
ϵ^{φ}	Spatial internal energy density	19
η	Material entropy density	20
$\hat{\eta}$	Material entropy volume source	21
$\hat{\eta}^{\varphi}$	Spatial entropy volume source	20
η^{φ}	Spatial specific entropy density	20
$\boldsymbol{F}$	Mass averaged deformation gradient	13
$\mathscr{F}_h(\Omega)$	Set of all faces in the triangulation	72
$\boldsymbol{g}$	Material boundary loading	18
$g^{\alpha/\beta}$	Gibbs free energy of the α-/β-phase	31
γ	Friction coefficient	26
$\boldsymbol{\Gamma}$	Surface stress tensor	28
Γ_T	Cylindric shell of the time space cylinder	10
$\boldsymbol{\Gamma}^{\alpha/\beta}$	Surface stress tensors of α-/β-phase	30
$\bar{\gamma}$	Interface energy	31
Γ_T^D	Dirichlet boundary part in the reference configuration	19
Γ_D	Dirichlet boundary part	40
Γ_T^N	Neumann boundary part in the reference configuration	18
Γ_N	Neumann boundary part	40
$\Gamma_T^{\varphi,D}$	Dirichlet boundary part of the actual configuration	17
$\Gamma_T^{\varphi,N}$	Neumann boundary part of the actual configuration	17
Γ_T^{φ}	Time space shell in the actual configuration	16
$\mathrm{GL}(\mathbb{R})$	General linear group	13
$\boldsymbol{g}^n$	Time discrete boundary loading	51
$\boldsymbol{g}_N$	Piecewise constant expansion of the boundary loading	51
$\boldsymbol{g}^{\varphi}$	Spatial boundary loading	17
h	Global mesh size	72
$H^s(\Gamma)$	Trace space	41
$H^{-\frac{1}{2}}(\Gamma_N)$	Dual space of the trace space	42
$H^l(\Omega)$	Sobolev space	41
h_τ	Local mesh size	72
$\widetilde{H}^{\frac{1}{2}}(\Gamma_N)$	Trace space	42
$h_{\boldsymbol{z}}$	Averaged local mesh size	73
$\boldsymbol{J}$	Material diffusive flux	16
$\boldsymbol{J}_k$	Material diffusive flux of component k	16
$\boldsymbol{J}_k^{\varphi}$	Spatial diffusive flux of component k	15
k	Component index in the mixture	10
$\boldsymbol{\mathcal{L}}$	Elasticity operator	84
$\underline{\boldsymbol{L}}$	Stiffness matrix	84
L_0	Characteristic length	27

W	Strain energy density	28
$\boldsymbol{X}(\Omega)$	Space of the displacement	42
$\boldsymbol{x}$	Material coordinate	10
X	Banach space	40
$X_h(\Omega)$	Trial space of piecewise linear functions	74
$\boldsymbol{X}_h(\Omega)$	Trial space of vector valued piecewise linear functions with homogeneous Dirichlet boundary conditions	74
$X_m(\Omega)$	Space with mass conservation	41
$X_{m,h}(\Omega)$	Trial space of piecewise linear functions with mass conservation	74
X'	Dual space of a Banach space	40
$\boldsymbol{x}^*$	Dimensionless coordinate	27
$\boldsymbol{Y}$	Thermodynamic process	22
$\boldsymbol{y}$	Spatial coordinate	11
y	Particle density	32
$Y_0(\Omega)$	Space with solvability condition	41

Bibliography

[1] M. Abramowitz and I. A. Stegun, editors. *Handbook of Mathematical Functions with Formulas, Graphs and Mathematical Tables*, volume 55 of *Applied Mathematic Series*. U.S. Department of Commerce, National Bureau of Standards, Washington D.C., 1972.

[2] R. A. Adams. *Sobolev Spaces*, volume 65 of *Pure and Applied Mathematics*. Academic Press, Inc., Boston, 1992.

[3] N. Akaiwa, K. Thornton, and P. W. Voorhees. Dynamics of late-stage phase separation in crystalline solids. *Physical Review Letters*, 86(7):1259–1263, 2001.

[4] N. Akaiwa, K. Thornton, and P. W. Voorhees. Large-scale simulations of microstructural evolution in elastically stressed solids. *Journal of Computational Physics*, 173:61–86, 2001.

[5] H. W. Alt. *Lineare Funktionalanalysis*. Springer Verlag, Berlin, Heidelberg, 4 edition, 2002.

[6] H. W. Alt and I. Pawlow. Thermodynamical models of phase transitions with multicomponent order parameter. In Manuel D. P. Monteiro Marques and other, editors, *Trends in applications of mathematics to mechanics*, volume 77 of *Pitman Monographs Surveys Pure and Applied Mathematics*, pages 87–98, Harlow, 1995. STAMM-94, Longman.

[7] H. W. Alt and I. Pawlow. On the entropy principle of phase transition models with a conserved order parameter. *Adv. Math. Sci. Appl.*, 6(1):291–376, 1996.

[8] L. S. Avila et al. *The VTK user's guide: updated for version 4.2*. Kitware, Inc. publishers, New York, 2003.

[9] J. W. Barrett and J. F. Blowey. Finite element approximation of a model for phase separation of a multi-component alloy with non-smooth free energy. *Numerische Mathematik*, 77(1):1–34, 1997.

[10] J. W. Barrett and J. F. Blowey. Finite element approximation of a model for phase separation of a multi-component alloy with a concentration-dependent mobility matrix. *IMA Journal of Numerical Analysis*, 18(2):287–328, 1998.

[11] J. W. Barrett, J. F. Blowey, and H. Garcke. On fully practical finite element approximations of degenerate Cahn-Hilliard systems. *Mathematical Modeling and Numerical Analysis*, 35(4):713–748, 2001.

[12] L. Bartkowiak and I. Pawlow. The Cahn-Hilliard-Gurtin system coupled with elasticity. to appear, 2004.

[13] E. Bonetti, P. Colli, W. Dreyer, G. Gilardi, G. Schimpera, and J. Sprekels. On a model for phase separation in binary alloys driven by mechanical effects. *Physica D*, 165:48–65, 2002.

[14] R.M. Bowen and J.C. Wiese. Diffusion in mixtures of elastic materials. *International Journal of Engineering Science*, 7:689–722, 1969.

[15] D. Braess. *Finite Elemente*. Springer Verlag, Berlin Heidelberg, 1997.

[16] J. H. Bramble, J. E. Pasciak, and O. Steinbach. On the stabitity of the L^2-projection in $H^1(\Omega)$. *Mathematics of Computation*, to appear, 2000.

[17] J. H. Bramble, J. E. Pasciak, and J. Xu. Parallel multilevel preconditioners. *Mathematics of Computation*, 55:1–22, 1990.

[18] S. C. Brenner and L. R. Scott. *The Mathematical Theory of Finite Element Methods*. Springer Verlag Inc., New York, 1994.

[19] J. W. Cahn. On spinodal decomposition. *Archives of Mechanics*, 9:795–801, 1961.

[20] J. W. Cahn and J. E. Hilliard. Free energy of a non-uniform system: I. interfacial free energy. *The Journal of Chemical Physics*, 28(2):258–267, 1958.

[21] J. W. Cahn and J. E. Hilliard. Free energy of a non-uniform system: III. nucleation in a two-component incompressible fluid. *The Journal of Chemical Physics*, 31(3):688–699, 1959.

[22] M. Carrive, A. Miranville, and A. Piétrus. The Cahn-Hilliard equation for deformable elastic continua. *Adv. Math. Sci. Appl.*, 10(2):539–569, 2000.

[23] X. Chen and M. Kowalczyk. Existence of equilibria for the Cahn-Hilliard equation via local minimisers of the perimeter. *Communications in Partial Differential Equations*, 21:1207–1233, 1996.

[24] P. G. Ciarlet. *Mathematical Elasticity*, volume 1, Three-dimensional Elasticity. North Holland, Amsterdam, 1993.

[25] P. G. Ciarlet. *The finite element method for elliptic problems*. SIAM, Philadelphia, 2002.

[26] P. Clément. Approximation by finite element functions using local regularization. *Revue Française d´Automatique, Informatique et Recherche Opérationnelle*, 9(R-2):77–84, 1975.

[27] R. Cool and P. Rabinowitz. Monomial cubature rules since "Stoud": a compilation. *Journal of Computational and Applied Mathematics*, 48:309–326, 1993.

[28] M. I. M. Copetti and C. M. Elliott. Numerical analysis of the Cahn-Hilliard equation with logarithmic free energy. *Numerische Mathematik*, 63:39–65, 1992.

[29] B. Dacorogna. *Direct Methods in the Calculus of Variations*. Springer Verlag, 1989.

[30] R. Dautray and J.-L. Lions. *Mathematical Analysis and Numerical Methods for Science and Technology*, volume 5 Evolution Problems I. Springer Verlag, Berlin Heidelberg, 1992.

[31] W. Dreyer and W. H. Müller. Computer modelling of micromorphological change by phase field models: applications to metals and ceramics. *Journal of the Australasian ceramic society*, 36(1):83–94, 2000.

[32] W. Dreyer and W. H. Müller. A study of the coarsening in tin/lead solders. *International Journal of Solids and Structures*, 37:3841–3871, 2000.

[33] W. Dreyer and W. H. Müller. Modelling diffusional coarsening in eutectic tin/lead solders: a quantitative approach. *International Journal of Solids and Structures*, 38:1433–1458, 2001.

[34] W. Dreyer and W. H. Müller. Modelling diffusional coarsening in microelectronic solders. Preprint 654, Weierstraß-Institut für Angewandte Analysis und Stochastik, Berlin, 2001.

[35] C. M. Elliott. The Cahn-Hilliard model for the kinetics of phase separation. In J. F. Rodrigues, editor, *Mathematical Models for Phase Change Problems*, volume 88 of *International Series of Numerical Mathematics*, pages 35–73. Birkhäuser Verlag, Basel, 1989.

[36] C. M. Elliott and D. A. French. Numerical studies of the Cahn-Hilliard equation for phase separation. *IMA Journal of Applied Mathematics*, 38:97–128, 1987.

[37] C. M. Elliott, D. A. French, and F. A. Milner. A 2nd order splitting method for the Cahn-Hilliard equation. *Numerische Mathematik*, 54:575–590, 1989.

[38] C. M. Elliott and H. Garcke. On the Cahn-Hilliard equation with degenerate mobility. *SIAM Journal on Mathematical Analysis*, 27(2):404–423, 1996.

[39] C. M. Elliott and S. Luckhaus. A generalised diffusion equation for phase separation of multi-component mixture with interfacial free energy. Preprint 195, SFB 256 University Bonn, Bonn, 1991.

[40] C. M. Elliott and Z. Songmu. On the Cahn-Hilliard equation. *Archive for Rational Mechanics and Analysis*, 96:339–357, 1986.

[41] C. M. Elliott and A. M. Stuart. The global dynamics of discrete semilinear parabolic equations. *SIAM Journal on Numerical Analysis*, 30(6):1622–1663, 1993.

[42] J. Elstrodt. *Maß- und Integrationstheorie*. Springer Verlag, Berlin Heidelberg, 1996.

[43] L. C. Evans. *Partial Differential Equations*. American Mathematical Society, 1998.

[44] P. Fratzl, O. Penrose, and J. L. Lebowitz. Modelling of phase separation in alloys with coherent elastic misfit. *Journal of Statistical Physics*, 95(5/6): 1429–1503, 1999.

[45] P. Fratzl, O. Penrose, J. L. Lebowitz, and J. Amar. Scaling functions, self similarity and the morphology of phase separating systems. *Physical Review B*, 44:4794–4811, 1991.

[46] E. Fried and M. E. Gurtin. Continuum theory of thermally induced phase transitions based on an order parameter. *Physica D*, 68:326–343, 1993.

[47] E. Fried and M. E. Gurtin. Dynamic solid-solid transitions with phase characterized by an order parameter. *Physica D*, 72:287–308, 1994.

[48] H. Garcke. On mathematical models for phase separation in elastically stressed solids. Habilitationsschrift, Friedrich-Wilhelms-Universität, Bonn, 2000.

[49] H. Garcke. On Cahn-Hillard systems with elasticity. Preprint 19, Priority Program (Schwerpunktprogramm 1095) DFG: Analysis, Modeling and Simulation of Multiscale Problems, 2001.

[50] H. Garcke, M. Rumpf, and U. Weikard. The Cahn-Hilliard equation with elasticity finite element approximation and qualitative studies. *Interfaces and Free Boundaries*, 3:101–118, 2001.

[51] H. Garcke and U. Weikard. Numerical approximation of the cahn-larche equation. Preprint 115, Priority Program (Schwerpunktprogramm 1095) DFG: Analysis, Modeling and Simulation of Multiscale Problems, 2004.

[52] M. Grinfeld and A. Novick-Cohen. The viscous Cahn-Hilliard equation: Morse decomposition and structure of the global attractor. *Transactions of the American Mathematical Society*, 351(6):2375–2406, 1999.

[53] P. Grisvard. *Elliptic Problems in Nonsmooth Domains*. Pitman Press, Bath, Avon, 1985.

[54] G. Grün and M. Rumpf. Simulation of singularities and instabilities arising in thin film flow. *European Journal of Applied Mathematics*, 12:293–320, 2001.

[55] M. E. Gurtin. *An Introduction to Continuum Mechanics*. Academic Press Inc., 1981.

[56] M. E. Gurtin. Generalized Ginzburg-Landau and Cahn-Hilliard equations based on a microforce balance. *Physica D*, 92:178–192, 1996.

[57] M. E. Gurtin. *Configurational Forces as Basic Concepts of Continuum Physics*. Springer Verlag, New York, 2000.

[58] M. Hestenes and E. Stiefel. Methods of conjugate gradients for solving linear systems. *Journal of Research of the National Bureau of Standards*, 49:409–436, 1952.

[59] H.-J. Jou, P.H. Leo, and J.S. Lowengrub. Microstructural evolution in inhomogeneous elastic media. *Journal of Computational Physics*, 131(1):109–148, 1997.

[60] M. Jung and U. Langer. *Methode der finiten Elemente für Ingenieure: eine Einführung in die numerischen Grundlagen und Computersimulation*. Teubner Verlagsgesellschaft, Stuttgart, Leipzig, Wiesbaden, 1 edition, 2001.

[61] K. Kawasaki and Y. Enomoto. Statistical theory of Ostwald ripening with elastic field interactions. *Physica A*, 150:463–498, 1988.

[62] A. G. Khachaturyan. *Theory of Structural Transformations in Solids*. John Wiley & Sons, Inc., New York, 1983.

[63] Inc. Kitware. ParaView, Version 1.8. http://www.paraview.org/, .

[64] Inc. Kitware. The Visualization Toolkit, Version 4.2. http://www.vtk.org/, .

[65] V. A. Kondrat'ev. Boundary value problems for elliptic equations in domains with conical or angular points. *Transactions of the Moscow Mathematical Society*, 10:227–313, 1967.

[66] T. Köpper and N. Masbaum. Simulations of particle growth and Ostwald ripening via Cahn-Hilliard equation. *Acta Metallugica et Materialia*, 42:1847–1858, 1994.

[67] V. A. Kozlov, V. G. Maz'ya, and J. Rossmann. *Elliptic Boundary Value Problems in Domains with Point Singularities*. American Mathematical Society, 1997.

[68] F. C. Larché and J. W. Cahn. The effect of self-stress on diffusion in solids. *Acta Metallurgica*, 30:1835–1845, 1982.

[69] P. H. Leo, W. W. Mullins, R. F. Sekerka, and J. Viñals. Effect of elasticity on late stage coarsening. *Acta Metallugica et Materialia*, 38:1573–1580, 1990.

[70] I. M. Lifshitz and V. V. Slyozov. The kinetics of precipitation from supersaturated solid solutions. *The Journal of Physics and Chemistry of Solids*, 19: 35–50, 1961.

[71] I.-S. Liu. Method of lagrange multipliers for exploitation of the entropy principle. *Archive for Rational Mechanics and Analysis*, 46:131–148, 1972.

[72] T. Merkle. Phase separation in solid mixtures under elastic loadings with application to solder material. Preprint 2003/006, Berichte aus dem Institut für Angewandte Analysis und Numerische Simulation, Universität Stuttgart, http://preprints.ians.uni-stuttgart.de, 2003.

[73] MTData. NPL Databank for Material Thermochemestry. National Physical Laboratory, Queens Rad Teddington Midlesex TW111 0LW, 1998.

[74] I. Müller. The coldness a universal function in thermoelastic bodies. *Archive for Rational Mechanics and Analysis*, 41:319–332, 1971.

[75] I. Müller. Die Kältefunktion eine universelle Funktion in der Thermodynamik viskoser wärmeleitender Flüssigleiten. *Archive for Rational Mechanics and Analysis*, 40:1–36, 1971.

[76] I. Müller. *Thermodynamik, Die Grundlagen der Materialtheorie*. Bertelsmann Universitätsverlag, 1973.

[77] W. W. Mullins and R. F. Sekerka. Morphological stability of a particle growing by diffusion or heat flow. *Journal of Applied Mechanics*, 34:323–329, 1963.

[78] S. Müller-Urbaniak. Eine Analyse des Zweischritt-θ-Verfahrens zur Lösung der instationären Navier-Stokes-Gleichung. Preprint 94-01, SFB 359, 1994.

[79] J. Nećas and I. Hlavaček. *Mathematical theory of elastic and elasto-plastic bodies*. Elsevier, Amsterdam, 1981.

[80] A. Novick-Cohen. Energy methods for the Cahn-Hilliard equation. *Quarterly of Applied Mathematics*, XLVI(4):681–690, December 1988.

[81] A. Novick-Cohen. The Cahn-Hilliard equation: Mathematical and modelling perspectives. *Adv. Math. Sci. Appl.*, 8(2):965–985, 1998.

[82] L. Onsager. Reciprocal relations in irreversible processes I. *Physical Review*, 37:405–426, 1931.

[83] L. Onsager. Reciprocal relations in irreversible processes II. *Physical Review*, 38:2265–2279, 1931.

[84] A. Onuki. Ginzburg-Landau approach to elastic effects in the phase separation of soilds. *Journal of the Physical Society of Japan*, 58:3065–3068, 1989.

[85] A. Quarteroni and A. Valli. *Numerical Approximation of Partial Differential Equations*. Springer Verlag, Berlin, Heidelberg, 1997.

[86] J. Radon. Zur mechanischen Kubatur. *Monatshefte für Mathematik*, 52:286–300, 1948.

[87] Y. Saad and M. H. Schultz. A generalized minimal residual algorithm for solving nonsymmetric linear systems. *SIAM Journal on Scientific Computing*, 7:856–869, 1985.

[88] H. R. Schwarz. *Numerische Mathematik*. Teubner Verlag, Stuttgart, 1997.

[89] J. R. Shewchuk. Triangle, Version 1.5: A two-dimensional quality mesh generator and delaunay triangulator. http://www-2.cs.cmu.edu/ quake/triangle.html.

[90] J. R. Shewchuk. Triangle: Engineering a 2D Quality Mesh Generator and Delaunay Triangulator. In M. C. Lin and D. Manocha, editors, *Applied Computational Geometry: Towards Geometric Engineering*, volume 1148 of *Lecture Notes in Computer Science*, pages 203–222. Springer-Verlag, 1996.

[91] J. Simon. Compact sets in the space $L_p(0,T;B)$. *Annali di Matematica Pura ed Applicata*, 146:65–96, 1987.

[92] O. Steinbach. Theorie und Algorithmen für Iterationsverfahren zur Lösung linearer Gleichungssysteme. Preprint 1994–4, Universität Stuttgart, 1994.

[93] O. Steinbach. *Numerische Näherungsverfahren für elliptische Randwertprobleme, Finite Elemente und Randelemente*. Advances in Numerical Mathematics. B. G. Teubner Verlag, Wiesbaden, 1. edition, 2003.

[94] G. Strang. On the construction and comparison of difference schemes. *SIAM Journal on Numerical Analysis*, 5:506–517, 1968.

[95] M. Struwe. *Variational methods. Applications to nonlinear partial differential equations and Hamiltonian systems*. Springer-Verlag, Berlin, 1990.

[96] V. Thomée. *Galerkin Finite Element Methods for Parabolic Equations*. Springer Verlag, Berlin Heidelberg, 1984.

[97] C. Truesdell. *Rational Thermodynamics*. Springer Verlag, New York, second edition edition, 1984.

[98] H. A. van der Vorst. Bicgstab: A fast and smoothly converging variant of bicg for the solution of nonsymmetric linear systems. *SIAM Journal on Scientific Computing*, 13(2):631–644, 1992.

[99] M. Šilhavý. *The Mechanics and Thermodynamics of Continuous Media*. Springer Verlag, Berlin Heidelberg, 1997.

[100] C. Wagner. Theorie der Alterung von Niederschlägen durch Umlösen. *Zeitschrift für Elektrochemie*, 65:581–594, 1961.

[101] W. Walter. *Gewöhnliche Differentialgleichungen*. Springer Verlag, Berlin, Heidelberg, 7. edition, 2000.

[102] U. Weikard. Numerische Lösungen der Cahn-Hilliard-Gleichung und der Cahn-Larché-Gleichung. Dissertationsschrift, Friedrich-Wilhelms-Universität, Bonn, 2002.

[103] T. Williams et al. Gnuplot, version 4.0. Technical report, Pixar Corporation, http://www.gnuplot.info/, 2004.

[104] J. Wloka. *Partielle Differentialgleichungen*. Teubner Verlag, Stuttgart, 1982.

[105] J. Xu. An introduction to multilevel methods. In *Wavelets, multilevel methods and elliptic PDEs*, Numerical mathematics and scientific computation, pages 213–302. Oxford University Press, 1997.

[106] E. Zeidler. *Nonlinear Functional Analysis and its Applications*, volume 2/A Linear Monotone Operators. Springer Verlag Inc., New York, 1986.

[107] E. Zeidler. *Nonlinear Functional Analysis and its Applications*, volume 2/B Nonlinear Monotone Operators. Springer Verlag Inc., New York, 1986.

[108] E. Zeidler. *Nonlinear Functional Analysis and its Applications*, volume 3 Variational Methods and Optimization. Springer Verlag Inc., New York, 1986.

Curriculum vitae

Personal information

Name:	Dipl.-Math. Thomas Merkle
Day of birth:	27th November 1974
Place of birth:	Göppingen
Marital status:	married, one daughter

Career

1981-1985	Schiller-Grundschule Faurndau
1985-1994	Werner-Heisenberg-Gymnasium Göppingen,
Juni 1994	Grade: Abitur
1994-1995	Alternative service at the Sozialstation St. Franziskus Göppingen
1995-2001	Study of mathematic at the University of Stuttgart Second subject: Computer science
February 2001	Grade: Diplom Diploma thesis: „Schadstofftransport in porösen Medien“
April 2001	Member of the scientific staff at the University of Stuttgart in the „Sonderforschungsbereich 404 projekt C5“ at apt. Prof. Dr. A.-M. Sändig
January 2002	Member of the scientific staff at the university of Stuttgart in the „Mathematischen Institut A“ at Prof. Dr. A. Mielke
April 2002	Phd student at „Engineering Design Powertrain, AE/EDP5, Robert Bosch GmbH“ in Reutlingen Project: „Mathematische Modellbildung und Analyse von Weichloten unter mechanischen und thermischen Belastungen mit Anwendung auf die Steuergeräte-konstruktion“
since April 2005	Computation Engineer at „Engineering Design Powertrain, AE/EDP5, Robert Bosch GmbH“ in Reutlingen